DISSERTATION

POLYMERIC FILMS, EMULSIONS, AND NANOFIBERS FOR MEDICAL APPLICATIONS

Submitted by

Janet Pamela Yapor

Department of Chemistry

In partial fulfillment of the requirements

For the Degree of Doctor of Philosophy

Colorado State University

Fort Collins, Colorado

Fall 2018

Doctoral Committee:

Advisor: Melissa M. Reynolds

Yan V. Li
Travis S. Bailey
Alan Van Orden

ABSTRACT

POLYMERIC FILMS, EMULSIONS, AND NANOFIBERS FOR MEDICAL APPLICATIONS

Natural polymers such as cellulose and proteinaceous materials including hair or animal tissue have been used since prehistory. Their use was appropriate until they no longer met the criteria for the intended applications. For example, for implantable materials, the requirements would include materials with higher rigidity or slower degradation than naturally-occurring polymers. For this reason, scientists have invented new materials that are able to emulate or have similar properties as physiological tissue.

New materials with a wide range of physical and chemical properties have been tailored to meet the highly diversified demands of modern technologies such as polyurethanes (PU) used for coatings, adhesives, fiber, foams, and thermoplastic elastomers. However, some of these have been derived from petroleum sources, which is a finite resource and its extraction causes environmental contamination. Furthermore, the synthesis of polymeric materials prepared from renewable resources and without the use of external catalysts has been an evolving field in materials science. Polymers such as polyesters have been developed with the goal of decreasing the use of petroleum sources. In addition, synthetic polymers can be tailored to mimic physiological responses. One method for the functionalization of these materials is through the addition of nitric oxide (NO) by the formation of *S*-nitrosothiol groups. NO is a relevant endogenous free radical that has important physiological roles such as vasodilation, cell proliferation, angiogenesis, and broad-spectrum antibacterial activity. Various NO-releasing

platforms have been developed with morphologies that range from viscous liquids and emulsions to films.

The synthesis of NO-releasing polyesters with potential applications in wound healing is discussed in this dissertation. Copolymers were prepared *via* bulk polycondensation with monomeric units including citric acid, maleic acid, and 1,8-octanediol. The first generation of materials required additional conjugation steps in order to add sulfhydryl groups, which were added using carbodiimide chemistry to couple cysteamine or ethyl cysteinate pendant groups. For the second generation of materials, the use of a sulfhydryl-containing monomer, thiomalic acid, eliminated the need for additional conjugation steps. The polyesters were formed using thiomalic acid and 1,8-octanediol alone, and with citric or maleic acid. The increased tensile mechanical properties of the second generation of polyesters yielded materials with Young's moduli similar to that of soft biological tissues such as meniscus, ligament and tendon. The results expanded the potential applications for such polyesters suggesting that the materials could be used as implantable devices or as scaffolds for tissue engineering. An issue with implantable devices arises from the fibrous encapsulation of the device, which is a physiological response referred to as the foreign body response that can be mitigated by NO. Furthermore, an NO-releasing emulsion with additives such as vitamin E and hyaluronic acid was developed, and its NO release profile was studied.

In addition to polymer applications, emulation of physiological activities includes materials that can elicit a response when exposed to a variety of chemical or physical environments. Polydiactelyenes (PDAs) are a class of conjugated polymers that have been studied for their potential applications as sensors that detect biological, chemical and thermal changes in the surroundings. These polymers exhibit a chromatic response from blue to red when

exposed to various stimuli. PDA nanofibers were prepared *via* elecrospinning with matrix polymers such as poly(ethylene oxide) and PU.

ACKNOWLEDGEMENTS

This is the last section of the dissertation to be written, but the first one in my mind when I started graduate school. I was fortunate to grow up in a caring family, surrounded by wonderful friends. I will be forever grateful for the love and joy that they have brought to my life. Thank you to my mom, Abigail, for teaching me about perseverance and optimism. She taught me that the magnitude of the adversities should not frighten you, instead, it should help you mold your attitude so that you can overcome difficult situations. Thank you to my sister, Abby, for being the best friend and companion ever possible. Her kindness and gentleness taught me that everyone deserves to be treated with respect. Thank you to my brother, Oscar, for reminding me that it takes time for flowers to bloom and that patience is a virtue that can be developed if it is put into practice. Other family members, such as Sophia, Emma, Memo, and Roger, I thank for their encouragement and help.

My time in graduate school was enjoyable, which would not have been possible without the guidance and support of my advisor, Prof. Melissa Reynolds. I am truly grateful for my committee members, and I thank them for believing in me and for their thoughtful feedback throughout my doctoral studies. Special appreciation to Prof. Debbie Crans for her contributions as a committee member substitute during the evaluations. I also thank my undergraduate research advisor, Prof. Melvin Druelinger, for educating me on the art of performing research. My high school chemistry teacher, Armida, who showed me the excitement there is in studying chemistry and conducting experiments in the laboratory. It is thanks to inspiring teachers that a new generation of scientists arises, and they deserve recognition for their effort. I leave Colorado

State University with great memories, knowing that, regardless of what the future holds for me, this institution will be remembered fondly.

In loving memory of Oscar Yapor Zepeda.

TABLE OF CONTENTS

CHAPTER 1

INTRODUCTION

1.1 Polymers for medical applications

Natural polymers have been used for centuries due to the wide range of applications and processing methods that can be used to develop materials into various morphologies.[1] Materials currently developed for medical applications can be designed and tailored to achieve specific aims depending on the end use.[2] Polymers are currently used in the medical field for applications that range from wound dressings and catheters to sensors.[3]

The preparation of polymeric materials for medical applications is one of the most rapidly evolving areas in materials science due to the diversity of processing methods that can be utilized for their preparation and broad range of applications. Materials have been successfully developed from naturally-occurring sources such as proteins,[4-6] polysaccharides,[7,8] and polyhydroxyalkanoates.[9,10] The type of sources used for the formulation of polymeric devices has expanded, however, since the intended applications have become more specific. Emerging technologies have utilized synthetic polymers as an alternative strategy for the development of medical devices. One of the advantages of synthetic polymers arises from the ability to create modulus-matched materials based on the desired application.[11] Synthetic materials have been studied in the field of materials research due to their potential application in the development of drug delivery therapies, medical device coatings, tissue regeneration, wound dressings, and biosensors.[12,13]

1.1.1 Biodegradable nitric oxide-releasing polyesters

Materials that undergo degradation are of particular interest because they can break down into smaller components and do not accumulate waste in the environment. Waste can be minimized by designing materials with monomeric units that are bonded through links that support degradation. Polyesters are a family of polymers with ester functional groups that were synthesized from a condensation reaction by Carothers in the 1930s.[14-16] Esterification is thermodynamically a reversible reaction.[17] Hence, theoretically, polyesters are degradable in the presence of water. This type of degradation is referred to as hydrolytic degradation and occurs when water causes cleavage of the main chain ester bonds.[18] Ester linkages can be formed by polycondensation reactions, which involve the formation of water as a byproduct. Polyesters are typically synthesized by a stepwise polymerization of difunctional monomers of the AB type, or from the combination of AA and BB difunctional monomers. Multifunctional monomers may be used as well, which may give rise to crosslinked networks. Polyesters can be synthesized from the reaction of a monomeric units such as diacids and diols, diacid chlorides and diols, or by transesterification of diesters with diols.[19] The degradation profiles of networked polymers can be correlated with the crosslinking density, where lower crosslinking densities may correspond to materials with slower degradation profiles.[20] Such results may be attributed to the linearity of the polymer chains that do not allow solvent permeation to occur to a greater extent compared to polymers with high crosslinking densities.[21,22] The degradation can also dependent on the hydrophobicity of the monomer units given that longer hydrocarbons may exhibit greater hydrophobicity.[23] Degradation experiments for biomaterials are usually performed at simulated physiological conditions that include a specific pH and temperature. In addition, analysis of the

hydrolytic degradation products by mass spectrometry can be useful to decipher the type of byproducts obtained.

A common issue that arises in the medical field is the occurrence of infection. Existing technologies used to treat wounds include growth factors,[24] bioengineered skin,[25] negative pressure wound therapy,[26] hydro-colloids,[27] foam dressings,[28] and antimicrobial dressings.[29] The appropriate dressing for the wound is determined by the specialist considering the position and state of the wound, fragility of surrounding skin, frequency of dressing changes, and patient comfort. An alternate method for the prevention of infection is through the use of nitric oxide (NO)-releasing substances that prevent and mitigate infection. An issue with NO releasing surfaces involves cytotoxicity issues given that NO can cause various physiological responses depending on the concentration. Therefore, cytotoxicity studies should be performed using viable cells to confirm the lack of toxicity of synthetic polymers. Fig. 1.1 illustrates the applications of NO-releasing polymers.

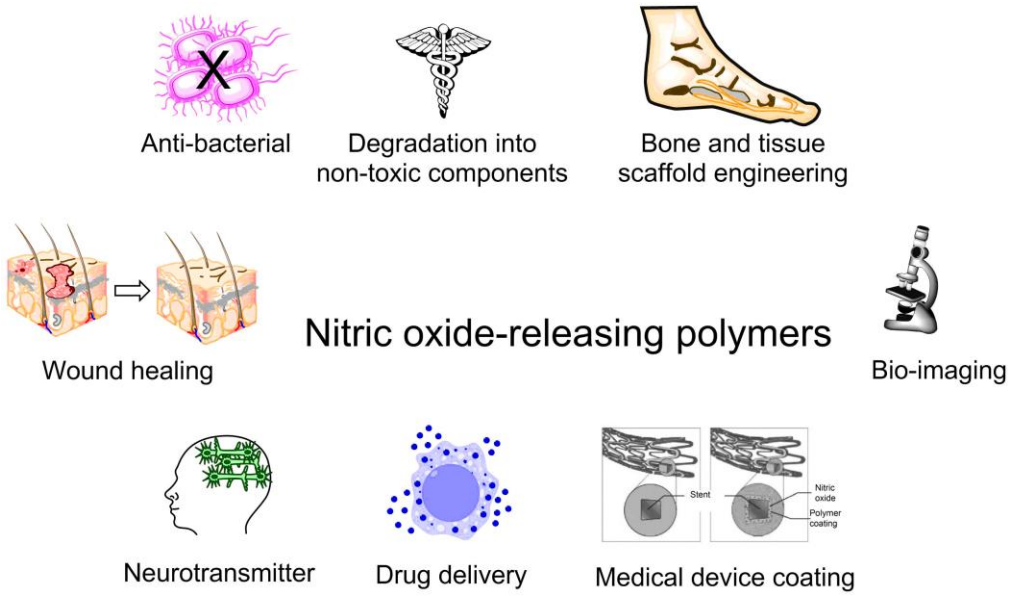

Figure 1.1 The illustration represents the potential applications of NO-releasing polymers.

1.1.1.1 Nitric oxide

A unique approach to prevent and combat bacterial infection is through the use of nitric oxide. The important role of NO in physiological pathways was discovered by Ignarro, Furchgott, and Murad; who jointly received the Nobel Prize in Physiology or Medicine in 1998 for the discovery of NO as an endothelial derived relaxation factor.[30-33] Prior to their discovery, NO was known an atmospheric pollutant produced from electrical storms, automobile exhaust, and industrial processes.[34]

Nitric oxide is an endogenous radical with important physiological roles such as blood vessel dilation,[35-40] immune response to infection,[41-43] neurotransmission in the brain,[44] platelet adhesion and aggregation,[45-47] wound repair,[48] as well as cancer biology and pathology.[49] NO is endogenously produced by a family of heme-bearing enzymes called nitric oxide synthase (NOS) by a 5-electron oxidation of the amino acid L-arginine to L-citrulline, which generates one equivalent of NO.[50,51] Another possible endogenous route for NO generation is through the reduction of nitrate to nitrite, nitric oxide and ammonia that is mediated by bacteria in the intestinal tract.[52] Continued NO release occurs at the surface of the endothelial cells (ECs), which effectively prevents platelets from activating or adhering to the walls of healthy blood vessels.[39,53-58] It has been estimated that the NO flux from normal ECs is between 0.5 and 1 $x10^{-10}$ mol cm^{-2} min^{-1}.[53,59] Due to the pivotal role of NO in human physiology, interruption in the homeostasis of NOS enzymes is typically correlated with a number of disease states.[60] Hence, strategies that regulate NOS activity or produce NO from exogenous sources have been developed with promising applications that range from cardiovascular,[51,61] cancer,[49] antibacterial,[62,63] and wound healing therapies.[64] However, the rapid reactivity of NO gas has been the limiting factor in the development of successful NO therapies.[65] Synthetic scaffolds

include NO-releasing albumin derivatives,[66] nanoparticles,[67,68] and polymers.[69-74] Current NO therapies are either drugs that alter physiological enzymatic NO production, or materials that release NO or one of NO's redox analogs.[75]

NO is able to trigger various physiological responses depending on the concentration at which it is delivered. At low doses (nM), the molecule can induce proliferative effects. At high concentrations, the molecule can cause apoptosis. Furthermore, scientists have developed methods to create a larger array of RSNOs that can be used with different quantities of NO to produce the desired physiological response.[76] Table 1.1 demonstrates physiological responses elicited by various concentrations of NO.

Table 1.1 Correlation of nitric oxide concentration and physiological responses.

Nitric Oxide Concentration	Physiological Response
< 1–30 nM	Mediation of proliferative and protective effects
30–60 nM	Apoptosis protection
100 nM	Tissue injury repair
400 nM	Cytostatic to apoptotic responses, cell cycle arrest
> 1 μM	Apoptosis, full cell cycle arrest

1.1.1.2 Nitric oxide donors

In order to achieve a controlled NO delivery, various NO donors have been developed such as organic nitrates, nitrites, metal NO-complexes, *N*-diazeniumdiolates (NONOates) and *S*-nitrosothiols (RSNOs).[77] The most widely used NO donor systems include NONOates and RSNOs given their ability to spontaneously release NO at physiological pH and temperature.

1.1.1.2.1 *N*-Diazeniumdiolates

NONOates were first discovered in 1961 by Drago *et al.* in a publication where inorganic chemists described the reaction of NO with selected nucleophiles.[78] NONOates can be synthesized by the reaction of secondary amines (*i.e.* diethylamine) with high pressures (*i.e.* 5 atm) of NO gas.[77] Nucleophilic attack on NO is the result of the deprotonation of the backbone amine by either an unreacted amine substrate or an added metal.[34] The charge of the anionic NONOate is stabilized by a cation, such as the protonated additional amine or metal from alkoxide base. NO release occurs upon deprotonation of the amine bearing the NONOate group. One of the advantages of NONOates involves the release of 2 moles of NO per mole of donor at physiological pH and temperature. As is the case with other functional groups, the structure of the amine precursor affects the NO release kinetics. A disadvantage for the use of NONOates arises from the release of NO under oxygenated conditions. In 1965, Drago *et al.* studied the decomposition of the adducts of diethylamine and isopropylamine with nitric oxide. The authors discovered that the reaction of diethylamine with NO produced a white powder, which, after being exposed to air overnight, was converted to the potent carcinogen *N*-nitrosodiethylamine.[79] In order to avoid the production of undesirable secondary *N*-nitrosamines, the diazeniumdiolate functional group could be attached to primary amines or carbon-based nucleophiles. Therefore, rigorous analysis of the byproducts of NO release should be done with NONOates and their contamination should be avoided to prevent toxicity issues.

1.1.1.2.2 *S*-Nitrosothiols

Alternate NO donors with lower toxicity concerns include RSNOs. The preferred use of these compounds is due to their endogenous nature. RSNOs have been studied for their potent smooth-muscle relaxation activity and inhibition of platelet aggregation. These compounds are believed to be the best candidates for the endogenous storage and transport of NO.[80-86] RSNOs such as *S*-nitrosoalbumin (BSNO) and *S*-nitrosoglutathione (GSNO) occur naturally *in vivo,* while other analogues such as *S*-nitroso-*N*-acetylpenicilamine (SNAP) have been synthesized. The synthesis of RSNOs involves the *S*-nitrosation reaction of the sulfhydryl-containing species.[87-89] Glutathione (GSH), the most abundant non-protein thiol produced endogenously, and L-cysteine (CySH) are naturally occurring sulfhydryl-containing peptides found in nearly all cells and they bear the sulfhydryl group in the cysteine residue. GSNO is the *S*-nitrosated analogue of GSH and is considered to be an endogenous NO carrier for multiple physiological functions.[80,81,88,90] CySH, the precursor of GSH, is involved as an intermediate (S-nitrosocysteine, CySNO) in transition reactions with alternate NO carriers.[91,92] Furthermore, *S*-nitrosation of certain cysteine species is predicted by highly conserved amino acids acting harmoniously in many proteins.[93,94] Specific enzymes and cell compartmentalization regulate this signaling biochemistry,[95-97] which has been proposed to be analogous to phosphorylation.[98,99] However, the reactions differ in the important ways since NO can be released by homolytic cleavage or transferred as nitrosonium (NO^+) between thiolate moieties.[100] Hence, changes in protein confirmation can drastically change the stability or reactivity of the S-NO bond in a specific protein. This change causes the transfer or release of an equivalent of NO to begin certain bioactivity. The lability of RSNOs also marks a difference from phosphorylation rendering RSNOs more difficult to identify and measure than phosphorylated proteins.[101] RSNOs

decompose through enzymatic, thermal, photolytic,[102,103] or transition metal ion-dependent pathways.[104] It is generally understood that RSNOs decompose by homolytic cleavage of the S–N bond.[105] The process generates a thiyl radical and nitric oxide followed by the formation of the corresponding disulfide.[106,107] The biological activity of RSNOs is not exclusively determined by the release of •NO since the chemistry of reactive nitrogen species is complex. Equations 1–3 and Fig. 1.2 illustrate reactions involved with NO release. RSNOs have also been reported to form NO^-, which can form either nitrous oxide[102,108,109] or peroxynitrite.[110,111] In addition, nitrosonium (NO^+) transfer to other thiolated moieties can occur through a process referred to as transnitrosation.[112,113]

$$RSNO \rightarrow RS\bullet + \bullet NO \quad (1)$$

$$2\ RS\bullet \rightarrow RS\text{–}SR \quad (2)$$

$$RSNO + RS\bullet \rightarrow \bullet NO + RSSR \quad (3)$$

Characterization of RSNOs can be performed by spectrophotometric techniques. RSNOs are generally pink, red or green. UV-vis spectra show characteristic absorption bands in the 330–350 nm region ($\varepsilon\ 10^3\ M^{-1}\ cm^{-1}$, $n_o \rightarrow \pi^*$) and at 550–600 nm ($\varepsilon\ 20\ M^{-1}\ cm^{-1}$, $n_N \rightarrow \pi^*$). These absorbances can be used to monitor RSNO decomposition and can be correlated to NO release to obtain an estimate of NO content. Infrared spectroscopy can also be employed for the characterization of RSNOs as the stretching and bending frequencies of the N–O bond have been detected at 1480–1530 cm^{-1}, as well as the C–S bond stretching frequency at 600–730 cm^{-1}. In addition, ^1H and ^{13}C NMR spectra have demonstrated that there is a downfield shift of the α-proton and α-carbon resonances after the *S*-nitrosation reaction.[114]

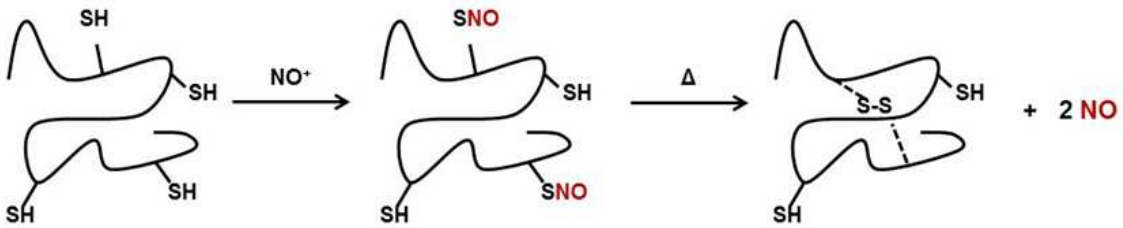

Figure 1.2 Generic *S*-nitrosation of thiolated polymer with a nitric oxide donor, followed by nitric oxide release as a result of thermal decomposition.

1.1.1.3 Quantification of NO release by RSNOs

NO release by RSNOs can be measured by several complementary types of assays. These include (a) chemiluminescence based analysis in which NO is photolytically cleaved from the SNO, or an NO^+ equivalent is reduced to NO, then reacted with ozone; (b) colorimetric assays in which NO is oxidized to nitrite and analyzed using spectrophotometry; (c) assays using fluorescent-based detection of released NO^+; (d) assays using antibodies directed to S-nitroso-cysteine (CSNO); (e) assays based on replacement of the thiolate bound NO^+ group with biotin; and (f) assays based on direct mass spectrometric identification of the RSNO containing species.[101] Table 1.2 demonstrates the advantages and disadvantages of each technique. The high sensitivity of the detection method using photolysis-chemiluminescence has made of this the preferable method for the detection of NO in the studies discussed herein.

Table 1.2 Summary of common *S*-nitrosothiol assay techniques.

Method	Principle	Detection limit	Selectivity	Advantage	Caveats
Photolysis-chemiluminescence [115-118]	Photoexcitation induced homolytic cleavage.	pmol-range	Fe nitrosyls also detected	Sensitive	False positives may occur if the oil overheats. Highly sensitive and expensive instruments.
Reductive chemiluminescence (CuCl, cysteine) [95,119-121]	Selective reduction of S–NO.	pmol-range	SNO selective	Specific and sensitive	Nitrite observed at low pH.
Indirect assay via nitrite quantification-KI chemiluminescence [117,121,122]	Conversion of thiol bound NO to NO^+, detected as nitrite after reduction in KI/acid.	pmol-range	Detects nitrite	Simple	Modification of the samples is required, but alters the SNO bond to make NOI. Iodide methods should not be used as stand-alone assays.
Saville (colorimetric) [100,123]	As above, but SNO generated NO^+ detected *via* Griess reagent.	500 nM	SNO selection	Simple, inexpensive	Insensitive
DAF-based fluorescence [120,124,125]	Conversion of DAF to fluorescent DAF-2T by NO^+.	Low nM	Variable	High-throughput capability	SNO quantified as gain of signal in paired samples +/- $HgCl_2$.
Mass spectrometry [126-132]	Selective monitoring of appropriate *m/z*.	Instrument specific ~200 nM solutions	Gold standard	Gold standard	LC separation phase must be designed to limit loss or gain of S–NO bonds. Requires internal standards labeled with ^{15}N. Alternatively, thiol-bound groups may be switched.

1.1.1.4 Tissue engineering

An approach to mitigate adverse reactions at the material interface is through the use of nitric oxide (NO) as a therapeutic agent.[133] NO has been extensively studied due to its role in physiological processes such as inhibition of platelet activation and broad-spectrum antibacterial activity, among others. In order to harness the benefits of NO, the molecule can be conjugated into polymeric substrates that release NO at a localized site. Previous research has shown that

NO has the ability to mitigate the foreign body response and prevent device fouling by simulating the natural NO release from the endothelium. It was demonstrated that NO is directly synthesized from the amino acid L-arginine by a family of NO synthase enzymes, which proved that the endogenous process occurs as a response mechanism to different stimuli in the cellular environment.[11]

The foreign body response (FBR) is a cascade of events where fibrous encapsulation is triggered by the presence of an external component and can lead to post-operatory interventions or additional surgical procedures to remove the implanted material.[134] When biological tissue is exposed to biomaterials, a response is triggered in a step-wise manner where inflammation is followed by wound healing and eventually scar formation or fibrous encapsulation.[135] The FBR is initiated by the absorption of plasma proteins on the surface of the foreign body, which causes the recruitment and activation of macrophages. Once activated, they form giant cells and generate functional vessels followed by fibrotic encapsulation of the implanted object. The FBR can be prevented by NO given its ability to inhibit platelet adhesion and activation.[136]

Implantable polymeric materials with antibacterial activity have been developed in an attempt to reduce the occurrence of infection on devices.[137] The relevant physiological activity of NO have led to the investigation and development of NO-releasing materials that deliver NO at biological interfaces. One route for the preparation of such materials is the incorporation of NO donor groups such as NONOates or RSNOs into polymeric systems to produce materials that release NO under physiological pH and temperature as a result of the NO donor decomposition.[138] As stated previously, RSNOs are preferred over NONOates given that the latter may produce carcinogenic *N*-nitrosamines as a byproduct of NO release under oxygenated conditions.[139,140]

Therapeutic NO release may lead to enhanced curative effects in materials such as polysaccharides,[141] polyurethanes,[142] and biodegradable polyesters.[143] Recently, biodegradable polyesters have been investigated for their potential biomedical applications. When used as tissue engineering materials, a three-dimensional polymer scaffold is implanted to support and orient cell growth toward the generation of new tissue.[144,145] However, issues may arise after implantation due to bacterial infection or the foreign body response. Thus, incorporation of NO-release functionality to polymeric systems may enhance their performance, given that NO can prevent such adverse reactions.

Mechanical stimulation is essential in the formation of elastic soft tissue such as blood vessels, cartilage and smooth muscle. Studies have shown that scaffolds with applied cyclic mechanical strains increase collagen and elastin production in vascular smooth muscle cells.[146] Thus, tissue-engineered constructs should resemble the physical properties of native tissue in order to withstand the mechanical demands asserted upon them after implantation, and be able to recover from deformations without causing irritation. Polymer matrices used as implants and wound dressings include biodegradable polyesters approved by the Food and Drug Administration (FDA) such as poly($_L$-lactide) (PLLA), poly(glycolide) (PGA), and poly(lactic-*co*-glycolic acid) (PLGA).[147] However, these systems are stiff and do not meet the criteria required for soft tissue-engineering, which could cause inflammation and scar tissue formation, ultimately leading to other complications.[148] One limitation of implantable polymers has been the foreign body response, which, as stated *supra*, results in fibrous encapsulation of implanted material that may result in implant failure. Therefore, the development of a biodegradable polymeric system with nitric oxide (NO)-release and lack of cytotoxicity would be a major contribution in the area of tissue engineering.[149]

In addition, NO has anti-infective effects on bacterial colonies, which are often the cause of infection on implantable devices or external wounds. Biofilms are highly organized bacterial environments that protect bacteria from the patient's immune response and antibiotic therapy. Therefore, the preparation of antimicrobial polymeric surfaces that can combat biofilm formation are needed to reduce the vast number of patients with infections.[150] Previous studies have demonstrated the use of NO-releasing materials to combat biofilm formation caused by bacterial strains such as *Escherichia coli* (*E.coli*) and *Staphylococcus aureus* (*S. aureus*). These bacterial strains are commonly found on implantable devices or infected wounds.[151] Studies have demonstrated the use of NO as an antimicrobial agent that is able to mitigate the foreign body response. The combination of NO release and similar Young's modulus as certain soft biological tissue, present an alternative platform for the preparation of medical devices.

1.1.2 Biosensors

Biosensors belong to a group of polymers that are currently in a field that is rapidly expanding due to the need for materials that can elicit a response when exposed to an external stimulus. Biosensors are of particular interest when the response can be qualitatively confirmed by a noticeable color change. In some cases, the color change can be attributed to variations in the surroundings that disrupt hydrogen bonding within the end groups of the polymer chains. Chromophores are relevant additives for polymers because they can undergo a color transformation triggered by an external stimulus. Such stimuli include live bacteria, pH changes, or temperature changes. Polydiacetylenes (PDAs) are a type of polymer that can undergo a color shift to the red phase when exposed to living organisms, pH or temperature changes and are thus categorized as a bio-, chemo-, and thermosensors.

The first PDA-containing materials were prepared by Wegner in 1969.[152] However, it was not until 1993 when Charych *et al*. explored their use as biosensors.[153] A (PDA) matrix monolayer was incubated with biomolecules such as the influenza virus, which cause the monolayer to undergo a color change from blue to red. Since then, researchers have tested the chromatic properties of these materials to develop new types of sensors. PDAs have been combined with various matrix polymers to analyze the colorimetric response in different environments.[154] The importance of the detection of pH or temperature changes arises from the ability to visually evaluate the conditions of certain systems and make the necessary adjustments to maintain those conditions. The applications for these materials include systems that can detect chemical and thermal changes, or for the preparation of bandages to detect live bacteria on wounds. Once the infection has been confirmed, the wound could be treated with broad-spectrum antibacterial agents that can eradicate living organisms, such as nitric oxide.

1.2 Dissertation overview

The studies presented herein demonstrate how the use of various material platforms and key reagents give rise to specific material characteristics and various end applications. Through the use of NO or polydiacetylenes, specific function was imparted uniquely to each material. In the case of NO, the materials were used for cytotoxicity assays and to confirm broad spectrum antibacterial efficacies. Polydiacetylenes were used to elicit a color changing mechanism that is caused by various stimuli, such as the metabolites of bacteria, heat, or pH changes.

Chapter 2. The research presented in this chapter addresses cytotoxicity issues related to the release of NO by *S*-nitrosothiols. Synthetic polyesters were prepared *via* bulk polycondensation through a step-growth mechanism. The materials were isolated and purified in

order to incorporate amines with thiol pendant groups that could provide a site for the formation of RSNOs by the reaction of *tert*-butyl nitrite and ethanol. The materials were characterized using chemiluminescence-based detection to confirm nitric oxide release for 4 to 6 days at physiological pH and temperature. In addition, the material composition and atom connectivity was studied through instrumental techniques for polymeric materials. Degradation studies performed by gravimetric analysis during the course of 4 weeks established hydrolytic degradation and suggested that the stability of the materials increases as nitric oxide is released due to the formation of disulfide linkages resulting as byproducts of nitric oxide release. Excitingly, cytotoxicity studies using human dermal fibroblasts demonstrated that toxic leachates were not observed at the limit of detection. Although nitric oxide release was optimal for short term antibacterial applications, the mechanical properties confirmed by thermal transitions, suggested that the viscoelastic properties were not ideal for the applications intended, such as wound dressings. The preparation of material platforms with sustained nitric oxide release gave rise polyesters with different nitric oxide release profiles that were dependent on the structure of the thiol moiety.

Chapter 3. The third chapter summarizes the synthesis of nitric oxide-releasing materials with mechanical properties that mimic the tensile strength of the meniscus, while maintaining a uniform molecular weight, glass transition temperature (T_g) and NO release properties. For this study, three different polyesters were prepared with similar monomeric units as those used for the second chapter, for cytotoxicity reasons. After the polymers were synthesized, they were purified and casted on PTFE molds to yield crosslinked polyesters with elastomeric properties. Nitric oxide release was also achieved from these materials, however, the release occurred during a shorter timeframe (20 h) given that the thiols pendant groups may have been

compromised by treatment with heat to achieve crosslinked polymers. Hence, the mechanical properties and nitric oxide release were found to be inversely proportional. The degradation profiles were analyzed at physiological conditions for 10 weeks confirming hydrolytic degradation for all samples and the difference of degradation profiles within each polymer, since some materials were minimally degraded. Degradation product analysis was performed using mass spectrometric techniques in order to assess understand their composition. Mechanical properties were studied by tensile mechanical tests suggesting that the young's modulus and crosslinking densities for the dehydrated materials were similar to that of soft biological tissue. Furthermore, the antibacterial activity of the *S*-nitrosated polyesters was tested against *Escherichia coli* and *Staphylococcus aureus*. A log-8 reduction of bacterial colonies was confirmed by the method of colony forming units, this result established broad-spectrum antibacterial activity given that the bacterial strains used were Gram negative and Gram positive. The industry standard for antibacterial agents is log-3, which means that the materials prepared herein and the methods employed gave rise to efficacious antibacterial agents that exceed those currently available to patients.

Chapter 4. Inspired by the antibacterial properties of the polyesters described in the third chapter and the lack of measurable toxic leachates of polymers in chapter 2, I aimed to prepare an emulsion with nitric oxide release. Previous reports have demonstrated the possibility of achieving nitric oxide release from viscous materials. However, the chemical composition was mostly polymer based and lacked components that were initially intended for topical uses. The emulsion prepared herein incorporates ingredients that act as humectants, as well as allowing dermal tissue to retain its moisture by using hyaluronic acid, and provide the benefits of vitamin E. The purpose of the emulsion was to increase cell proliferation on damaged dermal tissue.

Due to the concentration-dependent activity of NO, theoretically, the emulsion could be used to promote cell proliferation without causing local cytotoxicity. In addition, nitric oxide release was quantified for up to 52 h at physiological conditions. The pH of the emulsion was monitored over the course of 8 weeks to assess the shelf life of the formulation. Viscosity and density measurements were performed given that the emulsion should be able to be applied with minimal external force to avoid further damage to the skin. I found that an emulsion with vitamin E and hyaluronic acid can achieve sustained NO release.

Chapter 5. Lastly, a different concept was studied: the use of biosensors using polymer matrices. Polydiacetylene materials were prepared by the formation of nanofibers using an electrospinning apparatus. In addition, polydiacetylene vesicles were formed to assess the chromatic properties of such conjugated moieties in the absence of a supporting polymer. The colorimetric response of the materials was studied in terms of fiber morphology, diameter, bacteria presence and pH variations. It was found that the colorimetric response was independent of the polymer matrix used, such as polyethylene oxide and polyurethane. As expected, the materials were found to express chromatic changes from blue to red in the presence of *Escherichia coli* and at basic pH values. Based on my findings, I hypothesize that the metabolites of live bacteria that are secreted onto the agar have the capability of inducing a chromatic response.

Chapter 6. The concepts presented in the last chapter propose a study with the use of siloxane-based materials with potential applications in tissue engineering. The chapter encompasses some experimental techniques and methods utilized for the projects stated *supra.* A material that could be used for soft tissue regeneration would, most likely, require oxygen permeability and appropriate mechanical properties in order to remain in a contained site and

tolerate the mechanical load on certain tissue. As an example, a material that could mimic the activity of a meniscus would allow the surrounding tissue to regenerate. Nitric oxide would be a molecule of interest given that NO can mitigate the foreign body response, allowing the implant to serve its function without causing issues at the material interface. Such limitations could be examined by performing cytotoxicity studies using endothelial cells, as well as allowing cells to seed on the polymer. A material that could be prepared using 3D printing would allow for the formation of scaffolds that would be highly detailed and personalized. Tensile tests would verify that the Young's modulus is skin to that of the surrounding tissue to avoid incompliances. Given that infection could threaten the performance of the scaffold, the material should have a rough surface to avoid bacterial colonization on the surface of the polymer. For such an implantable device, the degradation should be minimal, which should be analyzed by gravimetric analysis. The degradation products should be analyzed using mass spectrometry and additional cytotoxicity studies should be done using such byproducts.

REFERENCES

1. Kulkarni Vishakha, S.; Butte Kishor, D.; Rathod Sudha, S. *Int. J. Pharm. Biomed.* **2012**, *3*, 1579.
2. Ikada, Y. *Biomaterials* **1994**, *15*, 725.
3. Frommelt, H. In *Makromol. Chem., Macromol. Symp.*; Wiley Online Library: 1987; Vol. 12, p 281.
4. Lee, C. H.; Singla, A.; Lee, Y. *Int. J. Pharm.* **2001**, *221*, 1.
5. Buttafoco, L.; Kolkman, N.; Engbers-Buijtenhuijs, P.; Poot, A. A.; Dijkstra, P. J.; Vermes, I.; Feijen, J. *Biomaterials* **2006**, *27*, 724.
6. Kundu, B.; Rajkhowa, R.; Kundu, S. C.; Wang, X. *Adv. Drug Deliv. Rev.* **2013**, *65*, 457.
7. Suh, J.-K. F.; Matthew, H. W. *Biomaterials* **2000**, *21*, 2589.
8. Luo, Y.; Kirker, K. R.; Prestwich, G. D. *J. Control. Release* **2000**, *69*, 169.
9. Chen, G.-Q.; Wu, Q. *Biomaterials* **2005**, *26*, 6565.
10. Freier, T.; Kunze, C.; Nischan, C.; Kramer, S.; Sternberg, K.; Saß, M.; Hopt, U. T.; Schmitz, K.-P. *Biomaterials* **2002**, *23*, 2649.
11. Seabra, A. *Nitric Oxide Donors: Novel Biomedical Applications and Perspectives*; Academic Press, 2017.
12. Hubbell, J. A. *Nat. Biotechnol.* **1995**, *13*, 565.
13. Nair, L. S.; Laurencin, C. T. *Prog. Polym. Sci.* **2007**, *32*, 762.
14. Carothers, W. H. *J. Am. Chem. Soc.* **1929**, *51*, 2548.
15. Carothers, W. H.; Arvin, J. *J. Am. Chem. Soc.* **1929**, *51*, 2560.
16. Carothers, W. H.; Natta, F. V. *J. Am. Chem. Soc.* **1930**, *52*, 314.

17. Pereira, C. S.; Pinho, S. P.; Silva, V. M.; Rodrigues, A. E. *Ind. Eng. Chem. Res.* **2008**, *47*, 1453.

18. Vert, M.; Li, S.; Garreau, H.; Mauduit, J.; Boustta, M.; Schwach, G.; Engel, R.; Coudane, J. *Angew. Makromol. Chem.* **1997**, *247*, 239.

19. Edlund, U.; Albertsson, A.-C. *Adv. Drug. Deliv. Rev.* **2003**, *55*, 585.

20. Tobita, H. *Polymer* **1995**, *36*, 2585.

21. Bhanushali, D.; Kloos, S.; Kurth, C.; Bhattacharyya, D. *J. Memb. Sci.* **2001**, *189*, 1.

22. Holloway, J. L.; Ma, H.; Rai, R.; Burdick, J. A. *J. Control. Release* **2014**, *191*, 63.

23. Middleton, J. C.; Tipton, A. J. *Biomaterials* **2000**, *21*, 2335.

24. Choi, J. U.; Lee, S. W.; Pangeni, R.; Byun, Y.; Yoon, I.-S.; Park, J. W. *Acta Biomater.* **2017**, *57*, 197.

25. Frykberg, R. G.; Gibbons, G. W.; Walters, J. L.; Wukich, D. K.; Milstein, F. C. *Int. Wound J.* **2017**, *14*, 569.

26. Saku, I.; Kanda, S.; Saito, T.; Fukushima, T.; Akiyama, T. *Int. J. Surg. Case Rep.* **2017**, *37*, 106.

27. Phillips, T. J.; Palko, M. J.; Bhawan, J. *J. Am. Acad. Dermatol.* **1994**, *30*, 61.

28. Davies, P.; McCarty, S.; Hamberg, K. *J. Wound Care.* **2017**, *26*, S1.

29. Dhand, C.; Venkatesh, M.; Barathi, V. A.; Harini, S.; Bairagi, S.; Goh Tze Leng, E.; Muruganandham, N.; Low, K. Z. W.; Fazil, M. H. U. T.; Loh, X. J.; Srinivasan, D. K.; Liu, S. P.; Beuerman, R. W.; Verma, N. K.; Ramakrishna, S.; Lakshminarayanan, R. *Biomaterials* **2017**, *138*, 153.

30. Furchgott, R. F.; Zawadzki, J. V. *Nature* **1980**, *288*, 373.

31. Ignarro, L. J. *Angew. Chem. Int. Ed.* **1999**, *38*, 1882.

32. Ignarro, L. J.; Buga, G. M.; Wood, K. S.; Byrns, R. E.; Chaudhuri, G. *Proc. Natl. Acad. Sci. U.S.A.* **1987**, *84*, 9265.

33. Arnold, W. P.; Mittal, C. K.; Katsuki, S.; Murad, F. *Proc. Natl. Acad. Sci. U.S.A.* **1977**, *74*, 3203.

34. Riccio, D. A.; Schoenfisch, M. H. *Chem. Soc. Rev.* **2012**, *41*, 3731.

35. Ferrige, A.; Moncada, S. *Nature* **1987**, *327*, 524.

36. Vanin, A.; Vedernikov, Y.; Galagan, M.; Kubrina, L.; Kuzmanis, Y.; Kalvinsh, I.; Mordvintsev, P. *Biokhimiya (Moscow)* **1990**, *55*, 1048.

37. Maragos, C. M.; Morley, D.; Wink, D. A.; Dunams, T. M.; Saavedra, J. E.; Hoffman, A.; Bove, A. A.; Isaac, L.; Hrabie, J. A.; Keefer, L. K. *J. Med. Chem.* **1991**, *34*, 3242.

38. Morley, D.; Maragos, C. M.; Zhang, X.-Y.; Boignon, M.; Wink, D. A.; Keefer, L. K. *J. Cardiovasc. Pharmacol.* **1993**, *21*, 670.

39. Diodati, J. G.; Quyyumi, A. A.; Keefer, L. K. *J. Cardiovasc. Pharmacol.* **1993**, *22*, 287.

40. Walford, G.; Loscalzo, J. *J. Thromb. Haemost.* **2003**, *1*, 2112.

41. Marletta, M. A.; Yoon, P. S.; Iyengar, R.; Leaf, C. D.; Wishnok, J. S. *Biochemistry* **1988**, *27*, 8706.

42. Hibbs Jr, J. B.; Taintor, R. R.; Vavrin, Z.; Rachlin, E. M. *Biochem. Biophys. Res. Commun.* **1988**, *157*, 87.

43. Fang, F. C. *J. Clin. Investig.* **1997**, *99*, 2818.

44. Garthwaite, J.; Charles, S. L.; Chess-Williams, R. *Nature* **1988**, *336*, 385.

45. Moncada, S.; Palmer, R. M.; Higgs, E. A. *Biochem. Pharmacol.* **1989**, *38*, 1709.

46. Diodati, J.; Quyyumi, A.; Hussain, N.; Keefer, L. *Thromb. Haemost.* **1993**, *70*, 654.

47. Hanson, S.; Hutsell, T.; Keefer, L.; Mooradian, D.; Smith, D. *Adv. Pharmacol.* **1995**, *34*, 383.

48. Luo, J.-D.; Chen, A. F. *Acta Pharmacol. Sin.* **2005**, *26*, 259.

49. Mocellin, S.; Bronte, V.; Nitti, D. *Med. Res. Rev.* **2007**, *27*, 317.

50. Schulz, R.; Rassaf, T.; Massion, P.; Kelm, M.; Balligand, J.-L. *Pharmacol. Ther.* **2005**, *108*, 225.

51. Liu, V. W.; Huang, P. L. *Cardiovasc. Res.* **2008**, *77*, 19.

52. Tiso, M.; Schechter, A. N. *PLoS ONE* **2015**, *10*, e0119712.

53. Radomski, M. W.; Palmer, R. M. J.; Moncada, S. *Biochem. Biophys. Res. Commun.* **1987**, *148*, 1482.

54. Moncada, S.; Higgs, E.; Hodson, H.; Knowles, R.; Lopez-Jaramillo, P.; McCall, T.; Palmer, R.; Radomski, M.; Rees, D.; Schulz, R. *J. Cardiovasc. Pharmacol.* **1991**, *17*, S1.

55. Marletta, M.; Tayeh, M.; Hevel, J. *Biofactors* **1990**, *2*, 219.

56. Furchgott, R. F. *Biosci. Rep.* **1999**, *19*, 235.

57. Gries, A.; Bode, C.; Peter, K.; Herr, A.; Böhrer, H.; Motsch, J.; Martin, E. *Circulation* **1998**, *97*, 1481.

58. Fleming, I.; Busse, R. In *Adv. Pharmacol.*; Elsevier: 1995; Vol. 34, p 187.

59. Vaughn, M. W.; Kuo, L.; Liao, J. C. *Am. J. Physiol. Heart Circ. Physiol.* **1998**, *274*, H2163.

60. Thomas, D. D.; Ridnour, L. A.; Isenberg, J. S.; Flores-Santana, W.; Switzer, C. H.; Donzelli, S.; Hussain, P.; Vecoli, C.; Paolocci, N.; Ambs, S.; Colton, C. A.; Harris, C. C.; Roberts, D. D.; Wink, D. A. *Free Radic. Biol. Med.* **2008**, *45*, 18.

61. Archer, S. L.; Huang, J.; Hampl, V.; Nelson, D. P.; Shultz, P. J.; Weir, E. K. *Proc. Natl. Acad. Sci. U.S.A.* **1994**, *91*, 7583.

62. Ghaffari, A.; Miller, C.; McMullin, B.; Ghahary, A. *Nitric oxide* **2006**, *14*, 21.

63. Hetrick, E. M.; Schoenfisch, M. H. *Biomaterials* **2007**, *28*, 1948.

64. Witte, M. B.; Barbul, A. *Am. J. Surg.* **2002**, *183*, 406.

65. Hetrick, E. M.; Schoenfisch, M. H. *Annu. Rev. Anal. Chem.* **2009**, *2*, 409.

66. Hrabie, J. A.; Saavedra, J. E.; Roller, P. P.; Southan, G. J.; Keefer, L. K. *Bioconjug. Chem.* **1999**, *10*, 838.

67. Polizzi, M. A.; Stasko, N. A.; Schoenfisch, M. H. *Langmuir* **2007**, *23*, 4938.

68. Shin, J. H.; Metzger, S. K.; Schoenfisch, M. H. *J. Am. Chem. Soc.* **2007**, *129*, 4612.

69. Zhou, Z.; Meyerhoff, M. E. *Biomacromolecules* **2005**, *6*, 780.

70. Damodaran, V. B.; Place, L. W.; Kipper, M. J.; Reynolds, M. M. *J. Mater. Chem.* **2012**, *22*, 23038.

71. Damodaran, V. B.; Reynolds, M. M. *Journal of Materials Chemistry* **2011**, *21*, 5870.

72. Lutzke, A.; Pegalajar-Jurado, A.; Neufeld, B. H.; Reynolds, M. M. *Journal of Materials Chemistry B* **2014**, *2*, 7449.

73. Yapor, J. P.; Lutzke, A.; Pegalajar-Jurado, A.; Neufeld, B. H.; Damodaran, V. B.; Reynolds, M. M. *J. Mater. Chem. B* **2015**, *3*, 9233.

74. Yapor, J. P.; Neufeld, B. H.; Tapia, J. B.; Reynolds, M. M. *J. Mater. Chem. B.* **2018**.

75. Carpenter, A. W.; Schoenfisch, M. H. *Chem. Soc. Rev.* **2012**, *41*, 3742.

76. Coneski, P. N.; Schoenfisch, M. H. *Chem. Soc. Rev.* **2012**, *41*, 3753.

77. Wang, P. G.; Xian, M.; Tang, X.; Wu, X.; Wen, Z.; Cai, T.; Janczuk, A. J. *Chem. Rev.* **2002**, *102*, 1091.

78. Drago, R. S.; Karstetter, B. R. *J. Am. Chem. Soc.* **1961**, *83*, 1819.

79. Ragsdale, R. O.; Karstetter, B. R.; Drago, R. S. *Inorg. Chem.* **1965**, *4*, 420.

80. Askew, S. C.; Butler, A. R.; Flitney, F. W.; Kemp, G. D.; Megson, I. L. *Bioorganic Med. Chem.* **1995**, *3*, 1.

81. Clancy, R. M.; Levartovsky, D.; Leszczynska-Piziak, J.; Yegudin, J.; Abramson, S. B. *Proc. Natl. Acad. Sci. U.S.A.* **1994**, *91*, 3680.

82. Mathews, W. R.; Kerr, S. W. *J. Pharmacol. Exp. Ther.* **1993**, *267*, 1529.

83. Gabor, G.; Allon, N.; Weetall, H. *Microchem. J.* **1997**, *56*, 177.

84. Kaye, D. M.; Wiviott, S. D.; Kobzik, L.; Kelly, R. A.; Smith, T. W. *Am. J. Physiol. Heart Circ. Physiol.* **1997**, *272*, H875.

85. Hogg, N. *Free Radic. Biol. Med.* **2000**, *28*, 1478.

86. Szaciłowski, K.; Stasicka, Z. *Prog. React. Kinet. Mec.* **2001**, *26*, 1.

87. Stamler, J. S.; Simon, D. I.; Osborne, J. A.; Mullins, M. E.; Jaraki, O.; Michel, T.; Singel, D. J.; Loscalzo, J. *Proc. Natl. Acad. Sci. U.S.A.* **1992**, *89*, 444.

88. Wink, D. A.; Nims, R. W.; Darbyshire, J. F.; Christodoulou, D.; Hanbauer, I.; Cox, G. W.; Laval, F.; Laval, J.; Cook, J. A. *Chem. Res. Toxicol.* **1994**, *7*, 519.

89. Jocelyn, P. C. *Biochemistry of the SH Group*; Academic Press: London & New York, 1972.

90. de Oliveira, M. G.; Shishido, S. M.; Seabra, A. B.; Morgon, N. H. *J. Phys. Chem. A* **2002**, *106*, 8963.

91. Liu, Z.; Rudd, M. A.; Freedman, J. E.; Loscalzo, J. *J. Pharmacol. Exp. Ther.* **1998**, *284*, 526.

92. Park, J.; Billman, G.; Means, G. *Biochem. Mol. Biol. Int.* **1993**, *30*, 885.

93. Stamler, J. S.; Toone, E. J.; Lipton, S. A.; Sucher, N. J. *Neuron* **1997**, *18*, 691.

94. Zhang, H.; Xu, Y.; Joseph, J.; Kalyanaraman, B. *J. Biol. Chem.* **2005**, *280*, 40684.

95. Mannick, J. B.; Schonhoff, C.; Papeta, N.; Ghafourifar, P.; Szibor, M.; Fang, K.; Gaston, B. *J. Cell Biol.* **2001**, *154*, 1111.

96. Gaston, B. M.; Carver, J.; Doctor, A.; Palmer, L. A. *Mol. Interv.* **2003**, *3*, 253.

97. Kim, S. F.; Huri, D. A.; Snyder, S. H. *Science* **2005**, *310*, 1966.

98. Hess, D. T.; Matsumoto, A.; Kim, S.-O.; Marshall, H. E.; Stamler, J. S. *Nat. Rev. Mol. Cell Biol.* **2005**, *6*, 150.

99. Gaston, B.; Singel, D.; Doctor, A.; Stamler, J. S. *Am. J. Respir. Crit. Care Med.* **2006**, *173*, 1186.

100. Arnelle, D. R.; Stamler, J. S. *Arch. Biochem. Biophys.* **1995**, *318*, 279.

101. Gow, A.; Doctor, A.; Mannick, J.; Gaston, B. *J. Chromatogr. B* **2007**, *851*, 140.

102. Singh, R. J.; Hogg, N.; Joseph, J.; Kalyanaraman, B. *FEBS Lett.* **1995**, *360*, 47.

103. Sexton, D. J.; Muruganandam, A.; McKenney, D. J.; Mutus, B. *Photochem. Photobiol.* **1994**, *59*, 463.

104. Lyn H áWilliams, D. *J. Chem. Soc. Chem. Commun.* **1993**, 1758.

105. Singh, R. J.; Hogg, N.; Joseph, J.; Kalyanaraman, B. *J. Biol. Chem.* **1996**, *271*, 18596.

106. Josephy, P. D.; Rehorek, D.; Janzen, E. G. *Tetrahedron Lett.* **1984**, *25*, 1685.

107. Williams, D. L. H. *Acc. Chem. Res.* **1999**, *32*, 869.

108. DeMaster, E. G.; Quast, B. J.; Redfern, B.; Nagasawa, H. T. *Biochemistry* **1995**, *34*, 11494.

109. Pryor, W. A.; Church, D. F.; Govindan, C.; Crank, G. *J. Org. Chem.* **1982**, *47*, 156.

110. Hogg, N.; Darley-Usmar, V.; Wilson, M.; Moncada, S. *Biochem. J.* **1992**, *281*, 419.

111. Donald, C. E.; Hughes, M. N.; Thompson, J. M.; Bonner, F. T. *Inorganic Chemistry* **1986**, *25*, 2676.

112. Barnett, D. J.; Rios, A.; Williams, D. L. H. *J. Chem. Soc., Perkin Trans. 2* **1995**, *0*, 1279.

113. Barnett, D. J.; McAninly, J.; Williams, D. L. H. *J. Chem. Soc., Perkin Trans. 2* **1994**, 1131.

114. Roy, B.; du Moulinet d'Hardemare, A.; Fontecave, M. *J. Org. Chem.* **1994**, *59*, 7019.

115. Pawloski, J. R.; Hess, D. T.; Stamler, J. S. *Nature* **2001**, *409*, 622.

116. Gow, A. J.; Stamler, J. S. *Nature* **1998**, *391*, 169.

117. Hausladen, A.; Rafikov, R.; Angelo, M.; Singel, D. J.; Nudler, E.; Stamler, J. S. *Proc. Natl. Acad. Sci. U.S.A.* **2007**, *104*, 2157.

118. Mannick, J. B.; Hausladen, A.; Liu, L.; Hess, D. T.; Zeng, M.; Miao, Q. X.; Kane, L. S.; Gow, A. J.; Stamler, J. S. *Science* **1999**, *284*, 651.

119. Doctor, A.; Gaston, B. *Blood* **2006**, *108*, 3225.

120. Doctor, A.; Platt, R.; Sheram, M. L.; Eischeid, A.; McMahon, T.; Maxey, T.; Doherty, J.; Axelrod, M.; Kline, J.; Gurka, M. *Proc. Natl. Acad. Sci. U.S.A.* **2005**, *102*, 5709.

121. Fang, K.; Ragsdale, N. V.; Carey, R. M.; MacDonald, T.; Gaston, B. *Biochem. Biophys. Res. Commun.* **1998**, *252*, 535.

122. Gladwin, M. T.; Schechter, A. N.; Shelhamer, J. H.; Pannell, L. K.; Conway, D. A.; Hrinczenko, B. W.; Nichols, J. S.; Pease-Fye, M. E.; Noguchi, C. T.; Rodgers, G. P. *J. Clin. Investig.* **1999**, *104*, 937.

123. Gaston, B.; Reilly, J.; Drazen, J. M.; Fackler, J.; Ramdev, P.; Arnelle, D.; Mullins, M. E.; Sugarbaker, D. J.; Chee, C.; Singel, D. J. *Proc. Natl. Acad. Sci. U.S.A.* **1993**, *90*, 10957.

124. McMahon, T. J.; Moon, R. E.; Luschinger, B. P.; Carraway, M. S.; Stone, A. E.; Stolp, B. W.; Gow, A. J.; Pawloski, J. R.; Watke, P.; Singel, D. J. *Nat. Med.* **2002**, *8*, 711.

125. King, M.; Gildemeister, O.; Gaston, B.; Mannick, J. B. *Anal. Biochem.* **2005**, *346*, 69.

126. Tsikas, D.; Sandmann, J.; Gutzki, F.-M.; Stichtenoth, D. O.; Frölich, J. C. *J. Chromatogr. B Biomed. Sci. Appl.* **1999**, *726*, 13.

127. Tsikas, D.; Raida, M.; Sandmann, J.; Rossa, S.; Forssmann, W.-G.; Frölich, J. C. *J. Chromatogr. B Biomed. Sci. Appl.* **2000**, *742*, 99.

128. Lipton, A. J.; Johnson, M. A.; Macdonald, T.; Lieberman, M. W.; Gozal, D.; Gaston, B. *Nature* **2001**, *413*, 171.

129. Tsikas, D.; Sandmann, J.; Frölich, J. C. *J. Chromatogr. B* **2002**, *772*, 335.

130. Tsikas, D.; Sandmann, J.; Rossa, S.; Gutzki, F.-M.; Frölich, J. C. *Anal. Biochem.* **1999**, *272*, 117.

131. Jaffrey, S. R.; Erdjument-Bromage, H.; Ferris, C. D.; Tempst, P.; Snyder, S. H. *Nat. Cell. Biol.* **2001**, *3*, 193.

132. Hao, G.; Derakhshan, B.; Shi, L.; Campagne, F.; Gross, S. S. *Proc. Natl. Acad. Sci. U.S.A.* **2006**, *103*, 1012.

133. Moncada, S.; Higgs, E. *Eur. J. Clin. Invest.* **1991**, *21*, 361.

134. Anderson, J. M. In *Biomaterials Science: An Introduction to Materials: Third Edition*; Elsevier Inc.: 2013.

135. Dondossola, E.; Holzapfel, B. M.; Alexander, S.; Filippini, S.; Hutmacher, D. W.; Friedl, P. *Nat. Biomed. Eng.* **2017**, *1*, 0007.

136. Hetrick, E. M.; Prichard, H. L.; Klitzman, B.; Schoenfisch, M. H. *Biomaterials* **2007**, *28*, 4571.

137. Donlan, R. M. *Emerg. Infect. Dis.* **2001**, *7*, 277.

138. Lutzke, A.; Pegalajar-Jurado, A.; Neufeld, B. H.; Reynolds, M. M. *J. Mater. Chem. B* **2014**, *2*, 7449.

139. Singh, R. J.; Hogg, N.; Joseph, J.; Kalyanaraman, B. *J. Biol. Chem.* **1996**, *271*, 18596.

140. Schmähl, D.; Habs, M. *Oncology* **1980**, *37*, 237.

141. Lu, Y.; Slomberg, D. L.; Schoenfisch, M. H. *Biomaterials* **2014**, *35*, 1716.

142. Koh, A.; Lu, Y.; Schoenfisch, M. H. *Anal. Chem.* **2013**, *85*, 10488.

143. Coneski, P. N.; Rao, K. S.; Schoenfisch, M. H. *Biomacromolecules* **2010**, *11*, 3208.

144. Amsden, B. *Soft Matter* **2007**, *3*, 1335.

145. Niklason, L.; Gao, J.; Abbott, W.; Hirschi, K.; Houser, S.; Marini, R.; Langer, R. *Science* **1999**, *284*, 489.

146. Waldman, S. D.; Spiteri, C. G.; Grynpas, M. D.; Pilliar, R. M.; Kandel, R. A. *J. Tissue Eng.* **2004**, *10*, 1323.

147. Makadia, H. K.; Siegel, S. J. *Polymers* **2011**, *3*, 1377.

148. Carrier, R. L.; Papadaki, M.; Rupnick, M.; Schoen, F. J.; Bursac, N.; Langer, R.; Freed, L. E.; Vunjak-Novakovic, G. *Biotechnol. Bioeng.* **1999**, *64*, 580.

149. Vroman, I.; Tighzert, L. *Materials* **2009**, *2*, 307.

150. Kuijer, R.; Jansen, E. J.; Emans, P. J.; Bulstra, S. K.; Riesle, J.; Pieper, J.; Grainger, D. W.; Busscher, H. J. *Biomaterials* **2007**, *28*, 5148.

151. Donlan, R. M. *Emerging Infect. Dis.* **2001**, *7*, 277.

152. Wegner, G. *Z. Naturforsch. B Chem. Sci.* **1969**, *24*, 824.

153. Charych, D. H.; Nagy, J. O.; Spevak, W.; Bednarski, M. D. *Science* **1993**, *261*, 585.

154. Chen, X.; Zhou, G.; Peng, X.; Yoon, J. *Chem. Soc. Rev.* **2012**, *41*, 4610.

CHAPTER 2

BIODEGRADABLE CITRATE-BASED POLYESTERS WITH *S*-NITROSOTHIOL FUNCTIONAL GROUPS FOR NITRIC OXIDE RELEASE

2.1 Synopsis

Nitric oxide (NO) is a biologically-active free radical involved in numerous physiological processes such as regulation of vasodilation, promotion of cell proliferation and angiogenesis, and modulation of the inflammatory and immune responses. Furthermore, NO has demonstrated the ability to mitigate the foreign body response that often results in the failure of implanted biomedical devices. Although NO has promising therapeutic value, the short physiological half-life of exogenous NO complicates its effective delivery. For this reason, the development of NO-releasing materials that permit the localized delivery of NO is an advantageous method of utilizing this molecule for biomedical applications. Herein, we report the synthesis and characterization of biodegradable NO-releasing polyesters prepared from citric acid, maleic acid, and 1,8-octanediol. NO release was achieved by incorporation of *S*-nitrosothiol donor groups through conjugation of cysteamine and ethyl cysteinate to the polyesters, followed by *S*-nitrosation with *tert*-butyl nitrite. The extent of NO loading and the release properties under physiological conditions (pH 7.4 PBS, 37 °C) were determined by chemiluminescence-based NO detection.

Reproduced from Yapor, J. P.; Lutzke, A.; Pegalajar-Jurado, A.; Neufeld, B. H.; Damodaran, V. B.; Reynolds, M. M. Biodegradable Citrate-Based Polyesters with *S*-nitrosothiol Functional Groups for Nitric Oxide Release. *J. Mater. Chem. B*. **2015**, *3*, 9233-9241 with permission from the Royal Society of Chemistry.

The average total NO content of poly(citric-*co*-maleic acid-*co*-1,8-octanediol)-cysteamine was determined to be 0.45 ± 0.07 mol NO g^{-1} polymer, while the NO content for poly(citric-*co*-maleic acid-*co*-1,8-octanediol)-ethyl cysteinate was 0.16 ± 0.04 mol NO g^{-1} polymer. Continuous NO release under physiological conditions was observed for at least 6 days for the cysteamine analog and 4 days for the ethyl cysteinate analog. Cell viability assays and morphological studies with human dermal fibroblasts indicated an absence of toxic leachates at a cytotoxic level and suggested that these citrate-based polyesters may be suitable for future biomedical applications. Figure 2.1 represents the main studies and conclusions of this project.

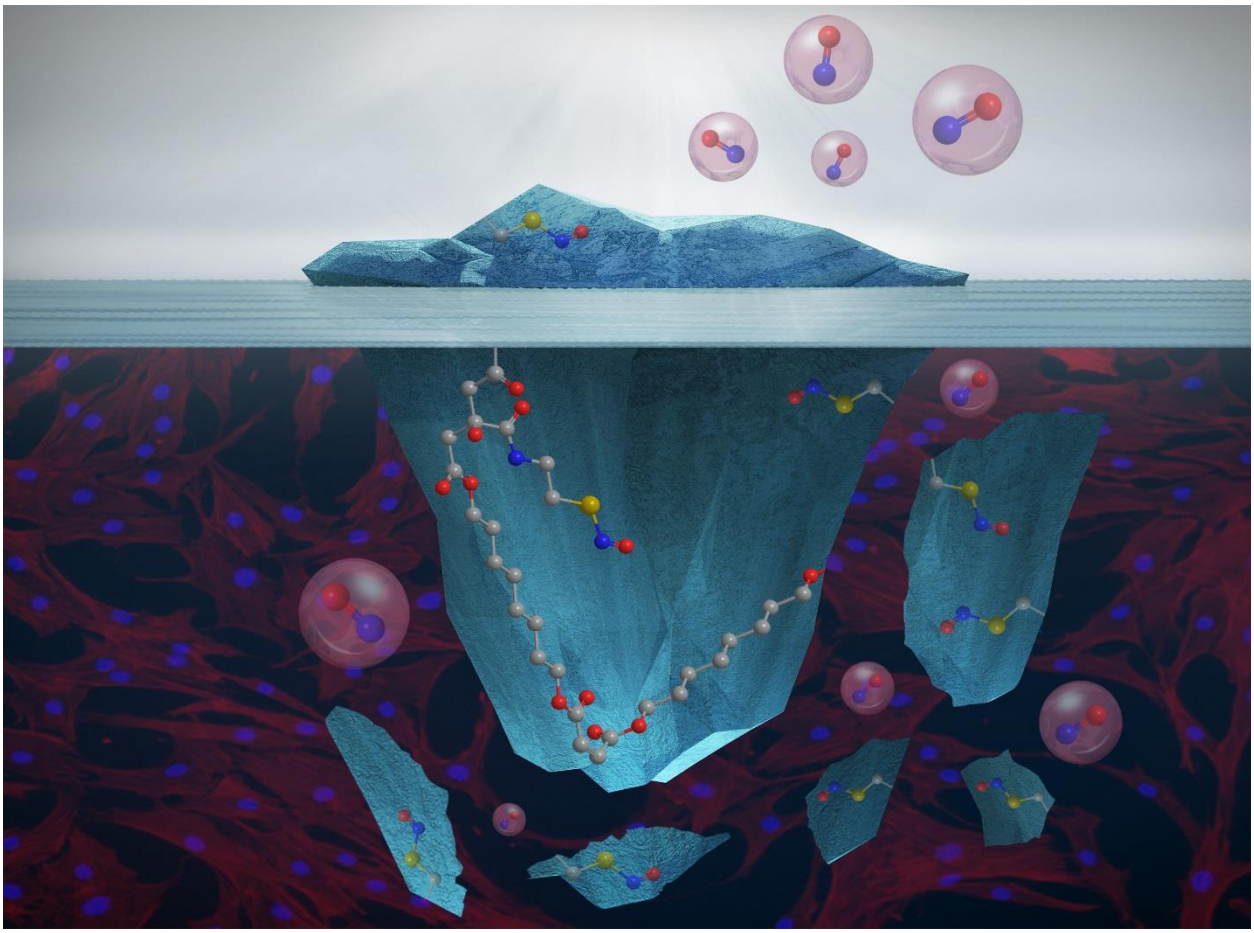

Figure 2.1 Selected artwork for the front cover of the publishing journal. The image summarizes the main results of the study. Reproduced with permission from the Royal Society of Chemistry.

2.2 Introduction

Current polymeric materials used for applications such as tissue engineering and the fabrication of biomedical devices are frequently exposed to adverse phenomena, including bacterial infections and the foreign body response.[1-3] These complications often require medical intervention and may ultimately result in the rejection and failure of biomedical implants.[4-6] In response to such harmful outcomes, consistent progress has been made toward the development of new polymeric materials for biomedical applications, and many recent efforts have focused on the incorporation of biomolecules or other therapeutic agents within polymer matrices to minimize adverse reactions. The combination of the bulk properties of the polymeric matrix with the controlled delivery of a therapeutic agent aims to enhance the overall material performance, and extend the lifetime of implantable devices.

Nitric oxide (NO) can be highlighted among the biomolecules that are the focus of study in the biomaterials community. The identification of NO in the late 1980s as a biologically-active molecule was an important development in the field of medicine.[7,8] Since then, it has been established that NO plays a crucial role in numerous biological processes such as cardiovascular homeostasis, immune response, neurotransmission, and inhibition of cancer cell growth.[9-12] From a biomaterials perspective, previous research has shown that NO has the ability to mitigate the foreign body response and reduce device fouling by simulating the natural NO release from the endothelium.[13] However, the relatively short biological half-life of NO under physiological conditions (0.09 to >2 s in extravascular tissue) has limited the use of exogenous NO as a method of addressing implant failure.[14] Therefore, one strategy to improve the performance of biomaterials has been the development of polymers that contain NO-releasing functional groups that serve as an NO source with greater stability.

Two broad categories of NO-releasing functional groups are *N*-diazeniumdiolates and *S*-nitrosothiols (RSNOs), which are coupled to polymeric substrates to afford materials that release NO under physiological conditions (pH 7.4, 37 °C).[15] Such materials permit the release of therapeutic NO directly at biological interfaces, and may lead to enhanced performance in polysaccharides, polyurethanes, and biodegradable polyesters.[16-20] Polyesters have been investigated as platforms for the development of NO-releasing materials due to the well-established biocompatibility and biodegradability of polyesters such as poly(lactic-*co*-glycolic acid) (PLGA), among others, and their common use in the development of degradable biomedical implants.[21] Coneski *et al.* have reported the synthesis of NO-releasing polyesters from glycerol or pentaerythritol and diacids.[22] NO release was achieved by the conjugation of thiols such as cysteamine and penicillamine to the polymers, followed by the formation of RSNO functional groups by reaction with sodium nitrite under acidic conditions. NO release was continuous for as many as 6 days, and it was demonstrated that this release reduced bacterial adhesion (*Pseudomonas aeruginosa*) by up to 80% compared with controls. The Ameer group has also reported the development of promising NO-releasing polyester systems based on low-toxicity citric acid and diols, where NO release was achieved by either blending the *N*-diazeniumdiolate derived from *N*,*N*-diethyldiethylenetriamine (DEDETA/NO) into the materials or by preparing a copolymer with *N*,*N*′-bis(2-hydroxyethyl)ethylenediamine that contained secondary amine groups, followed by subsequent *N*-diazeniumdiolation.[23,24] However, the NO release from *N*-diazeniumdiolates under oxygenated conditions is known to produce nitrosating species such as N_2O_3, that subsequently react with secondary amines to form carcinogenic secondary *N*-nitrosamines, which may pose a considerable health risk.[25-29]

Herein, we present an alternative approach to the synthesis of citrate-based NO-releasing polyesters that is intended to avoid any potential complications associated with secondary *N*-nitrosamine formation. Our work focuses on the development of biodegradable NO-releasing polyesters from citrate-based poly(citric-*co*-maleic acid-*co*-1,8-octanediol) (PCMO). Due to the inherently low toxicity of citric acid, polyesters that incorporate citric acid as a component of their structure have been investigated for a variety of biomedical uses including cardiac tissue engineering, drug delivery, and bio-imaging.[30-32] Furthermore, the inclusion of maleic acid provides a site for further chemical modification of the polymers. To avoid the use of *N*-diazeniumdiolates, we achieved NO release through covalent incorporation of the bioavailable thiols cysteamine and cysteine (as the ethyl ester), followed by *S*-nitrosation to yield the corresponding RSNOs.[33,34] Unlike *N*-diazeniumdiolates, RSNOs are known to occur naturally in the form of endogenous *S*-nitrosoglutathione and macromolecular *S*-nitrosoalbumin, among others.[35] RSNOs serve as NO donors under physiological conditions through thermal or metal-catalyzed decomposition, and are understood to form disulfide as their major decomposition product.[36] The NO loading and release properties of the *S*-nitrosated citrate polymers was characterized using chemiluminescence-based NO detection, demonstrating that these materials were able to sustain NO release over 4 to 6 days under physiological conditions. The cytotoxicity of both *S*-nitrosated PCMO derivatives was assessed using LIVE/DEAD and CellTiter-Blue® viability assays, in addition to morphological studies, to evaluate the suitability of these materials for biomedical applications. Figure 2.2 illustrates a simplified version of the theory studied in this project.

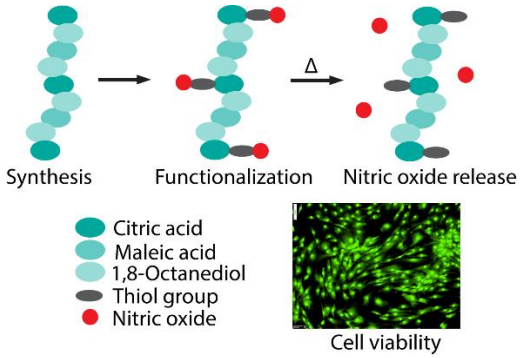

Figure 2.2 Summary of the main concepts explored in the study. Reproduced with permission from the Royal Society of Chemistry.

2.3 Materials and methods

2.3.1 Materials

Citric acid (99.5%), maleic acid (98%), 1,8-octanediol (98%), and triethylamine (TEA) were obtained from Alfa Aesar (Ward Hill, MA, USA). Cysteamine hydrochloride (97%) and *tert*-butyl nitrite (*t*-BuONO, 90%) were purchased from Sigma-Aldrich (St. Louis, MO, USA). L-Cysteine ethyl ester hydrochloride (99%) and 1-ethyl-(3-dimethylaminopropyl)carbodiimide hydrochloride (EDC·HCl, 99%) were from Chem-Impex International (Wood Dale, IL, USA). *N*-Hydroxysuccinimide (NHS, 98%) was obtained from Acros Organics (Somerville, NJ, USA). Phosphate buffered saline (PBS) tablets were procured from EMD Chemicals (Gibbstown, NJ, USA). DL-Dithiothreitol (DTT, 99%) was obtained from AMRESCO (Solon, OH, USA). Bis(2,4-dinitrophenyl) disulfide (80%) was obtained from TCI (Tokyo, Japan). Human dermal fibroblasts (HDF) were purchased from ZenBio, Inc. (Durham, NC, USA). Amphotericin B, gentamicin, and Media 106 fetal bovine serum supplement were purchased from Gibco (Grand Island, NY, USA). Alexa Fluor® 568 Phalloidin, DAPI, propidium iodide (PI), SYTO9, and trypsin-EDTA (0.25%) were purchased from Life Technologies (Grand Island, NY, USA). CellTiter-Blue® was obtained from Promega (Madison, WI, USA). 25T tissue culture (TC) plates were purchased from VWR (Denver, CO, USA). All chemicals were used as received.

2.3.2 Characterization techniques

^{1}H NMR spectra were obtained in dimethylsulfoxide-d_6 (DMSO-d_6) using an Agilent (Varian) Inova 400 MHz FT-NMR (Agilent Technologies, Inc., Santa Clara, CA, USA). Chemical shifts for ^{1}H NMR spectra were recorded in parts per million (ppm), and were referenced relative to tetramethylsilane (TMS, 0.00 ppm) as an internal standard. FTIR-ATR spectra were recorded in the range of 650-4000 cm^{-1} using a Nicolet 6700 FTIR spectrometer (Thermo Electron Corporation, Madison, WI, USA). UV-Vis absorption studies were performed using a Nicolet Evolution 300 UV-Vis spectrophotometer (Thermo Electron Corporation). Polymer molecular weight was characterized by gel permeation chromatography (GPC) using a Waters University 1500 GPC instrument (Waters, Milford, MA, USA). Thermal transitions were detected by differential scanning calorimetry (DSC) with a TA modulated 2920 DSC and the decomposition temperature of the materials was determined by thermogravimetric analysis (TGA) utilizing a TA thermogravimetric analyzer 2950 (TA Instruments, New Castle, DE, USA).

Ellman's assay for thiol quantification. Quantification of incorporated thiol was performed using a modified Ellman's assay as described elsewhere.[37] Briefly, samples of each polymer ($n \geq 3$) were suspended in dimethylformamide (DMF) and treated with 100 μL of 4.00 mM bis(2,4-dinitrophenyl) disulfide. The samples were then agitated for 1 h at room temperature. Aliquots were transferred to a 1 cm quartz cuvette and absorbance values were acquired at λ_{max} = 478 nm. Thiol content was calculated using *N*-acetyl cysteine standards.

Polymer degradation under physiological conditions. In order to confirm the hydrolytic degradability of the materials, gravimetric analysis was performed to assess changes in weight after incubating the materials under physiological conditions.[38] PCMO and *S*-nitrosated PCMO derivatives were placed in 5 mL phosphate buffered saline (PBS) at pH 7.4 and incubated at 37 °C

for up to 4 weeks. Samples were collected every 7 days, washed with Millipore water (18.2 MΩ·cm), and lyophilized for 24 h prior to measurement. For samples incubated longer than 1 week, the buffer solution was replaced at the end of each week.

Chemiluminescence-based NO analysis. NO release from *S*-nitrosated citrate polyester samples was evaluated using Sievers chemiluminescence NO analyzers (NOA 280i, GE Analytical, Boulder, CO, USA), following our earlier reported procedure.[39] The instruments were calibrated prior to each analysis using nitrogen (zero gas) and 45 ppm NO/nitrogen, and the nitrogen sweep gas flow during analysis was maintained at 200 mL/min. Total NO content was obtained by heating polymer samples and appropriate controls ($n \geq 3$) to 120 °C, which initiated the NO-releasing thermal decomposition of the RSNO groups.[18] The NO emission from this process was measured and used to quantify the amount of thermally releasable NO present in each material. To determine NO release under physiological conditions, polymer samples ($n \geq 3$) were suspended in deoxygenated 10 mM PBS (pH 7.4) at 37 °C, and the NO release was measured for 4 to 6 days, depending on the release properties of the material. All samples were shielded from direct exposure to light in order to prevent photodecomposition of the light sensitive RSNO.[40]

2.3.3 Synthesis of materials

Poly(citric-*co*-maleic acid-*co*-1,8-octanediol) (PCMO) (1). The biodegradable citrate-based polymer was prepared by a melt-phase polycondensation between maleic acid (2.32 g, 20.0 mmol), citric acid (5.76 g, 30.0 mmol), and 1,8-octanediol (7.31 g, 50.0 mmol). The polycondensation was carried out without an exogenous catalyst following a modification of a previously reported procedure.[41,42] The reagents were added to a vented 250 mL flask equipped with a nitrogen inlet and the reaction mass was stirred under a high flow of nitrogen for 30 min,

then heated to 140 °C with constant stirring to initiate the polycondensation. The colorless melted mass was maintained at 140 °C for 2 h under nitrogen flow to obtain the polymer. The crude polymer was then dissolved by sonication in absolute ethanol (35 mL) and added over 30 min to Millipore water (200 mL) containing Tween-80 to remove any unreacted materials. The mixture was stirred for 1 h and allowed to settle at 4 °C. The supernatant was decanted, and the polymer was washed 3 times with Millipore water (200 mL) and lyophilized for 4 days. ^{1}H NMR δ_H/ppm (400 MHz, DMSO-d_6): 1.20-1.65 (-$(CH_2)_6$-), 2.66-2.76 (-CH_2CO_2-), 3.95-4.03 (-OCH_2-), 6.35 (-HC=CH-), 12.6 (-CO_2H); IR ν_{max}/cm^{-1}: 3600-3200 (O-H alcohol, carboxylic acid), 2930-2856 (C-H), 1724 (C=O, carbonyl), 1167 (C-O). A synthetic scheme that illustrates the synthesis of polyester analogs is given in Figure 2.3.

PCMO-cysteamine (PCMO-CysAm) (2a). PCMO (12.4 g) was dissolved by sonication in DMF (100 mL). Free carboxylic acid groups of PCMO were reacted with EDC·HCl (3.06 g, 16.0 mmol) and NHS (2.81 g, 24.0 mmol) at 0 °C, and the reaction was maintained at this temperature for 1 h. The mixture was then allowed to warm to RT and was stirred overnight to activate the carboxylic acid groups. A solution of dry cysteamine hydrochloride (3.26 g, 28.7 mmol) in DMF (20 mL) and was added to the NHS activated polymer with 6.0 mL of TEA. The polymer solution was protected from direct exposure to light and stirred under nitrogen for 48 h. The polymer was then isolated after filtration through Celite and evaporation of the solvent under vacuum. The crude material was subsequently redissolved in absolute ethanol (40 mL) and treated with DTT (0.200 g, 1.30 mmol) and TEA (0.18 mL). The polymer solution was added over 30 min to Millipore water (200 mL) containing Tween-80 and stirred for 1 h, then allowed to settle at 4 °C and washed as previously described for PCMO. The purified material was recovered by lyophilization. ^{1}H NMR δ_H/ppm (400 MHz, DMSO-d_6): 1.20-1.65 (-$(CH_2)_6$-), 2.66-2.76 (-

CH_2CO_2-), 2.98 (-CH_2SH), 3.22 ((CO)NHCH-), 3.95-4.03 (-OCH_2-), 6.35 (-HC=CH-), 7.82-7.92 (-(CO)NH-); IR ν_{max}/cm^{-1}: 3600-3200 (O-H), 2930-2856 (C-H), 1724 (C=O, carbonyl), 1656 (amide I), 1531 (amide II), 1167 (C-O).

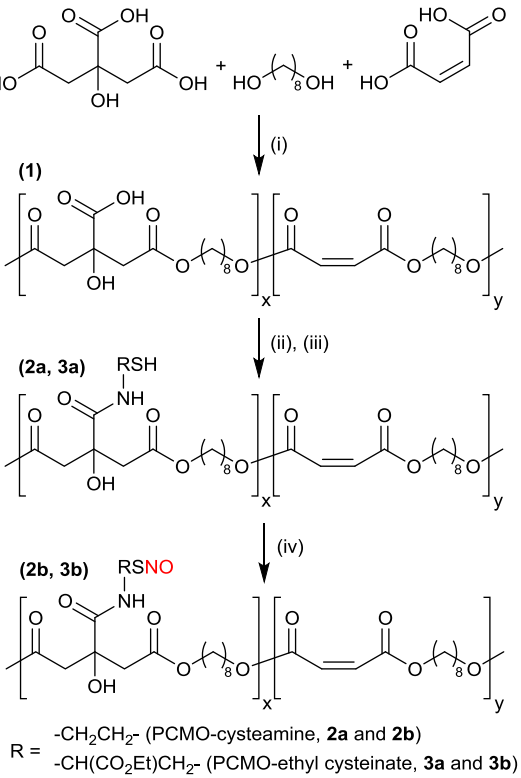

Figure 2.3 Synthesis of PCMO and both thiolated (2a, 3a) and *S*-nitrosated (2b, 3b) derivatives. (i) 140 °C, 2 h, (ii) NHS, EDC·HCl, 0 °C to RT, overnight, cysteamine hydrochloride/ethyl cysteinate hydrochloride, RT, 48 h, (iii) DTT, TEA, RT, 1 h, (iv) *t*-BuONO, EtOH, RT, 4h. Reproduced with permission from the Royal Society of Chemistry.

***S*-nitrosated PCMO-cysteamine (PCMO-CysAm-NO) (2b).** A mixture of PCMO-cysteamine/ethanol (2a) (25 mg/mL) and *t*-BuONO (0.500 mL) was stirred at RT for 4 h in a vial protected from light. After *S*-nitrosation, the material was stirred under vacuum to remove solvent, residual *t*-BuONO, and volatile byproducts. IR ν_{max}/cm^{-1}: 3600-3200 (O-H alcohol, carboxylic acid), 2930-2856 (C-H), 1728 (C=O, carbonyl), 1653 (amide I), 1529 (amide II), 1173 (C-O). UV-Vis λ_{max}/nm: 335 (RSNO, $n_O \rightarrow \pi^*$), 550 (RSNO, $n_N \rightarrow \pi^*$).

PCMO-ethyl cysteinate (PCMO-EtCys) (3a). An analog was prepared following the general method provided for 2a using cysteine ethyl ester hydrochloride (5.33 g, 28.7 mmol). ^{1}H NMR δ_H/ppm (400 MHz, DMSO-d_6): 1.18-1.22 (-CH_3) 1.20-1.65 (-$(CH_2)_6$-), 2.66-2.76 (-CH_2CO_2-), 3.70 (-CH_2SH), 4.42 (-(CO)NH-CH_2-), 3.95-4.03 (-OCH_2-), 6.35 (-HC=CH-), 7.84-7.94 (-(CO)NH-); IR ν_{max}/cm^{-1}: 3600-3200 (O-H alcohol, carboxylic acid), 2930-2856 (C-H), 1724 (C=O, carbonyl), 1673 (amide I), 1518 (amide II), 1167 (C-O).

***S*-nitrosated PCMO-ethyl cysteinate (PCMO-EtCys-NO) (3b).** An analog was prepared from 3a using the procedure described for 2b. IR ν_{max}/cm^{-1}: 3600-3200 (O-H alcohol, carboxylic acid), 2930-2856 (C-H), 1733 (C=O, carbonyl), 1684 (amide I), 1517 (amide II), 1176 (C-O). UV-Vis λ_{max}/nm: 336 (RSNO, $n_O \rightarrow \pi^*$), 549 (RSNO, $n_N \rightarrow \pi^*$).

2.3.4 Cell studies

For cell studies, HDF were cultured in media 106 supplemented with 2% v/v fetal bovine serum, 1 µg/mL hydrocortisone, 10 ng/mL human epidermal growth factor, 3 ng/mL basic fibroblast growth factor, 10 µg/mL heparin, 125 µg/mL amphotericin B, and 5 mg/mL gentamicin in a 25T flask. HDF were incubated at 37 °C in a humid atmosphere with 5% CO_2. Prior to the experiments, cells were collected from a 25T flask by addition of 1 mL of a trypsin-EDTA (0.25%) solution, and re-suspended at different concentrations (cells/mL) depending on the specific experiment.

Preparation of extracts. All cytotoxicity experiments were performed according to ISO standards.[43] Extracts from both *S*-nitrosated PCMO derivatives were obtained at physiological temperature (37 °C in a humid atmosphere with 5% CO_2). To prepare extracts, each material was incubated in the above described cell media (concentration of 0.5 mg material/mL cell media) for

24 h in sterilized 20 mL amber vials. After 24 h, the resulting extracts were used for cell experiments. As a control, cell media was kept under the same conditions and used to replace media in the positive and negative control samples.

Extract experiments. To perform experiments with extracts, 5.0 x 10^4 cells per well were seeded in a 24-well plate for assessing the morphology of the cells, 2.5 x 10^4 cells per well were seeded in a 24-well plate for CellTiter-Blue® viability assays and 2.5 x 10^4 cells per well were seeded in a 24-well plate for LIVE/DEAD assay. HDF cells were incubated for 48 h prior to exposure to the different extracts (37 °C in a humid atmosphere with 5% CO_2) followed by 24 h in the presence of the extracts at 37 °C in a humid atmosphere with 5% CO_2. All biological assays were repeated $n \geq 9$.

Morphological studies. Each time, three wells were used for positive control and three wells were used for each material extract. After rinsing all samples twice with PBS, cells were fixed by exposing them to 3.7% methanol-free formaldehyde (300 µL) in PBS for 10 min at RT. All wells were rinsed twice with PBS and exposed to acetone (200 µL), cooled to 0 °C for 3 min, rinsed twice again with PBS, and stained using 200 µL of staining solution for 20 min at RT. Staining solution consisted of DAPI and Alexa Fluor® 568 Phalloidin at concentrations of 7.60 µM and 6.60 µM, respectively, and was prepared in PBS. All wells were finally rinsed twice with DI water and imaged. Fluorescence microscopy images were taken using an Olympus IX73 fluorescence microscope. An excitation wavelength of 358 nm was used for DAPI (461 nm emission observed), and a wavelength of 578 nm was used for Alexa Fluor® 568 Phalloidin (600 nm emission observed). Images of cells are composed of two overlaid images (DAPI and Alexa) combined using the Olympus CellSens software.

CellTiter-Blue® viability assay. For each experiment, three wells containing cells were used as a positive control (labeled TC), three wells were used as a negative control, and three wells containing cells were exposed to each material extract. For the negative control, wells were rinsed twice with PBS and cells were exposed to methanol (100 µL per well) for 45 min to reduce viability. Methanol was removed and all wells were rinsed twice with PBS and 300 µL of CellTiter-Blue® solution was added. CellTiter-Blue® solution was prepared by mixing 20 µL of CellTiter-Blue® solution for each 100 µL of warm cell media. After 4 h incubation at 37 °C in a humid atmosphere with 5% CO_2, absorbance readings were measured with a plate reader (BioTek Synergy 2) at 570 nm and 600 nm.

LIVE/DEAD assay. Each time, three wells were used for positive control, three were used for negative control, and three wells were used for each material extract. For the negative control, cells were exposed to methanol as described above. In this case, the PBS was removed after the second wash and 200 µL of LIVE/DEAD solution was added to each well. Samples were incubated for 1 h at RT. Subsequently, the LIVE/DEAD solution was removed and DI water was added to each well. To prepare the LIVE/DEAD solution, PI and SYTO9 were added to 0.85% w/v NaCl solution at concentrations of 3 µM and 0.5 µM, respectively. Fluorescence microscopy images were obtained using an Olympus IX73 fluorescence microscope. An excitation wavelength of 543 nm was used for PI (617 nm emission observed), and a wavelength of 488 nm was used for SYTO9 (500 nm emission observed). Images of cells used for LIVE/DEAD assay are composed of two overlaid images (PI and SYTO9), combined using the Olympus CellSens software.

2.4 Results and discussion

2.4.1 Synthesis and characterization of poly(citric-*co*-maleic acid-*co*-1,8-octanediol)

PCMO was synthesized from citric acid, maleic acid, and 1,8-octanediol following a modified literature protocol to yield an amorphous polyester.[41,42] Citric acid is generally regarded as non-toxic and occurs endogenously as citrate, where it participates in several crucial metabolic pathways.[44,45] As a tri-functional carboxylic acid, citric acid permits both crosslinking through the formation of multiple ester linkages and the conjugation of pendant groups using carbodiimide-mediated coupling reactions.[46] Furthermore, it has been established that certain citrate-based polymers exhibit excellent hemocompatibility and such materials have frequently been proposed for blood-contacting applications.[47,48] It was previously demonstrated that the incorporation of maleic acid as a component of polyesters allows post-polymerization crosslinking to occur through exposure to UV light, and the hydrophobic 1,8-octanediol acts to balance the inherent hydrophilicity of citrate.[49] The catalyst-free polycondensation was carried out in the melt-phase at 140 °C for 2 h with a constant nitrogen flow to remove water, and the structure of PCMO was independently confirmed by ^{1}H NMR (Fig. A.1) and compared to previous reports.[23] The multiplet at 2.66-2.76 ppm corresponds to the methylene protons from citrate units, while peaks at 1.20-1.65 (-CH_2-) and 3.95-4.03 (-OCH_2-) ppm confirmed incorporation of 1,8-octanediol. The alkenyl protons of the maleate group appeared at 6.35 ppm. The broad feature centered at 12.6 ppm is attributable to remaining free carboxyl groups from either the citrate or maleate units. The FTIR-ATR spectrum (shown in Fig. A.4 and A.5) features an ester carbonyl C=O stretching band at 1724 cm^{-1}, which confirmed the ester linkages between the monomers, while the contribution of carboxylic acid O-H stretching to the broad feature between 3600-3200 cm^{-1} supported the preservation of free carboxylic acids groups for further post-polymerization modifications. GPC

analysis with polystyrene standards showed a weight average molecular weight (M_w) of 175,000 g mol^{-1}, a number average molecular weight (M_n) of 33,100 g mol^{-1} and a polydispersity index (PDI) of 5.29. TGA indicated an onset decomposition temperature of 178 °C, and the glass transition temperature of -16 °C was determined by DSC.

2.4.2 Synthesis and characterization of thiolated poly(citric-*co*-maleic acid-*co*-1,8-octanediol)

The thiols cysteamine and ethyl cysteinate were conjugated to PCMO by formation of amide linkages between the primary. amine of the thiols and the remaining free carboxylic acid groups of the polyester. This was accomplished *via* a carbodiimide-mediated coupling reaction in a modification of a previously reported literature protocol.[39] This process results in the covalent incorporation of thiol groups that permit the subsequent formation of NO-releasing RSNO groups.[50] Incorporation of the thiols was confirmed by ^{1}H NMR, where the appearance of additional multiplets at 2.98 and 3.22 ppm was attributable to the methylene protons of cysteamine, while features at 1.18 – 1.22 (-CH_3), 3.70 (-CH_2SH), and 4.42 (-(CO)NHCH-) ppm corresponded to ethyl cysteinate (Fig. A.2 and A.3). The feature at approximately 7.8 – 7.9 ppm for both derivatives indicated the formation of amide bonds between the thiol and the polymer. In addition, the development of characteristic amide absorbance bands in the FTIR-ATR spectrum of the thiolated polymers further supported the successful formation of amide linkages.[51] In the case of PCMO-CysAm, these prominent features occur at 1656 (amide I) and 1531 cm^{-1} (amide II), while PCMO-EtCys displays equivalent features at 1673 and 1518 cm^{-1} (Fig. A.4 and A.5). These features are absent in the FTIR-ATR spectrum of unmodified PCMO. Although the comparative weakness of the IR features associated with thiol groups prevented their identification in the

spectra of the thiolated polymers, the presence of thiol groups was confirmed using a modified Ellman's assay protocol with bis(2,4-dinitrophenyl) disulfide in DMF (Table 2.1).[52] Use of the more common Ellman's reagent 5,5′-dithiobis(2-nitrobenzoic) acid (DTNB) in aqueous base was not possible due to the lack of water solubility exhibited by PCMO derivatives and the general hydrophobicity of the polymer, which limited water permeation and reduced the accessibility of the thiol groups.[53] GPC analysis of the thiolated derivatives was complicated by crosslinking from disulfide formation and was limited to characterization of the parent polyester.

Table 2.1 Summarized thiol and NO content data for PCMO derivatives

Material	Thiol Content[a] (mmol g^{-1})	Total NO Content[b] (mmol g^{-1})	Cumulative NO Release[c] (mmol g^{-1})	% NO/Thiol Content
PCMO-Cysteamine (**2a**, **2b**)	0.856 ± 0.030	0.45 ± 0.07	0.29 ± 0.05	52 ± 8
PCMO-Ethyl cysteinate (**3a**, **3b**)	0.797 ± 0.038	0.16 ± 0.04	0.066 ± 0.003	13 ± 3

[a]Values determined for 2a and 3a using a modified Ellman's assay protocol in DMF. [b]Values determined by NO analysis of 2b and 3b through thermal decomposition of the RSNO. [c]Release measured under physiological conditions (pH 7.4, 37 °C) in 10 mM PBS over 6 days (2b) and 4 days (3b). Measurements were ended when the detected NO release was below 3 ppb. For all experiments, $n \geq 3$ and results are reported as the mean ± SD.

2.4.3 Synthesis and characterization of *S*-nitrosated poly(citric-*co*-maleic acid-*co*-1,8-octanediol)

S-Nitrosation of the thiolated polymers was carried out in ethanol under anhydrous conditions using the alkyl nitrite *t*-BuONO as the nitrosating agent.[54] This comparatively mild procedure avoids the use of sodium nitrite and aqueous acid that could lead to parallel hydrolysis of the polymeric ester linkages, and permits removal of unreacted *t*-BuONO and volatile byproducts under vacuum.[18,55] The successful conversion of thiol groups to the corresponding RSNO was supported by UV-Vis spectrophotometry in DMSO, where characteristic RSNO

absorptions at 335 ($n_O \rightarrow \pi^*$) and 550 nm ($n_N \rightarrow \pi^*$) for PCMO-CysAm-NO and equivalent absorptions for PCMO-EtCys-NO at 336 and 549 nm were observed (Fig. A.6 and A.7).[36] Identification of the $n_N \rightarrow \pi^*$ transition near 550 nm was supported by the use of diffuse reflectance UV-Vis, since the low molar extinction coefficient of that absorbance feature complicated its detection in DMSO due to solubility limitations. No features developed that could be attributable to the formation of undesirable *N*-nitrosamide or alkyl nitrite species, which typically result in pronounced and distinctive absorptions in the range of 260 - 400 nm.[54,56] The FTIR-ATR spectra of both *S*-nitrosated materials indicated that the primary structural features of the polyester were preserved, with bands at 3600-3200 (O-H), 2930-2856 (C-H), 1728 (C=O, carbonyl), 1653 (amide I), 1529 (amide II), and 1173 cm^{-1} (C-O) for PCMO-CysAm-NO that are consistent with those of the parent thiolated polyester (Fig. A.4). These features appear at 3600-3200, 2931-2856, 1733, 1684, 1517, and 1176 cm^{-1} in the case of PCMO-EtCys-NO (Fig. A.5). For both thiolated PCMO derivatives, the efficacy of the *S*-nitrosation process (as evaluated by UV-Vis) was greatest using ethanol as a solvent, where the polymers exhibited appreciable solubility. The conversion of thiol to RSNO (% total NO/thiol content) under identical conditions was 52 ± 8% for PCMO-CysAm-NO, and 13 ± 3% for PCMO-EtCys-NO. A previous report identified a similar reduction in *S*-nitrosation efficiency in the case of a PLGA derivative bearing cysteine pendant groups, where this outcome was attributed to the influence of the additional neighboring carbonyl group that was not present in cysteamine derivatives.[50] In addition, the extent of *S*-nitrosation may be limited due to parallel decomposition of the RSNO.[36]

The total NO content of each polymer was directly quantified using highly selective chemiluminescence-based NO detection.[57,58] Samples of each *S*-nitrosated material were heated to 120 °C in a stepwise manner under deoxygenated conditions in custom gas-flow cells with a

constant flow of nitrogen, following a previously reported method.[17] The thermal decomposition of the RSNO groups resulted in the quantifiable release of NO, which was detected by the instrument as it occurred. The instrument output (NO concentration) was converted to total NO release using a calibration constant obtained from gases of known NO concentration and used to calculate the amount of thermally-releasable NO present in the polymer samples. In all cases, the samples were heated until no further NO emission was detected. Controls consisted of thiolated PCMO derivatives heated under identical conditions, a process that was not observed to result in statistically relevant NO release.[59] NO release under physiological conditions was determined in gas-flow cells by immersing the materials in pH 7.4 PBS at 37 °C while protected from direct exposure to light (Fig. 2.4a). The gradual decomposition of the RSNO functional groups resulted in the release of NO. Experiments were performed in triplicate and an average of 0.29 ± 0.05 mmol NO g^{-1} was released under these conditions over the course of 6 days from PCMO-CysAm-NO, and 0.066 ± 0.003 mmol NO g^{-1} was released from PCMO-EtCys-NO in 4 days (Fig. 2.4b). The experiments were terminated when continuing NO release fell below 3.0 ppb. In a prior report, Zhao et al. calculated total NO release (by Griess assay) from an *N*-diazeniumdiolated copolymer consisting of citric acid, 1,8-octanediol, and *N*,*N*′-bis(2-hydroxyethyl)ethylenediamine coated on expanded poly(tetrafluoroethylene) vascular grafts in the range of 0.4 - 0.5 μmol/g polymer. In comparison, PCMO-CysAm-NO and PCMO-EtCys-NO demonstrate greater total NO release under physiological conditions and do not exhibit the concomitant formation of potentially hazardous *N*-nitrosamine that was observed for a citrate-based polymer system containing blended DEDETA/NO.[23] The overall quantity of NO released under physiological conditions was largely proportional to the total NO content of the materials. In addition, the general similarity of the physiological NO release properties for both *S*-nitrosated PCMO derivatives indicated that the

morphology and hydrophobicity of the polymer itself was responsible for the release characteristics of the materials. The duration of NO release in *S*-nitrosated materials is frequently attributable to the stability of the RSNO, a property that is greatly dependent upon the prevailing conditions.[35,50,60] It has been previously observed that greater hydrophilicity and solvent permeation under physiological conditions promoted rapid RSNO decomposition, while isolation within hydrophobic polymer matrices improved the duration of NO release.[17] For this reason, the 4 to 6 day release from hydrophobic *S*-nitrosated PCMO derivatives is primarily attributable to reduced solvent accessibility, which inhibits the NO-releasing decomposition of RSNO to NO and disulfide (2RSNO → 2NO + RSSR).[36]

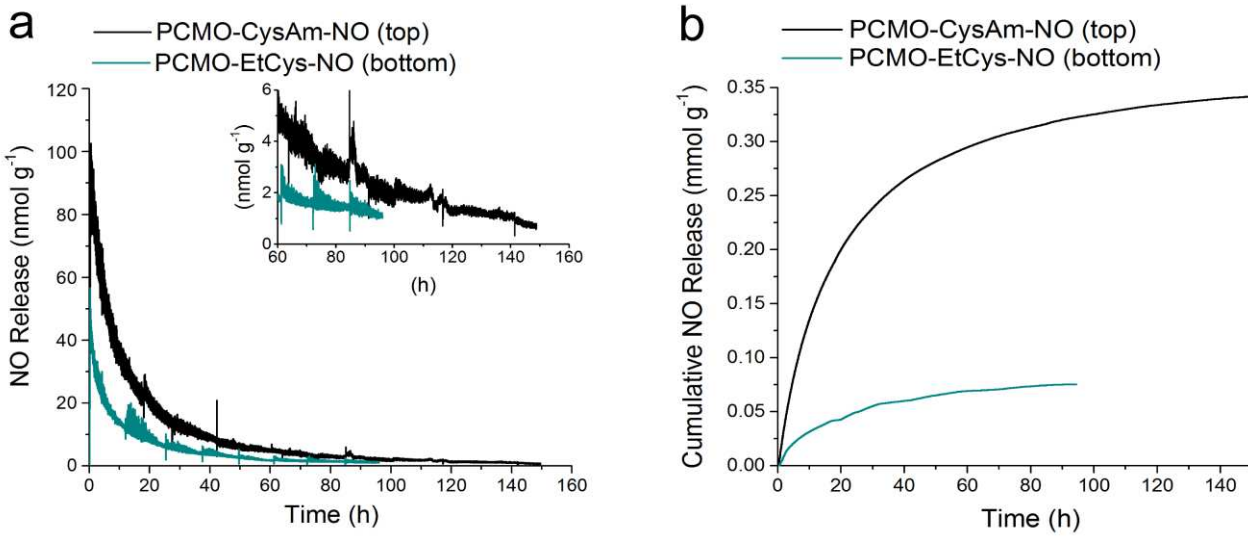

Figure 2.4 (a) Representative real-time NO release profiles for PCMO-CysAm-NO (top) and PCMO-EtCys-NO (bottom) under physiological conditions (pH 7.4, 37 °C) in 10 mM PBS. Inset: NO release after 60 hours. (b) Representative cumulative NO release profiles under physiological conditions. Reproduced with permission from the Royal Society of Chemistry.

2.4.4 Polymer degradation under physiological conditions

The potential biodegradability of the polymers was assessed by immersing samples ($n = 3$) of PCMO, PCMO-CysAm-NO, and PCMO-EtCys-NO in 10 mM pH 7.4 PBS buffer at 37 °C in

the absence of light for up to 4 weeks (Fig. 2.5). The results indicate relatively rapid degradation for the unmodified PCMO during this time period. A dramatic decrease in polymer weight occurring between week 2 and 3 was observed, where 65% of the polymer mass was lost (Table A.1). The rapid degradation of the parent PCMO was largely attributable to the exposure of additional surface area as the degradation proceeded. In comparison, the *S*-nitrosated derivatives exhibited only a 50% reduction in initial weight at the end of the 4 week period. The reduced degradation rate of the *S*-nitrosated polymers can be attributed to crosslinking arising from the formation of disulfide linkages.

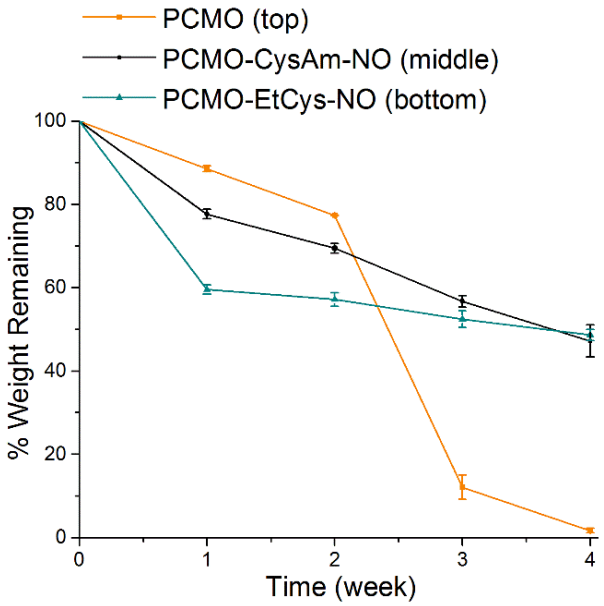

Figure 2.5 Degradation profiles of PCMO and *S*-nitrosated derivatives under physiological conditions (pH 7.4 PBS, 37 °C). Each data point represents an average of $n \geq 3$ replicates and the standard deviation. Reproduced with permission from the Royal Society of Chemistry.

2.4.5 Cytotoxicity studies

The relative cytotoxicity of potential leachates from the two *S*-nitrosated citrate-based polyesters (PCMO-CysAm-NO and PCMO-EtCys-NO) with respect to HDF was evaluated using an extract approach, based on the commonly accepted ISO regulation 10993 part 5.[43] Morphological studies and two cytotoxicity tests (CellTiter-Blue® viability and LIVE/DEAD)

were performed to ensure the suitability of these materials for biomedical applications. Figure 2.6a reveals cells with the anticipated morphology for HDF fixed to a TC plate after reaching 90% confluency. Both *S*-nitrosated PCMO derivatives show comparable morphology to the positive control sample, confirming that neither of the extracts induces any changes in cell morphology (Fig. 2.6b and 2.6c).

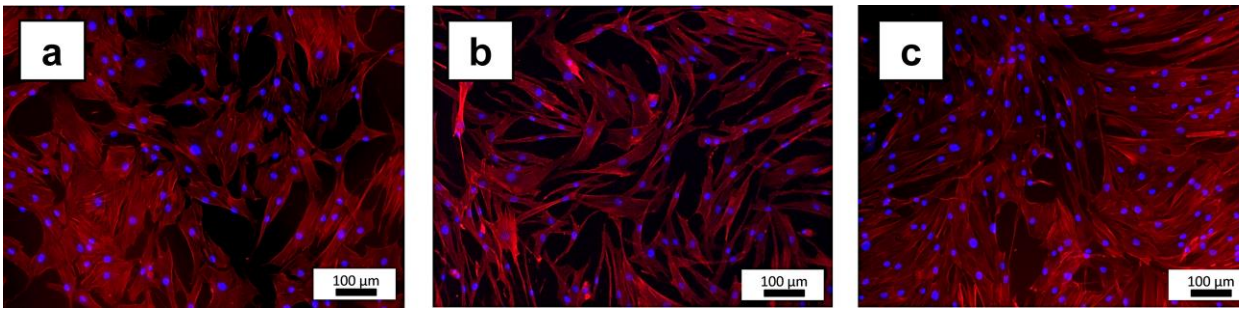

Figure 2.6 *Morphological studies*. Overlaid fluorescence microscopy images of human dermal fibroblasts attached to a TC plate for 72 h using: (a) cell media (positive control), (b) extract from PCMO-CysAm-NO, and (c) extract from PCMO-EtCys-NO. Blue areas are cell nuclei and red areas are cell actin cytoskeletons. For all experiments, $n \geq 9$. Reproduced with permission from the Royal Society of Chemistry.

CellTiter-Blue® viability assay was used to assess the percentage of viable cells present in the control samples as well as in the presence of the different extracts. CellTiter-Blue® viability assay functions similarly to the commonly used 3-(4,5-dimethylthiazol-2-yl)-2,5-diphenyltetrazolium bromide (MTT) assay, with the advantage that only one step is required as the reduced product is water soluble. In both cases, the mitochondrial activity in live cells is tested, therefore this assay is an excellent indicator of the cell viability.[61] Figure 2.7 shows the viability results for TC and cells exposed to extracts from both *S*-nitrosated PCMO derivatives. Negative control samples (values not included in the graph) indicated that there were no viable cells after exposure to methanol for 45 minutes, and the absorbance from these samples was equivalent to a CellTiter-Blue® solution. For PCMO-CysAm-NO and PCMO-EtCys-NO extracts, the percentage

of viable cells was very similar to the positive control indicating that there was no decrease in cellular viability (normalized with the positive control sample) when cells were exposed to the extracts. These results suggest that there were no toxic leachates and/or toxic degradation products at a cytotoxic concentration present in either of the extracts.

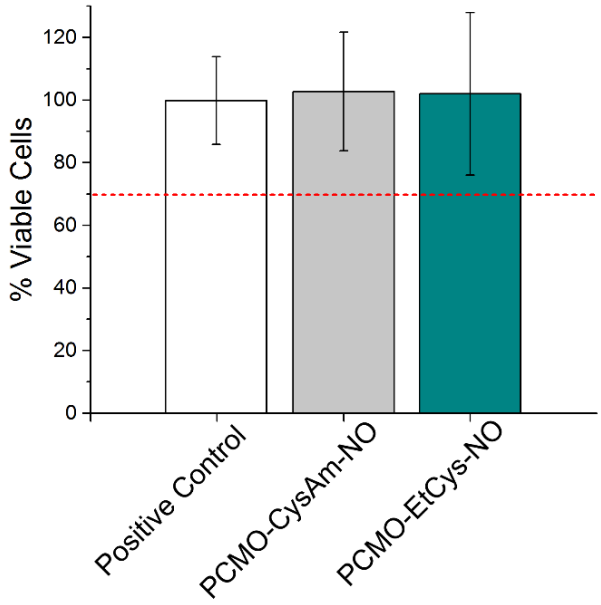

Figure 2.7 *CellTiter-Blue® viability assays.* % Viable human dermal fibroblasts cultured in cell media (positive control), in extract from PCMO-CysAm-NO, and in extract from PCMO-EtCys-NO. Red line indicates the 70% threshold for viability assessment. For all experiments, $n \geq 9$. Reproduced with permission from the Royal Society of Chemistry.

Similar results to CellTiter-Blue® viability assay were observed when the LIVE/DEAD assay was performed. Results from LIVE/DEAD assay are presented in Figure 2.8. HDF cells attached to TC plates were used as positive control and cells exposed to methanol prior to staining were used as negative control. A similar area covered with HDF was observed in the positive control sample and the wells exposed to PCMO-CysAm-NO and PCMO-EtCys-NO extracts. Figure 2.8a shows positive control cells where the majority of the cells are observed in green indicating that the cell membrane is intact and the cells are considered alive.

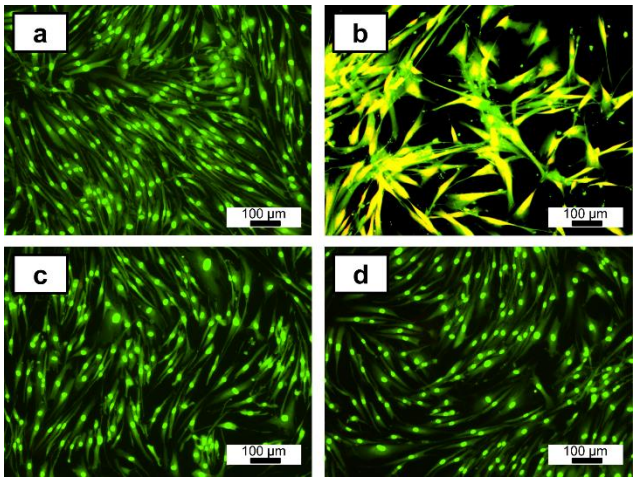

Figure 2.8 *LIVE/DEAD studies*. Overlaid fluorescence microscopy images of human dermal fibroblasts attached to a TC plate for 72 h using: (a) cell media (positive control), (b) cell media and exposure to methanol prior to staining (negative control), (c) extract from PCMO-CysAm-NO, and (d) extract from PCMO-EtCys-NO. Green cells are considered alive and red cells are considered dead. For all experiments, n ≥ 9. Reproduced with permission from the Royal Society of Chemistry.

Figure 2.8b illustrates cells that were exposed to methanol prior to staining. The yellow color indicates that the cell membrane was disrupted, therefore, a mixture of red and green staining is observed. Figure 2.8c and 2.8d display HDF that have been exposed to extracts from PCMO-CysAm-NO and PCMO-EtCys-NO, respectively. Both images display green cells indicating that neither of the material extracts damage the cell wall. Cytotoxicity results were consistent with those performed by Wang *et al.* where it was demonstrated that the citrate-based parent material did not hinder cell growth.[23]

2.5 Conclusions

The work presented here is the first, to our knowledge, that reports the synthesis and characterization of *S*-nitrosated citrate-based polyesters with quantified extended NO release. In the case of PCMO-CysAm-NO, total NO content of 0.45 mmol g^{-1} was obtained, while the NO content of PCMO-EtCys-NO was found to be 0.16 mmol g^{-1}. The polymers released quantifiable

NO over the course of at least 4 (PCMO-EtCys-NO) to 6 days (PCMO-CysAm-NO) with respective average cumulative NO releases of 0.066 and 0.29 mmol g^{-1}. In both cases, *S*-nitrosation was not found to alter the backbone structure of the polymer and no toxic *N*-nitroso species were detected by UV-Vis or FTIR-ATR. Cell viability studies with HDF indicated viability above the cytotoxicity threshold as compared to a positive control, and morphological studies confirmed that the polymer extracts did not induce changes to cell morphology. Taken together, these results suggest that PCMO derivatives may be candidates for potential biomedical applications.

Individual contributions and funding sources

A. Lutzke helped with the method development for the modified Ellman's assay and degradation studies. V. B. Damodaran provided the synthetic methods for thiolated materials. Cytotoxicity studies performed by A. Pegalajar-Jurado and B. H. Neufeld, who were the primary authors of section 2.3.4. All other work carried out by J. P. Yapor. Funding for this research was provided by the Department of Defense Congressionally Directed Medical Research Program (W81XWH-11-2-0113). A. P. J. also thanks the Dreyfus Foundation for support *via* the Camille and Henry Dreyfus Foundation Postdoctoral Program in Environmental Chemistry. J. P. Yapor acknowledges the National Science Foundation for support *via* the Alliance for Graduate Education and the Professoriate Fellowship 2013-2014 and fellowship extension 2014-2015 (PO0000062901).

REFERENCES

1. Ratner, B. D. *J. Biomed. Mater. Res.* **1993**, *27*, 283.
2. Ratner, B. D. *Biomaterials* **2007**, *28*, 5144.
3. Anderson, J. M. *Annu. Rev. Mater. Sci.* **2001**, *31*, 81.
4. Costerton, J. W.; Stewart, P. S.; Greenberg, E. *Science* **1999**, *284*, 1318.
5. Donlan, R. M. *Emerg. Infect. Dis.* **2001**, *7*, 277.
6. Pegalajar-Jurado, A.; Joslin, J. M.; Hawker, M. J.; Reynolds, M. M.; Fisher, E. R. *ACS Appl. Mater. Interfaces* **2014**, *6*, 12307.
7. Culotta, E., Joshland Jr., D. E. *Science* **1992**, *258*, 1862.
8. Moncada, S. *J. R. Soc. Med.* **1999**, *92*, 164.
9. Schulz, R.; Rassaf, T.; Massion, P.; Kelm, M.; Balligand, J. *Pharmacol. Ther.* **2005**, *108*, 225.
10. Bogdan, C. *Nat. Immunol.* **2001**, *2*, 907.
11. Rand, M.; Li, C. *Annu. Rev. Immunol.* **1995**, *57*, 659.
12. Weiming, X.; Liu, L. Z.; Loizidou, M.; Ahmed, M.; Charles, I. G. *Cell Res.* **2002**, *12*, 311.
13. Seabra, A. B.; Duran, N. *J. Mater. Chem.* **2010**, *20*, 1624.
14. Thomas, D. D.; Liu, X.; Kantrow, S. P.; Lancaster, J. R. *Proc. Nat. Acad. Sci.* **2001**, *98*, 355.
15. Jen, M. C.; Serrano, M. C.; van Lith, R.; Ameer, G. A. *Adv. Funct. Mater.* **2012**, *22*, 239.
16. Lu, Y.; Slomberg, D. L.; Schoenfisch, M. H. *Biomaterials* **2014**, *35*, 1716.

17. Lutzke, A.; Pegalajar-Jurado, A.; Neufeld, B. H.; Reynolds, M. M. *J. Mater. Chem. B* **2014**, *2*, 7449.

18. Damodaran, V. B.; Place, L. W.; Kipper, M. J.; Reynolds, M. M. *J. Mater. Chem.* **2012**, *22*, 23038.

19. Koh, A.; Lu, Y.; Schoenfisch, M. H. *Anal. Chem.* **2013**, *85*, 10488.

20. Coneski, P. N.; Schoenfisch, M. H. *Polym. Chem.* **2011**, *2*, 906.

21. Makadia, H. K.; Siegel, S. J. *Polymers* **2011**, *3*, 1377.

22. Coneski, P. N.; Rao, K. S.; Schoenfisch, M. H. *Biomacromolecules* **2010**, *11*, 3208.

23. Wang, Y.; Kibbe, M. R.; Ameer, G. A. *Biomater. Sci.* **2013**, *1*, 625.

24. Zhao, H.; Serrano, M. C.; Popowich, D. A.; Kibbe, M. R.; Ameer, G. A. *J. Biomed. Mater. Res. Part A* **2010**, *93*, 356.

25. Keefer, L. K. *ACS Chem. Biol.* **2011**, *6*, 1147.

26. Magee, P. *Food Cosmet. Toxicol.* **1971**, *9*, 207.

27. Schmähl, D.; Habs, M. *Oncology* **1980**, *37*, 237.

28. Coneski, P. N.; Schoenfisch, M. H. *Org. Lett.* **2009**, *11*, 5462.

29. Batchelor, M. M.; Reoma, S. L.; Fleser, P. S.; Nuthakki, V. K.; Callahan, R. E.; Shanley, C. J.; Politis, J. K.; Elmore, J.; Merz, S. I.; Meyerhoff, M. E. *J. Med. Chem.* **2003**, *46*, 5153.

30. Prabhakaran, M. P.; Nair, A. S.; Kai, D.; Ramakrishna, S. *Biopolymers* **2012**, *97*, 529.

31. Serrano, M. C.; Gutiérrez, M. C.; Jiménez, R.; Ferrer, M. L.; del Monte, F. *Chem. Commun.* **2012**, *48*, 579.

32. Yang, J.; Zhang, Y.; Gautam, S.; Liu, L.; Dey, J.; Chen, W.; Mason, R. P.; Serrano, C. A.; Schug, K. A.; Tang, L. *Proc. Nat. Acad. Sci.* **2009**, *106*, 10086.

33. Vos, O. *Adv. Space Res.* **1992**, *12*, 201.

34. Stipanuk, M. H.; Dominy, J. E.; Lee, J. I.; Coloso, R. M. *J. Nutr.* **2006**, *136*, 1652S.

35. Stamler, J. S. *Circ. Res.* **2004**, *94*, 414.

36. Williams, D. L. H. *Acc. Chem. Res.* **1999**, *32*, 869.

37. Gabor, G.; Vincze, A. *Anal. Chim. Acta* **1977**, *92*, 429.

38. Williams, D. *J. Mater. Sci.* **1982**, *17*, 1233.

39. Damodaran, V. B.; Reynolds, M. M. *J. Mater. Chem.* **2011**, *21*, 5870.

40. Szacilowski, K.; Stasicka, Z. *Prog. React. Kinet. Mec.* **2001**, *26*, 1.

41. Yang, J.; Webb, A. R.; Ameer, G. A. *Adv. Mater.* **2004**, *16*, 511.

42. Tran, R. T.; Wang, L.; Zhang, C.; Huang, M.; Tang, W.; Zhang, C.; Zhang, Z.; Jin, D.; Banik, B.; Brown, J. L. *J. Biomed. Mater. Res. Part A* **2014**, *102*, 2521.

43. International Organization for Standardization, Biological evaluation of medical devices - Part 5: Test for *in vitro* cytotoxicity. ISO 10993-5, Geneva, Switzerland, 2009, pp.1-34.

44. Krebs, H. A.; Johnson, W. A. *FEBS Lett.* **1980**, *117*, K2.

45. Kornberg, H. *Nat. Rev. Mol. Cell Biol.* **2000**, *1*, 225.

46. Valeur, E.; Bradley, M. *Chem. Soc. Rev.* **2009**, *38*, 606.

47. Tran, R. T.; Zhang, Y.; Gyawali, D.; Yang, J. *Recent Pat. Biomed. Eng.* **2009**, *2*, 216.

48. Chung, E. J.; Kodali, P.; Laskin, W.; Koh, J. L.; Ameer, G. A. *J. Mater. Sci. Mater. Med.* **2011**, *22*, 2131.

49. Gyawali, D.; Tran, R. T.; Guleserian, K. J.; Tang, L.; Yang, J. *J. Biomater. Sci., Polym. Ed.* **2010**, *21*, 1761.

50. Stamler, J. In *The Role of Nitric Oxide in Physiology and Pathophysiology*; Springer: 1995, p 19.

51. Damodaran, V. B.; Joslin, J. M.; Wold, K. A.; Lantvit, S. M.; Reynolds, M. M. *J. Mater. Chem.* **2012**, *22*, 5990.

52. Coates, J. *Encyclopedia of Analytical Chemistry, RA Meyers Ed, 10815–10837*; John Wiley & Sons Ltd, Chichester, 2000.

53. Reynolds, M. M.; Frost, M. C.; Meyerhoff, M. E. *Free Radical Biol. Med.* **2004**, *37*, 926.

54. Wang, P. G.; Xian, M.; Tang, X.; Wu, X.; Wen, Z.; Cai, T.; Janczuk, A. J. *Chem. Rev.* **2002**, *102*, 1091.

55. Ridd, J. *Q. Rev. Chem. Soc.* **1961**, *15*, 418.

56. Ungnade, H. E.; Smiley, R. A. *J. Org. Chem.* **1956**, *21*, 993.

57. Fontijn, A.; Sabadell, A. J.; Ronco, R. J. *Anal. Chem.* **1970**, *42*, 575.

58. Reynolds, M. M.; Hrabie, J. A.; Oh, B. K.; Politis, J. K.; Citro, M. L.; Keefer, L. K.; Meyerhoff, M. E. *Biomacromolecules* **2006**, *7*, 987.

59. Seo, K. S.; Cloyd, J. D. *J. Appl. Polym. Sci.* **1991**, *42*, 845.

60. De Oliveira, M. G.; Shishido, S. M.; Seabra, A. B.; Morgon, N. H. *J. Phys. Chem. A* **2002**, *106*, 8963.

61. Promega, CellTiter 96 Aqueous One Solution Cell Proliferation Assay, Technical Bulletin, 2012.

CHAPTER 3

BIODEGRADABLE CROSSLINKED POLYESTERS DERIVED FROM THIOMALIC ACID AND *S*-NITROSOTHIOL ANALOGUES FOR NITRIC OXIDE RELEASE

3.1 Synopsis

Crosslinked polyesters with Young's moduli similar to that of certain soft biological tissues were prepared *via* bulk polycondensation of thiomalic acid and 1,8-octanediol alone, and with citric or maleic acid. The copolymers were converted to nitric oxide (NO)-releasing *S*-nitrosothiol (RSNO) analogues by reaction with *tert*-butyl nitrite. Additional conjugation steps were avoided by inclusion of the thiolated monomer during the polycondensation to permit thiol conversion to RSNOs. NO release at physiological pH and temperature (pH 7.4, 37 °C) was determined by chemiluminescence-based NO detection. The average total NO content for poly(thiomalic-*co*-maleic acid-*co*-1,8-octanediol), poly(thiomalic-*co*-citric acid-*co*-1,8-octanediol), and poly(thiomalic acid-*co*-1,8-octanediol) was 130 ± 39 μmol g^{-1}, 200 ± 35 μmol g^{-1}, and 130 ± 11 μmol g^{-1}, respectively. The antibacterial properties of the *S*-nitrosated analogues were confirmed against *Escherichia coli* and *Staphylococcus aureus.* The hydrolytic degradation products were analyzed by time-of-flight mass spectrometry after a 10-week study to investigate their compositions. Tensile mechanical tests were performed on the non-nitrosated polymers as well as their *S*-nitrosated derivatives and suggested that the materials have appropriate Young's moduli and elongation values for biomedical applications. Figure 3.1 presents a summary of the project.

Reproduced from Yapor, J. P.; L.; Neufeld, B. H.; Tapia, J. B.; Reynolds, M. M. Biodegradable Crosslinked Polyesters Derived from Thiomalic Acid and *S*-nitrosothiol Analogues for Nitric Oxide Release. *J. Mater. Chem. B.* **2018**, *6*, 4071-4081 with permission from the Royal Society of Chemistry.

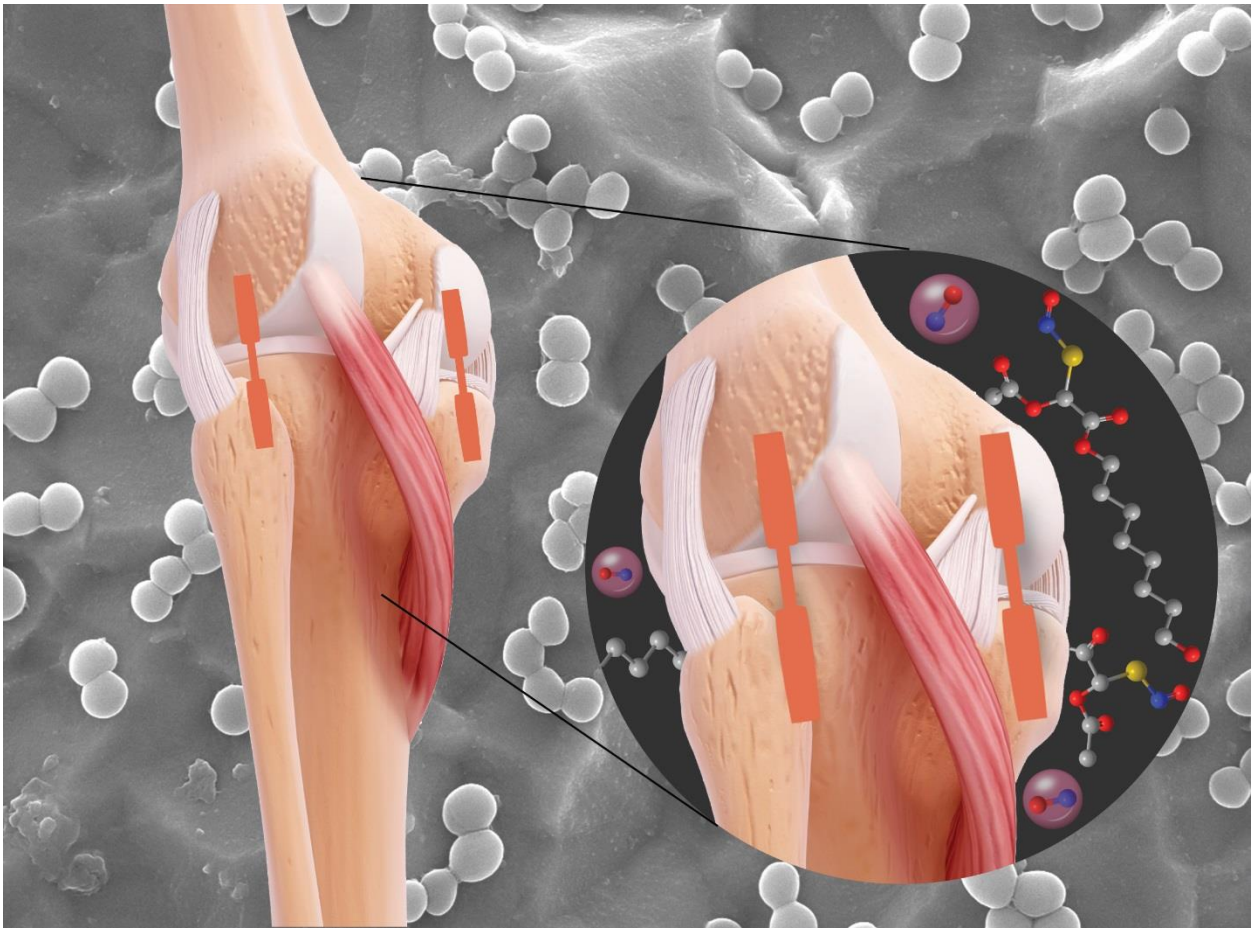

Figure 3.1 Selected cover artwork of the publishing journal. The image depicts the main findings of the study. Reproduced with permission from the Royal Society of Chemistry.

3.2 Introduction

Biodegradable polyesters have been extensively studied in the field of materials research due to their applications in drug delivery therapies, tissue engineering, and wound dressings.[1,2] Such polymers are of particular interest given the broad range of processing methods that can be utilized for their preparation, their hydrolytic degradation, and the ability to create modulus-matched materials.[3-5] Polyesters utilized for the preparation of biomaterials such as sutures and hernia meshes include poly(lactic acid) (PLA), poly(glycolic acid) (PGA), their copolymer poly(lactic-*co*-glycolic acid) (PLGA), and poly(ε-caprolactone) (PCL).[6] The limitations for their use as biomaterials, however, include lack of appropriate mechanical properties and adverse

reactions at the material interface. The latter phenomena may be caused by the interaction of the polymer with the surrounding biological environment, which may result in bacterial infection or the foreign body response.[7] An approach to mitigate or prevent the occurrence of these events is through the use of nitric oxide (NO) as a therapeutic agent.

Research in the field of biomedical devices has significantly advanced with the development of NO-releasing materials. This is due to the immense role that NO plays within biological systems, including antibacterial action, mitigation of the foreign body response, and prevention of platelet aggregation. Incorporation of NO donor groups such as *N*-diazeniumdiolates or *S*-nitrosothiols (RSNOs) into polymeric systems produce materials that release NO at physiological pH and temperature as a result of NO donor decomposition.[8] Such processes facilitate the use of materials in a unique drug delivery therapy that harnesses the benefits of NO for its delivery at a localized site. RSNOs are the most commonly used NO sources given their low toxicity and natural occurrence in the form of *S*-nitrosoalbumin and *S*-nitrosoglutathione.[9] RSNOs decompose through thermal, photolytic, or transition metal-catalyzed reactions to yield NO and the corresponding disulfide as expressed by the equation: $2RSNO \rightarrow 2NO + RSSR$.[10] Previous studies have reported the thermal and photolytic decomposition of RSNOs as a twofold process. The initial process is generally understood to involve homolytic cleavage of the S–N bond to form the radical species nitric oxide and a thiyl radical (NO• and RS•). The formation of the thiyl radical is followed by the dimerization of RS• to yield the disulfide RSSR.[11,12] Contrary to RSNOs, *N*-diazeniumdiolates decompose to form secondary amines. Such compounds have been reported to produce carcinogenic secondary *N*-nitrosamines as byproducts under oxygenated conditions.[13,14] Therefore, the use of RSNOs as NO donor groups provides a release pathway without the health risks associated with *N*-nitrosamines.

Prior research has extensively explored the preparation and use of NO-releasing polyester materials. Seabra *et al.* have reported the synthesis of NO-releasing polyesters from poly(ethylene glycol) and thiomalic acid. NO was coupled to the thiolated polyester by bubbling a mixture of NO/synthetic air through the liquid polyester. The *S*-nitrosated polyester was blended with poly(methyl methacrylate) (PMMA) and used to coat PMMA plates and stainless steel intracoronary stents. The films were shown to reduce platelet adhesion after their direct contact with whole blood, suggesting that the strategy could be used to improve blood compatibility and thrombogenicity of different medical devices. NO release from these materials was indirectly measured by the Griess assay, which monitors the formation of nitrite (NO_2^-) by spectrophotometric analysis.[15] The materials released 0.15 μmol g^{-1} of NO for approximately 24 h, at 37 °C.[16] Yang *et al.* developed hyperbranched polyesters with bis(hydroxymethyl)propionic acid in a similar fashion as the materials reported in this study through a one-pot reaction. However, the conjugation of a thiolated moiety was reported as an additional reaction. The *S*-nitrosation procedure was performed using sodium nitrite in hydrochloric acid. The influence of the thiol structure and the polymer scaffold were studied in terms of NO release. The measured NO payloads (2 μmol g^{-1}) for up to 20 h *via* chemiluminescence-based analysis were claimed to represent the largest level for a biodegradable material at the time of the study in 2016.[17]

Herein, we report the synthesis of *S*-nitrosated polyesters with NO-releasing properties. Three materials were prepared from the combination of various monomeric units such as thiomalic acid, citric acid, maleic acid, and 1,8-octanediol. The prepolymer was prepared *via* one-pot, melt phase polycondensation, with subsequent thermal curing to yield crosslinked products that can be processed into various morphologies for the desired application.[18,19] The synthetic route circumvents the use of additional coupling reactions for the covalent functionalization of the

material to yield a thiolated polymer, which is the prevailing method for the preparation of such materials. The crosslinked polyesters and their *S*-nitrosated analogues were the subject of bacterial studies in order to assess their antibacterial properties. *Escherichia coli* (*E. coli*) and *Staphylococcus aureus* (*S. aureus*) were exposed to the *S*-nitrosated materials as well as the non-nitrosated polymers, which were used as controls. The materials were found to be efficacious antibacterial agents, in their ability to successfully kill Gram-negative and Gram-positive bacteria strains, characteristic of broad-spectrum therapies. The degradation profiles at physiological pH and temperature were investigated by gravimetric analysis in order to establish material degradation. The degradation products of the polymers were analyzed by mass spectrometry to study the outcome of hydrolysis within the polymer chains. Tensile mechanical tests were conducted to analyze the mechanical properties of the materials and explore their potential applications based on the Young's modulus.

The optimization of mechanical properties for antibacterial polymeric substrates in conjunction with a more efficient synthetic route, have led to the development of materials with high tensile strain and promising applications for combating bacterial infection on damaged dermal tissue.[20,21] Figure 3.2 depicts a summary of the findings for this study.

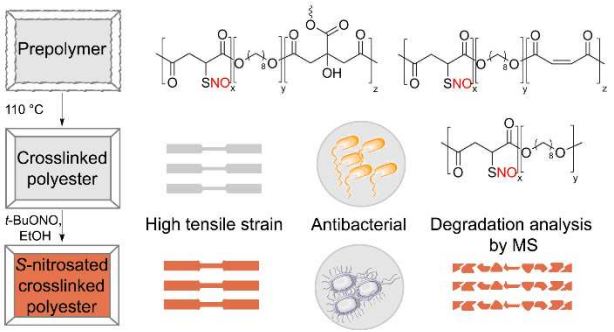

Figure 3.2 Summary of methods and results for *S*-nitrosated crosslinked polyesters and non-nitrosated analogues. Reproduced with permission from the Royal Society of Chemistry.

3.3 Materials and methods

3.3.1 Materials

Thiomalic acid (98%), citric acid (99.5%), maleic acid (98%), 1,8-octanediol (98%), and triethylamine (TEA) were obtained from Alfa Aesar (Ward Hill, MA, USA). *tert*-Butyl nitrite (*t*-BuONO, 90%) was purchased from Sigma-Aldrich (St. Louis, MO, USA). Tetrahydrofuran (THF) and anhydrous diethyl ether were purchased from Thermo Fisher Scientific (Pittsburgh, PA, USA). Phosphate buffered saline (PBS) tablets and anhydrous N,N-dimethylformamide (DMF) were procured from EMD Chemicals (Gibbstown, NJ, USA). DL-Dithiothreitol (DTT, 99%) was obtained from AMRESCO (Solon, OH, USA). Oxoid™ nutrient broth media (NBM, OXCM0001B), Oxoid™ nutrient agar (NA, OXCM0003B), and sodium chloride were purchased from Fisher Scientific (Fair Lawn, NJ, USA). 24-well tissue culture treated plates were obtained from Corning (Corning, NY, USA). *E. coli* (ATCC 25922) and *S. aureus* (ATCC 29213) were purchased from American Type Culture Collection (ATCC, USA). LC-MS grade methanol was purchased from VWR (Denver, CO, USA).

3.3.2 Characterization techniques

^{1}H NMR, ^{13}C NMR, homonuclear correlation spectroscopy (COSY) 2D NMR, and heteronuclear single quantum correlation (HSQC) 2D NMR spectra were obtained in dimethylsulfoxide-d_6 (DMSO-d_6) using an Agilent (Varian) Inova 400 MHz FT-NMR (Agilent Technologies, Inc., Santa Clara, CA, USA). FTIR-ATR spectra were recorded in the range of 650–4000 cm^{-1} using a Nicolet 6700 FTIR spectrometer (Thermo Electron Corporation, Madison, WI, USA). UV-Vis absorption studies were performed using a Nicolet Evolution 300 UV-Vis spectrophotometer (Thermo Electron Corporation). Polymer molecular weight was characterized

by gel permeation chromatography (GPC) in DMF using polystyrene standards with a Waters University 1500 GPC instrument (Waters, Milford, MA, USA). Thermal transitions were determined by differential scanning calorimetry (DSC) with a TA modulated 2920 DSC and the decomposition temperature was measured by thermogravimetric analysis (TGA) utilizing a TA thermogravimetric analyzer 2950 (TA Instruments, New Castle, DE, USA). Tensile mechanical tests were conducted based on ASTM standard D638 on an Instron 4442 mechanical tester equipped with a 50 N load cell (Instron, Norwood, MA, USA). Briefly, the dog-bone-shaped specimens were pulled at a rate of 100 mm/min. Values obtained from the stress-strain curves were used to calculate the Young's modulus and crosslinking density of each material.

Polymer degradation at physiological pH and temperature. Gravimetric analysis was performed to assess changes in weight after incubating the materials at physiological pH and temperature, which in turn confirmed the occurrence of hydrolytic degradation. Three different types of polyesters and their *S*-nitrosated analogues were incubated in 10 mM PBS (pH 7.4) at 37 °C for up to 10 weeks. Samples were collected every 7 days ($n = 3$), washed with Millipore water, and lyophilized for 24 h prior to measurement. For samples incubated longer than 1 week, the buffer solution was replaced at the end of each week.

Mass spectrometric identification of degradation products. The degradation products from the polymer degradation studies were identified using time-of-flight mass spectrometry (TOF-MS). All mass spectrometric analyses were performed on an Agilent 6224 TOF LC/MS (Agilent Technologies, Palo Alto, CA, USA). The instrument was equipped with an Agilent multimode ion (MMI) source capable of electrospray ionization (ESI) and atmospheric pressure chemical ionization (APCI). For all experiments, mixed-mode ionization in negative polarity was employed with the range of mass analysis set at 100–3200 *m/z*. The collected sample solutions

were directly introduced into the ion source by flow injection, without a pre-separation step, at a flow rate of 0.22 mL/min *via* the ESI nebulizer with methanol as the mobile phase ($n \geq 3$). The ion source conditions were as follows: capillary voltage, 2500 V; fragmentor voltage, 120 V; skimmer voltage, 60 V; charge voltage, 2000 V; drying gas temperature, 310 °C; drying gas flow rate (N_2), 10 L/min; and nebulizer pressure, 45 psig. All data were analyzed with Agilent MassHunter Qualitative Analysis B.07.00.

Chemiluminescence-based NO analysis. NO release from *S*-nitrosated crosslinked polyesters was evaluated using Sievers chemiluminescence NO analyzers (NOA 280i, GE Analytical, Boulder, CO, USA) following our previously reported procedure.[22] The instruments were calibrated prior to each analysis using nitrogen (zero gas) and 45 ppm NO/nitrogen. The nitrogen sweep gas flow during analysis was maintained at 200 mL min^{-1}. Total NO content was obtained by heating the polymer samples ($n \geq 3$) and appropriate controls at 150 °C in the absence of solvent followed by irradiation of light at 365 nm, which promoted the thermal and photodecomposition of the RSNO groups. The NO release from this process was used to quantify the amount of thermally and photo-releasable NO present in each material. In addition, NO release at physiological pH and temperature was determined. Polymer samples ($n \geq 3$) were suspended in deoxygenated 10 mM PBS (pH 7.4) at 37 °C, and NO release was measured for 6 to 20 h, depending on the release properties of the material. For the latter experiments, the samples were shielded from direct exposure to light to prevent further photodecomposition of the RSNO.

3.3.3 Synthesis of materials

Poly(thiomalic-*co*-maleic acid-*co*-1,8-octanediol (PTMO) (1). The polymer was prepared *via* melt-phase polycondensation reaction using thiomalic acid (4.31 g, 28.8 mmol),

maleic acid (2.90 g, 25.0 mmol), and 1,8-octanediol (7.31 g, 50.0 mmol). The polymerization was achieved without an exogenous catalyst and in the absence of solvent. The reagents were added to a vented 500 mL flask equipped with a nitrogen inlet and outlet. The mixture was stirred under nitrogen flow for 30 min, then heated to 140 °C with constant stirring to initiate the polycondensation. The colorless melted mass was maintained at 140 °C for 38 min under nitrogen flow to obtain a viscous polymer. The crude polymer was dissolved in absolute ethanol (40 mL) by sonication then treated with DTT (0.203 g, 1.31 mmol) and TEA (183 μL, 1.31 mmol) to reduce disulfide bonds formed during the reaction. The solution was stirred for 1 h then added over 30 min to Millipore water (200 mL) (18.2 MΩ·cm) containing Tween-80 to remove any unreacted materials. The mixture was stirred for 1 h at room temperature, then cooled at 4 °C for 1 h. The supernatant was decanted, and the polymer was washed twice with Millipore water (200 mL) and lyophilized for 7 days. After lyophilization, the prepolymer was characterized by various NMR techniques and GPC, to avoid solubility restraints caused by the following crosslinking procedure. A 20% (w/v) polymer solution in THF was prepared to cast films on a polytetrafluoroethylene (PTFE) mold, which was heated at 110 °C for 136 min under nitrogen flow to obtain a crosslinked material. The crosslinked polymer was used for the remaining characterization techniques stated previously. ^{1}H NMR δ_H/ppm (400 MHz, DMSO-d_6): 12.73 (–CO_2*H*), 6.67–6.73 (–*H*C=C*H*–), 3.94–4.07 (–OC*H*$_2$–), 3.72–3.89 (–S–C*H*–CO_2–), 3.32–3.35 (–C*H*$_2$OH), 2.58–2.91 (–C*H*$_2$$CO_2$–), 1.52–1.60 (–C*H*$_2$–$(CH_2)_4$–C*H*$_2$–), 1.34–1.39 (–C*H*$_2$–$CH_2$OH), 1.24 (–$(CH_2)_4$–). ^{13}C NMR δ_C/ppm (100 MHz, DMSO-d_6): 170.3–172.6 (–*C*O_2–), 130.4–133.6 (–H*C*=*C*H–), 64.8–65.5 (–C*H*$_2$OH), 61.2 (–O*C*H_2–), 41.9–42.0 (–S–*C*H–CO_2–), 35.9–37.1 (–*C*$H_2$$CO_2$–), 33.0 (–*C*$H_2$–$CH_2$OH), 29.0–29.3 (–$(CH_2)_2$–), 28.4–28.5 (–*C*$H_2$–$(CH_2)_4$–*C*$H_2$–), 25.7–25.9 (–$(CH_2)_2$–). IR υ_{max}/cm^{-1}: 3468–

2400 (O–H), 2929–2856 (C–H), 1725 (C=O) and 1159 (C–O). A synthetic scheme that illustrates the synthesis of PTMO and its *S*-nitrosated analog is given in Fig. 3.3.

***S*-nitrosated poly(thiomalic-*co*-maleic acid-*co*-1,8-octanediol) (PTMO–NO) (1a).** A mixture of crosslinked PTMO/ethanol (**1**) (25 mg/mL) and *t*-BuONO (0.250 mL) was stirred at room temperature for 20 min in a vial protected from light. The solvent was evaporated under vacuum for 2 h to obtain an *S*-nitrosated crosslinked material. Given that RSNOs decompose through thermal and photolytic pathways, all materials reported herein were stored at −20 °C in sealed vessels protected from light until further use. IR υ_{max}/cm^{-1}: 3468–2400 (O–H), 2930–2856 (C–H), 1725 (C=O) and 1159 (C–O). UV-Vis λ_{max}/nm: 335 (RSNO, $\pi \rightarrow \pi^*$) and 544 (RSNO, $n_N \rightarrow \pi^*$).

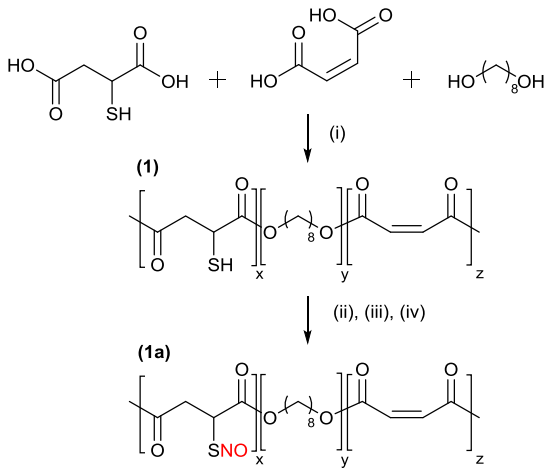

Figure 3.3 Synthesis of PTMO (**1**) and and *S*-nitrosated PTMO (**1a**). (i) 140 °C, 38 min, (ii), DTT, TEA, 1 h, (iii) 110 °C, 136 min, (iv) *t*-BuONO, EtOH, 20 min. Reproduced with permission from the Royal Society of Chemistry.

Poly(thiomalic-*co*-citric acid-*co*-1,8-octanediol) (PTCO) (2). A polyester was prepared following the general method provided for material **1** using thiomalic acid (2.19 g, 14.3 mmol), citric acid (2.40 g, 12.5 mmol), and 1,8-octanediol (3.66 g, 25.0 mmol). The polycondensation reaction was performed at 140 °C for 1 h under nitrogen flow to obtain a viscous polymer. The

viscous polymer was dissolved in absolute ethanol (20 mL) by sonication and treated with DTT (0.107 g, 0.69 mmol) and TEA (96.6 μL, 0.690 mmol). The prepolymer was characterized by NMR techniques and GPC given that the crosslinking procedure renders the material insoluble. Films were casted on PTFE molds using a 20% (w/v) polymer solution in THF. Films were dried at RT, then heated at 110 °C for 24 h under nitrogen flow to obtain a crosslinked material. The crosslinked polymer was used for the remaining characterization techniques. ^{1}H NMR δ_H/ppm (400 MHz, DMSO-d_6): 5.56 (–C–O*H*), 3.93–4.07 (–OCH_2–), 3.58–3.69 (–S–C*H*–CO_2), 3.32–3.36 (–CH_2OH), 2.61–2.91 (–CH_2CO_2–), 1.51–1.53 (–CH_2–$(CH_2)_4$–CH_2–), 1.36–1.39 (–CH_2–CH_2OH), 1.25 (–$(CH_2)_4$–). ^{13}C NMR δ_C/ppm (100 MHz, DMSO-d_6): 169.6–174.9 (–CO_2–), 72.9–73.3 (–*C*–OH), 64.4–65.3 (–O*C*H_2–), 61.2 (–*C*H_2OH), 41.9–42.0 (–*C*H_2CO_2–), 35.8–35.9 (–S–*C*H–CO_2–), 33.0 (–$(CH_2)_2$–), 28.4–28.5 (–*C*H_2–$(CH_2)_4$–*C*H_2–), 25.6–25.9 (–$(CH_2)_2$–). IR υ_{max}/cm^{-1}: 3494–2400 (O–H), 2928–2855 (C–H), 1725 (C=O), 1167 (C–O). A synthetic scheme that depicts the synthesis of PTCO and *S*-nitrosated PTCO is given in Fig. 3.4.

***S*-nitrosated poly(thiomalic-*co*-citric acid-*co*-1,8-octanediol) (PTCO–NO) (2a).** Crosslinked PTCO was *S*-nitrosated following the general procedure for **1a**. PTCO/ethanol (**2**) (25 mg/mL) and *t*-BuONO (0.250 mL) was stirred for 20 min, followed by solvent evaporation for 2 h under vacuum. IR υ_{max}/cm^{-1}: 3468–2400 (O–H), 2930–2856 (C–H), 1727 (C=O), 1167 (C–O). UV-Vis λ_{max}/nm: 331 (RSNO, $\pi \rightarrow \pi^*$) and 544 (RSNO, $n_N \rightarrow \pi^*$).

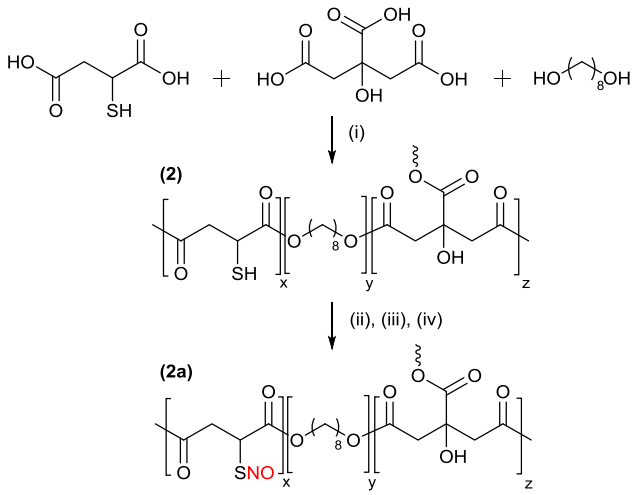

Figure 3.4 Synthesis of PTCO (**2**) and *S*-nitrosated PTCO (**2a**). (i) 140 °C, 1 h, (ii), DTT, TEA, 1 h, (iii) 110 °C, 24 h, (iv) *t*-BuONO, EtOH, 20 min. Reproduced with permission from the Royal Society of Chemistry.

Poly(thiomalic acid-*co*-1,8-octanediol) (PTO) (3). The material was synthesized following the procedure for polymer **1** using thiomalic acid (3.99 g, 26.6 mmol) and 1,8-octanediol (3.89 g, 26.6 mmol). The reaction mass was maintained at 140 °C for 17 h under nitrogen flow to obtain a viscous polymer. The crude polymer was dissolved in ethyl ether anhydrous (20 mL) by sonication and treated with DTT (0.104 g, 0.68 mmol) and TEA (94.4 μL, 0.68 mmol). The prepolymer was characterized by NMR and GPC before the crosslinking step to avoid solubility restraints. Layers of a 20% (w/v) polymer solution in THF were casted on PTFE molds for the film preparation. After the solvent evaporated, the molds were heated at 110 °C for 82 h under nitrogen flow to obtain a flexible polyester. The crosslinked polymer was used for the remaining characterization techniques. ^{1}H NMR δ_H/ppm (400 MHz, DMSO-d_6): 3.94–4.06 (–OC*H*$_2$–), 3.66–3.70 (–S–C*H*–CO$_2$–), 2.71–2.91 (–C*H*$_2$CO$_2$–), 1.57 (–C*H*$_2$–(CH$_2$)$_4$–C*H*$_2$–), 1.25–1.30 (–(C*H*$_2$)$_4$–). ^{13}C NMR δ_C/ppm (100 MHz, DMSO-d_6): 170.4–173.7 (–*C*O$_2$–), 64.7–65.2 (–O*C*H$_2$–), 39.8 (–*C*H$_2$CO$_2$–), 35.9–36.1 (–S–*C*H–CO$_2$–), 29.0 (–*C*H$_2$–(CH$_2$)$_4$–*C*H$_2$–), 28.4–28.5 (–(*C*H$_2$)$_2$–), 25.6–

25.7 (–(CH_2)$_2$–). IR υ_{max}/cm^{-1}: 3544–2400 (O–H), 2930–2856 (C–H), 1727 (C=O), 1158 (C–O). The synthetic scheme for the synthesis of PTO and its *S*-nitrosated analog is given in Fig. 3.5.

***S*-nitrosated poly(thiomalic acid-*co*-1,8-octanediol) (PTO–NO) (3a).** The general method provided for material **1a** was followed for the preparation of PTO–NO with a variation in solution concentration. PTO/ethanol (**3**) (12.5 mg/mL) and *t*-BuONO (0.250 mL) was stirred for 20 min followed by solvent removal under vacuum for 7.3 h. IR υ_{max}/cm^{-1}: 3544–2400 (O–H), 2927–2900 (C–H), 1728 (C=O), 1159 (C–O). UV-Vis λ_{max}/nm: 333 (RSNO, $\pi \rightarrow \pi^*$) and 540 (RSNO, $n_N \rightarrow \pi^*$).

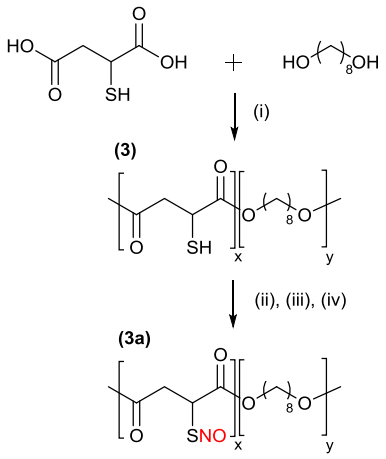

Figure 3.5 Synthesis of PTO (**3**) and *S*-nitrosated PTO (**3a**). (i) 140 °C, 17 h, (ii), DTT, TEA, 1 h, (iii) 110 °C, 82 h, (iv) *t*-BuONO, EtOH, 20 min. Reproduced with permission from the Royal Society of Chemistry.

3.3.4 Bacteria studies

***E. coli* and *S. aureus* bacteria culture.** Initial stock cultures of *E. coli and S. aureus* were obtained by streaking agar plates and inoculating the bacteria in nutrient broth. The stock culture was grown overnight in NBM to an O.D.$_{600nm}$ ~1.0. The bacterial solution was then combined with glycerol (30% v/v) in a 1:1 fashion to obtain a final glycerol concentration of 15% (v/v). These solutions were stored at −80 °C until further use. Prior to each bacterial assay, a 10 mL frozen culture was allowed to thaw at room temperature and centrifuged at 4700 rpm for 10 min. The

supernatant was discarded and the pellet was resuspended in 5 mL warmed NBM. The solution was transferred to an additional 45 mL NBM and allowed to grow overnight in a 37 °C incubator under stirring conditions until the $O.D_{600nm}$ reached ~1.0. The following day, the culture was diluted using NBM to a working concentration corresponding to an $O.D._{600nm}$ ~0.35.

Antibacterial activity of polyesters. Samples of both non-nitrosated and *S*-nitrosated polymer (50 mg) were added to 24-well plates in triplicate before the addition of bacterial solution (1 mL). The plate was placed in a 37 °C incubator for 6 or 24 h under shaking conditions before 100 μL aliquots were removed from each well and 10-fold serial dilutions were performed in sterilized saline solution (0.85% w/v NaCl). After dilution, 50 μL aliquots were plated on agar before being placed in a 37 °C incubator. The number of colony-forming units (CFU) were counted the following day and converted to CFU/mL for comparison to positive control (bacteria solution in the absence of polymer samples). All samples were tested in replicate ($n \geq 6$).[23-25]

3.4 Results and discussion

Three polyesters, PTMO, PTCO and PTO were synthesized from a combination of thiomalic acid, citric acid, maleic acid, and 1,8-octanediol following a modified literature protocol to yield crosslinked polyesters.[16,26] In particular, thiomalic acid was included in order to avoid the use of coupling reactions to incorporate the thiol moiety. These thiol pendant groups serve as functionalization sites to form RSNOs**.** The naturally-occurring monomer, citric acid, was utilized given its trifunctional connectivity, its well-studied hemocompatibility, and use in devices for drug delivery and cardiac-tissue engineering. Maleic acid was a relevant monomer to potentially increase the crosslinking density of the material through the alkene. Lastly, 1,8-octanediol enabled the formation of ester linkages and increased the hydrophobicity of materials**.**[27]

The structure of each material was independently confirmed by ^{1}H NMR and ^{13}C NMR. (Fig. B.1–B.6). The connectivity of the monomeric units was determined by two-dimensional NMR experiments such as COSY and HSQC spectroscopy (Fig. B.7–B.12). For all materials, the multiplets at 2.58–2.91 and 3.58–3.89 ppm correspond to thiomalic acid, while peaks at 1.24–1.60 and 3.93–4.07 ppm confirmed incorporation of 1,8-octanediol. For PTCO, the singlet at 5.56 ppm corresponds to citric acid. For PTMO, the doublets at 6.67–6.73 ppm represent the available alkenes of maleic acid and the occurrence of isomerization.

According to 2D NMR techniques, the carbons from 25.6–29.3 ppm have correlation with protons at 1.25–1.57 ppm. The atoms correspond to the inner carbons of 1,8-octanediol as they have correlations within each other and with protons at 3.96–4.06 ppm, which represent the outer 1,8-octanediol atoms adjacent to the ester linkages with carbons at 64.4–65.5 ppm. Thiomalic acid protons were detected at 2.71–2.91 ppm with homonuclear correlations at 3.66–3.70 ppm, and heteronuclear correlations at 35.8–42.0 ppm. The features are similar for all materials, with additional correlations for PTMO at 3.32–3.35 ppm with homonuclear correlations at 1.34–1.39 ppm and heteronuclear correlations at 64.8–65.5 ppm. Comparable correlations were found for PTCO at 3.32–3.36 ppm with homonuclear correlations at 1.36–1.39 ppm, and heteronuclear correlations at 61.2 ppm. The signals represent 1,8-octanediol protons on carbons bearing terminal hydroxyl groups, which indicate the presence of oligomers given that the step-growth polycondensation was stopped in order to characterize the prepolymers.[28] Protons at 6.67–6.73 ppm represent sp^2 hybridized maleic acid carbons, with heteronuclear correlations at 129–132 ppm. For PTCO, the multiplet at 2.61–2.91 ppm corresponds to protons from thiomalic and citric acid, with homonuclear correlations at 3.6 ppm and heteronuclear correlations at 35.8–35.9 and 41.9–42.0 ppm. The results and their interpretation were consistent with ^{1}H NMR and ^{13}C NMR spectra

of similar polyesters.[29-31] No features developed that could be attributable to the formation of thioester species, which typically result in features at 195 ppm.[32] The FTIR-ATR spectra (shown in Fig. B.13–B.15) feature ester carbonyl stretches at approximately 1700 cm^{-1}, which confirm the presence of ester linkages between the monomers. The contribution of carbonyl groups C=O stretching to the sharp feature at 1700 cm^{-1} supported the presence of ester linkages in the materials.[33]

GPC analysis with polystyrene standards indicated that the prepolymers had a number average molecular weight (M_n) higher than that of previously reported prepolymers (<1000 g mol^{-1}) with similar characteristics such as NO release and degradability.[34] This suggests that other prepolymers have been characterized at earlier stages of the polymerization, and the final properties of the materials such as Young's modulus may be more informative for comparison. The glass transition temperature (T_g) of these materials is comparable to that of previously reported materials, except PTO, which reached lower values. A decrease in T_g can be attributed to the presence of oligomeric or monomeric components that function as plasticizers.[35] Ideal T_g values for the applications intended would be below physiological temperature, the results confirm that this was achieved for all materials. In this case, the longer polymerization times increased the molecular weight of the material and reduced the T_g and the number of different sized oligomers, which can be deduced from the dispersity index ($Đ$).[36] The prepolymers were characterized by GPC instead of the crosslinked polymers due to solubility restraints. Hence, the value for $Đ$ deviates from unity given that the polymerization reaction had not reached completion at the stage of GPC analysis in order to obtain a soluble material. The crystallization temperature (T_c) and melting temperature (T_m) were identified, which denote that the materials are not completely amorphous and crystalline regions were detected.[37] The values were similar for all materials where

T_c ranged from 73.2–73.9 °C, and T_m ranged from 83.1–84.0 °C. All thiolated polyesters were flexible, colorless, transparent materials, which would be the preferred characteristics for the preparation of certain devices.

Thermal transitions, degradation profiles and the crosslinking density of the polyesters were influenced by the reaction time and the monomeric units employed for the synthesis of each material. The increased functionality of each monomer gave rise to more crosslinked polyesters. The crosslinking density and Young's modulus was inversely proportional to the elongation at break of the specimens. The exception to the tendency occurred with PTMO, which had relatively high elongation at approximately 300% and high Young's modulus and crosslinking density. Such finding suggests that the alkene-bearing monomer, maleic acid, increased the crosslinking density of the material without affecting the final elongation. The degradation time and thermal transitions were also proportional, as it was determined that the materials with lower T_g values were less prone to hydrolytic degradation. The results have comparable trends to those reported by Coneski *et al*.[34]

3.4.1 Synthesis and characterization of poly(thiomalic-*co*-maleic acid-*co*-1,8-octanediol)

The catalyst-free polycondensation was carried out in the melt-phase at 140 °C for 38 minutes with a constant nitrogen flow to remove water, and the structure of PTMO was independently confirmed by ^{1}H NMR, ^{13}C NMR, COSY 2D NMR, and HSQC 2D NMR (Fig. B.1, B.4, B.7, and B.10), consistent with previous reports.[29,38] The ^{1}H NMR spectrum shows multiplets at 2.58–2.91 (–C*H*$_2$CO$_2$–) and 3.72–3.89 ppm (–S–C*H*–CO$_2$–) that correspond to the protons on thiomalate units, while peaks at 1.24 (–(C*H*$_2$)$_4$–), 1.34–1.39 (–C*H*$_2$–CH$_2$OH), 1.52–1.60 (–C*H*$_2$–(CH$_2$)$_4$–C*H*$_2$–), 3.32–3.35 (–C*H*$_2$OH), and 3.94–4.07 (–OC*H*$_2$–) ppm confirm the incorporation of 1,8-octanediol. The split alkenyl protons of the maleate group appeared at 6.67–6.73 (–*H*C=C*H*–)

ppm. The broad feature at 12.73 (–CO_2H) ppm is attributed to the remaining free carboxyl groups from thiomalate units. Assignment of peaks on the ^{1}H NMR spectrum was confirmed by recording the proton correlations with COSY 2D NMR. ^{13}C NMR spectrum represents the different carbon environments present in the polymer, which were assigned by noting the protons bonded to carbons using HSQC 2D NMR. The carbon spectrum demonstrates peaks at 25.7–25.9 (–(CH_2)$_2$–), 28.4–28.5 (–CH_2–(CH_2)$_4$–CH_2–), 29.0–29.3 (–(CH_2)$_2$–), 33.0 (–CH_2–CH_2OH), 61.2 (–OCH_2–), and 64.8–65.5 (–CH_2OH) ppm that correspond to 1,8–octanediol, while peaks at 35.9–37.1 (–CH_2CO_2–), 41.9–42.0 (–S–CH–CO_2–), and 170.3–172.6 (–CO_2–) ppm are attributed to thiomalate carbons. The sp^2 hybridized carbons at 130.4–133.6 ppm (–CH=CH–) represent the incorporation of maleate units in the material. The FTIR-ATR spectrum features an ester carbonyl (C=O) stretching band at 1726 cm^{-1}, which confirmed the ester linkages between the monomer. GPC analysis of the prepolymer demonstrated a M_n of 95.8 kDa and a $Đ$ of 2.72. The dispersity index demonstrated that the material contains different sized oligomers. As determined by TGA, the decomposition temperature of the crosslinked polymer was 352.8 °C. Thermal transitions were analyzed by DSC, where it was established that the T_g was -4.18 °C.

3.4.2 Synthesis and characterization of poly(thiomalic-*co*-citric acid-*co*-1,8-octanediol)

The ^{1}H NMR spectrum shows multiplets at 2.61–2.91 (–CH_2CO_2–) attributed to the protons on the citrate and thiomalate units and at 3.58–3.69 (–S–C*H*–CO_2) ppm that corresponds to the protons on the thiomalate units. The peaks at 1.25 (–(CH_2)$_4$–), 1.36–1.39 (–CH_2–CH_2OH), 1.51–1.53 (–CH_2–(CH_2)$_4$–CH_2–), 3.32–3.36 (–CH_2OH), and 3.93–4.07 (–OCH_2–) ppm confirm the incorporation of 1,8-octanediol. The singlet at 5.56 (–C–O*H*) ppm represents the hydroxyl group on the citrate unit (Fig. B.2). ^{13}C NMR spectrum (depicted in Fig. B.5) represents the

different carbon environments present in the polymer, which were assigned by noting the nuclear correlations using COSY and HSQC 2D NMR (Fig. B.8 and B.11). The carbon spectrum demonstrates peaks at 25.6–25.9 (–(CH$_2$)$_2$–), 28.4–28.5 (–CH$_2$–(CH$_2$)$_4$–CH$_2$–), 33.0 (–(CH$_2$)$_2$–), 61.2 (–CH$_2$OH), and 64.4–65.3 (–OCH$_2$–) ppm that correspond to 1,8–octanediol, while peaks at 35.8–35.9 (–S–CH–CO$_2$–), 41.9–42.0 (–CH$_2$CO$_2$–), and 169.6–174.9 (–CO$_2$–) ppm are attributed to thiomalate carbons. The signal at 72.9–73.3 (–C–OH) ppm represents the incorporation of citrate units in the material. The FTIR-ATR spectrum features an ester carbonyl C=O stretching band at 1726 cm^{-1}, which confirmed the ester linkages between the monomer (Fig. B.14,). GPC analysis with polystyrene standards showed a M_n of 130 kDa and a $Đ$ of 2.53. The crosslinked polymer was used for TGA and DSC where it was established that the decomposition temperature was 322.0 °C and the T_g was −23.7 °C. The T_g value was lower given that the material was able to reach a higher crosslinking density due to the trifunctional monomer, citric acid.[36]

3.4.3 Synthesis and characterization of poly(thiomalic acid-*co*-1,8-octanediol)

The material had higher linearity compared to the other polyesters due to the absence of functional groups that permit a higher crosslinking density to be reached.[37] However, the thiol moiety on thiomalic acid provided some crosslinking sites, which increased the Young's modulus of the material. The ^{1}H NMR spectrum shows multiplets at 2.71–2.91 (–CH_2CO$_2$–) and 3.66–3.70 (–S–CH–CO$_2$–) ppm that correspond to the protons on thiomalate units, while peaks at 1.25–1.25–1.30 (–(CH_2)$_4$–), 1.57 (–CH_2–(CH$_2$)$_4$–CH_2–) and 3.96–4.06 ppm (–OCH_2–) confirm the incorporation of 1,8-octanediol (Fig. B.3). ^{13}C NMR spectrum (shown in Fig. B.6) represents the different carbon environments present in the polymer, which were confirmed by COSY and HSQC 2D NMR experimental techniques (Fig. B.9 and B.12). The carbon spectrum demonstrates peaks

at 25.6–25.7 (–(CH$_2$)$_2$–), 28.4–28.5 (–(CH$_2$)$_2$–), 29.0 (–CH$_2$–(CH$_2$)$_4$–CH$_2$–), and 64.7–65.2 (–OCH$_2$–) ppm that correspond to 1,8–octanediol, while peaks at 35.9–36.1 (–S–CH–CO$_2$–), 39.8 (–CH$_2$CO$_2$–), and 170.4–173.7 (–CO$_2$–) ppm are attributed to thiomalate carbons. The FTIR-ATR spectrum features an ester carbonyl (C=O) stretching band at 1727 cm^{-1}, which confirmed the ester linkages between the monomer, while the contribution of thiomalic acid (S–H) broad feature at 2557 cm^{-1} supported the preservation of free thiol groups for further functionalization into RSNOs (Fig. B.15). Opposite to PTMO and PTCO, a resonance feature was observed for the thiol groups given that only two monomeric units were used for PTO. Therefore, the molar ratio of thiols to other functional groups is greater in this case. GPC analysis with polystyrene standards showed a M_n of 412 kDa and a $Đ$ of 1.77. The larger molecular weight of this material is attributed to the longer reaction time, as well as the higher linearity that prevents crosslinking at various sites and elongates the polymer chains. The crosslinking procedure was performed for 82 h at 110 °C, which gave rise to a highly elastic material with a low crosslinking density. The crosslinked polymer was used to determine thermal properties using TGA and DSC. The decomposition temperature was 346.9 °C and the T_g was −33.5 °C. Minor degradation was measured over a 10-week experiment at physiological pH and temperature. The lack of degradation may be attributed to the increased hydrophobicity of the polymer chains due to the higher monomeric ratio of 1,8-octanediol to thiomalic acid in the material.

3.4.4 Synthesis and characterization of *S*-nitrosated poly(thiomalic-*co*-maleic acid-*co*-1,8-octanediol), *S*-nitrosated poly(thiomalic-*co*-citric acid-*co*-1,8-octanediol), and *S*-nitrosated poly(thiomalic-*co*-maleic acid-*co*-1,8-octanediol)

S-Nitrosation of the thiol-bearing polyesters was carried out in ethanol under anhydrous conditions using the alkyl nitrite, *t*-BuONO, as a nitrosating agent. The procedure exposes the material to milder conditions in comparison to other procedures. In addition, it avoids the use of sodium nitrite in aqueous acid that could lead to parallel hydrolysis of the polymeric ester linkages, and permits removal of unreacted *t*-BuONO and volatile products under vacuum. The conversion of thiol groups to the corresponding RSNO was supported by UV-Vis spectrophotometry in DMSO, where absorptions characteristic to RSNOs were observed at 335 ($\pi \rightarrow \pi^*$) and 544 nm ($n_N \rightarrow \pi^*$) for PTMO–NO, at 331 and 544 nm for PTCO–NO, and at 333 and 540 nm for PTO (Fig. B.16–B.18). No features developed that could be attributable to the formation of undesirable alkyl nitrite species, which typically result in distinctive absorptions in the range of 260–400 nm.[39] The FTIR-ATR of *S*-nitrosated materials indicated the preservation of the primary structural features of the polyester with bands at 3500–2400 (O–H), 2933–2857 (C–H), 1729 (C=O), and 1160 (C–O) cm^{-1} for PTMO–NO were consistent with those of the non-nitrosated polyester. These features appeared at 3500–2400 (O–H), 2933–2857 (C–H), 1729 (C=O), 1160 (C–O) cm^{-1} for PTCO–NO, and at 3500–2400 (O–H), 2989–2900 (C–H), 1727 (C=O), 1158 (C–O) cm^{-1} for PTO–NO (Fig. B.13–B.15).

The total NO content of the materials was quantified using real-time chemiluminescence-based detection of NO. Samples were heated at 150 °C followed by irradiation of light at 365 nm in a custom glass vessel with constant flow of nitrogen.[40] This process leads to the thermal and photo-decomposition of RSNO groups resulting in the quantifiable release of NO. The moles of

NO released per gram of material were calculated using a calibration constant obtained from known concentrations of NO. The experiments continued until the NO release was equivalent to the baseline (Table 3.1).

Table 3.1 Summarized NO data for PTMO–NO, PTCO–NO and PTO–NO. All samples were tested in replicate ($n \geq 3$) and results are reported as the mean ± standard deviation.

Material	Cumulative NO release[a] (μmol g^1)	Total NO content[b] (μmol g^{-1})
PTMO–NO (**1a**)	90 ± 20	130 ± 39
PTCO–NO (**2a**)	80 ± 15	200 ± 35
PTO–NO (**3a**)	30 ± 6	130 ± 11

[a] Release measured at pH 7.4, 37 °C in 10 mM PBS. [b] Values determined by NO analysis through thermal decomposition of the RSNO at 150 °C.

Experiments were performed in triplicate for all materials, and it was calculated that PTMO–NO had the highest cumulative NO release normalized by mass at physiological pH and temperature 90 ± 20 μmol g^{-1}, followed by PTCO–NO 80 ± 15 μmol g^{-1}, and PTO–NO 30 ± 6 μmol g^{-1}. The materials released NO for different periods of time; PTCO–NO released for 20 h, PTO–NO for 12 h, and PTMO–NO for more than 6 h. A potential reason for the time variation of NO release is the degradation of the materials. As seen in Fig. 3.6, the NO release time follows a similar trend as the degradation at physiological pH and temperature, where PTCO–NO degraded the slowest followed by PTO–NO and PTMO–NO. Thus, the material susceptibility for hydrolytic degradation influenced the NO release time. Of note, the concentration of the solution used for the *S*-nitrosation reaction (*t*-BuONO in ethanol) could be decreased to obtain NO values that lie within the range for the intended application. The thiol-bearing polyesters produced by Seabra *et al*. have been reported to release NO at lower concentrations (0.15 μmol g^{-1}) for approximately 24 h at 37 °C as calculated with the Griess assay. The *S*-nitrosation procedure varied in this case since NO gas was bubbled through the liquid polyester. The preparation of films using PMMA in acetonitrile

after the *S*-nitrosation procedure may have lowered the amount of releasable NO, since the solvent was allowed to evaporate at 10 °C for 12 h.[16] In a different study with thiolated polyesters, RSNOs were formed *via* exposure to aqueous solutions of acidified nitrite. The total NO release at near physiological conditions in $CuBr_2$ supplemented PBS solution ranged from 1.60–1.97 μmol g^{-1}.[17] While the intended application for the latter materials may differ from those reported herein, it is noteworthy that higher NO payloads were achieved by our methods.

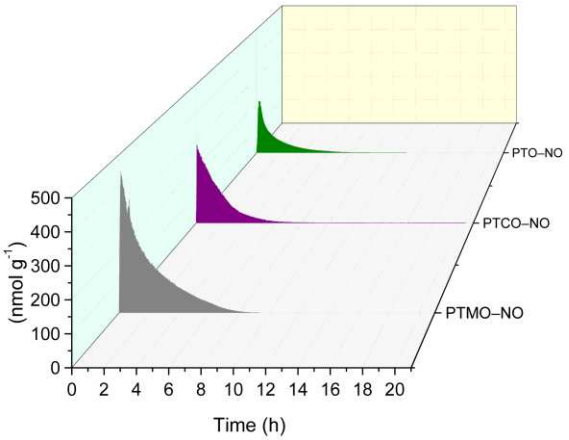

Figure 3.6 Representative real-time NO release profiles for PTMO–NO, PTCO–NO, PTO–NO under aqueous conditions (pH 7.4, 37 °C). Reproduced with permission from the Royal Society of Chemistry.

3.4.5 Polymer degradation at physiological pH and temperature

The potential biodegradability of the polymers was assessed by immersing samples (n = 3) of PTMO, PTMO–NO, PTCO, PTCO–NO, PTO, and PTO–NO in 10 mM PBS buffer (pH 7.4) at 37 °C in the absence of light for up to 10 weeks (Fig. 3.7). The results indicated a fast degradation for PTMO and PTMO–NO during the 10-week experiment. PTMO had a remaining mass percent of 33 ± 18 % and PTMO–NO had 7 ± 4 %. PTCO and PTCO–NO demonstrated a slower degradation under these conditions, where the mass percent remaining for PTCO was 90 ± 1 % and PTCO–NO had 86 ± 3 % mass remaining. For the previously mentioned polymers, hydrolytic degradation lead to the fragmentation of crosslinked polymer chains. The polymer with the higher

linearity, PTO, was not significantly degraded after the experiment concluded with a remaining mass percent of 97 ± 0.05 %. However, PTO–NO degraded slowly after the first week, but retained 88 ± 0.9 % of its mass at the end of the experiment. In all cases, the *S*-nitrosated material had a more rapid degradation that the unmodified material. The results suggest that *S*-nitrosated polymers have a lower molecular weight caused by the *S*-nitrosation methodology. It was not possible to measure the molecular weight of *S*-nitrosated polymers due to their impaired solubility after the functionalization procedures. The outcome indicates that, even though disulfide bonds were formed as byproducts of NO release, the formation of such bonds did not improve the robustness of the materials in aqueous conditions. However, potential crosslinking from disulfide formation does not offset the cleavage of ester linkages. The finding suggests that the process of disulfide formation is not particularly relevant for the stability of these systems. Also, it insinuates that the reaction conditions used for the *S*-nitrosation reaction mildly modify the polymer backbone, which leads to a faster degradation.

The alkene bearing polymer, PTMO and PTMO–NO, demonstrated the highest degradation rates of the materials that were the subject of these experiments. PTCO and its *S*-nitrosated analogue had a slower degradation than PTMO and PTMO–NO. This behavior can be attributed to the trifunctional monomer, citric acid, which provides additional reaction sites and allows for a higher crosslinking density. PTO and PTO–NO had the slowest degradation, according to the gravimetric techniques utilized. Degradation time was determined to be proportional to the polymerization and crosslinking time for each material as well as the T_g. Hence, the materials that underwent longer polymerization times did not readily degrade during the 10-week experiment. As studied using GPC, the materials contain oligomers of various molecular weights that allow the polymer chains to produce smaller fragmented sections. The most significant mass loss

occurred during the first week, which suggests that the bulk material readily releases oligomeric species upon immersion in PBS solution. The slow degradation combined with NO release at physiologically relevant levels suggest that the polymers may have potential applications as materials for wound dressings. The initial release of NO would prevent the risk of bacterial infection, while the slow degradation of the material would allow the materials to remain in place and provide moisture to the regenerating dermal tissue.[41]

Prior studies with non-nitrosated polyesters report degradation profiles that indicate mass remaining percentages from 0% to 90% with various combinations of the monomeric units such as adipic acid, glutaric acid, glycerol and pentaerythritol.[34] The composition of the materials based on the functionality of the monomers and crosslinking times and temperature were related to the degradation profiles. The study suggests that materials synthesized at higher temperatures and with a certain monomer combination, generally demonstrate slower hydrolytic degradation, which is in agreement with our findings.

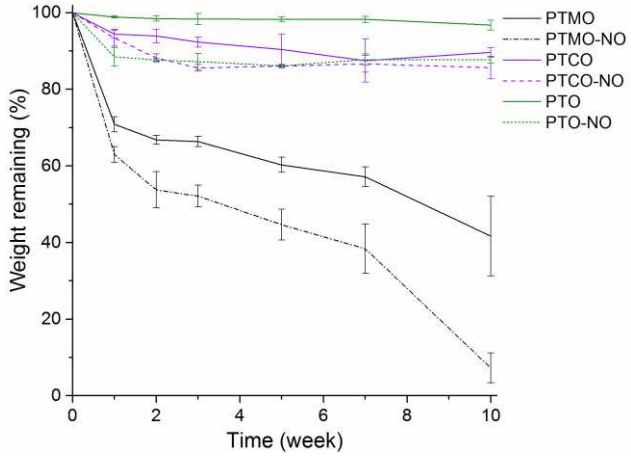

Figure 3.7 Degradation profiles of PTMO, PTCO, PTO and *S*-nitrosated derivatives at physiological pH and temperature (pH 7.4, 37 °C). Each data point represents an average of $n \geq 3$ replicates and the standard deviation. Reproduced with permission from the Royal Society of Chemistry.

3.4.6 Time-of-flight mass spectrometric identification of polymer degradation products

The degradation products found for PTO and PTO–NO were PTO-P1 ($C_{12}H_{20}O_5$), PTO-P2 ($C_{12}H_{22}O_5S$), PTO-P3 ($C_{16}H_{26}O_9S$) and PTO-P4 ($C_{24}H_{42}O_{10}S$). The degradation products found for PTMO and PTMO-NO were PTMO-P1 ($C_{12}H_{20}O_5$), PTMO-P2 ($C_{12}H_{22}O_5S$), PTMO-P3 ($C_{16}H_{26}O_9S$) and PTMO-P4 ($C_{24}H_{42}O_{10}S$). The degradation products for PTCO and PTCO–NO were PTCO- P1 ($C_{12}H_{20}O_5$), PTCO-P2 ($C_{12}H_{22}O_5S$), PTCO-P3 ($C_{14}H_{24}O_8$), PTCO-P4 ($C_{16}H_{26}O_8S_2$), PTCO-P5 ($C_{18}H_{28}O_{11}S$), PTCO-P6 ($C_{26}H_{44}O_{12}S$), and PTCO-P7 ($C_{12}H_{22}O_5$). The measured masses and formulas for each degradation product are shown in Table 3.2.

Table 3.2 TOF-MS identification of polymer degradation products.

Label	Formula	Molecular weight $[M-H]^-$
PTMO-P1*‡	$C_{12}H_{20}O_5$	243.1254
PTMO-P2‡	$C_{12}H_{22}O_5S$	277.1138
PTMO-P3*	$C_{16}H_{26}O_9S$	393.1246
PTMO-P4*	$C_{24}H_{42}O_{10}S$	521.2452
PTCO-P1‡	$C_{12}H_{20}O_5$	243.1245
PTCO-P2‡	$C_{12}H_{22}O_5S$	277.1131
PTCO-P3	$C_{14}H_{24}O_8$	319.1285
PTCO-P4	$C_{16}H_{26}O_8S_2$	409.1006
PTCO-P5	$C_{18}H_{28}O_{11}S$	451.1290
PTCO-P6	$C_{26}H_{44}O_{12}S$	579.2487
PTCO-P7*†	$C_{12}H_{22}O_5$	245.1407
PTO-P1*‡	$C_{12}H_{20}O_5$	243.1253
PTO-P2‡	$C_{12}H_{22}O_5S$	277.1120
PTO-P3*	$C_{16}H_{26}O_9S$	393.1246
PTO-P4*	$C_{24}H_{42}O_{10}S$	521.2450

*Ions also found as byproducts from *S*-nitrosated polymers (PTMO–NO, PTCO–NO and PTO–NO). ‡Ions common to all polymers (PTMO, PTMO–NO, PTCO, PTCO–NO, PTO and PTO–NO) corresponding to dimers composed of the bonded monomers. †Ion only found as byproduct from the *S*-nitrosated polymer PTCO–NO.

The collected spectra indicated that most of the ions identified correspond to a combination of the monomer units used for the synthetic procedure. All six polymers formed the ions *m/z* 243 and 277, which correspond to products formed from 1,8-octanediol – maleic acid, and 1,8-

octanediol – thiomalic acid, respectively. A major difference specific to PTCO was the presence of the ion *m/z* 319, which corresponds to a conjugate formed from 1,8-octanediol – citric acid (Fig. B.19). Identification of the majority of the degradation products as esters was encouraging, since the starting monomers (citric acid, maleic acid, thiomalic acid) were not prevalent.

3.4.7 Tensile mechanical test of crosslinked polyesters

The tensile modulus of the materials was measured using a tensiometer equipped with a 50 N load cell. The materials were elongated to failure in order to calculate the maximum extension as well as the Young's modulus from the initial slope of the stress-strain curves. The crosslink density of the polyesters, expressed by n (moles of active network chains per unit volume) was calculated using the equation derived from rubber elasticity theory: $n=E_0/3RT$, where E_0 is Young's modulus, R is the universal gas constant (8.314 J mol^{-1} K^{-1}), and T is the temperature in K (Table 3.3).[42]

Table 3.3 Summarized tensile mechanical test results of PTMO, PTCO, PTO, and *S*-nitrosated derivatives. All samples were tested in replicate ($n \geq 4$) and results are reported as the mean ± standard deviation.

Material	Young's Modulus[a] (MPa)	Elongation at Break[a] (%)	Crosslinking Density[b] (mol m^{-3})
PTMO (**1**)	0.6 ± 0.2	300 ± 60	80 ± 22
PTMO–NO (**1a**)	0.24 ± 0.08	240 ± 60	30 ± 11
PTCO (**2**)	1.00 ± 0.06	220 ± 24	140 ± 8
PTCO–NO (**2a**)	1.1 ± 0.1	97 ± 5	150 ± 17
PTO (**3**)	0.18 ± 0.02	800 ± 54	24 ± 3
PTO–NO (**3a**)	0.22 ± 0.03	330 ± 37	30 ± 4

[a] Values determined by tensile mechanical tests on a tensiometer with a 50 N load cell. [b] Values calculated from equation derived from rubber elasticity theory.

Non-linear stress-strain curves are typical for crosslinked materials, similar to those of ligament, especially PTCO and its *S*-nitrosated derivative (Fig. 3.8).[43-45] The tensile Young's

modulus of the materials was similar to other polyesters made from glycerol and sebacic acid 0.282 ± 0.025 MPa.[46] The material with the highest Young's modulus was PTCO–NO, followed by PTCO. Such materials had the lowest elongation due to the high crosslinking density of the polymer chains that afforded crosslinked networks through the trifunctional monomer, citric acid. The value of the Young's modulus of the materials is akin to that of ligaments, in the kPa scale, which contain mostly elastin and some collagen. The values are also in the range of tendons, which is in the GPa scale given their high collagen content.[47-49] Furthermore, material modulus may be matched to that of soft tissue by varying their monomeric constitution based on the desired degree of crosslinking. Compared to soft tissue with higher moduli, the values are also in the range of human meniscal tissue, which was reported to have an instantaneous modulus at 1 MPa, equilibrium values approx. 0.2 MPa, and dynamic modulus values 0.7–0.8 MPa.[50] Additionally, the instantaneous or dynamic moduli of ovine meniscus at 0.6 MPa is also within range of PTCO and PTCO–NO.[51,52] In all cases, except for PTMO–NO, the crosslinking density increased for the *S*-nitrosated polymers. These crosslinking events may be the result of disulfide formation through the thiol-bearing, thiomalic acid, as NO is released from the sample. Uniquely, PTO and PTO–NO had the lowest crosslinking densities due to the linearity of the structure, where chain entanglement gave rise to a crosslinked network. The crosslinking densities of the materials were comparable to previously reported polyesters with values that ranged from 16 ± 3 to 207 ± 3 mol m^{-3}. The elongation of such materials was lower, with a range from 51–327%.[30] The elongation at break is similar to that of arteries and veins, which is up to 260%, and larger than that of tendons at 18%.[53,54] PTO and PTO–NO showed the highest elongation, where PTO reached approximately 800% elongation at break. PTO had the longest reaction times, highest molecular weight, and showed minor degradation at physiological pH and temperature, which suggests that the applications for

this polymer may differ from those of the rest of the materials reported herein. The high elongation values suggest that the materials could be used as bandages for wound dressings given that they could be placed on a site that is continuously moving without damaging the films. In addition, the incorporation of NO to materials with similar modulus as that of soft biological tissue may expand the potential application of the materials given the occurrence of infection in implantable devices.[7,55]

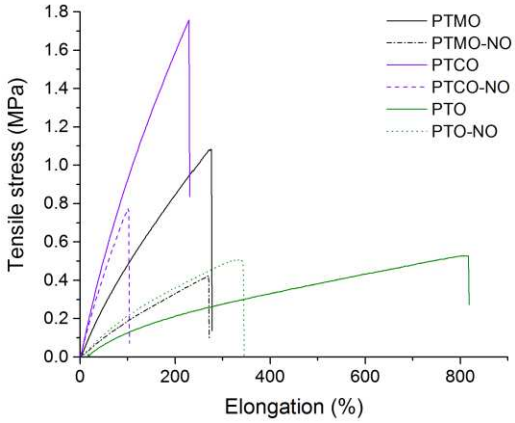

Figure 3.8 Representative stress-strain curves of PTMO, PTCO, PTO and *S*-nitrosated derivatives. Reproduced with permission from the Royal Society of Chemistry.

3.4.8 Bacteria studies

Although NO has been shown to participate in numerous biological functions, its use as a broad-spectrum antibacterial agent has been widely exploited for biomedical applications. The mechanism of antibacterial action is both from NO itself, which is thought to cause intracellular DNA damage, as well as from NO byproducts, which may cause oxidative and nitrosative stress on the viable bacteria. The potential antibacterial activity from the *S*-nitrosated polymers was tested against two bacteria strains (Gram-negative and Gram-positive) at two time points (6 and 24 h) using an agar plating assay. The *S*-nitrosated polymers were exposed to a solution of bacteria in NBM and maintained at 37 °C to ensure the integrity of the bacteria were not compromised by improper growing conditions. Additionally, use of the agar plating method enables high sensitivity

in order to achieve extremely large log-reductions obtained between the controls and the *S*-nitrosated polymers. Two clinically relevant bacteria strains were chosen (*E. coli* and *S. aureus*) to demonstrate the importance of these materials against strains associated with hospital-acquired infections and to highlight the broad-spectrum action of these NO-releasing materials. The activity was evaluated after a 6 h exposure period, as this is considered the critical time period associated with infection between a material and biological interface, but again at 24 h in order to ensure there was no regrowth of the bacteria after initial exposure. The lack of bacterial regrowth after NO had been depleted from the polymers suggests that diminished NO release capabilities would not necessarily diminish the antibacterial performance of the materials.[56]

Table 3.4 displays the results from the bacteria studies, where the log-reductions in bacterial viability based on the agar plating method after 6 and 24 h exposure to the *S*-nitrosated polymers can be seen (raw CFU values can be found in Table B.1). In the first 6 h of exposure to *E. coli*, a significant reduction in planktonic bacteria is observed for all three *S*-nitrosated polymers, with PTMO resulting in an astounding log-8 reduction, representing the limit of detection (LOD) for this technique. After 24 h exposure to *E. coli*, PTCO also reaches the LOD with a log-8 reduction, a reduction that is retained for PTMO. Interestingly, the PTO species shows slight regrowth of the bacteria from a log-5 to log-4 reduction in planktonic, however this still represents a significant reduction in planktonic bacteria to attain and is ultimately considered greater antibacterial efficacy than the current industry standard (log-3). An even greater reduction is observed when the polymers are exposed to *S. aureus*, yielding a log-7 reduction (LOD) within the first 6 h of exposure for all *S*-nitrosated polymers. This substantial reduction is ultimately maintained over the full 24 h exposure period. Indeed, these reductions using ~50 mg of material are extremely noteworthy, given the current industry standard of a log-3 (equivalent to 99.9%)

reduction in viable bacteria. To ensure that the observed antibacterial action was a direct result of the *S*-nitrosation and not the parent compound itself, the non-nitrosated polymers were also tested under identical conditions. The results from this control study indicated no decrease in cellular viability for either bacterial strain in the presence of the non-nitrosated polymers, suggesting that the *S*-nitrosation itself is responsible for the observed effect. Taken together, these results suggest that all three *S*-nitrosated polymers are capable of effectively killing planktonic bacteria of multiple strains within a 24 h period, ultimately presenting an ideal material for combating bacterial infections.[57]

Table 3.4 Log-reductions in viable bacteria obtained using the agar plating method after 6 and 24 h exposure to *S*-nitrosated polymers. All reductions are relative to a positive control containing bacteria in the absence of polymer ($n \geq 6$).

	Log-Reduction in Bacteria			
	E. coli		*S. aureus*	
	6 h	24 h	6 h	24 h
PTMO–NO (**1a**)	8	8	7	9
PTCO–NO (**2a**)	2	8	7	9
PTO–NO(**3a**)	5	4	7	9

3.5 Conclusions

The work presented here is the first, to our knowledge, that reports the synthesis of thiolated polyesters *via* one-pot reactions that were *S*-nitrosated in organic conditions. The method for the production of *S*-nitrosated analogues was optimized to reduce the reaction time and increase NO loading. All materials demonstrated hydrolytic degradation after a 10-week study at physiological pH and temperature, as quantified by gravimetric analysis. The hydrolytic degradation products of the materials at physiological temperature demonstrated the presence of esterified conjugates. Furthermore, the antibacterial activity of *S*-nitrosated materials was assessed against *E. coli* and *S. aureus* and resulted in a log-8 reduction in cellular viability with the majority of the materials,

representing broad-spectrum therapies. As determined by tensile mechanical tests, the materials have appropriate tensile modulus for the preparation of medical devices or wound dressings that require particular elongation. In addition, the materials have Young's moduli and elongation values akin to those of soft biological tissue such as meniscus, tendon, and arteries. The combination of therapeutic NO release for antibacterial applications, and similar mechanical properties as soft biological tissue, make this system a relevant platform for biomedical applications.

Individual contributions and funding sources

Bacteria studies were performed by B. H. Neufeld and mass spectroscopic analysis were carried out by J. B. Tapia. All other experiments were done by J. P. Yapor. Funding for this research was provided by the National Institutes of Health – National Institute of Biomedical Imaging and Bioengineering (5R21EB016838) and Colorado State University.

REFERENCES

1. Bettinger, C. J. *Pure Appl. Chem.* **2010**, *83*, 9.
2. Dhand, C.; Venkatesh, M.; Barathi, V. A.; Harini, S.; Bairagi, S.; Goh Tze Leng, E.; Muruganandham, N.; Low, K. Z. W.; Fazil, M. H. U. T.; Loh, X. J.; Srinivasan, D. K.; Liu, S. P.; Beuerman, R. W.; Verma, N. K.; Ramakrishna, S.; Lakshminarayanan, R. *Biomaterials* **2017**, *138*, 153.
3. Hubbell, J. A. *Nat. Biotechnol.* **1995**, *13*, 565.
4. Nair, L. S.; Laurencin, C. T. *Prog. Polym. Sci.* **2007**, *32*, 762.
5. Li, S. *J. Biomed. Mater. Res.* **1999**, *48*, 342.
6. Makadia, H. K.; Siegel, S. J. *Polymers* **2011**, *3*, 1377.
7. Kuijer, R.; Jansen, E. J.; Emans, P. J.; Bulstra, S. K.; Riesle, J.; Pieper, J.; Grainger, D. W.; Busscher, H. J. *Biomaterials* **2007**, *28*, 5148.
8. Lutzke, A.; Pegalajar-Jurado, A.; Neufeld, B. H.; Reynolds, M. M. *J. Mater. Chem. B* **2014**, *2*, 7449.
9. Williams, D. L. H. *Chem. Commun.* **1996**, 1085.
10. Singh, R. J.; Hogg, N.; Joseph, J.; Kalyanaraman, B. *J. Biol. Chem.* **1996**, *271*, 18596.
11. Marazzi, M.; López-Delgado, A.; Fernández-González, M. A.; Castaño, O.; Frutos, L. M.; Temprado, M. *J. Phys. Chem. A* **2012**, *116*, 7039.
12. Fernández-González, M. A.; Marazzi, M.; López-Delgado, A.; Zapata, F.; García-Iriepa, C.; Rivero, D.; Castaño, O.; Temprado, M.; Frutos, L. M. *J. Chem. Theory Comput.* **2012**, *8*, 3293.
13. Keefer, L. K. *ACS Chem. Biol.* **2011**, *6*, 1147.

14. Schmähl, D.; Habs, M. *Oncology* **1980**, *37*, 237.

15. Tsikas, D.; Gutzki, F. M.; Rossa, S.; Bauer, H.; Neumann, C.; Dockendorff, K.; Sandmann, J.; Frölich, J. C. *Anal. Biochem.* **1997**, *244*, 208.

16. Seabra, A. B.; Da Silva, R.; De Souza, G. F.; De Oliveira, M. G. *Artif. Organs* **2008**, *32*, 262.

17. Yang, L.; Lu, Y.; Soto, R. J.; Shah, A.; Ahonen, M. J. R.; Schoenfisch, M. H. *Polym. Chem.* **2016**, *7*, 7161.

18. Flory, P. J. *Chem. Rev.* **1946**, *39*, 137.

19. Pang, K.; Kotek, R.; Tonelli, A. *Prog. Polym. Sci.* **2006**, *31*, 1009.

20. Jones, M.; Ganopolsky, J. G.; Labbé, A.; Gilardino, M.; Wahl, C.; Martoni, C.; Prakash, S. *Int. Wound J.* **2012**, *9*, 330.

21. Vercelino, R.; Ferreira, E. S.; de Oliveira, M. G. *Nitric Oxide* **2012**, *27*, S33.

22. Damodaran, V. B.; Reynolds, M. M. *J. Mater. Chem.* **2011**, *21*, 5870.

23. Sutton, S. *J. Validation Tecnhol.* **2011**, *17*, 42.

24. Sutton, S. *J. GXP Compliance* **2012**, *16*, 74.

25. Hamilton, M. A. "The log reduction (LR) measure of disinfectant efficacy," MSU Center for Biofilm Engineering: Montana, 2010.

26. Yapor, J. P.; Lutzke, A.; Pegalajar-Jurado, A.; Neufeld, B. H.; Damodaran, V. B.; Reynolds, M. M. *J. Mater. Chem. B* **2015**, *3*, 9233.

27. Jiang, M.; Liu, Q.; Zhang, Q.; Ye, C.; Zhou, G. *J. Polym. Sci. A* **2012**, *50*, 1026.

28. Žagar, E.; Žigon, M. *Prog. Polym. Sci.* **2011**, *36*, 53.

29. Wang, Y.; Kibbe, M. R.; Ameer, G. A. *Biomater. Sci.* **2013**, *1*, 625.

30. Tran, R. T.; Thevenot, P.; Gyawali, D.; Chiao, J.-C.; Tang, L.; Yang, J. *Soft Matter* **2010**, *6*, 2449.

31. Seebacher, W.; Simic, N.; Weis, R.; Saf, R.; Kunert, O. *Magn. Reson. Chem.* **2003**, *41*, 636.

32. Lütke-Eversloh, T.; Bergander, K.; Luftmann, H.; Steinbüchel, A. *Microbiology* **2001**, *147*, 11.

33. Seabra, A. B.; da Silva, R.; de Oliveira, M. G. *Biomacromolecules* **2005**, *6*, 2512.

34. Coneski, P. N.; Rao, K. S.; Schoenfisch, M. H. *Biomacromolecules* **2010**, *11*, 3208.

35. Snejdrova, E.; Dittrich, M. In *Recent advances in plasticizers*; InTech: 2012.

36. Shibayama, K.; Suzuki, Y. *J. Polym. Sci. A* **1965**, *3*, 2637.

37. Malmström, E.; Johansson, M.; Hult, A. *Macromolecules* **1995**, *28*, 1698.

38. Barrère, M.; Landfester, K. *Polymer* **2003**, *44*, 2833.

39. Wang, P. G.; Xian, M.; Tang, X.; Wu, X.; Wen, Z.; Cai, T.; Janczuk, A. J. *Chem. Rev.* **2002**, *102*, 1091.

40. Damodaran, V. B.; Place, L. W.; Kipper, M. J.; Reynolds, M. M. *J. Mater. Chem.* **2012**, *22*, 23038.

41. Schairer, D. O.; Chouake, J. S.; Nosanchuk, J. D.; Friedman, A. J. *Virulence* **2012**, *3*, 271.

42. Sperling, L. H. *Introduction to physical polymer science*; John Wiley & Sons: New York, 2005.

43. Yamaguchi, S. *Arch. Oral Biol.* **1992**, *37*, 439.

44. Chiba, M.; Komatsu, K. *J. Biomech.* **1993**, *26*, 561.

45. Komatsu, K.; Chiba, M. *Arch. Oral Biol.* **1993**, *38*, 369.

46. Wang, Y.; Ameer, G. A.; Sheppard, B. J.; Langer, R. *Nat. Biotechnol.* **2002**, *20*, 602.

47. Fratzl, P.; Misof, K.; Zizak, I.; Rapp, G.; Amenitsch, H.; Bernstorff, S. *J. Struct. Biol.* **1998**, *122*, 119.

48. Wang, J. L.; Parnianpour, M.; Shirazi-Adl, A.; Engin, A. E. *Theor. Appl. Fract. Mec.* **1997**, *27*, 1.

49. Misof, K.; Rapp, G.; Fratzl, P. *Biophys. J.* **1997**, *72*, 1376.

50. Danso, E. K.; Mäkelä, J. T. A.; Tanska, P.; Mononen, M. E.; Honkanen, J. T. J.; Jurvelin, J. S.; Töyräs, J.; Julkunen, P.; Korhonen, R. K. *J. Biomech.* **2015**, *48*, 1499.

51. Fischenich, K. M.; Boncella, K.; Lewis, J. T.; Bailey, T. S.; Haut Donahue, T. L. *J. Biomed. Mater. Res. A* **2017**.

52. Galley, N. K.; Gleghorn, J. P.; Rodeo, S.; Warren, R. F.; Maher, S. A.; Bonassar, L. J. *Clin. Orthop. Relat. Res.* **2011**, *469*, 2817.

53. Lee, M. C.; Haut, R. C. *J. Biomech.* **1992**, *25*, 925.

54. Haut, R. C. *J. Biomech. Eng.* **1985**, *107*, 166.

55. Donlan, R. M. *Emerging Infect. Dis.* **2001**, *7*, 277.

56. Jones, M. L.; Ganopolsky, J. G.; Labbé, A.; Wahl, C.; Prakash, S. *Appl. Microbiol. Biotechnol.* **2010**, *88*, 401.

57. Kenawy, E. R.; Worley, S. D.; Broughton, R. *Biomacromolecules* **2007**, *8*, 1359.

CHAPTER 4

NITRIC OXIDE-RELEASING EMULSION ENFORCED WITH ADDITIVES FOR DERMAL TISSUE REGENERATION

4.1 Synopsis

S-nitrosoglutathione (GSNO) is a naturally available *S*-nitrosothiol that can be incorporated to non-toxic formulations intended for topical use. The value of nitric oxide (NO) delivered topically relates to its well-studied physiological functions such as vasodilation, angiogenesis, cell proliferation and broad-spectrum antibacterial activity. Previously reported topical NO-releasing substrates include polymeric materials that exhibit non-toxic behaviors on dermal tissue such as polyethylene glycol. However, they do not serve as humectants or provide vitamins to the skin. In this study, GSNO was added to an emulsion that was fortified with vitamin E and hyaluronic acid to improve and accelerate the wound healing process. The average total NO content for the NO-releasing emulsion was $58 \pm 7.7\ \mu mol\ g^{-1}$ at 150 °C and the cumulative NO release over 53 h at physiological temperature was $46 \pm 4.4\ \mu mol\ g^{-1}$. The GSNO concentration in the lotion was optimized in order to reach a pH value similar to that of human skin (pH 5.5). The viscosity of the samples was analyzed using a rotational viscometer for the *S*-nitrosated and the non-nitrosated emulsions to obtain a material that can be readily spread without disturbing the surrounding tissue. Cytotoxicity studies using human dermal fibroblast will indicate if the material elicits toxic responses when exposed to cells, which will be assessed by morphological, CellTiter-Blue® viability, and LIVE/DEAD assays. The findings indicate that the emulsion has potential applications to treat non-healing wounds or ulcers by

promoting cell proliferation, blood flow and oxygenation on damaged tissue. Fig. 4.1 presents a summary of the experiments that are explored in this study.

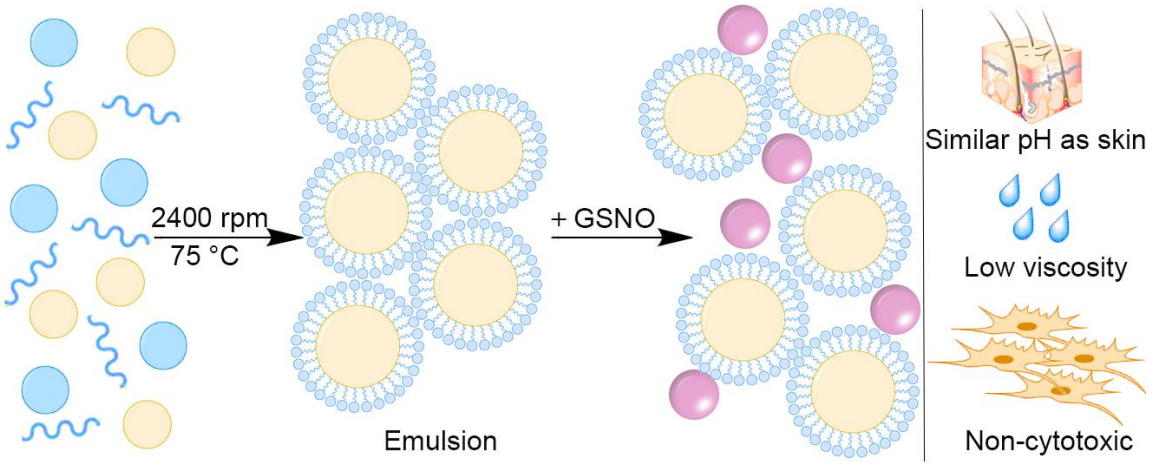

Figure 4.1 Summarized methodology for the preparation of NO-releasing emulsion.

4.2 Introduction

Infected wounds are an area of concern in the medical field due to the high number of individuals affected each year, increasing health care costs, and an aging population.[1] More specifically, chronic wounds pose a life-threatening condition to patients whose wounds do not heal after four weeks and often require special treatment or hospitalization.[2] Chronic wounds occur when multiple species of bacteria live cooperatively in highly organized biofilms. The biofilm protects bacteria from the patient's immune response and antibiotic therapy. Among others, cutaneous wounds are prone to infection by methicillin-resistant *Staphylococcus aureus*.[3] Such wounds can lead to complications or fatality in patients with a compromised immune system or underlying conditions such as diabetes or cardiovascular diseases. Approximately, 20 million patients in the world suffer from chronic wounds.[4] Unfortunately, in many of these cases, amputation is required due to the extent of infection. Therefore, the preparation of NO-releasing emulsions that can prevent infections and promote dermal cell proliferation are needed to reduce the high number of patients with non-healing wounds. Existing technologies used to treat

wounds include growth factors,[5] bioengineered skin,[4] negative pressure wound therapy,[6] hydrocolloids,[7] foam dressings,[8] and antimicrobial dressings.[9] The appropriate dressing for the wound is determined by the specialist considering the position and state of the wound, fragility of surrounding skin, frequency of dressing changes, and patient comfort.

Nitric oxide (NO) is an endogenous molecule involved in various physiological processes including vasodilation, angiogenesis, inhibition of platelet activation and broad-spectrum antibacterial activity. The applications for NO and their beneficial effects at low concentrations have inspired scientists to create new NO-releasing platforms for a wider range of applications. NO releasing surfaces have shown that a controlled release is able to mimic physiological pathways such as immune responses against opportunistic bacteria, and promotion of cell proliferation.[10,11] However, NO releasing matrices for topical applications have not been studied as widely due to cytotoxicity concerns. Topical NO delivery may be beneficial to patients with chronic wounds by increasing blood flow around the wound, stimulating angiogenesis and promoting cell proliferation.

One approach to prevent infections is to mimic the endothelium and release NO locally by incorporating the endogenous free radical, in the form of *S*-nitrosothiols (RSNOs), to the surface of materials. NO is a highly reactive gas with a short half–life, thus, emulsions may be formulated to deliver NO. This process facilitates the use of materials in a unique and localized drug delivery therapy that harnesses the benefits of NO. NO-releasing materials are commonly obtained from RSNOs and *N*-diazeniumdiolates (NONOates). NONOates release 2 moles of NO per mole of NO donor under acidic conditions. However, they have been reported to produce carcinogenic secondary *N*-nitrosamines under oxygenated conditions as a byproduct. RSNOs are the most commonly used NO sources given their natural occurrence in the form of *S*-

nitrosohemoglobin, *S*-nitrosoglutathione and *S*-nitrosoalbumin. These molecules decompose by thermal, photolytic or transition metal ion-dependent pathways to release NO and form disulfide bonds.

Previous studies have shown the benefits and potential applications of NO-releasing materials. Such applications range from antibacterial effects to vasodilation and oxygenation of dermal tissue. Seabra *et al.* reported the synthesis of liquid poly(ethylene glycol)(PEG)/H_2O matrices that were *S*-nitrosated by bubbling a mixture of NO/synthetic air through the matrix compound (PEG/H_2O) and glutathione in a quartz cuvette. NO release was measured using mass spectrometry to monitor the release of NO gas from the liquid sample. Spectrophotometric techniques were also used to characterize NO release by calculating the amount of *S*-nitrosoglutathione (GSNO) decomposed measuring absorbance changes at 545 nm. Kinetic curves were analyzed for up to 16 h of NO release, with calculated initial rates of 0.98 ± 0.02 mmol L^{-1} h^{-1}.[12]

A different study explored the use of an NO-releasing polyesters made from ethylene glycol or poly(ethylene glycol) and mercaptosuccinic acid. The material was also *S*-nitrosated by bubbling NO/synthetic air through the liquid polyester, where the reaction completion was monitored by spectrophotometric techniques and the gas was bubbled until the signals at 336 and 545 nm plateaued. Using the initial rate of NO release at 5.2 mmol L^{-1} h^{-1}, it was calculated that the total amount of NO released after 24 h was 45 μmol mL^{-1}. Drops of the material were applied to the skin of two human subjects for 7 min under ambient light, which caused hyperemia due to local vasodilation. Kinetic curves were obtained by immersing the polyesters in a Griess solution, which indirectly measured NO release.[13] A different report presented the preparation of NO-releasing hydrogels from a commercial triblock copolymer poly(ethylene

oxide)$_{99}$–poly(propylene oxide)$_{65}$–poly(ethylene oxide)$_{99}$ to which GSNO or *S*-nitroso-*N*-acetylcysteine (SNAC) were added. NO release was monitored by spectrophotometric techniques as described previously. The *S*-nitrosated hydrogels were placed on the forearm of eight human subjects and blood flow was measured by laser Doppler flowmetry and nitrite concentration was measured using dermal microdialysis catheters. They concluded that dermal nitrite concentration is generally directly correlated with blood flow. However, NO release was not reported given that it was not the focus of the study.[14]

Herein, an emulsion with non-toxic components was formulated and used as the medium to incorporate the naturally-occurring RSNO, *S*-nitrosoglutathione, as well as vitamin E and hyaluronic acid. Additives were used to fortify the emulsion considering that vitamin E is a naturally-occurring compound in the skin that is obtained through dietary sources requiring cellular metabolism breakdown.[15] The human sebaceous gland produces and secretes sebum in order to transport digested vitamin E to the surface of the skin.[16] Furthermore, vitamin E may be applied topically for a more exclusive application and the ability to provide more specific forms of the antioxidant that are unachievable through the diet alone.[17] The most common form of Vitamin E is α-tocopherol, which promotes plasma membrane repair within the epidermis and protection to the skin.[18] This type of vitamin E was successfully incorporated into the formulation as a beneficial additive. Studies have shown that topical use plays a role in photoprotection,[19] works as an anti-inflammatory agent,[20] promotes the healing of wounds,[21] and supplements moisturizing effects.[22]

Hyaluronic acid was also incorporated given that it is naturally occurring biomolecule found in all organs of the human body. It is produced in the membrane of mammalian cells by an enzyme called hyaluronic acid synthases (HAS).[23] Hyaluronic acid is most abundant within the

skin, where 50% of its total concentration is found.[24] Skin ages from both intrinsic and extrinsic factors that affect the overall ability to retain moisture and produce its own hyaluronic acid.[25] Topical application of the lotion will deliver hyaluronic acid to the top layer of skin. Used in injections and formulations, it is believed and studied that hyaluronic acid is a valuable solution for retaining moisture within the skin. [26]

GSNO served as the NO donor in this system where the concentration of RSNO was optimized in order to achieve NO release at levels that are physiologically relevant to promote vasodilation and cell proliferation. The purpose of preparing an NO-releasing lotion is to provide greater blood flow to damaged dermal tissue. The increase of blood flow would be beneficial in order to oxygenate the tissue where the lotion is applied to regenerate damaged skin. The viscosity of the emulsions was analyzed to obtain an appropriate consistency for a sample that could be applied without disturbing the regenerating surrounding tissue. pH was measured over 10 weeks to investigate the stability of the *S*-nitrosated emulsion. Cell studies will be performed using human dermal fibroblasts to assess the cytotoxicity of the *S*-nitrosated emulsion and non-nitrosated samples were used as controls. The combination of beneficial additives that allow dermal tissue to retain its moisture, in combination with NO-release make of this system a relevant platform with potential applications for wound healing.

4.3 Materials and methods

4.3.1 Materials

Vitamin E acetate (97%), *n*-propyl-4-hydroxybenzoate (99%), methyl 4-hydroxybenzoate (99%), 1-hexadecanol (98%), isopropyl tetradecanoate (98%), triethanolamine (98+%) were purchased from Alfa Aesar (Ward Hill, MA, USA). Hyaluronic acid sodium salt from

Streptococcus equi and mineral oil (light) were procured from Sigma Aldrich (St. Louis, MO, USA). Glycerol was purchased from Mallinckrodt (Phillipsburg, NJ, USA). Stearic acid (>98%) was obtained from TCI (Tokyo, Japan). Glyceryl stearate SE and carbomer 980 HQ were procured from MakingCosmetics Inc (Snoqualmie, WA, USA). Reduced glutathione (GSH) was purchased from VWR International (Radnor, PA, USA). Hydrochloric acid (HCl) and EPA vials were obtained from Thermo Fisher Scientific (Waltham, MA, USA). Sodium nitrite ($NaNO_2$) was purchased from EMD Millipore (Burlington, MA, USA).

4.3.2 Characterization techniques

UV-Vis absorption studies were performed using a Nicolet Evolution 300 UV-Vis spectrophotometer (Thermo Electron Corporation, Madison, WI, USA). pH values were obtained during the course of 10 weeks using a Mettler Toledo Seven Easy pH meter equipped with a Mettler Toledo InLab® Routine Pro pH probe (Mettler Toledo, Columbus, OH, USA). Dilutions for pH tests were prepared using Millipore water to make 11.1% w/v solutions at room temperature. Viscosity was analyzed using *S*-nitrosated samples as well as non-nitrosated emulsions without performing any dilutions. The instrument used was a Fungilab Viscolead Pro rotational viscometer equipped with spindles L4 Fungilab at 60 rpm for the *S*-nitrosated samples and L3 Fungilab at 12 rpm for the non-nitrosated samples (Fungilab, Bacelona, Spain). The sample temperature was controlled with a water bath and maintained at 25 °C.

4.3.3 Emulsion preparation

The emulsion preparation consisted of stirring vigorously an aqueous phase with a lipophilic phase. For the aqueous phase, a 2% w/v solution of carbomer 980 HQ was prepared in

Millipore water (18.2 MΩ cm) at room temperature 24 h prior to the emulsification. The following day, Millipore water was heated to 75 °C and 79.7 mL were added to glycerol (3 g), triethanolamine (0.9 g), methyl 4-hydroxybenzoate (0.1 g), and carbomer 980 HQ 2 % w/v in Millipore water (5 g). The aqueous phase was maintained at 75 °C in a cylindrical glass vessel with dimensions 6 cm x 19 cm. The lipophilic phase consisted of 1-hexadecanol (2 g), stearic acid (0.8 g), glyceryl stereate SE (1.5 g), *n*-propyl-4-hydroxybenzoate (0.05 g), isopropyl tetradecanoate (0.85 g), vitamin E (0.995 g) and mineral oil (0.85 g), which were heated to 75 °C until melted. The lipophilic phase was slowly added to the aqueous phase and stirred at 2400 revolutions per minute (rpm) for 30 min at 75 °C. Emulsification was achieved using a IKA® RW 20 digital mechanical stirrer (IKA Works, Inc., Wilmington, NC, USA). The white emulsion was transferred to a glass container with a cap and stored at room temperature shielded from direct exposure to light.

4.3.4 Synthesis and characterization of *S*-nitrosoglutathione

S-nitrosoglutathione (GSNO), the NO-donor in this study, was synthesized based on a previous reported method.[27] Briefly, a mixture of 5 mmol of reduced glutathione (GSH), 8 mL of cold H_2O, and 2.5 mL of 2 M hydrochloric acid (HCl) was stirred over ice for 10 min, followed by adding 5 mmol of sodium nitrite ($NaNO_2$) into this solution to initiate *S*-nitrosation. The mixture was stirred further for 40 min over ice before the addition of 10 mL of cold acetone. The resulting GSNO was collected and washed before dried under vacuum for 4 h. The purity of GSNO was characterized using UV-Vis spectrophotometric techniques by measuring the absorbance at 336 nm to ensure >95% purity.[28] The GSNO was stored in an EPA amber vial at −20 °C before use to prevent both photolytic and thermal decomposition.

4.3.5 Addition of *S*-nitrosoglutathione to emulsion

Hyaluronic acid (50 mg) was added to the emulsion (5 g) to obtain a 1% w/w mixture in an amber vial. The mixture was vortexed briefly to incorporate all solids to the emulsion, then stirred at 725 rpm overnight at room temperature. The process is followed by the addition of *S*-nitrosoglutathione (88 mg) to obtain a 1.75 w/w % concentration. The mixture was alternately vortexed for 2 min and stirred at 1100 rpm for 4 minutes during the course of 1 hour. The samples were stored at 4 °C until further use.

4.3.6 Chemiluminescence-based nitric oxide analysis

NO release from *S*-nitrosated emulsions was evaluated using Sievers chemiluminescence NO analyzers (NOA 280i, GE Analytical, Boulder, CO, USA) following our previously reported procedure.[29] The instruments were calibrated prior to each analysis using nitrogen as the zero gas and 43.6 ppm NO/nitrogen as the calibration gas. The nitrogen sweep gas flow during the analysis was maintained at 200 mL min^{-1}. Total NO content was obtained by heating *S*-nitrosated emulsions (n = 3, 9 mg) and appropriate controls at 150 °C in the absence of solvent followed by irradiation of light at 365 nm, which promoted the thermal and photodecomposition of the RSNO groups. The NO emission from this process was used to quantify the thermally and photo-releasable NO present in each material. In addition, NO release at physiological temperature was determined by heating *S*-nitrosated emulsion samples (n = 3) in the absence of solvent at 37 °C. NO release was measured for 53 h in vessels protected from direct exposure to light to prevent further photodecomposition of the RSNO.

4.4 Results and discussion

4.4.1 Emulsion preparation

The emulsion was prepared with the purpose of providing a carrier platform for GSNO, which would act as the NO donor. Initially, poly(acrylic acid) had been chosen as the main thickener. However, emulsification was not achieved due to the increased acidity of the solution or the low molecular weight of poly(acrylic acid). Therefore, a commercially available carbomer, composed of poly(acrylic acid) of various molecular weights, was used to substitute for the polymer used initially. Each component of the formulation served a purpose in the overall composition of the lotion. The list of ingredients and additives can be found in the materials section along with the quantities utilized. The list contains both aqueous phase and lipophilic phase components that were emulsified.

The aqueous phase consisted of water, carbomer (2% w/v), glycerol, methyl 4-hydroxybenzoate, and triethanolamine. Water was used as a diluent and was the most abundant ingredient in the emulsion. Millipore water was used to increase the purity of the emulsion. Carbomer at a 2% w/v concentration acted as a thickener that stabilized the emulsion to prevent the separation of the oil and water phases. Glycerol was the humectant that operated to attract water and pulled additional moisture into the epidermis.[30] Each phase received a preservative, as scuh, methyl 4-hydroxybenzoate was used in the water-soluble portion. Triethanolamine was used as a neutralizer in order to balanced the pH.

The lipophilic phase was comprised of 1-hexadecanol, stearic acid, glyceryl stearate SE, *n*-propyl-4-hydroxybenzoate, isopropyl tetradecanoate, and mineral oil. 1-Hexadecanol was a coemulsifier and increased stability in the emulsion. Stearic acid and glyceryl stearate SE are common emulsifiers that allowed this to be an oil in water mixture. The preservative for the

lipophilic phase utilized *n*-propyl-4-hydroxybenzoate. This phase of the lotion moisturizes because of the added occlusive agents, isopropyl tetradecanoate and mineral oil. Furthermore, occlusive compounds form a physical layer atop the skin and prevent the loss of water.[30]

4.4.2 Chemiluminescence-based nitric oxide analysis

The pH of the solution was adjusted by the addition of GSNO after the additives; vitamin E and hyaluronic acid had been incorporated to the emulsion. The desired NO concentration for an NO-releasing sample for tissue regeneration is in the range of 1–100 nM. Previous reports have demonstrated that different physiological responses are observed at certain instantaneous NO concentrations. Mediation of proliferative and protective effects occurs at <1–30 nM, followed by apoptosis protection, which occurs at 30–60 nM, and tissue injury protection at 100 nM. For this reason, the concentration of the GSNO was determined to be ideal at 1.75 % w/w. At this concentration, the NO release calculated for 53 h at physiological temperature was 46 ± 4.4 μmol g^{-1} and the total NO content was 58 ± 7.7 μmol g^{-1}. (Table 4.1) The analysis of total NO contents was performed at 150 °C followed by irradiation of light (365 nm) to promote the thermal- and photodecomposition of the RSNO groups. In addition, the experiment was done at 150 °C given that the temperature is similar to the reported decomposition temperature of GSNO. Total NO content can be used to compare how much NO is present in the emulsion compared to the NO released at physiological temperature. The theoretical availability of GSNO in a solution of 1.75% GSNO is 52 μmol g^{-1}, which is comparable to the results obtained for total NO content. Previous reports have shown similar results in terms of NO release such as 45 μmol mL^{-1} over 24 h.[13] The advantage of a longer release profile for 53 h with a low NO release

is that NO can continue reacting on the skin without causing apoptotic effects, which are typically associated with NO concentrations higher than 1 μM.

The release profile depicted in Fig. 4.2 shows a typical release profile for RSNOs, and Fig. 4.3 depicts the cumulative release, where an initial NO release is higher before the release reaches a plateau. The release at physiological temperature demonstrated the decomposition of GSNO as it shows a generic exponential decay plot. The release shows a decreased NO release after the first hours, which is ideal for the intended applications. A high NO release would be needed initially to mitigate the occurrence of infection by acting as a broad-spectrum antibacterial agent. A slower release would be beneficial for the remaining hours to provide a low NO release and provide proliferative and tissue protection effects.

Table 4.1 Summarized NO content data. All samples were tested in replicate ($n \geq 3$) and the results are reported as the mean ± standard deviation.

	Cummulative NO Release[a] ($\mu mol\ g^{-1}$)	Total NO Content[b] ($\mu mol\ g^{-1}$)
S-nitrosated emulsion	46 ± 4.4	58 ± 7.7

[a] Release measured at physiological temperature for 53 h. [b] Values determined by NO analysis through thermal decomposition of the RSNO at 150 °C.

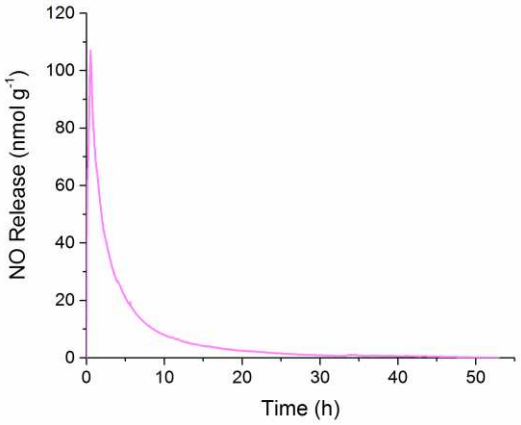

Figure 4.2 Representative NO release profile of *S*-nitrosated emulsion at physiological temperature.

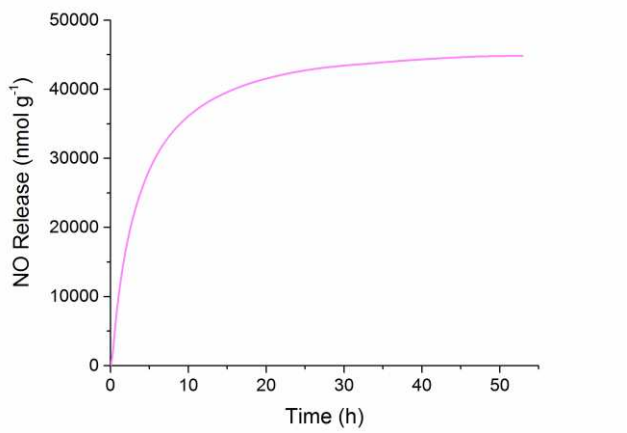

Figure 4.3 Representative cumulative NO release data of *S*-nitrosated emulsion at physiological temperature.

The presence of RSNOs was confirmed by UV-Vis spectrophotometry using diffuse reflectance mode. The method was chosen given the limited solubility of the sample in most solvents. The sample holder was baselined with a spectralon that reflects all wavelengths of light. Smoother spectra were obtained when a spectralon polymer was used as the baseline, compared to using the non-nitrosated emulsion as the baseline. Fig. 4.4 shows a representative UV-Vis spectrum of the *S*-nitrosated emulsion. Characteristic RSNO absorptions peaks were observed at 339 ± 1.5 ($\pi \rightarrow \pi^*$) and 546 ± 0.6 nm ($n_N \rightarrow \pi^*$). All samples were tested in replicate ($n \geq 3$) and the results are reported as the mean ± standard deviation.

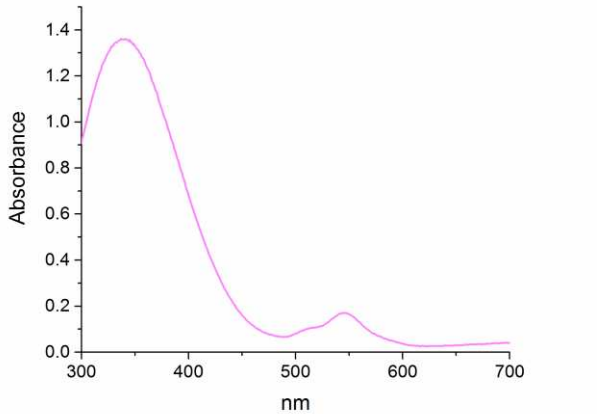

Figure 4.4 UV-Vis spectrum of *S*-nitrosated emulsion with characteristic RSNO features.

4.4.3 Kinematic viscosity analysis

The analysis of kinematic viscosity was performed in order to establish a viscosity range that would be beneficial for the intended application. Emulsion samples were obtained from non-nitrosated and *S*-nitrosated analogues without diluting the samples. The materials were tested at a constant temperature of 25 °C. The viscosity of the non-nitrosated lotion was tested using a spindle type L3 Fungilab, which was spun at 12 rpm. The *S*-nitrosated samples were tested using a spindle type L4 Fungilab at 60 rpm. Different spindles were needed given the insolubility of hyaluronic acid, which formed small particles within the *S*-nitrosated lotion. Table 4.2 demonstrates the kinematic viscosity and density values obtained for each material. The viscosity of the S-nitrosated samples was greater due to the hyaluronic acid and GSNO that yielded a more viscous sample as RSNOs decomposed to form disulfide bonds (Fig. 4.5).

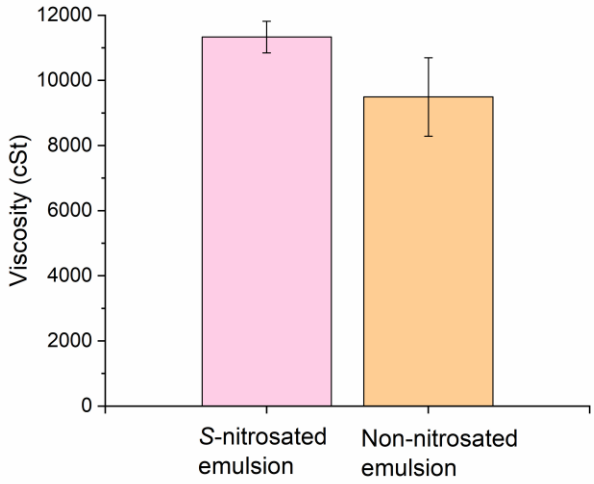

Figure 4.5 Kinematic viscosity of *S*-nitrosated and non-nitrosated emulsion samples. All samples were tested in replicate ($n \geq 3$) and the results are reported as the mean ± standard deviation.

The results demonstrated that the addition of hyaluronic acid and GSNO have an effect on the stability of the emulsion. The viscosity of the emulsion increased due to the presence of hyaluronic acid, which swelled and gave rise to an emulsion with a thicker, less viscous

consistency. On the other hand, the density of the *S*-nitrosated emulsion decreased with the addition of hyaluronic acid and GSNO (Fig. 4.6). The density of the emulsion decreased when the nitric oxide release functionality was added to the material, which may suggest that the decreased pH of the *S*-nitrosated emulsion rendered a more unstable, less dense emulsion. The density was statistically different, while the viscosity was not statistically different ($p < 0.05$).

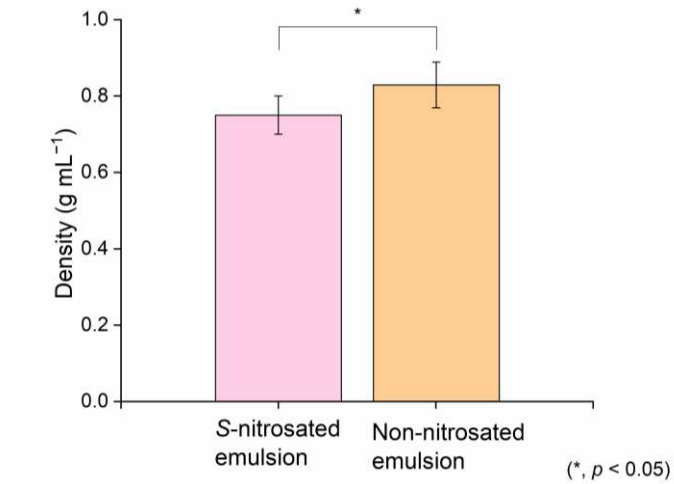

Figure 4.6 Density of *S*-nitrosated and non-nitrosated emulsion samples. All samples were tested in replicate ($n \geq 3$) and the results are reported as the mean ± standard deviation.

Table 4.2 Summarized kinematic viscosity and density results. All samples were tested in replicate ($n \geq 3$) and the results are reported as the mean ± standard deviation.

	Kinematic Viscosity[a] (cSt)	Density[b] (g mL^{-1})
S-nitrosated emulsion	11330 ± 485	0.75 ± 0.05
Non-nitrosated emulsion	9501 ± 1203	0.83 ± 0.06

[a] Values obtained using a Fungilab rotational viscometer. [b] Values determined experimentally by noting the mass of a specific volume of sample.

4.4.4 Analysis of pH

Even though it was determined that a 1.75 % w/w concentration would provide the appropriate NO release, and physiological pH, the concentration may be altered followed by a pH adjustment. It was observed that pH was inversely proportional to GSNO concentration. Hence, if a lower NO release were desired, then the pH would be adjusted to increase the acidity of the emulsion. pH adjustments can be done by using citric or lactic acid solutions during the emulsification, or by increasing the molar quantity of the stearic acid, which is currently used in the formulation as an emulsifier. The pH of the emulsion was measured at different GSNO concentrations including, 1.0%, 1.5%, 2.0%, 2.5 %, 3.0% and 6.0% w/w, with resulting pH values of 7.43, 6.75, 5.36, 4.37, 3.88, and 3.24, respectively. The emulsion was unstable when the GSNO concentration was greater than 3.0% w/w because of the increased acidity of the emulsion. Of note, the pH of the emulsion with only vitamin E and with vitamin E and hyaluronic acid were measured following the same procedure as with the *S*-nitrosated emulsion. The pH of the emulsion with vitamin E (1% w/w) as the only additive was 8.40 ± 0.03, while the pH of the emulsion both additives, with vitamin E and hyaluronic acid (1% w/w) was 8.17 ± 0.02. Thus, the hyaluronic acid does decrease the pH of the emulsion.

In addition, pH was measured in triplicate during the course of 10 weeks. Dilutions were made using Millipore water to obtain a final concentration of 11.1% w/v. Samples were stirred vigorously prior to pH tests. The results obtained from the analyses are shown in table 4.3. The pH decreased during the course of the experiment given that the RSNOs decomposed to form disulfide bonds. In addition, the generation of nitrous acid (HNO_2) or nitric acid (HNO_3) from the reaction with water and oxygen may cause a decrease in pH for the *S*-nitrosated emulsions.

Table 4.3 pH analysis of the *S*-nitrosated emulsion. All samples were tested in replicate ($n \geq 3$) and the results are reported as the mean ± standard deviation.

	pH of *S*-nitrosated emulsion[a]
Week 0	5.5 ± 0.4
Week 1	5.3 ± 0.2
Week 2	4.0 ± 0.1
Week 3	3.9 ± 0.02
Week 8	3.9 ± 0.01
Week 10	3.9 ± 0.1

[a] Values obtained using a Mettler Toledo Seven Easy pH meter equipped with a Mettler Toledo InLab® Routine Pro pH probe.

The initial pH of the emulsion with vitamin E as its only additive was higher than the intended pH range for the emulsion (~5.5). The value is represented in Fig. 4.7. In order to increase the acidity of the emulsion, and to provide an agent that aids in moisture retention, hyaluronic acid was added. The addition of GSNO also increased the acidity of the emulsion due to the carboxylic acid groups bared by the *S*-nitrosated moiety.

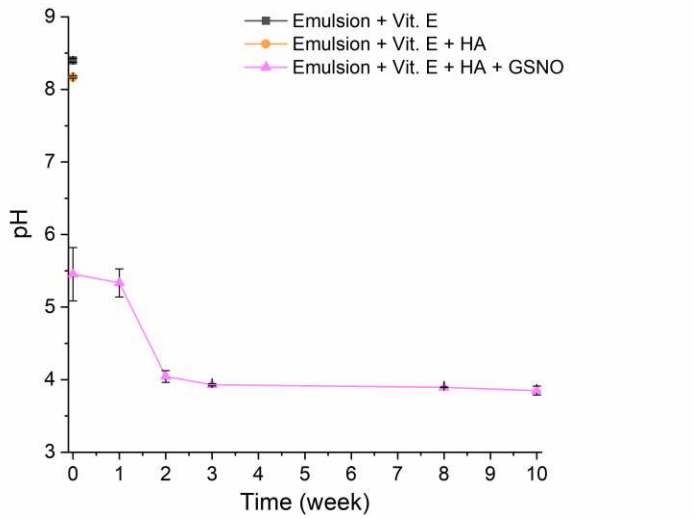

Figure 4.7 Analysis of pH of the emulsion with various additives. Each data point represents an average of $n \geq 3$ replicates and the standard deviation.

4.5 Conclusions

The study reports the preparation of an NO releasing emulsion with *S*-nitrosothiol groups. The matrix was prepared using a formulation that is intended for topical use and additives such as vitamin E and hyaluronic acid were incorporated in order to expand the benefits of the emulsion on dermal tissue. GSNO was added to the emulsion to serve as an NO donor at a concentration that allowed for a low NO release. Such release was quantified *via* chemiluminescence-based detection of NO. The targeted NO release was adjusted in order to obtain NO release values that would have specific physiological reactions such as cell proliferation and tissue injury protection. The pH of the emulsion was measured over the course of 10 weeks a decrease in pH values was observed. Although the pH of the emulsion decreased during the first weeks, it was seen that the pH did not change drastically as measured in week 8 and 10. Therefore, the ideal storage conditions for this sample involve refrigeration at 4 °C. Using kinematic viscosity, it was determined that the emulsion viscosity is appropriate to be used on delicate areas where external force is not needed or would damage the surrounding tissue. Future studies will include cell assays to provide insight regarding cell viability and morphology. The preparation of an emulsion with beneficial properties to the skin such as the addition of vitamin E and hyaluronic acid, with GSNO provide a relevant platform for the treatment of non-healing wounds or ulcers.

Individual contributions and funding sources

Y. Zang prepared the GSNO and performed purity analysis. C. Henderson aided in the formulation of emulsions, viscosity and NO analysis in addition to performing pH and density analyses. J. Gordon will assess the cytotoxicity of the emulsion using human dermal fibroblasts

and/or bacteria. All other experiments were performed by J. P. Yapor. Funding for this project was provided by Colorado State University.

REFERENCES

1. Sen, C. K.; Gordillo, G. M.; Roy, S.; Kirsner, R.; Lambert, L.; Hunt, T. K.; Gottrup, F.; Gurtner, G. C.; Longaker, M. T. *Wound Repair Regen.* **2009**, *17*, 763.
2. Järbrink, K.; Ni, G.; Sönnergren, H.; Schmidtchen, A.; Pang, C.; Bajpai, R.; Car, J. *Syst. Rev.* **2017**, *6*, 15.
3. Loh, J. V.; Percival, S. L.; Woods, E. J.; Williams, N. J.; Cochrane, C. A. *Int. J. Nutr.* **2009**, *6*, 32.
4. Frykberg, R. G.; Gibbons, G. W.; Walters, J. L.; Wukich, D. K.; Milstein, F. C. *Int. Wound. J.* **2017**, *14*, 569.
5. Choi, J. U.; Lee, S. W.; Pangeni, R.; Byun, Y.; Yoon, I.-S.; Park, J. W. *Acta Biomater.* **2017**, *57*, 197.
6. Saku, I.; Kanda, S.; Saito, T.; Fukushima, T.; Akiyama, T. *Int. J. Surg. Case Rep.* **2017**, *37*, 106.
7. Phillips, T. J.; Palko, M. J.; Bhawan, J. *J. Am. Acad. Dermatol.* **1994**, *30*, 61.
8. Davies, P.; McCarty, S.; Hamberg, K. *J. Wound Care* **2017**, *26*, S1.
9. Dhand, C.; Venkatesh, M.; Barathi, V. A.; Harini, S.; Bairagi, S.; Leng, E. G. T.; Muruganandham, N.; Low, K. Z. W.; Fazil, M. H. U. T.; Loh, X. J. *Biomaterials* **2017**, *138*, 153.
10. Yapor, J. P.; Neufeld, B. H.; Tapia, J. B.; Reynolds, M. M. *J. Mater. Chem. B* **2018**.
11. Napoli, C.; Paolisso, G.; Casamassimi, A.; Al-Omran, M.; Barbieri, M.; Sommese, L.; Infante, T.; Ignarro, L. J. *J. Am. Coll. Cardiol.* **2013**, *62*, 89.

12. Seabra, A. B.; de Souza, G. F. P.; da Rocha, L. L.; Eberlin, M. N.; de Oliveira, M. G. *Nitric Oxide* **2004**, *11*, 263.

13. Seabra, A. B.; da Silva, R.; de Oliveira, M. G. *Biomacromolecules* **2005**, *6*, 2512.

14. Seabra, A.; Fitzpatrick, A.; Paul, J.; De Oliveira, M.; Weller, R. *Br. J. Dermatol.* **2004**, *151*, 977.

15. Keen, M.; Hassan, I. *Indian Dermatol. Online J.* **2016**, *7*, 311.

16. Ekanayake-Mudiyanselage, S.; Thiele, J. J. *Hautarzt* **2006**, *57*, 291.

17. Ikeda, S.; Toyoshima, K.; Yamashita, K. *Int. J. Nutr.* **2001**, *131*, 2892.

18. Howard, A. C.; McNeil, A. K.; McNeil, P. L. *Nat. Commun.* **2011**, *2*, 597.

19. Kagan, V.; Witt, E.; Goldman, R.; Scita, G.; Packer, L. *Free Radic. Res.* **1992**, *16*, 51.

20. Prakoeswa, C. S.; Natallya, F.; Harnindya, D.; Thohiroh, A.; Oktaviyanti, R.; Pratiwi, K.; Rubianti, M.; Yogatri, B.; Primasari, P.; Herwanto, N. *J. Dermatolog. Treat.* **2018**, 1.

21. Hobson, R. *Int. Wound. J.* **2016**, *13*, 331.

22. Kato, E.; Takahashi, N. *Bioorganic Med. Chem.* **2012**, *20*, 3837.

23. de Oliveira, J. D.; Carvalho, L. S.; Gomes, A. M. V.; Queiroz, L. R.; Magalhães, B. S.; Parachin, N. S. *Microb. Cell Fact.* **2016**, *15*, 119.

24. Papakonstantinou, E.; Roth, M.; Karakiulakis, G. *Dermatoendocrinol.* **2012**, *4*, 253.

25. Zhang, S.; Duan, E. *Cell Transplant.* **2018**, *27*, 729.

26. Jegasothy, S. M.; Zabolotniaia, V.; Bielfeldt, S. *J. Clin. Aesthet. Dermatol.* **2014**, *7*, 27.

27. Hart, T. W. *Tetrahedron Lett.* **1985**, *26*, 2013.

28. Williams, D. L. H. *Acc. Chem. Res.* **1999**, *32*, 869.

29. Damodaran, V. B.; Reynolds, M. M. *J. Mater. Chem.* **2011**, *21*, 5870.

30. Sethi, A.; Kaur, T.; Malhotra, S.; Gambhir, M. *Indian J. Dermatol.* **2016**, *61*, 279.

CHAPTER 5

POLYDIACETYLENE NANOFIBER COMPOSITES AS A COLORIMETRIC SENSOR RESPONDING TO *ESCHERICHIA COLI* AND pH

5.1 Synopsis

Polydiacetylenes (PDA) are conjugated polymers that demonstrate color changes as a response to an external stimulus. In this study, 10,12–pentacosadiynoic acid (PCDA) was mixed with a supporting polymer including poly(ethylene oxide) (PEO) and polyurethane (PU), and the mixture solution was electrospun to construct fiber composites. The electrospun fibers were then photopolymerized using UV irradiation to produce PEO–PDA and PU–PDA nanofiber mats with a fiber diameter ranging from 130 nm to 2.5 μm. The morphologies of both PEO–PDA and PU–PDA nanofibers were dependent on electrospinning parameters such as the ratio of PCDA to PEO or PCDA to PU and the total polymer concentrations. Scanning electron microscopy images showed beaded fibers of PEO–PDA and PU–PDA at 2% w/v and 18% w/v concentration, respectively. Smooth fibers were found when the solvent concentration was increased to 3.75% w/v in PEO–PDA and 25% w/v in PU–PDA fibers, respectively. Both PEO–PDA and PU–PDA nanofiber composites demonstrated excellent colorimetric responses to the presence of *E. coli* ATCC25922 bacterial cells and the changes in pH as external stimuli. The nanofibers underwent a rapid colorimetric response when exposed directly to *E. coli* ATCC25922 grown on Luria Bertani (LB) agar.

Reprinted with permission from Yapor, J. P.; Alharby, A.; Gentry-Weeks, C.; Reynolds, M. M.; Mashud Alam, A. K. M.; Li, Y. V. Polydiacetylene Nanofiber Composites as a Colorimetric Sensor Responding To Escherichia coli and pH. *ACS Omega*. **2017**, *2(10)*, 7334-7342.

The comparison between the PEO–PDA and PU–PDA suggested that the combination of PEO and PDA is favorable since it provides a sensitive response to the presence of *E. coli*. The results were compared with samples of PDA polymer in the absence of a matrix polymer. The colorimetric response was similar when the PDA polymer and the PDA nanofiber composites were exposed to pH changes and the color change was found to occur at pH 10, and enhanced at pH 11–13. The PDA-containing nanofiber composites showed stronger colorimetric responses than those of the PDA polymer only, suggesting their potential as biosensors and chemosensors.

5.2 Introduction

Bacterial infection of wounds, including burns, diabetic foot ulcers and surgical-site infections impact approximately 2 million people and cost more than $18 billion in direct medical cost annually in the United States.[1] For example, chronically infected diabetic foot ulcers are the most critical wound care problem worldwide and 14–24% of these cases eventually suffer an amputation.[2] Wound dressings are typically used to protect the wound and surrounding tissue from contamination and to promote wound healing. Conventional wound dressings are generally not suitable for chronic and acute wounds nor are they suitable for treatment or monitoring the infection status of chronic and acute wounds. Novel strategies are in great need for early detection of wound infection, to prevent further complications and to enhance the healing process. One recently used strategy is to introduce biosensors that can monitor *in situ* the presence of bacteria in wounds and hence improve wound care and management. A biosensor is an analytical device that is made of an analyte in combination with a biological element such as an enzyme, antibody, or nucleic acid.[3,4] The biological element interacts with the analyte, resulting in a biological response that can be converted into electrical or electrochemical signals.[5] In particular,

colorimetric biosensors have been attractive due to their ease of use, rapid response, high prevision, accuracy, and cost effectiveness.[6] If colorimetric biosensors could be integrated into wound dressings, the wound dressings could potentially enable early detection of infections in wounds by providing *in situ* monitoring of the wound condition *via* colorimetric indication.[7] Biosensors can function in different transducers, including electrochemical, optical, electronic, piezoelectric, gravimetric, and pyroelectric.[8] In electrochemical biosensor development, conjugated polymers can be used to create the bio-transducer components in the sensor.[9] Polyaniline, polypyrrole and polydiacetylene are mostly used conjugative polymers to construct electrochemical biosensors because their electrochemical properties are usually associated with visible colorimetric changes.[10] Polydiacetylenes (PDAs) are specially attractive because they exhibit a blue-to-red color transition visible to the naked eye when they are subjected to external stimuli such as changes in temperature,[7,11-13] pH,[14] and the presence of bacterial cells,[15] and aromatic compounds.[16] PDAs were first synthesized by Wegner *et al.* in 1969, who identified the polymerization as a 1,4-addition reaction.[17] The potential use of PDAs in developing biosensors was first reported in 1993 when Bednarski *et al.* who coated a glass slide with a polydiacetylene bilayer and developed a direct colorimetric detection method for sialic acid, a receptor-specific ligand for the influenza virus.[18] Since then, a range of sensing systems were developed using PDAs such as films,[19] crystals,[20] and fibers.[21] Our previous studies showed that PDAs can be used in nanofiber composites for sensor applications, demonstrating their potential use in wound dressings and medical textiles.[7] Sensor sensitivity is generally increased *via* an increase in the contact surface area of biosensors. The surface area of nanofibers can be exceptionally high due to small diameters and high aspect ratios such as diameter to length ratio. Nanofiber composites exhibit excellent flexibility as well as high permeability, which meet ergonomic and physiological preferences in the application of medical

textiles such as wound bandages and surgical dressings. Due to the high cost and low spinnability of PDAs, the PDAs have been successfully incorporated into fiber/nanofiber composites with other polymers, such as polymethyl methacrylate (PMMA), polystyrene (PS), tetraethyl orthosilicate (TEOS), poly(ethylene oxide) (PEO), which serve as supporting components or matrix polymers in the composites. The PDA-containing nanofiber composites could be used to develop wound bandages and surgical dressings with biosensing capabilities.[10,22]

In this study, supporting polymers of polyethylene oxide (PEO) or polyurethane (PU), were separately mixed with the PDA monomer, 10,12-pentacosadiynoic acid (PCDA), and the mixtures were used in an electrospinning apparatus to create nanofiber composites. The nanofibers were then photopolymerized *via* UV irradiation resulting in PEO–PDA and PU–PDA nanofiber composites. The biosensing properties of the PEO–PDA and PU–PDA nanofiber composites were evaluated for their potential application as wound bandages and surgical dressings. PEO is a linear, semi-crystalline, biocompatible, nontoxic polymer approved for internal use in food, cosmetics, pharmaceutical and personal care products.[23] PEO is widely used due to its amphiphilic properties as well as its solubility in aqueous and organic solvents,[24] and its stability in air.[25] On the other hand, PU is also frequently used in medical products due to its good barrier properties and oxygen permeability. PU has been traditionally proven to be bio- and hemocompatible material.[26] The electrospun nanofibers of PEO–PDA and PU–PDA were exposed to *E. coli* (ATCC®25922) culture and the colorimetric behaviors were monitored to evaluate their biosensing properties. It was found that both nanofiber composites demonstrated colorimetric responses to *E. coli*, however the colorimetric changes in the PEO–PDA nanofibers responded differently than those changes in PU–PDA nanofibers. The colorimetric properties were measured using a photospectrometer as a function of exposure time to *E. coli*. The conditions of the bacterial culture, such as pH in Luria

Bertani (LB) media have great impact on the bacteria and their growth. Thus, colorimetric responses in the nanofiber composites were also monitored using the photospectrometer as a function of pH in a buffer solution without the presence of *E. coli* to study the correlation between biosensing behaviors and pH. The results showed no visible color changes in the PDA nanofibers at the pH < 11. Since most of known bacteria live in pH from 6 to 7, the results suggested that no false signal in detecting bacteria would occur at physiological pH. Our results suggested great potential of using the PDA-containing nanofiber composites in wound bandages and surgical dressings to detect the presence of bacterial infection and to continuously monitor wound health status. A schematic for the preparation of nanofibers is shown in Fig. 5.1.

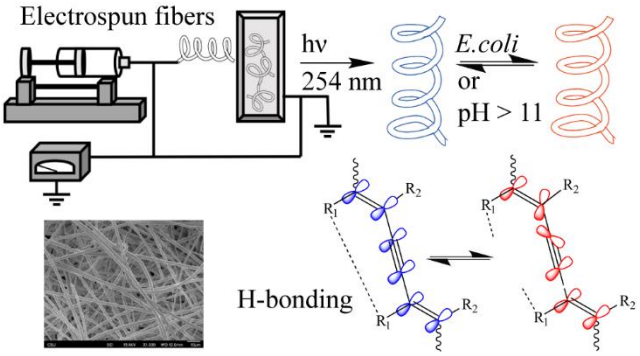

Figure 5.1 Schematic depicting the fabrication of nanofibers and chromatic changes. Reproduced with permission from the American Chemical Society.

5.3 Materials and methods

10,12-Pentacosadiynoic acid (PCDA, 98%) was purchased from GFS Organics (Columbus, OH) the PCDA monomer was used to synthesize polydiacetylenes (PDA) in the electrospinning. Poly(ethylene oxide) (PEO, M_w = 300,000 g/mol) was purchased from Sigma-Aldrich (St. Louis, MO). Polyurethane (PU) Tecoflex™ SG-80A was kindly donated by Lubrizol Corporation (Brecksville, OH). PEO and PU were used separately as matrix polymers in nanofiber composites. Luria Bertani (LB) and chloroform (≥ 99.8%) were purchased from Sigma-Aldrich

(St. Louis, MO). Tetrahydrofuran (THF, 99%), *N*,*N*-dimethylformamide (DMF, 99.8%, extra dry, AcroSeal®), and potassium hydroxide (KOH) were purchased from Fisher Scientific (Waltham, MA). LB broth/agar was used as the bacterial growth media. Chloroform, THF and DMF were solvents for the preparation of electrospinning solutions. Hydrochloric acid (HCl) was purchased from EMD chemicals (Gibbstown, NJ, USA). HCl and KOH were used to analyze the polymers at various pH values. *Escherichia coli* (*Migula*) *castellani* and *chalmers* ATCC 25922™ were purchased from ATCC (Manassas, VA). Reagents were used as received without further purification.

5.3.1 Polydiacetylene synthesis

The diacetylene monomer, PCDA, was used in the polymerization of PDAs. PDA polymerized from PCDA was synthesized following our previously reported procedure.[7] Briefly, 2.56 g PCDA (6.83 mmol) was dissolved in diethyl ether (35 mL) and filtered to remove any contaminants. Millipore water (18.2 MΩ·cm) was added to yield a 1.07 % w/v suspension, which was sonicated at 65 °C for 30 min. The suspension was allowed to cool to room temperature, then stored at 4 °C overnight. The suspension was transferred to a crystallizing dish with a magnetic stir bar and irradiated with UV light (254 nm) for 8 min.[27] After the photo-polymerization, the dark blue suspension was transferred to a round bottom flask protected from light to remove the solvent under vacuum. The solid PDA was then stored at 4 °C and characterized by ATR-FTIR and ultraviolet-visible (UV-Vis) spectrophotometer in diffuse reflectance mode.

5.3.2 Preparation of electrospinning solution

For the preparation of PDA-containing nanofiber composites, PCDA was mixed with PEO or PU to prepare electrospinning solutions by varying concentrations (w/w %) and mass ratios of PEO to PCDA and PU to PCDA. The mixture solution of PEO and PCDA was prepared by adding the calculated amount of PEO and PCDA in chloroform, followed by stirring overnight at room temperature on a hotplate stirrer at 600 rpm until a homogeneous solution in light pink was obtained. In mixing PU and PCDA, a binary solvent of 1:1 THF and DMF was used to prepare uniform solutions. It was attributed to the effect of solvent properties on the viscosity and surface tension of the solution. DMF is a dipolar aprotic solvent and has a high dielectric constant (36.7 at 25 °C) and dipole moment (3.8 D) as compared to the THF, which has a low dielectric constant (7.6 at 25 °C) and dipole moment (1.7 D).[28] A 1:1 by volume mixture of these two solvents achieved a balance of solution viscosity and conductivity, which was favorable for the formation of PU–PDA nanofibers *via* electrospinning. The mixture solution of PU and PCDA was prepared by dissolving the required amount of PU and PCDA in THF and stirring the mixture overnight at room temperature. The mixture was then added to the same volume of DMF and continuously stirred until a uniform solution in light pink was obtained.

5.3.3 Electrospinning and polydiactylene polymerization

A customized vertical electrospinning apparatus was used to prepare nanofiber composites. The apparatus primarily consisted of a Gamma High Voltage Research ES50P power supply, a plastic syringe, a stainless steel needle, a Harvard PHD 2000 syringe pump, and an aluminum plate type collector. A mixture solution of PEO and PCDA or PU and PCDA, respectively, was injected at 0.2 mL/h and 15 kV, resulting nanofibers collected at a collection distance of 25 cm. The time

for electrospinning a solution was 4 h to obtain a thick and colorless fiber mat. The as-spun fibers were stored in the dark overnight to avoid any changes due to light before the photopolymerization of PCDAs. A UV-light (Spectroline, Longlife™ filter, New York, USA) at 254 nm was used to photopolymerize PCDAs for 3 min, resulting PDAs embedded in PEO or PU nanofibers and creating PEO–PDA or PU–PDA nanofiber composites. After the UV irradiation, the color of the nanofiber composites became blue within 30 sec and then became deep blue within 3 min.

5.3.4 Scanning electron microscopy

The size and morphology of electrospun nanofibers were studied using a scanning electron microscope (SEM) (JEOL, JSM 6500F, Tokyo, Japan). The fiber mats were kept overnight under vacuum to evaporate any residual solvent or moisture, followed by sputter-coating with 10 nm of gold to improve the conductivity of the fiber samples.

5.3.5 Fourier transform infrared spectroscopy

Attenuated Total Reflectance Fourier Transform Infrared (ATR-FTIR) spectra of PCDA, PEO–PDA nanofibers, and PU–PDA nanofibers were collected on a Nicolet 6700 FTIR spectrometer (Thermo Electron Corp., Madison, WI) fitted with a Smart iTR ATR sampling accessory and ZnSe crystal plate.

5.3.6 Colorimetric response to pH

Colorimetric response of PDAs to pH was investigated. The tested PDAs included 100% PDA powders (PPCDA synthesized in this study) and the PDA composites (PEO–PDA nanofibers obtained at 2:1 mass ratio and 3.75% and PU–PDA nanofibers obtained at 2:1 mass ratio and 25%).

Buffer solutions were prepared by mixing HCl and KOH, resulting in a range of pH values from 0 to 14. The PDA polymer, and the PEO–PDA and PU–PDA nanofiber composites were individually dispersed with 1 % w/v in the buffer solutions. All of the suspension solutions were stirred for 1 h to improve uniformity of the solutions. In order to obtain dry, solid materials, the solvent was removed using a lyophilizer and the samples were analyzed using a Nicolet Evolution 300 UV-Vis spectrophotometer in diffuse reflectance mode. The colorimetric response (% CR) was calculated using equation 1 as below.[14]

$$\%CR = \left[\frac{(PB_0 - PB)}{PB_0}\right] \times 100 \qquad (1)$$

where the initial percent blue (PB_0) is the percent blue before color change and percent blue (PB) is the final percent blue after exposure to external stimuli. The PB value was calculated using equation 2.

$$PB = \frac{A_{blue}}{(A_{red} + A_{blue})} \qquad (2)$$

where A_{blue} the absorbance at 648 nm and A_{red} the absorbance at 537 nm.

5.3.7 Bacterial culture

*E. coli (*ATCC®25922) was streaked on LB agar and was grown to saturation at 37 °C for 24 h. One colony was inoculated into LB broth medium and incubated at 37 °C with shaking at 200 rpm using MaxQ Shaker for 18 h. An aliquot (100 µl) of the overnight bacterial culture was spread on LB agar and incubated at 37 °C for 36 h. The *E. coli* culture was used to test the colorimetric responses of the obtained nanofiber composites.

5.3.8 Colorimetric response to bacteria

The colorimetric transition of the nanofiber composites upon direct exposure to *E. coli* was evaluated using a spectrophotometer (HunterLab ColorQuest XE) as a function of exposure time (0.5 h, 1.0 h, 1.5 h, 2.0 h, 2.5 h, 3.0 h). Electrospun fiber mats were cut into 6.5 cm^2 mats. Each 6.5 cm^2 fiber mat was then placed flat in a clear petri dish where *E. coli* was cultured, and the dish was closed and sealed tightly. This set-up allowed bacteria to be in direct contact with the *E. coli* in the petri dish. Because the fiber mat was flat on the bottom of the petri dish and the petri dish was clear, it was possible to conduct spectrophotometer measurements with the appropriate baseline. The method avoided cross-contamination and allowed the measurements to be taken in real time, without removing the fiber mat from the dish. Spectrophotometric measurements were then taken by placing the petri dishes on the spectrophotometer measurement outlet while the fiber mats were still in the petri dish. The colorimetric reflectance of the fiber mat was measured every 30 min for 3 h. The outside of the petri dishes was wiped and cleaned with ethanol before each spectrophotometric measurement. For these measurements, three fiber samples obtained at each electrospinning condition were used in the spectrophotometer. At each time interval, three spectrophotometric measurements were conducted for the colorimetric analysis in each fiber mat. An average of the colorimetric reflectance of each fiber mat was calculated and used in the analysis of colorimetric response. The experimental procedure was also followed for the controls, which included fiber samples in LB agar only, the supernatant, or the pellet. The LB agar was pristine and not used for previous bacteria growth. The supernatant and the pellet were obtained after the solution was centrifuged and filtered.

A reflectance value was obtained for all the fiber mat samples using the ColorQuest spectrophotometer. Therefore, it was necessary to convert reflectance to absorbance so that

colorimetric response could be calculated using equations 1 and 2. The absorbance of the blue and red phases can be calculated based on the reflectance values using equation 3 as below.

$$\text{Absorbance} = \log[\frac{1}{\text{Reflectance}/100}] \qquad (3)$$

The resulted absorbance value was used to calculate the colorimetric response to measure the efficiency of the color change of PDA in the fibers responding to *E. coli*. The reflectance of the blue phase in the spectrophotometer spectrum was measured at 640 nm, and the red reflectance was measured at 540 nm. These reflectance values were first converted into absorbance then used to calculate the colorimetric response that represents the relative change from blue to red color of PDA before and after exposure to the bacterial cells.

In summary, Fig. 5.2 shows the experimental design for preparing electrospinning solutions, specified concentrations, mass ratios and tests performed of PEO–PDA and PU–PDA fibers.

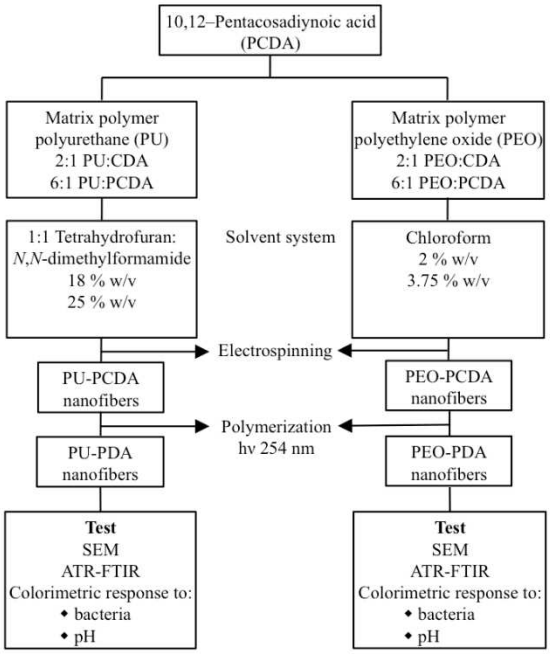

Figure 5.2 Experimental design scheme of polydiacetylene electrospun fibers. Reproduced with permission from the American Chemical Society.

5.4 Results and discussion

5.4.1 Fiber morphology

Fig. 5.3a and 5.3b show the SEM images of PU–PDA and PEO–PDA electrospun fibers obtained at different spinning conditions. Polymer concentration and mass ratios of matrix polymer to PCDA (the monomer of PDA) had great impact on fiber morphology. The morphology of PU–PDA fibers was generally different from that of PEO–PDA fibers. Beads on fibers were present in the PEO–PDA fibers obtained at 2% w/v concentrations and the PU–PDA fibers obtained at 18 % w/v concentrations when the mass ratio of matrix polymer to PCDA was 2:1. During electrospinning, PDA solutions with low viscosity experienced a low viscoelastic force resulting in partial break up in the electrical jet. Due to the effect of surface tension, free solvent molecules in the solution accumulated into a spherical shape causing a formation of beads. The number of beads was significantly reduced when the concentrations were higher at 25 % w/v for PU–PDA fibers and 3.75 % w/v for PEO–PDA fibers, respectively. The mass ratio between matrix polymer to PCDA had a similar effect on fiber morphology. Fewer beads were formed at the high mass ratio (6:1) for both PU–PDA and PEO–PDA fibers. The formation of beads was attributed to the insufficient polymer chain entanglement at low concentrations. In principle, the polymer chains are stretched by electrostatic forces during electrospinning, resulting in linear fibers only if sufficient polymer chain entanglements prevent breakage and discontinuity in the solidified fibers. A low concentration of the polymers results in insufficient chain entanglements that result in beaded fibers.[23,29]

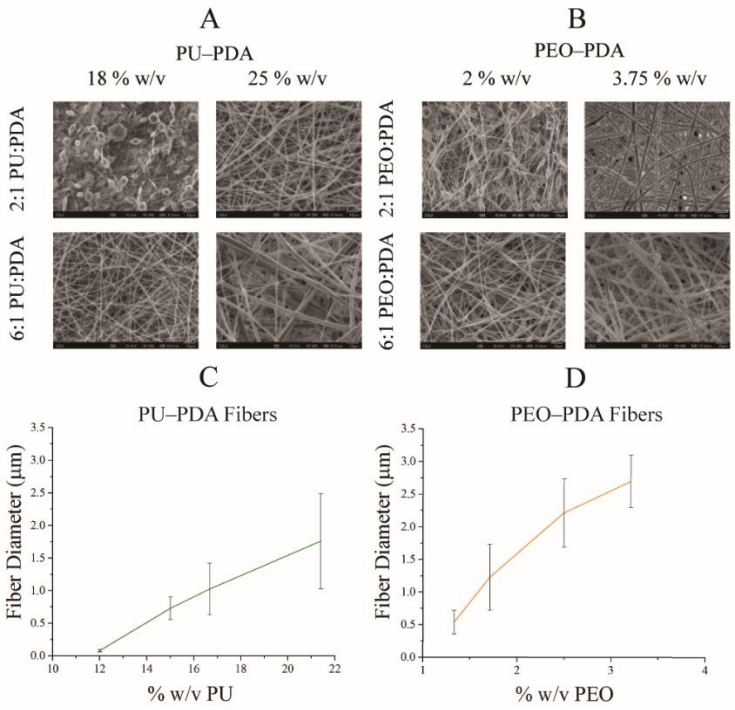

Figure 5.3 SEM images of PU–PDA (A) and PEO–PCDA (B) electrospun fibers are presented in section A and B. Graphs C and D depict the average diameter of electrospun fibers for PU–PDA and PEO–PDA, respectively. Each data point represents an average of $n \geq 3$ replicates and the standard deviation. Reproduced with permission from the American Chemical Society.

Matrix polymers used in the electrospinning are primarily to enhance the spinnability of PDAs, since it is difficult to electrospin PDAs alone due to their impaired solubility and low viscosity. Therefore, the concentration of the matrix polymer (PU or PEO) was calculated, based upon the mass ratio and total polymer concentration. Fig. 5.3b and 5.3c show the correlation between the fiber diameter and the concentration of PU and PEO, respectively. The fiber diameters of the PDA fibers prepared with both PU and PEO varied with the change in mass ratio. The diameter of fiber samples of PU–PDA and PEO–PDA increased linearly with the increase of matrix polymer concentration (PU/PEO), which is attributed to the higher viscosity and surface tension of the electrospinning solution.[30] In addition, beads on the string were formed at low concentrations due to the low viscosity of the electrospun solution. Coarse fibers were formed at the high mass ratio of matrix polymer (PU or PEO) to PCDA. On the other hand, the SEM images

shown in Fig. 5.3 suggest that the surface roughness of the fibers increased with an increase in fiber diameter. The surface roughness of PU–PDA and PEO–PDA fibers appeared slightly different. This might be due not only to the nature of different matrix polymer but also to the different solvents used. Surface morphology of PEO and PDA electrospun fibers was previously reported differently when different solvents were used including chloroform, methylene chloride, and dimethyl formamide.[31]

5.4.2 Chemical analysis *via* attenuated total reflection-Fourier transform infrared spectroscopy

Colorimetric changes in conjugated polymers are usually due to conformational changes in the conjugated macromolecules, such as PDAs. In this study, PDAs were mixed with PEO or PU, resulting in PEO–PDA and PU–PDA nanofiber composites. It leads a question whether the PEO or PU mixed with PDA has an effect on conjugated macromolecules at a molecular level and hence influence on electrochemical properties in the nanofiber composites. Therefore, chemical analysis was carried out *via* ATR-FTIR for PDAs including PDAs embedded in PEO and PU fibers, and PDA in the absence of matrix polymers. ATR-FTIR measurements were conducted on samples in the blue phase prior to chromatic changes and the spectra are shown in Fig. 5.4. Spectrum A corresponds to the PU–PDA fibers, where the following resonance features were interpreted for characterization; IR νmax/cm^{-1}: 3324 cm^{-1} (N–H stretch), 2919–2847 cm^{-1} (C–H stretch), 1692 cm^{-1} (C=O stretch), 1104 cm^{-1} (C–O stretch), and 723 cm^{-1} (C–H bend). Similar features were observed in spectrum B representing PEO–PDA fibers; IR νmax/cm^{-1}: 2919–2847 cm^{-1} (C–H stretch), 1691 cm^{-1} (C=O stretch), 1097 cm^{-1} (C–O stretch), 723 cm^{-1} (C–H bend). The resulting resonance features were similar to previously reported results for PDAs, and the spectra

were consistent with the anticipated structures.[7,32] PDAs synthesized in the absence of a matrix polymer were also characterized by ATR-FTIR before the color transition and are shown in Fig. 5.4. Spectrum C represents PDA in the absence of matrix polymer with key vibrational bands originating at IR νmax/cm^{-1}: 2918–2847 cm^{-1} (C–H stretch), 1690 cm^{-1} (C=O stretch), 722 cm^{-1} (C–H bend). Resonance features that indicate the presence of PDAs are seen on all spectra, where the most prominent stretch is due to the carbonyl. Substitution at the terminal hydroxyl groups of the dicarboxylic acid monomers is shown by the absence of resonance features that correspond to those groups. The results suggest that the characteristic macromolecular structures of PDA were not altered after the composite polymer was formed with the matrix polymer. Thus, the electrochemical and colorimetric properties are not significantly altered in the nanofiber composites.[33]

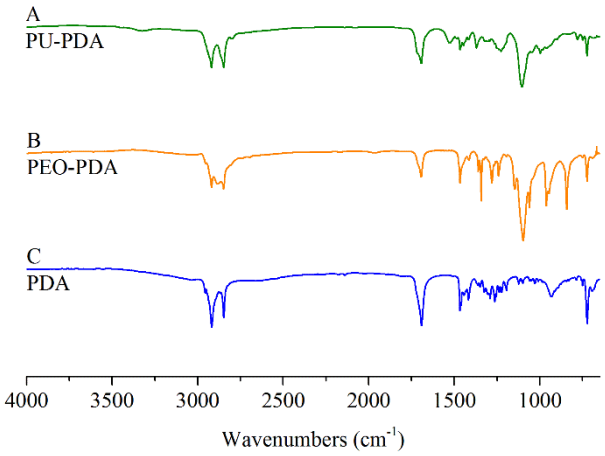

Figure 5.4 ATR-FTIR spectra of polymeric fibers and PDA polymers. The signals correspond to: PU–PDA fibers (A), PEO–PDA fibers (B), PDA (C). Reproduced with permission from the American Chemical Society.

5.4.3 Colorimetric response to bacteria

PEO–PDA and PU–PDA fiber composites were immersed in *E. coli* culture and their colorimetric properties were monitored as a function of contact time. The fibers were in the blue phase before they were immersed and after immersion the fibers demonstrated color changes to

red immediately. The fiber samples that were immersed in a control dish containing only LB agar prepared without *E. coli* remained blue and no visible colorimetric change was observed. In order to confirm our hypothesis involving membrane-secreted compounds, additional controls were investigated by using the pellet or the supernatant. Our findings indicated that the fiber in contact with the pellet underwent a color transition from blue to red, whereas the fiber in contact with the supernatant did not fully show a red shift. The fiber mat that was exposed to the supernatant appeared purple. The change suggests that bacterially secreted proteins that were present in the media might be capable of initiating the color transition.[15]

Fig. C.1 and C.2 show photographs of colorimetric responses of the PU–PDA and PEO–PDA fibers every 30 min from t = 0 min to t = 3 h, respectively. The color changes were different in the fibers obtained at various electrospinning parameters.

The color transition from blue to red was rapid in the fibers with a high mass ratio (6:1). The slowest transition of color was observed in the fibers that were prepared at lowest concentrations and lowest mass ratio. It was found that the color of beaded fibers remained unchanged for longer time than that of the fibers without a significant amount of beads. The beads on the fibers might disturb the interaction with bacterial cells and cause a delay in color transition. Continuous fibers without beads exhibited a fast and prominent color change. The color change became less drastic in the PEO–PDA fibers at 1.5 h and in the PU–PDA fibers at 2.5 h, respectively. The intensity of the red in the PEO–PDA fibers reached its maximum color intensity after 3 h. A similar trend was found in the PU–PDA fibers. The color transition continued and no significant color change was observed after 3 h. The PU–PDA fibers obtained at a mass ratio of 6:1 and 18 % w/v concentration exhibited an early and vivid color transition as compared to the

rest of fibers. The color change became more distinct as the pH of the solution increased and the concentration of bacteria increased.

Representative reflectance spectra are shown in Fig. 5.5 for the PEO–PDA fiber mat that was obtained at 2:1 mass ratio and 3.75 % w/v solvent concentration. Untreated polymerized blue fiber mats that were used as controls showed a slight increase in the reflectance value at 640 nm, but remained unchanged at 540 nm. After the fibers were exposed to *E. coli* for 30 min, they started to change color and exhibited a wide reflectance peak at 610 nm, which bypassed the original peak at 640 nm. The reflectance switch on the spectra was continuously developed when the interaction between the fibers and *E. coli* continued for 3 h.

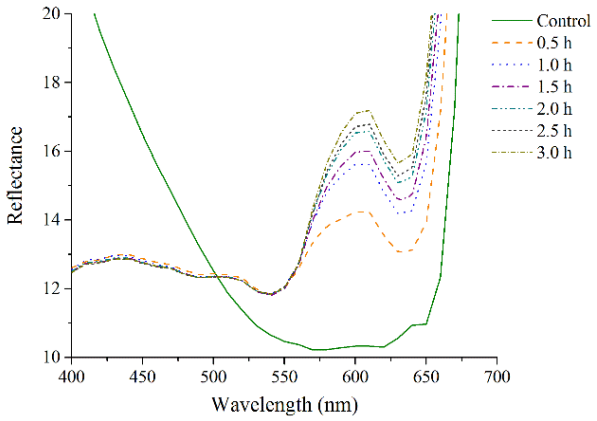

Figure 5.5 Reflectance spectra of the PEO–PDA fiber mat 2:1 mass ratio and 3.75 % w/v solvent concentration over time after the exposure to *E. coli*. The solid line represents the blue PDA fibers (control), and the different dotted lines represent the fibers after exposure to *E. coli* for different time periods. Reproduced with permission from the American Chemical Society.

A comparison between the PEO–PDA and PU–PDA fibers is made to investigate the colorimetric transition in different fiber composites. Both the PEO–PDA and PU–PDA fibers obtained at 6:1 mass ratio showed a pronounced reflectance switch. It was found that the low switch was shown by the fine fibers obtained at 2:1 PEO: PDA ratio and 2 w/v % polymer concentration, while a high switch was shown by the coarse fiber obtained at 6:1 PEO: PCDA ratio and 3.75 w/v % polymer concentration. Our earlier discussion on fiber size indicated that an

increase in the amount of PEO in electrospinning solution influenced the fiber size, resulting in an increase of the fiber diameter. The increase of the fiber diameter thus expanded the exposed surface area and enhanced color transition from blue to red. Additionally, the fiber surface became rough with the increase of the fiber diameter. The high reflectance of the color switch from blue to red that was associated with the coarser fibers was probably due to the high reflectance surface area of the rough fibers.

Previous studies proposed that the mechanism responsible for the color change might be attributed to the release of endotoxins, such as lypopolysaccharides, from the gram-negative bacterial strain. As membrane-active compounds are secreted by proliferating bacteria, the PDA undergoes conformational transitions by perturbations that disrupt hydrogen bonding of the head-groups and favor binding of positively charged ions.[15] Further studies that explore the interaction between bacterial cells and PDAs are needed to investigate the driving force of the color change as a response to *E. coli*.

The colorimetric response of PEO–PDA and PU–PDA fibers is presented in Fig. 5.6. The % CR between the blue and red reflectance correlates to the intensity of color transition. Fig. 5.6a shows that at the same time integral, the PEO–PDA fibers obtained at the PEO:PCDA mass ratio of 2:1 and the concentrations of 2 w/v % demonstrated lowest % CRs (2.6–3.6), which represent the lowest color transition. Fig. 5.6b shows that at the same time integral, the PU–PDA fibers obtained at the PU:PCDA mass ratio of 2:1 and the concentrations of 18 % also presented lowest % CRs (1.7–2.9), showing the lowest color transition. The increases in both mass ratio and concentration for both fibers were able to enhance the colorimetric response of the PDA-containing composites. It is in agreement with previous conclusion that the increase in the concentration of the matrix polymer (PEO) increases the surface area of the fiber that is in contact with the bacterial

cells and enhances colorimetric response behaviors. In addition, it is important to notice that, by comparison of Fig. 5.6a and 5.6b, the % CRs of the PEO–PDA composites were higher than those of the PU–PDA composites at the similar spinning conditions, suggesting faster color transition occurring in the PU–PDA composites. For example, the maximum % CR by the PEO–PDA and PU–PDA are 15.2 and 10.6, respectively. This may be due to the interaction between the two components in the composites, which include the sensing component of PDA and the matrix polymer. The results show that the combination of PEO and PDA give rise to a favorable and sensitive response in the presence of *E. coli*. The mechanism of sensitive response by the PEO–PDA composites needs further investigation.

It can be noticed that both PU–PDA (6:1 mass ratio and 18%) and PEO–PDA (2:1 mass ratio and 3.75%) fibers demonstrated a high % CR. These values were also associated with relatively large variation shown, suggesting that strong colorimetric responses might not necessarily indicate high sensitivity and stability of color changes in these fibers.

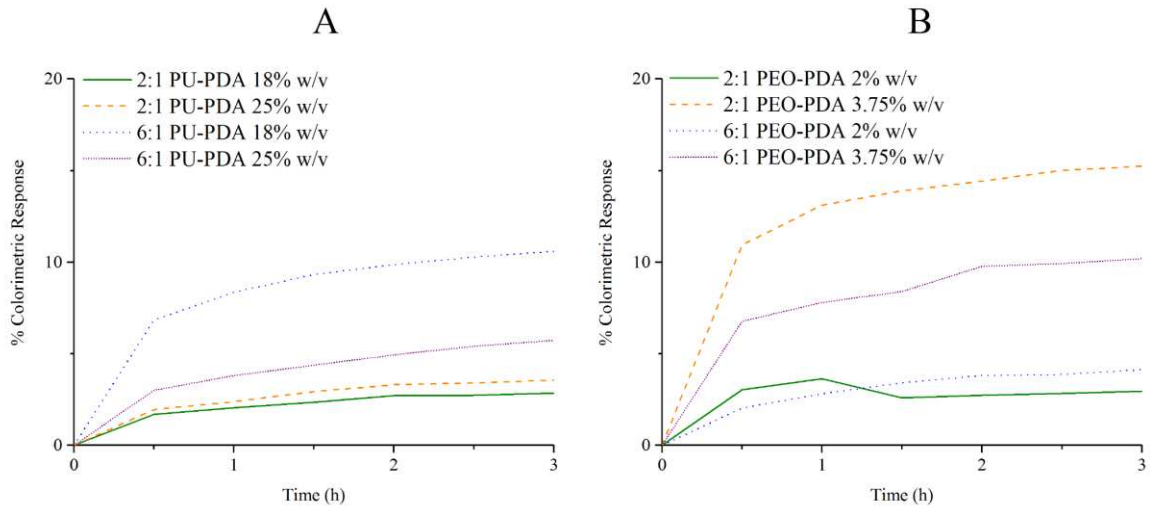

Figure 5.6 Representative colorimetric response values of PU–PDA and PEO–PDA fibers after direct contact with *E. coli* for 3 h. Graph A and B depict PU–PDA and PEO–PDA fibers, respectively, that were prepared by varying the matrix polymer ratio to PDA. Reproduced with permission from the American Chemical Society.

PEO–PDA and PU–PDA nanofiber composites, and PDA in the absence of matrix polymer were separately dispersed in buffer solutions where the pH varied in the range of 0 to 14. The suspensions were measured using UV-Vis and the absorbance was used to calculate colorimetric responses. The absorbance spectra of the samples immersed in the buffer solution with pH 0–9 were nearly overlapped, suggesting no color change in this range of pH. When the pH increased to 10, 11, 12, and 13, the color of the PEO–PDA and PU–PDA nanofiber suspensions changed from blue to purple and finally to red. The color shift was significant at pH 11–13. The changes were likely due to the high concentration of hydroxide ion at pH 11–13, which had significant impact on chemical environment and hydrogen bonding of the PDAs.[18,34] Previous work suggested that pH changes in the PDA can alter the hydrogen bonding of the carboxylic acid head groups inducing a conformational change in the PDA backbone that leads to a color transition of the polymer.[18,35] In this case, changes in the chemical environment cause a reflectance shift due to shortening of the p-conjugated bonds in the backbone of the polymer.[36] In the blue phase, π electrons within the polymer backbone are delocalized.[37] As the hydrogen bonding is disrupted by external stimuli, the π electrons become distorted and the polymer reaches the red phase.[38]

The intensity of color transition was clear at pH 11 when the PDA demonstrated a color of purple given that the color transition was reversible and was not fully completed at pH 11. When the pH was further increased to 12, the PDA nanofibers in the solution became red. The color change was captured by the increase of the colorimetric response calculated by the absorbance at 640 nm (blue phase) and 540 nm (red phase). The colorimetric responses were plotted against the pH in the buffer solutions and the plots are shown in Fig. 5.7. It was found that the color transition from blue to red was promoted at pH 12 and 13. Then the colorimetric responses slightly dropped at the extremely alkaline condition (pH = 14).

Similar results were obtained using 100% PDAs in the absence of matrix polymers as the PDA fibers. No color change was seen in pH values ranging from 0 to 9. The colorimetric response began at pH 11. At high pH values (12–14), the PDA polymer followed a similar pattern of colorimetric response as the PDA nanofiber composites.

In comparison between the PDA polymer and the PDA nanofiber composites, it is important to notice that the colorimetric responses of the PDA nanofiber composites are higher than those of the PDA polymer at pH 11. The colorimetric response is due to the self-assembled PDA macromolecular chains, also called "synthetic vesicles".[33] The electrospinning significantly enhanced the formation of self-assemblies of the PDA macromolecules and then improved the organization of synthetic vesicles within the nanofibers. Therefore, the colorimetric response was enhanced in the PDA nanofiber composites. In addition, the high surface area of the electrospun nanofibers was able to increase the colorimetric response as well. The results suggested that the PDA nanofiber composites are good candidates for biosensor applications.

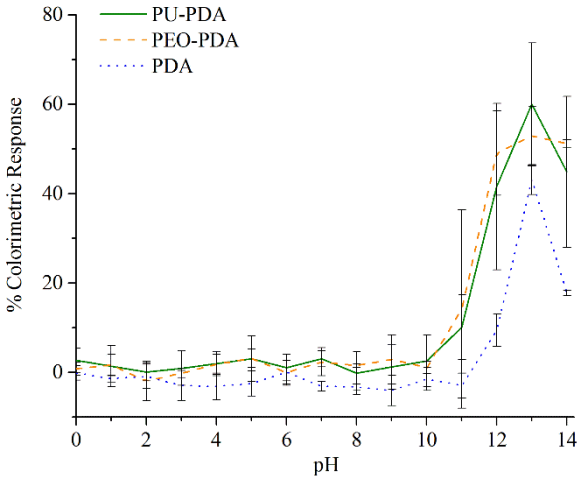

Figure 5.7 The colorimetric response of 100% PDA polymer, PEO–PDA, and PU–PDA nanofiber composites as a function of pH when immersed in buffer solutions. Each data point represents an average of $n \geq 3$ replicates and the standard deviation. Reproduced with permission from the American Chemical Society.

5.5 Conclusions

Two polymers, PEO and PU, were separately mixed with diacetylene (DA) monomers and the mixtures were used to create PEO–PDA and PU–PDA nanofiber composites using an electrospinning method. Smooth and uniform nanofibers with diameters ranging from 130 nm to 2.5 μm were obtained at high concentrations and mass ratios. The variation in the nanofiber morphology was attributed to the mixture solutions and spinning conditions in the electrospinning. Although the PDAs are known with colorimetric properties due to external stimuli, to the best of our knowledge, we are the first to report that the PDA nanofiber composites were able to respond to the presence of *E. coli* and the change of pH in buffer solutions. The colorimetric response to *E. coli* was more pronounced for 6:1 PEO:PDA at 3.75% w/v concentration than for 2:1 PEO:PDA at 2% w/v concentration. The % CR to *E. coli* was more intense in 6:1 PU–PDA at 25% w/v concentration than for 6:1 PU–PDA at 18 % w/v concentration. The results suggest that the increase in fiber diameter and surface area enhanced the colorimetric sensitivity to *E. coli*. Both the PEO–PDA and PU–PDA nanofiber composites demonstrated a sensitive colorimetric response due to the presence of *E. coli*. The comparison results show that the combination of PEO and PDA is favorable in sensitive response to *E. coli*. ATR-FTIR analysis confirmed that the colorimetric response was not caused by a variation of the functional groups within the polymer. Such results are in accordance with previous reports which suggest that the color change was induced by a conformational change in the molecular configuration of PDA when the PDA interacted with *E. coli*. The colorimetric responses of the PDA only, PEO–PDA and PU–PDA nanofiber composites were also investigated in buffer solutions with pH 0–14. Similar responses were found that the colorimetric response did not occur until pH 10, then increased at pH 11, 12, 13, followed by a slight drop at pH 14. Our results demonstrate that the PDA-containing nanofiber composites can

be used in developing sensitive, flexible, and lightweight biosensors that are easy-use, durable, and do not require a power supply. The potential applications include lab-on-chip sensors, wearable sensors, and medical sensing textiles such as wound dressing and bandages.

Individual contributions and funding sources

A. Alharby performed bacteria experiments, prepared fiber samples as needed, and aided with colorimetric response analysis with respect to pH variation. A. K. M. Mashud prepared fibrous samples and performed microscopic analysis. All other characterization was carried out by J. P. Yapor. This work was funded by Agricultural Experiment State at Colorado State University (COL00628) and Colorado Clinical & Translational Sciences Institute Pilot Program supported by the University of Denver.

REFERENCES

1. DeLeon, S.; Clinton, A.; Fowler, H.; Everett, J.; Horswill, A. R.; Rumbaugh, K. P. *Infect. Immun.* 2014, *82*, 4718.
2. Leese, G.; Reid, F.; Green, V.; McAlpine, R.; Cunningham, S.; Emslie-Smith, A.; Morris, A.; McMurray, B.; Connacher, A. *Int. J. Clin. Pract* 2006, *60*, 541.
3. Ivnitski, D.; Abdel-Hamid, I.; Atanasov, P.; Wilkins, E. *Biosens. Bioelectron.* 1999, *14*, 599.
4. Owicki, J. C.; Parce, J. W. *Biosens. Bioelectron.* 1992, *7*, 255.
5. Cooper, M. A. *Nat. Rev. Drug Discov.* 2002, *1*, 515.
6. Chen, X.; Zhou, G.; Peng, X.; Yoon, J. *Chem. Soc. Rev.* 2012, *41*, 4610.
7. Alam, A.; Yapor, J. P.; Reynolds, M. M.; Li, Y. V. *Materials* 2016, *9*, 202.
8. Sethi, R. S. *Biosens. Bioelectron.* 1994, *9*, 243.
9. Ronkainen, N. J.; Halsall, H. B.; Heineman, W. R. *Chem. Soc. Rev.* 2010, *39*, 1747.
10. Dargaville, T. R.; Farrugia, B. L.; Broadbent, J. A.; Pace, S.; Upton, Z.; Voelcker, N. H. *Biosens. Bioelectron.* 2013, *41*, 30.
11. Chen, X.; Kang, S.; Kim, M. J.; Kim, J.; Kim, Y. S.; Kim, H.; Chi, B.; Kim, S. J.; Lee, J. Y.; Yoon, J. *Angew. Chem. Int. Ed.* 2010, *49*, 1422.
12. Lee, S.; Kim, J.-Y.; Chen, X.; Yoon, J. *Chem. Commun.* 2016, *52*, 9178.
13. Park, I. S.; Park, H. J.; Kim, J.-M. *ACS Appl. Mater. Interfaces* 2013, *5*, 8805.
14. Charoenthai, N.; Pattanatornchai, T.; Wacharasindhu, S.; Sukwattanasinitt, M.; Traiphol, R. *J. Colloid Interface Sci.* 2011, *360*, 565.

15. Silbert, L.; Shlush, I. B.; Israel, E.; Porgador, A.; Kolusheva, S.; Jelinek, R. *Appl. Environ. Microbiol.* 2006, *72*, 7339.

16. Scoville, S. P.; Shirley, W. M. *J. Appl. Polym. Sci.* 2011, *120*, 2809.

17. Wegner, G. *Z. Naturforsch. B Chem. Sci.* 1969, *24*, 824.

18. Charych, D. H.; Nagy, J. O.; Spevak, W.; Bednarski, M. D. *Science* 1993, *261*, 585.

19. Lee, J.; Jun, H.; Kim, J. *Adv. Mater.* 2009, *21*, 3674.

20. Chen, X.; Li, L.; Sun, X.; Liu, Y.; Luo, B.; Wang, C.; Bao, Y.; Xu, H.; Peng, H. *Angew. Chem. Int. Ed.* 2011, *50*, 5486.

21. Sheikh, F. A.; Macossay, J.; Cantu, T.; Zhang, X.; Hassan, M. S.; Salinas, M. E.; Farhangi, C. S.; Ahmad, H.; Kim, H.; Bowlin, G. L. *J. Mech. Behav. Biomed. Mater.* 2015, *41*, 189.

22. Aplander, K.; Marttila, M.; Manner, S.; Arnberg, N.; Sterner, O.; Ellervik, U. *J. Med. Chem.* 2011, *54*, 6670.

23. Shenoy, D.; Little, S.; Langer, R.; Amiji, M. *Mol. Pharm.* 2005, *2*, 357.

24. Hu, Y.; Jiang, X.; Ding, Y.; Zhang, L.; Yang, C.; Zhang, J.; Chen, J.; Yang, Y. *Biomaterials* 2003, *24*, 2395.

25. Jeon, H.; Lee, J.; Kim, M. H.; Yoon, J. *Macromol. Rapid Commun.* 2012, *33*, 972.

26. Zdrahala, R. J.; Zdrahala, I. J. *J. Biomater. Appl.* 1999, *14*, 67.

27. Champaiboon, T.; Tumcharern, G.; Potisatityuenyong, A.; Wacharasindhu, S.; Sukwattanasinitt, M. *Sens. Actuators B Chem.* 2009, *139*, 532.

28. Erdem, R.; Usta, I.; Akalin, M.; Atak, O.; Yuksek, M.; Pars, A. *Appl. Surf. Sci.* 2015, *334*, 227.

29. Nie, H.; He, A.; Wu, W.; Zheng, J.; Xu, S.; Li, J.; Han, C. C. *Polymer* 2009, *50*, 4926.

30. Lee, K. H.; Kim, H. Y.; Ryu, Y. J.; Kim, K. W.; Choi, S. W. *J. Polym. Sci. Part B Polym. Phys.* 2003, *41*, 1256.

31. Yoon, J.; Chae, S. K.; Kim, J.-M. *J. Am. Chem. Soc.* 2007, *129*, 3038.

32. Pratt, F.; Wong, K.; Hayes, W.; Bloor, D. *J. Phys. C : Solid State Phys.* 1987, *20*, L41.

33. Okada, S.; Peng, S.; Spevak, W.; Charych, D. *Acc. Chem. Res.* 1998, *31*, 229.

34. Kew, S. J.; Hall, E. A. *Anal. Chem.* 2006, *78*, 2231.

35. Zhou, G.; Wang, F.; Wang, H.; Kambam, S.; Chen, X. *Macromol. Rapid Commun.* 2013, *34*, 944.

36. Cheng, Q.; Stevens, R. C. *Adv. Mater.* 1997, *9*, 481.

37. Morigaki, K.; Baumgart, T.; Jonas, U.; Offenhäusser, A.; Knoll, W. *Langmuir* 2002, *18*, 4082.

38. Ahn, D. J.; Chae, E. H.; Lee, G. S.; Shim, H. Y.; Chang, T. E.; Ahn, K. D.; Kim, J. M. *J. Am. Chem. Soc.* 2003, *125*, 8976.

CHAPTER 6

PRACTICAL CONSIDERATIONS AND FUTURE DIRECTIONS

6.1 The use of polyesters as platforms for the delivery of nitric oxide

***S*-nitrosated PCMO-penicillamine.** Polyesters have been used in the field of medical applications due to the wide array of materials that can be prepared from polycondensation reactions. Chapter 1 described the used of carbodiimide chemistry to couple thiol-bearing amines as pendant groups for the formation of RSNOs. Cysteamine hydrochloride and L-cysteine ethyl ester hydrochloride were successfully used for the preparation of thiol-bearing polyesters. However, the use of D-penicillamine (4.196 g, 28.12 mmol) purchased from Sigma-Aldrich (St. Louis, MO, USA), during the carbodiimide coupling reaction yielded a material with increased water solubility. The general method for the formation of PCMO-cysteamine described in Chapter 1 was followed to produce an orange-brown viscous polyester. The *S*-nitrosation reaction was also performed using a mixture of PCMO-penicillamine/ethanol (25 mg mL^{-1}) and *t*-BuONO (0.500 mL) that was stirred at RT for 4 h, time after which the solvent was removed under vacuum. The material obtained after the *S*-nitrosation reaction was a green viscous material with blue undertones. Given that D-penicillamine is composed of a tertiary thiol, the green hue was expected since it is a characteristic absorbance features for tertiary RSNOs occur at approximately 340 and 600 nm.[1,2] The total nitric oxide release of *S*-nitrosated-PCMO-penicillamine was 0.079 ± 0.041 mmol g^{-1}. The total nitric oxide release was calculated from thermal decomposition of the material at 120 °C in the absence of solvent. A limitation with the use of *S*-nitrosated-PCMO-penicillamine arises from its solubility in aqueous solutions. Hydrolytic degradation studies at physiological pH and temperature were not successful for this

material given that the polyester was soluble in the solution used (PBS, pH 7.4). Gravimetric analysis confirmed that the material had approximately 0 % remaining weight after the first week of incubation. The accelerated degradation profile of the material complicated its use for the intended application, so the material was not used for the remaining experiments in the study. Fig. 6.1 and 6.2 depict chemical characterization techniques used for this material.

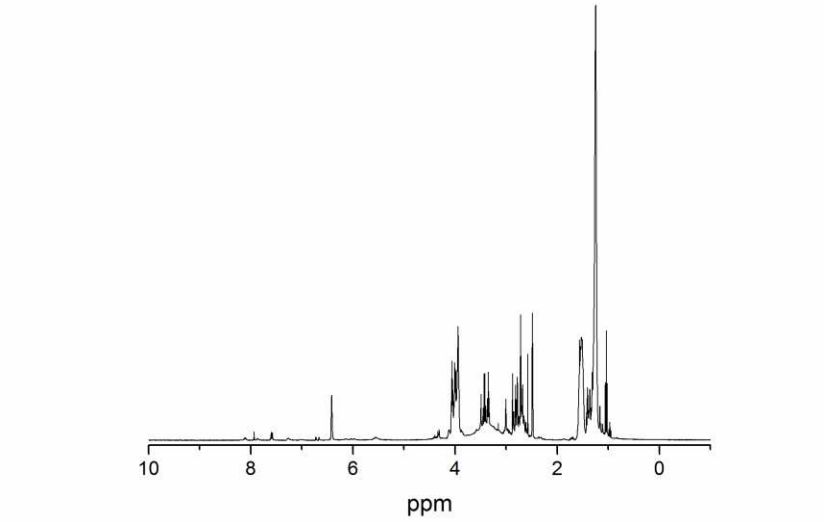

Figure 6.1 ^{1}H NMR spectrum of PCMO-penicillamine.

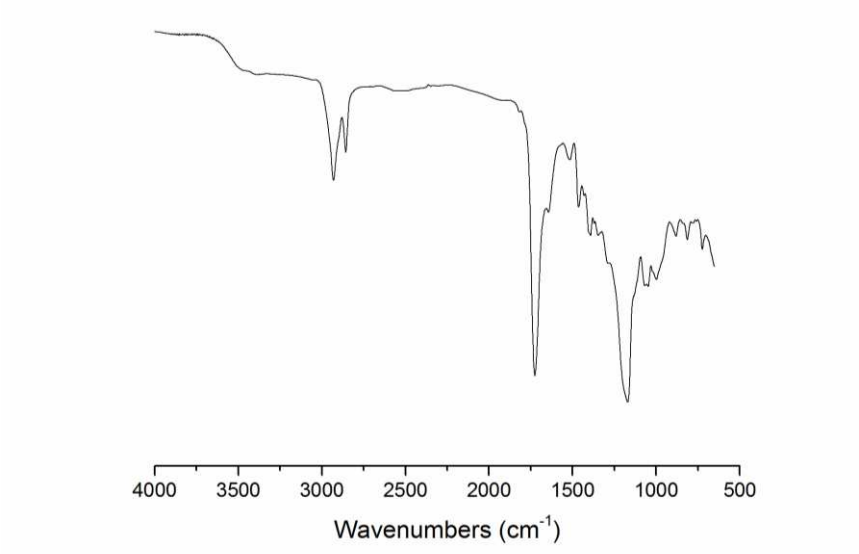

Figure 6.2 FTIR-ATR spectrum of PCMO-penicillamine.

Poly(citrate-*co*-malic acid-*co*-1,8-octanediol). Various polyesters were prepared form the combination of monomeric units such as diacids and diols. The general procedure for the formation of PCMO was followed for the synthesis of an analogue with L-(−)-malic acid procured from Fluka Analytical (College Park, GA, USA). Citric acid (5.793 g, 30 mmol), L-(−)-malic acid (2.983 g, 22 mmol), and 1,8-octanediol (7.462 g, 51 mmol) were stirred at 350 rpm under nitrogen flow for 10 min at RT. Diethyl ether (5 mL) was added to incorporate all solids to the bottom of the round bottom flask to optimal stoichiometric quantities. The temperature was maintained at 140 °C with constant stirring for 2 h. At the end of the experiment, the polyester has become quite viscous and impeded the stir bar from rotating. The polycondensation was stopped and the elastomeric material was used for solubility assessment. It was concluded that the material was a thermoset given that solubility was not achieved in dichloromethane, chloroform, dimethylformamide, 1,4-dioxane, methylene chloride, or ethanol. Chemical characterization was performed using FTIR, which is shown in Fig 6.3. A peak appearing at 1100 cm^{-1} was the main difference from other soluble materials, which suggests that the C-O bond is responsible for crosslinking.

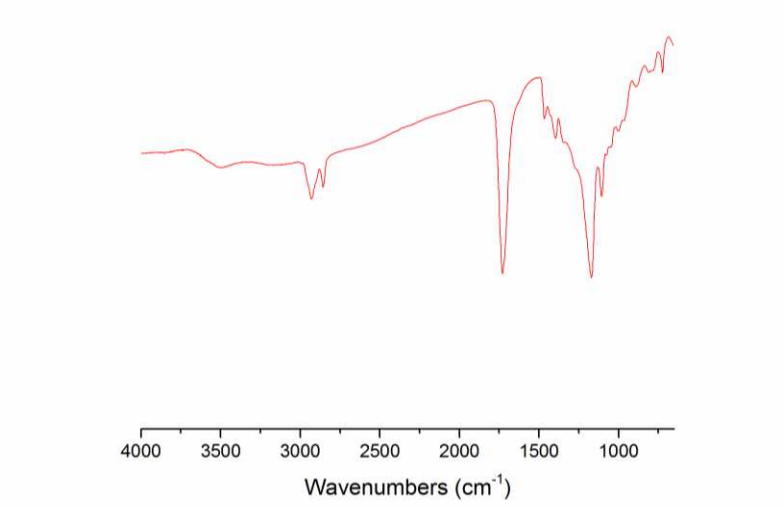

Figure 6.3 FTIR-ATR spectrum of poly(citrate-*co*-malic acid-*co*-1,8-octanediol).

Poly(citrate-*co*-succinic anhydride-*co*-1,8-octanediol). In a similar fashion, citric acid (5.793 g, 30 mmol), succinic anhydride (2.001 g, 20 mmol) from Sigma-Aldrich (St. Louis, MO, USA), and 1,8-octanediol (7.461 g, 51 mmol) were stirred in a round bottom flask with a nitrogen inlet and outlet at 140 °C for 4 h. The material was an elastomeric polyester insoluble in dichloromethane, acetone, dimethylformamide, and methylene chloride. Preliminary mechanical tensile test with a sample with an irregular morphology were conducted.

Poly(thiomalic acid-*co*-pentaerythritol). Thiomalic acid (8.587 g, 57 mmol) and pentaerythritol (3.622 g, 27 mmol) procured from Alfa Aesar (Ward Hill, MA, USA) were used for the preparation of the material. The reagents were stirred following the general procedure reported in Chapter 1. The temperature was maintained at 145 °C for 2 h with a constant nitrogen flow, protected from direct exposure to light. After the reaction, the material obtained was a brittle and partially soluble in acetone. In order to test if any available thiol groups were present in the polymer, *t*-BuONO was added in the absence of solvent to visually assess the formation of RSNOs. Although the qualitative findings were not corroborated with instrumental techniques such as UV-Vis, the surface of the material became pink, suggesting that RSNOs had formed. The material was characterized using FTIR (shown in Fig.6.4). The FTIR-ATR spectrum showed peaks at 2559 cm^{-1} that correspond to the S-H stretch, the resonance feature at 1716 demonstrates the presence of C=O functional groups, and a stretch at 1002 can be attributed to the formation of C=S. For this material, the crosslinking density may have been facilitated by the presence of four hydroxyl groups in pentaerythritol.

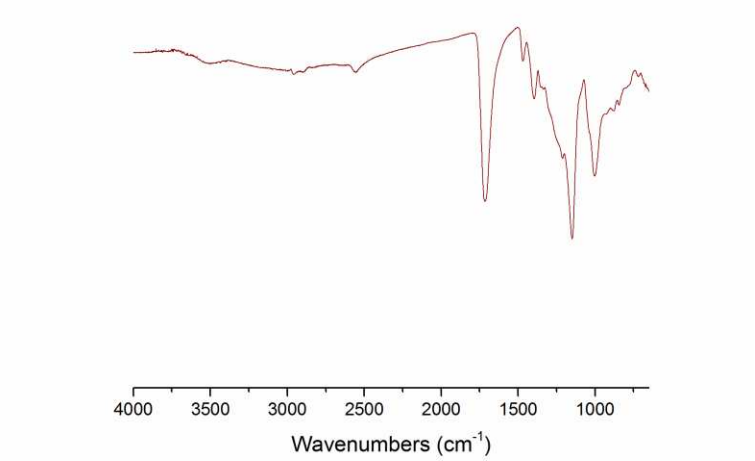

Figure 6.4 FTIR-ATR spectrum of poly(thiomalic acid-*co*-pentaerythritol).

Poly(thiomalic acid-*co*-1-thioglycerol-*co*-1,8-octanediol). The elastomer was prepared by a melt-phase polycondensation reaction using mercaptosuccinic acid (4.29 g, 28.6 mmol), 1-thioglycerol (1.44 mL, 16.6 mmol), and 1,8-octanediol (1.46 g, 9.98 mmol). The polymerization was achieved without an exogenous catalyst. The reagents were added to a vented 500 mL flask equipped with a nitrogen inlet and a condenser. The monomers were stirred under nitrogen flow for 30 min, then heated to 120 °C with constant stirring to initiate the polycondensation. The colorless melted mass was maintained at 120 °C for less than 12 h under nitrogen flow to obtain a viscous polymer. The material can be heated for longer periods of time to obtain a crosslinked material that is partially soluble in acetone. The crosslinked material is a yellow elastomeric sample that is deformed easily and returns to its original shape within seconds. Chemical characterization is shown in Fig. 6.5. IR ν_{max}/cm^{-1}: 3468 (O-H alcohol, carboxylic acid), 2929-2855 (C-H), 2560 (S-H), 1727 (C=O, carbonyl), 1166 (C-O).

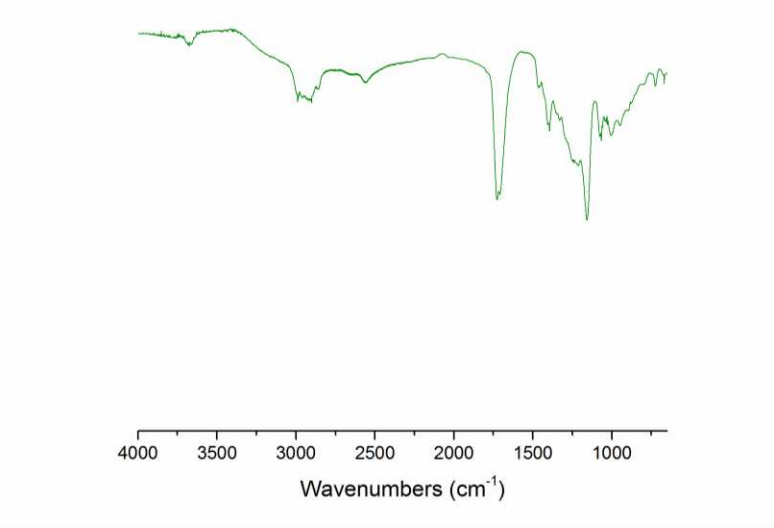

Figure 6.5 FTIR-ATR spectrum of poly(thiomalic acid-*co*-1-thioglycerol-*co*-1,8-octanediol).

6.2 The use of polydiacetylenes as sensors

Poly(10,12-docosadiynedioic acid) (PDCDA). The diacetylene monomer DCDA (4.03 g, 11.1 mmol) procured from Alfa Aesar (Ward Hill, MA, USA), was dissolved in diethyl ether (35 mL) and filtered to remove any contaminants. The solvent was evaporated under vacuum in order to isolate the monomer in a flask protected from direct exposure to light. Millipore water (18.2 MΩ·cm) was added to yield a 1.68 % w/v suspension, which was sonicated at 65 °C for 30 min. The suspension was allowed to cool to room temperature, then stored at 4 °C overnight. The suspension was transferred to a crystallizing dish with a magnetic stir bar and irradiated with UV light (254 nm) for 216 min.[3] After the photo-polymerization, the light blue suspension was transferred to a round bottom flask protected from light to remove the solvent under vacuum. The solid PDCDA was then stored at 4 °C and characterized by FTIR (Fig. 6.6). ^{1}H NMR characterization was not possible due to the impaired solubility of the material. IR ν_{max}/cm^{-1}: 2918-2847 cm^{-1} (H-C-H), 1690 cm^{-1} (C=O, ester), 725 cm^{-1} (C=C).

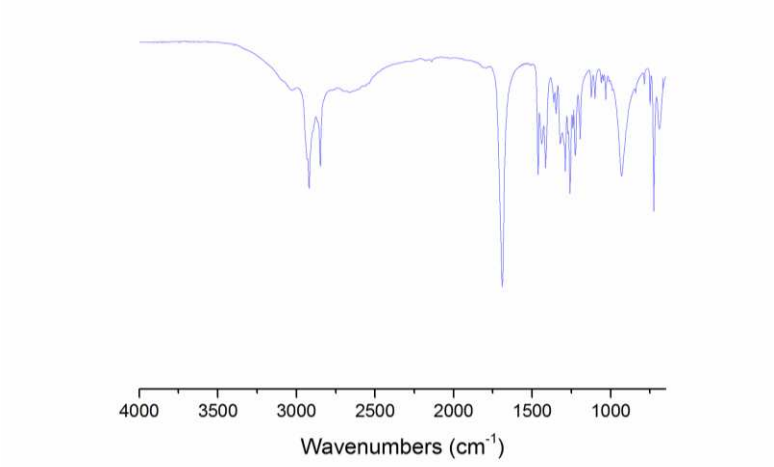

Figure 6.6 FTIR-ATR spectrum of poly(10,12-docosadiynedioic acid) vesicles in the blue phase.

The colorimetric response of PPCDA and PDCDA was studied at various pH values using aqueous solutions of HCl or KOH. The polymerized materials were used to prepare vesicle suspensions with concentration 1.00 % w/v using solvents with pH values that ranged from 1-14. The suspensions were stirred at room temperature and the solvent was removed under vacuum. The dried samples were analyzed using a Nicolet Evolution 300 UV-Vis spectrophotometer in diffuse reflectance mode. Fig. 6.7 depicts the results obtained for colorimetric response using PDCDA.

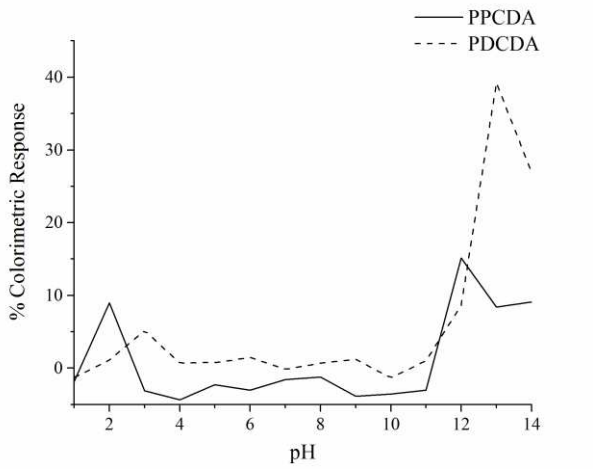

Figure 6.7 Colorimetric response with respect to pH including PDCDA results.

6.3 Synthesis of NO-releasing, 3D Printed Siloxane-Based Polymer with Textured Surface for Cell Seeding and Tissue Engineering

6.3.1 Synopsis

The main objective of the proposed studies is to synthesize siloxane-based polymers that can be used as scaffolds for cell seeding and tissue engineering. The overall objective addresses important topics such as mitigation of implant rejection and infection. This approach changes the dependence of immobilizing regenerating tissue that is normally at continuous movement, such as ligament. Synthetic, mechanistic, and characterization methods will be employed to achieve 7 specific aims*:* a) nitric oxide release at physiologically relevant levels for cell proliferation, b) cytotoxicity assays and cell seeding with endothelial cells, c) 3D printed materials to achieve various morphologies and efficient material processing, d) appropriate tensile strength for the intended application, e) surface roughness for prevention of bacterial infection, f) mass spectrometric analysis and quantification of degradation products at physiological pH and temperature, and g) study of degradation profiles and cytotoxicity studies using degradation products.

6.3.2 Introduction

Implantable devices are beneficial for applications where an external device is needed in order to complete or achieve a specific physiological function that has not been achieved due to a malfunction or impediment in the patient. These devices often ameliorate the condition, however, there are several risks involved with implantable devices such as infection or implant rejection. An approach to mitigate adverse reactions at the material interface is through the use of nitric oxide (NO) as a therapeutic agent.[4] NO has been extensively studied due to its role in

physiological processes such as inhibition of platelet activation and broad-spectrum antibacterial activity, among others. In order to harness the benefits of NO, the molecule can be conjugated into polymeric substrates that release NO at a localized site. Previous research has shown that NO has the ability to mitigate the foreign body response and prevent device fouling by simulating the natural NO release from the endothelium. It was demonstrated that NO is directly synthesized from the amino acid L-arginine by a family of NO synthase enzymes, which proved that the endogenous process occurs as a response mechanism to different stimuli in the cellular environment.[5]

Studies have demonstrated the use of NO as an antimicrobial agent that is able to mitigate the foreign body response. A textured surface made from polyurethane and *S*-nitroso-*N*-acetylpenicillamine (SNAP) was used in a study to establish the antimicrobial activity of NO. The materials released NO from 2 to 10 days at physiological conditions depending on the composition. Interestingly, it was reported that the synthetic polymer was able to inhibit biofilm formation for more than 28 days, even after the NO release was not quantifiable using nitric oxide analyzers.[6] A different study investigated the anticlotting and antimicrobial properties of NO with a material made from silicon, polyurethane, and SNAP that released NO for 4 hours.[7]

The purpose of this study is to synthesize NO-releasing siloxane-based polymers with texturized surfaces. Materials that bear siloxane moieties have high oxygen permeability, low intermolecular forces, and relatively unhindered single bonds that link the silicon and oxygen backbone chain atoms together. The result of these interactions leads to a high amount of free volume and high degree of chain mobility.[8] Thermoplasticity would be an ideal property for the material in order to increase the types of processing methods that can be used to develop various devices by 3D printing. Previous *S*-nitrosated materials have been developed from silicon-

containing compounds, however, some limitations include the use of a light source, copper(II) ions or ascorbate to trigger the release of NO from these interfaces.[9] Such materials were developed using thiol species (cysteine, *N*-acetylcysteine, *N*-cetylpenicillamine) anchored to fumed silica particles, which were blended in polyurethane and silicone rubber. RSNOs were prepared by reaction with *t*-butyl nitrite, and it was reported that the total NO loading was 0.14 ± 0.029 μmol NO mg^{-1} for 12 hours. An additional report explored NO release as a function of various NO release triggers, and the stability of nitrosated silane-derived xerogels that were synthesized from a thiol-terminated alkoxysilane. For the latter study, the thiol utilized for the preparation of RSNOs was 3-mercaptopropyltrimethoxysilane, which was hydrolyzed and co-condensed with alkoxysilanes (methyltrimethoxysilane, ethyltrimethoxysilane, and isobutyltrimethoxysilane).[10] However, the xerogel was *S*-nitrosated in acidified nitrite, which may compromise the stability of the polymer backbone. Additionally, NO release at physiological pH and temperature was measured for 2 weeks and it was reported that the xerogels were capable of storing up to 1.31 ± 0.07 μmol NO mg^{-1}. For the future study, a thiol-bearing alkoxysilane would be used for the preparation of RSNOs. In order to increase the stability of the RSNO and prolong NO release time, a silane with a tertiary thiol would be used with a matrix polymer composed of non-hindered alkoxysilane.

6.3.3 Research design and methods

Specific aim 1. Nitric oxide release will be achieved from the siloxane-based polymer by the reaction of a tertiary thiol with an alkoxysilane. The reaction will take place with diphenylacetaldehyde. The diphenyl-containing molecule will be reacted with disulfide dichloride in a solvent that where both reagents are solvated and inert. The reaction procedure

will take place in a three-neck round bottom flask equipped with an addition funnel, a condenser with a rubber septum used as an inlet for N_2 and a thermometer.[11] The reaction should proceed over the course of 3 to 15 hours, time after which a disulfide will be formed. This can be assessed visually by noting a color change in the solution that should have a yellow hue. Ozone will be used in order to oxidize the aldehyde to form a carboxylic acid. Ideally, the oxidizing agent would not oxidize the disulfide, so a mild oxidizing agent should be used (Fig. 6.8).

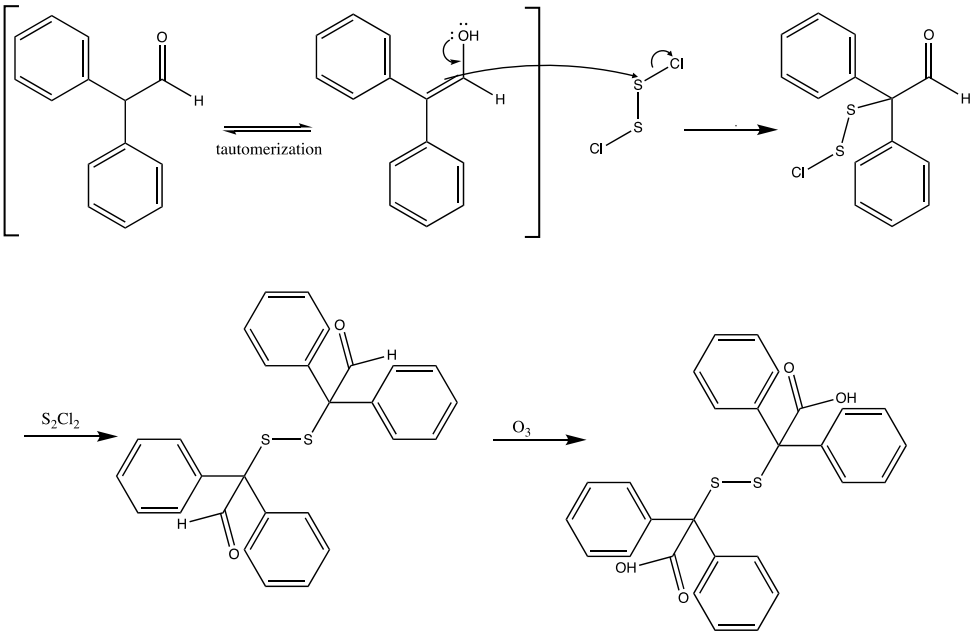

Figure 6.8 Synthetic scheme of tertiary disulfide using diphenylacetaldehyde.

The disulfide bond will be reduced to the corresponding thiol by using a reducing agent such as sodium borohydride. After the reaction, the product should be precipitated with sodium hydroxide in a solvent such as diethyl ether to obtain a salt with a tertiary thiol (Fig. 6.9).

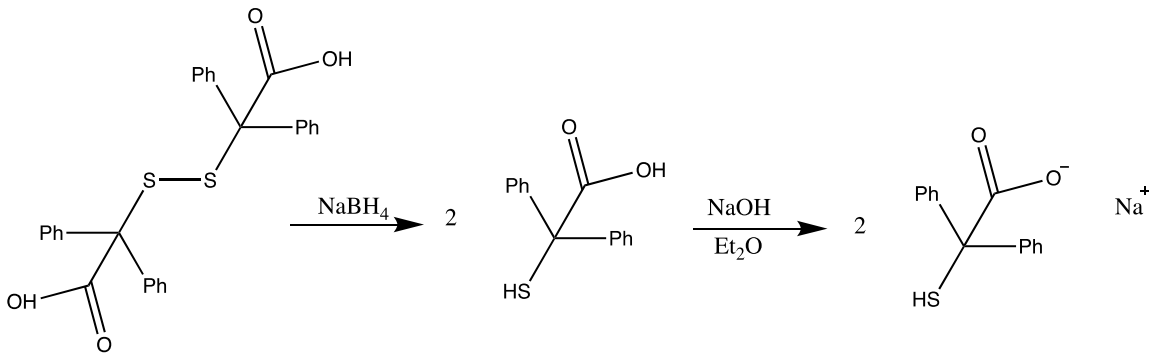

Figure 6.9 Reaction scheme for the reduction of disulfide to produce a tertiary thiol.

Carbodiimide coupling will be used to bond the tertiary thiol with an allkoxysilane such as aminopropyltrimethoxysilane. For the latter reaction *N*-hydroxysuccinimide (NHS) and dicyclohexanedicarbodiimide (DCC) will be used in tetrahydrofuran (THF) (Fig. 6.10).

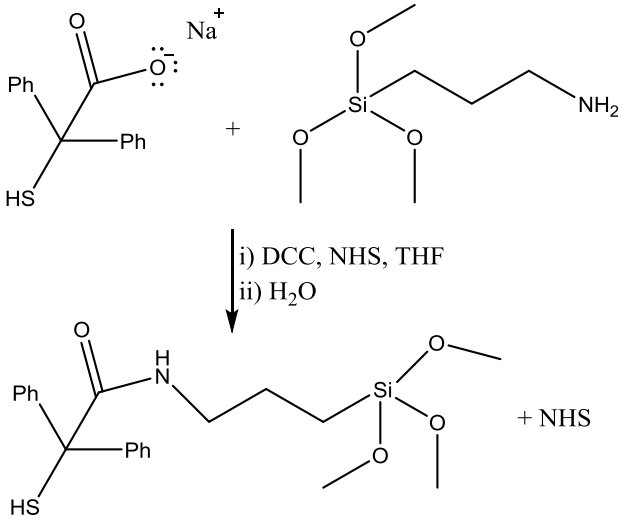

Figure 6.10 Carbodiimide coupling of aminopropyltrimethoxysilane.

The reaction product would be an alkoxysilane with a tertiary thiol that will be reacted with an alkoxysilane such as methyltrimethoxysilane using water and ethanol as the solvent (Fig. 6.11). The thiolated product will be analyzed using ^{1}H-NMR and ^{29}Si-NMR, as well as COSY and HSQC 2D NMR techniques. ATR-FTIR will also be used to confirm the presence of certain functional groups. The material would be further characterized by TGA, DSC and GPC to obtain a more complete analysis of thermal transitions and molecular weight of the polymer.

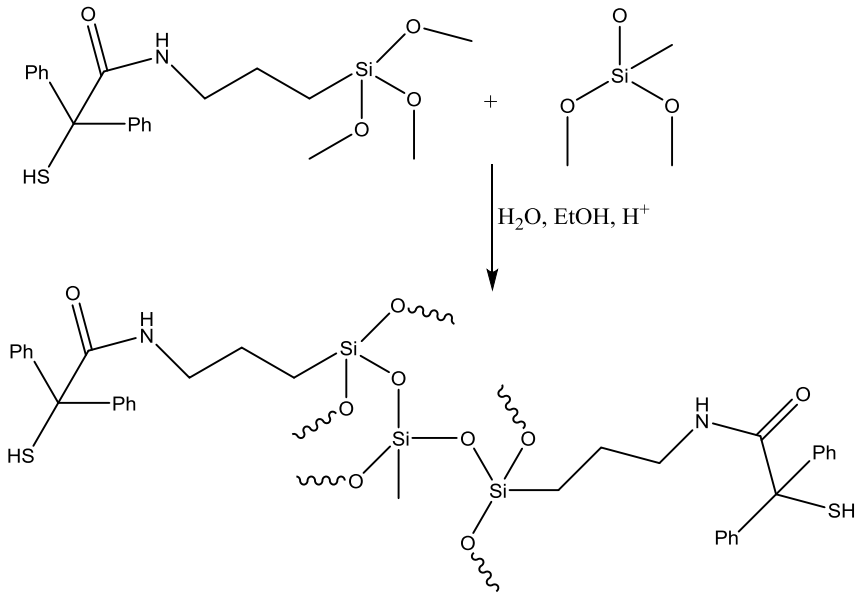

Figure 6.11 Synthetic reaction of thiol-bearing polymer.

Once the thiolated alkoxysilane has been made, the *S*-nitrosation will be performed using a mixture of NO/synthetic air (Fig. 6.12). The advantage of using NO gas as a nitrosating agent is twofold, the material would not be exposed to additional solvents once the desired morphology has been made by 3D printing. Such solvents could compromise the stability of the material. In addition, the need for drying the sample after the reaction would be eliminated. Qualitative experiments will be done using UV-Vis in order to confirm typical absorptions of RSNOs at approximately 335 ($\pi \rightarrow \pi^*$) and 540 nm ($n_N \rightarrow \pi^*$). Nitric oxide release would be quantified using nitric oxide analyzers where the material would be submerged in a solution that would emulate physiological conditions (phosphate buffered saline (PBS) pH 7.4, 37 °C). The success criteria for this specific aim would require NO release at 1−100 nM to provide proliferative effects, apoptosis protection and tissue injury protection.[12]

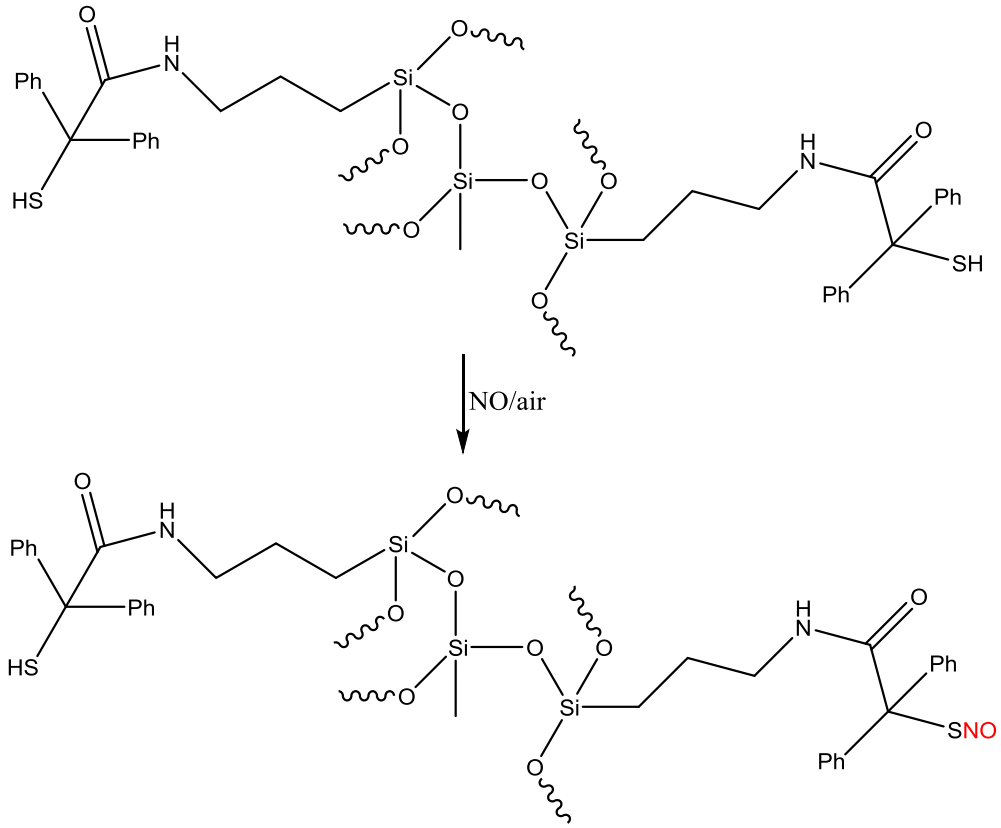

Figure 6.12 *S*-nitrosation of polymer in the absence of solvent.

Specific aim 2. Cell seeding will be performed on *S*-nitrosated materials as well as non-nitrosated ones, as a control. Endothelial cells will be used in order to assess the cell proliferative effects of NO and modulate how they would behave in the presence of an external material. Cells will be cultures in media 106 supplemented with 2 % v/v fetal bovine serum, 1 μg mL^{-1} hydrocortisone, 10 ng mL^{-1} heparin, 125 μg mL^{-1} amphotericin B, and 5 mg mL^{-1} gentamicin in a 25T flask. Cells will be incubated at 37 °C in a humid environment with 5 % CO_2. Cytotoxicity studies will be performed according to ISO standards.[13] Cytotoxicity assays will be performed in order to verify the absence of toxic leachates in the material extracts. LIVE/DEAD, morphological and viability assays will be done prior to cell seeding with all material analogs as described previously.[14] Cell seeding will be done by placing 50 mg of material in 24-well plates followed by addition of endothelial cells and incubation at 37 °C for 24 to 72 h. A similar

methodology as that followed for the LIVE/DEAD assay will be used to stain live cells on the material and counterstain dead cells. Fluorescence microscopy will be used to determine the presence of cells on the surface of the material. In order to analyze the core of the material, the polymer can be cut in half to examine if cells have migrated to the bulk of the material. The success criteria for establishing successful cell seeding would be determined by fluorescence microscopy to verify that live cells have proliferated on the surface of the material.

Specific aim 3. 3D printing will be attempted with this system given the broad range of applications for 3D printed materials in fields such as manufacturing, medicine, architecture, and custom design. 3D printed materials will be prepared by fused deposition modeling technology.[15] A virtual model would be created on a 3D modeling application or software to design the intended device. The model can then be sliced by the software to create a 2D file that will be printed on a texturized mold. Each layer is printed on the mold by heating and extruding the thermoplastic filament through the nozzle and onto the base.

Specific aim 4. Tensile strength will be measured using a tensiometer equipped with a 50 or 500 N load cell. Extension and compression tensile tests will be performed using dog bone shapes cut with cutting dye type III or IV following ASTM D638. Extension tests will be performed at 50 mm min^{-1} or 500 mm min^{-1}, and compression tests will be done at the same rate. Film preparation will be done by casting layers of the material dissolved in a volatile solvent. The polymerization will take place on polytetrafluoroethylene molds unless the tested polymer is a thermoplastic that dissolves in organic solvents without compromising the robustness of the polymeric backbone. In that case, the material will be dissolved in the solvent and allowed to dry on the mold. Young's modulus and crosslinking density will be calculated with information

obtained from the stress vs. strain curves. The same experiments will take place using the *S*-nitrosated materials after the presence of *S*-nitrosothiols is confirmed using UV-Vis.

Specific aim 5. Surface textures can be categorized into different types depending on the desired cell response. Ordered textures are constructed *via* microfabrication techniques that are often limited to materials such as silicon or quartz. In addition, laser machining can be used to directly fabricate topography in biomedical materials. The latter can also be achieved by allowing replication of microfabricated topographies into a biomedical device by nanoimprint lithography, nanoembossing, or replication molding.[16,17]

Previous reports have demonstrated inhibition of platelet attachment and activation through the use of textured polymers such as polyurethane.[18] Adhesion-resistant materials have also shown reduction of staphylococcal bacterial adhesion and biofilm formation.[19] Therefore, methods for the control and prevention of bacterial adhesion that circumvent the use of antibiotics or biocides are of great clinical interest. It has been reported that surface modifications on implants affect the initial attachment of microorganisms and reduce the number of persistent pathogens.[20] Surface texturing has been proven to have important effects on biological cell behavior. It was noted that parallel grooves cause cells to align along the direction of the grooves and that cells grow more readily on pillars compared with wells.[21] In addition, random pillars may increase or decrease cell adhesion depending on the pillar geometry.[22]

In order to create texturized surfaces the method of replication molding will be followed. In this manner, a microfabricated master pattern will be made creating a relief of photoresist pillars on a silicon wafer. The mold can be created by casting a silicon wafer over the master pattern, then the silicon sample will be cured and released to create a mold. Finally, the material that should be textured (thiolated polysiloxane) can be casted on the silicon mold and released,

resulting in direct replication of the master template relief.[23] Various sizes of nanostructures on different molds will provide a variety of textured surfaces.[20] Thus, the success criteria would be dependent cell proliferation on different types and sizes of texturized material surfaces.

Specific aim 6. Degradation products at physiological pH and temperature will be analyzed by submerging *S*-nitrosated and non-nitrosated materials in deuterium oxide (D_2O) at 37 °C in a water bath stirred a 15 rpm. The instrument used would be a time-of-flight mass spectrometer. Three vials will be removed from water bath each week (for 20 weeks) and aliquots of the supernatant will be introduced into the ion source by flow injection. The flow rate of 0.22 mL/min would be used *via* electrospray ionization (ESI) nebulized with methanol as the mobile phase. A method could be developed for the quantification of degradation products, which, ideally, would be negligible.

Specific aim 7. Degradation profiles will be obtained by performing gravimetric analysis on the materials which will be suspended in 5 mL of a 100 mmol PBS solution (pH 7.4) at 37 °C in a water bath. The degradation studies should take place for approximately 20 weeks with *S*-nitrosated and non-nitrosated materials. Initially, the weight of the vials should be recorded and the caps should be labeled appropriately. The material should be weighted to the nearest one hundredth of a milligram, and the vials sealed with parafilm and covered with foil should be placed in the water bath. Each week, all vials will be taken out of the water bath and allowed to reach room temperature. The liquid of each vial will be discarded after measuring and recording the pH. The vial containing the material to be tested will be washed twice with 5 mL of Millipore water (18.2 MΩ·cm) and lyophilized for 24 h. Once the solvent has completely evaporated from the sample, the vial with the material will be weighed and the percent remaining mass will be calculated. For the materials that are not the subject of gravimetric analysis that week, the PBS

solution should be replaced with new buffer solution and the vial should return to the water bath. In order to extend the measurement of the material degradation only the first three weeks of degradation will be measured consecutively. After the third week, the buffer should be replaced for all vials. However, no gravimetric analysis will be performed for the fourth week, instead the material will be analyzed on the sixth week. This method will allow the degradation to be tested for approximately a year, if two-week breaks are taken after the third week. In addition, such degradation products may be the subject of cytotoxicity studies in order to assess cellular behavior on leachates that are produced over a longer period of time.

REFERENCES

1. Riccio, D. A.; Coneski, P. N.; Nichols, S. P.; Broadnax, A. D.; Schoenfisch, M. H. *ACS Appl. Mater. Interfaces* **2012**, *4*, 796.
2. Lutzke, A.; Tapia, J. B.; Neufeld, M. J.; Reynolds, M. M. *ACS Appl. Mater. Interfaces* **2017**, *9*, 2104.
3. Champaiboon, T.; Tumcharern, G.; Potisatityuenyong, A.; Wacharasindhu, S.; Sukwattanasinitt, M. *Sensors and Actuators B: Chemical* **2009**, *139*, 532.
4. Moncada, S.; Higgs, E. *Eur. J. Clin. Invest.* **1991**, *21*, 361.
5. Seabra, A. *Nitric Oxide Donors: Novel Biomedical Applications and Perspectives*; Academic Press, 2017.
6. Xu, L.-C.; Wo, Y.; Meyerhoff, M. E.; Siedlecki, C. A. *Acta Biomater.* **2017**, *51*, 53.
7. Goudie, M. J.; Brainard, B. M.; Schmiedt, C. W.; Handa, H. *J. Biomed. Mater. Res. A* **2017**, *105*, 539.
8. Polmanteer, K. *Rubber Chem. Technol.* **1981**, *54*, 1051.
9. Frost, M. C.; Meyerhoff, M. E. *J. Biomed. Mater. Res. A* **2005**, *72*, 409.
10. Riccio, D. A.; Dobmeier, K. P.; Hetrick, E. M.; Privett, B. J.; Paul, H. S.; Schoenfisch, M. H. *Biomaterials* **2009**, *30*, 4494.
11. Roy, B.; Du Moulinet d'Hardemare, A.; Fontecave, M. *J. Org. Chem.* **1994**, *59*, 7019.
12. Coneski, P. N.; Schoenfisch, M. H. *Chem. Soc. Rev.* **2012**, *41*, 3753.
13. Standardization, I. O. f. In *Part 5: Test for in vitro cytotoxicity.* Geneva, 2009, p 1.
14. Yapor, J. P.; Lutzke, A.; Pegalajar-Jurado, A.; Neufeld, B. H.; Damodaran, V. B.; Reynolds, M. M. *J. Mater. Chem. B* **2015**, *3*, 9233.

15. Ventola, C. L. *Pharmacy and Therapeutics* **2014**, *39*, 704.

16. Flemming, R.; Murphy, C.; Abrams, G.; Goodman, S.; Nealey, P. *Biomaterials* **1999**, *20*, 573.

17. Walboomers, X.; Monaghan, W.; Curtis, A.; Jansen, J. *J. Biomed. Mater. Res. A* **1999**, *46*, 212.

18. Milner, K. R.; Snyder, A. J.; Siedlecki, C. A. *J. Biomed. Mater. Res. A* **2006**, *76*, 561.

19. Den Braber, E.; De Ruijter, J.; Smits, H.; Ginsel, L.; Von Recum, A.; Jansen, J. *Biomaterials* **1996**, *17*, 1093.

20. Xu, L.-C.; Siedlecki, C. A. *Acta Biomater.* **2012**, *8*, 72.

21. Turner, A.; Dowell, N.; Turner, S.; Kam, L.; Isaacson, M.; Turner, J.; Craighead, H.; Shain, W. *J. Biomed. Mater. Res.* **2000**, *51*, 430.

22. Dalby, M.; Riehle, M.; Johnstone, H.; Affrossman, S.; Curtis, A. *J. Tissue Eng.* **2002**, *8*, 1099.

23. Milner, K. R.; Siedlecki, C. A. *J. Biomed. Mater. Res. A* **2007**, *82*, 80.

APPENDIX A

EXPERIMENTAL DETAILS AND SUPPORTING INFORMATION FOR CHAPTER 2

A.1 Additional figures and tables

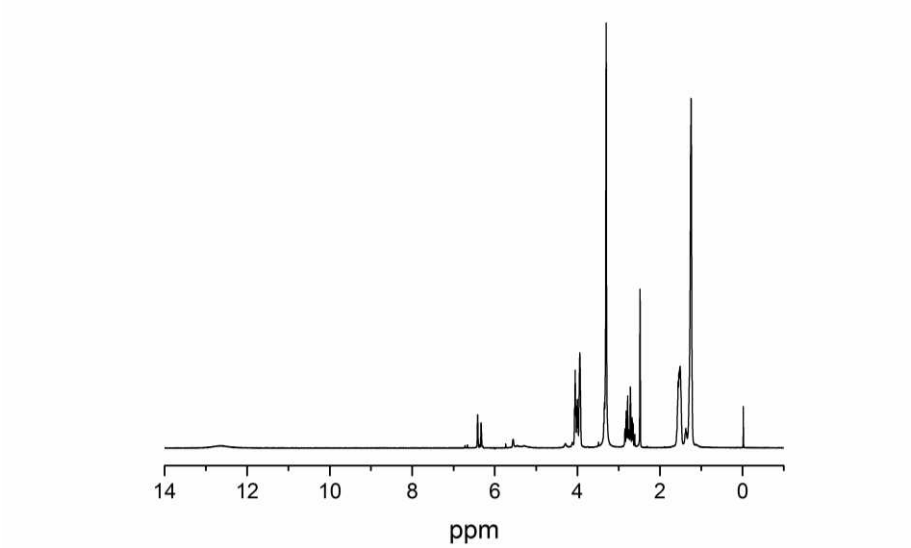

Figure A.1 ^{1}H NMR spectrum of PCMO. ^{1}H NMR δ_H/ppm (400 MHz, DMSO-d_6): 1.20–1.65 (–(C**H**$_2$)$_6$–), 2.66–2.76 (–C**H**$_2$CO$_2$–), 3.95–4.03 (–O**CH**$_2$–), 6.35 (–**H**C=C**H**–), 12.6 (–CO$_2$**H**).

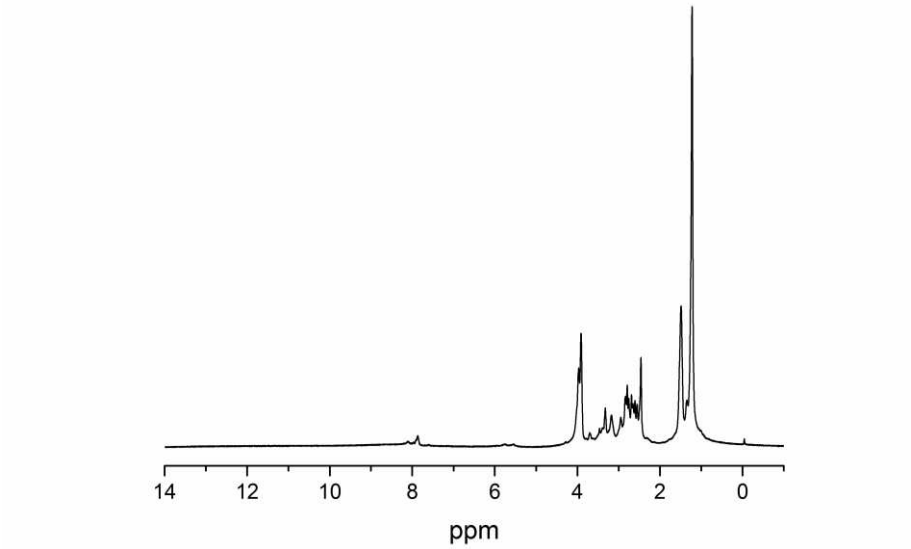

Figure A.2 ^{1}H NMR spectrum of PCMO-cysteamine. ^{1}H NMR δ_H/ppm (400 MHz, DMSO-d_6): 1.20–1.65 (–(C**H**$_2$)$_6$–), 2.66–2.76 (–C**H**$_2$CO$_2$–), 2.98 (–C**H**$_2$SH), 3.22 (–(CO)NHC**H**–), 3.95–4.03 (–O–C**H**$_2$–), 6.35 (–**H**C=C**H**–), 7.82–7.92 (–(CO)N**H**–).

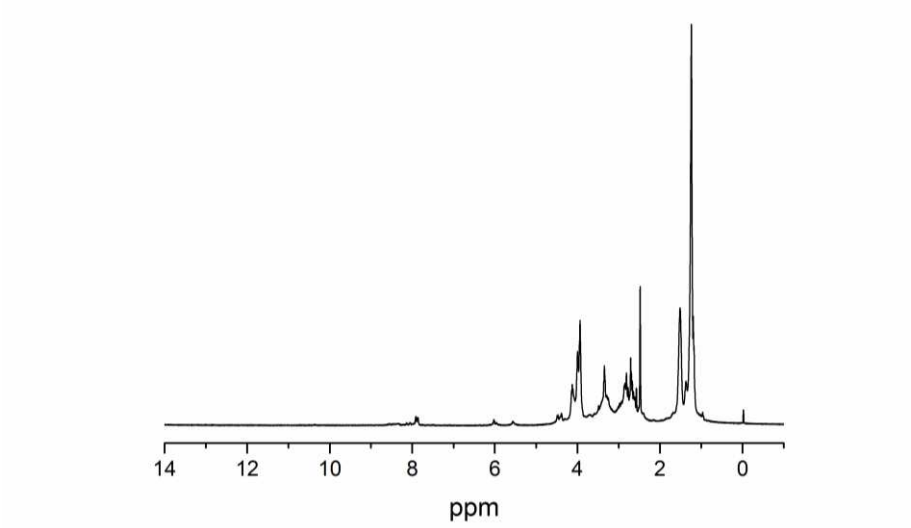

Figure A.3 ^{1}H NMR spectrum of PCMO-ethyl cysteinate. ^{1}H NMR δ_H/ppm (400 MHz, DMSO-d_6): 1.18–1.22 (–C**H**$_3$) 1.20–1.65 (–(C**H**$_2$)$_6$–), 2.66–2.76 (–C**H**$_2$CO$_2$–), 3.70 (–C**H**$_2$SH), 4.42 (–(CO)NHC**H**–), 3.95–4.03 (–OC**H**$_2$–), 6.35 (–**H**C=C**H**–), 7.84–7.94 (–(CO)N**H**–).

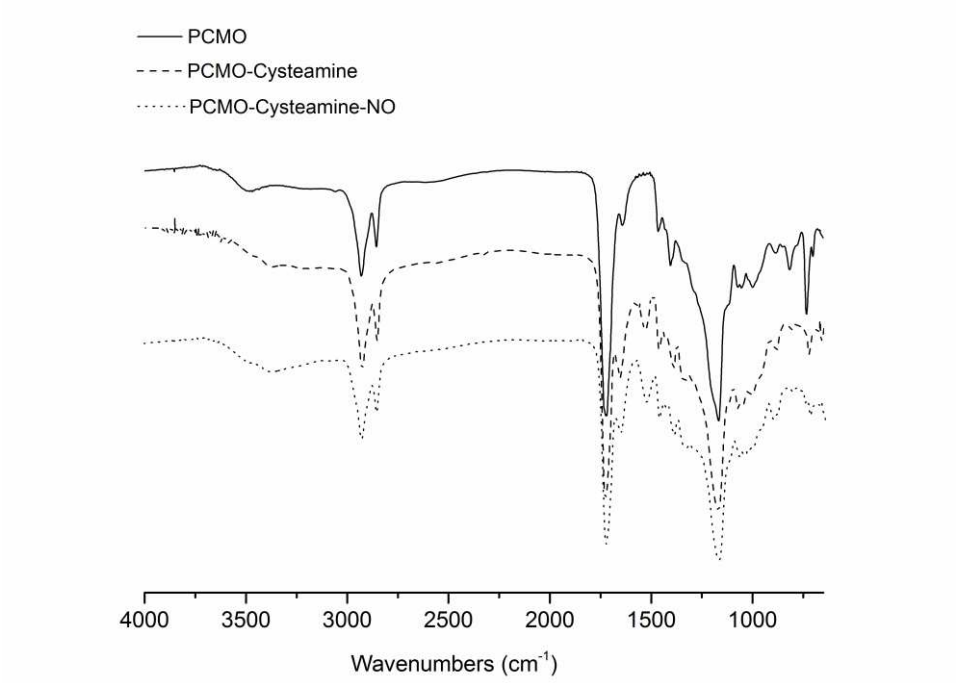

Figure A.4 FTIR-ATR spectra of PCMO, PCMO-cysteamine, and PCMO-cysteamine-NO. PCMO – IR ν_{max}/cm^{-1}: 3600-3200 (O-H alcohol, carboxylic acid), 2930-2856 (C-H), 1724 (C=O, carbonyl), 1167 (C-O). PCMO-cysteamine – IR ν_{max}/cm^{-1}: 3600-3200 (O-H), 2930-2856 (C-H), 1724 (C=O, carbonyl), 1656 (amide I), 1531 (amide II), 1167 (C-O). PCMO-cysteamine-NO – IR ν_{max}/cm^{-1}: 3600-3200 (O-H alcohol, carboxylic acid), 2930-2856 (C-H), 1728 (C=O, carbonyl), 1653 (amide I), 1529 (amide II), 1173 (C-O).

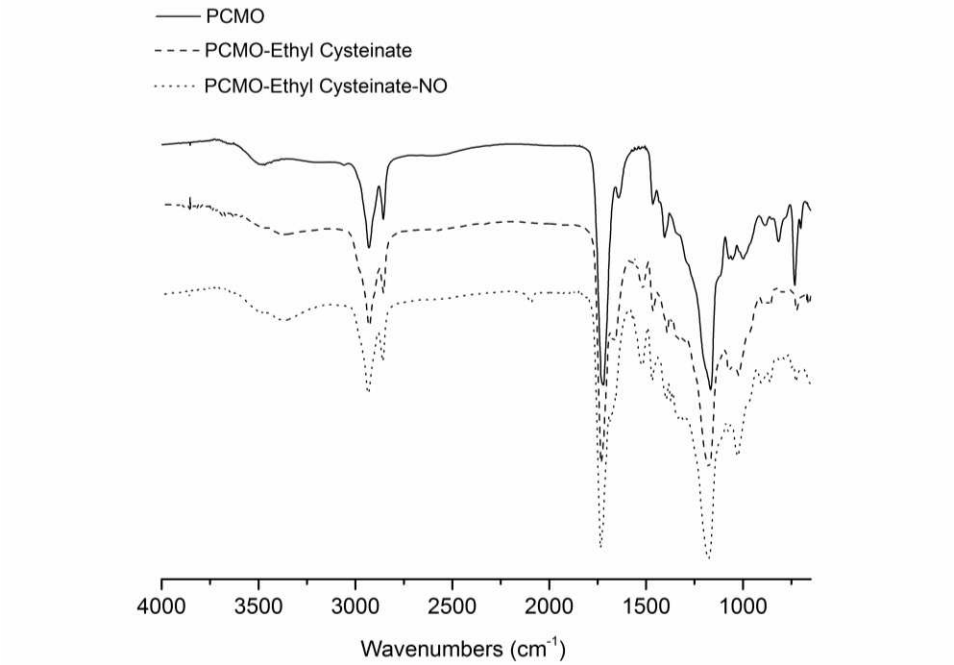

Figure A.5 FTIR-ATR spectrum of PCMO, PCMO-ethyl cysteinate, and PCMO-ethyl cysteinate-NO. PCMO – IR ν_{max}/cm^{-1}: 3600-3200 (O-H alcohol, carboxylic acid), 2930-2856 (C-H), 1724 (C=O, carbonyl), 1167 (C-O). PCMO-ethyl cysteinate – IR ν_{max}/cm^{-1}: 3600-3200 (O-H alcohol, carboxylic acid), 2930-2856 (C-H), 1724 (C=O, carbonyl), 1673 (amide I), 1518 (amide II), 1167 (C-O). PCMO-ethyl cysteinate – IR ν_{max}/cm^{-1}: 3600-3200 (O-H alcohol, carboxylic acid), 2930-2856 (C-H), 1733 (C=O, carbonyl), 1684 (amide I), 1517 (amide II), 1176 (C-O).

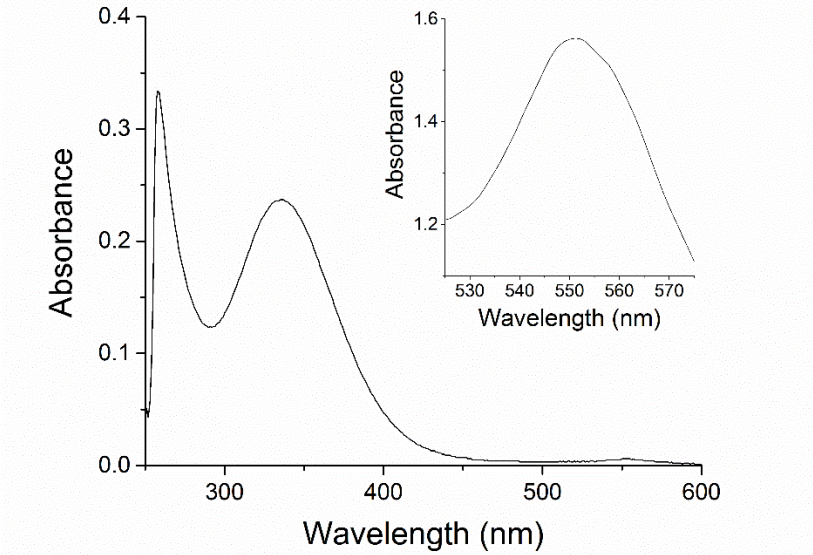

Figure A.6 UV-Vis spectrum of PCMO-cysteamine-NO in DMSO. **Inset**: Diffuse reflectance UV-Vis spectrum. The spectra depict the characteristic transitions of *S*-nitrosothiols at 335 ($n_O \rightarrow \pi^*$) and 550 nm ($n_N \rightarrow \pi^*$). Diffuse reflectance was used to identify the peak corresponding to the $n_N \rightarrow \pi^*$ transition since the small molar extinction coefficient prevents unambiguous solution-phase measurements within the solubility range of the polymer.

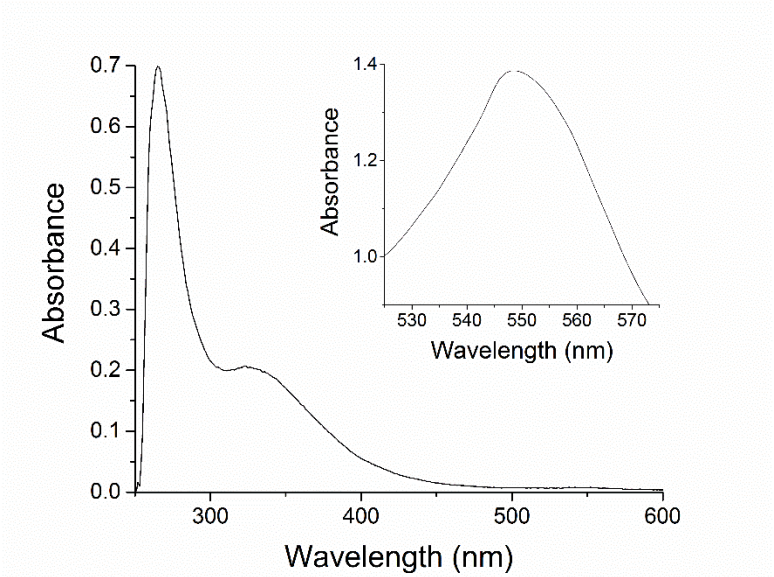

Figure A.7 UV-Vis spectrum of PCMO-ethyl cysteinate-NO in DMSO. **Inset:** Diffuse reflectance UV-Vis spectrum. The spectra depict the characteristic transitions of *S*-nitrosothiols at 336 ($n_O \rightarrow \pi^*$) and 549 nm ($n_N \rightarrow \pi^*$). Diffuse reflectance was used to identify the peak corresponding to the $n_N \rightarrow \pi^*$ transition since the small molar extinction coefficient prevents unambiguous solution-phase measurements within the solubility range of the polymer.

Table A.1 Hydrolytic degradation of PCMO and *S*-nitrosated derivatives.

		% Weight Remaining			
Material	Initial	Week 1	Week 2	Week 3	Week 4
PCMO	100	88.5 ± 0.7	77.4 ± 0.1	12.1 ± 3.0	1.70 ± 0.5
PCMO-CysAm-NO (**2a**)	100	77.7 ± 1.1	69.5 ± 1.1	56.7 ± 1.4	47.2 ± 3.8
PCMO-EtCys-NO (**3a**)	100	59.6 ± 1.1	57.2 ± 1.7	52.4 ± 2.0	48.6 ± 1.4

Hydrolytic degradation of the *S*-nitrosated materials was evaluated under physiological conditions (pH 7.4, 37 °C) in 10 mM PBS over 4 weeks. Each week, the buffer was replaced and the materials were lyophilized for 24 h before data collection. For all experiments, $n \geq 3$ and results are reported as the mean ± SD.

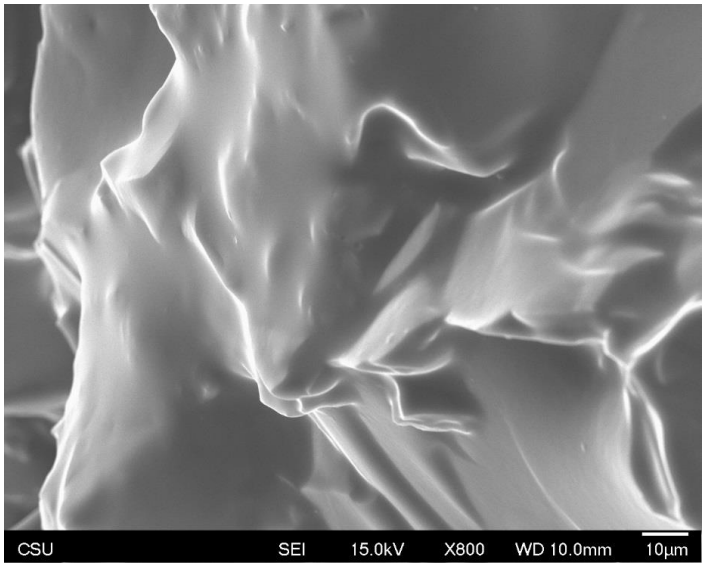

Figure A.8 The morphology of PCMO is depicted in the image obtained using a scanning electron microscope. The sample was dried in a vacuum oven at room temperature for 24 h prior to the analysis. Gold sputtering was performed and the sample was mounted on carbon tape.

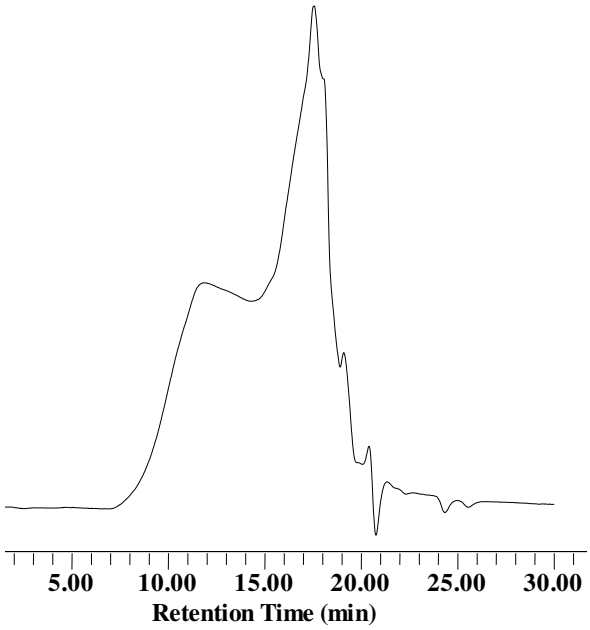

Figure A.9 Gel permeation chromatography plot obtained from a solution of PCMO in DMF (0.25% w/v). The sample was analyzed using polystyrene standards.

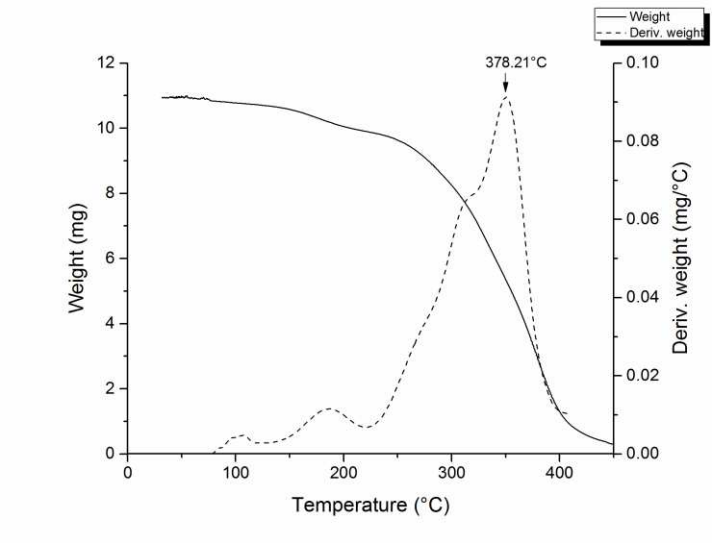

Figure A.10 Thermogravimetric analysis plot of PCMO. During the experiment, the temperature of the instrument was set to ramp to 450 °C at a rate of 20 °C min^{-1}. The process was followed by an isothermal step for 2 min.

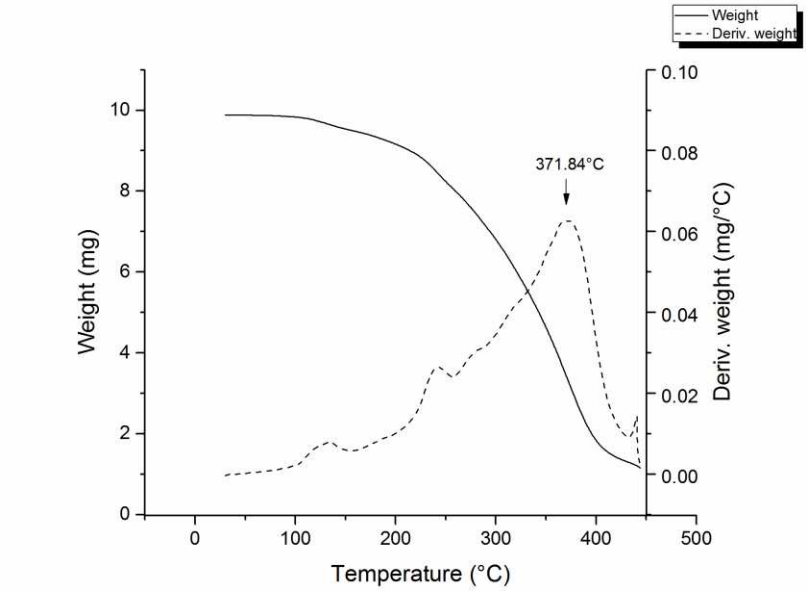

Figure A.11 Thermogravimetric analysis plot of PCMO-cysteamine. The temperature of the instrument was set to ramp to 450 °C at a rate of 20 °C min^{-1}, followed by an isothermal step for 2 min.

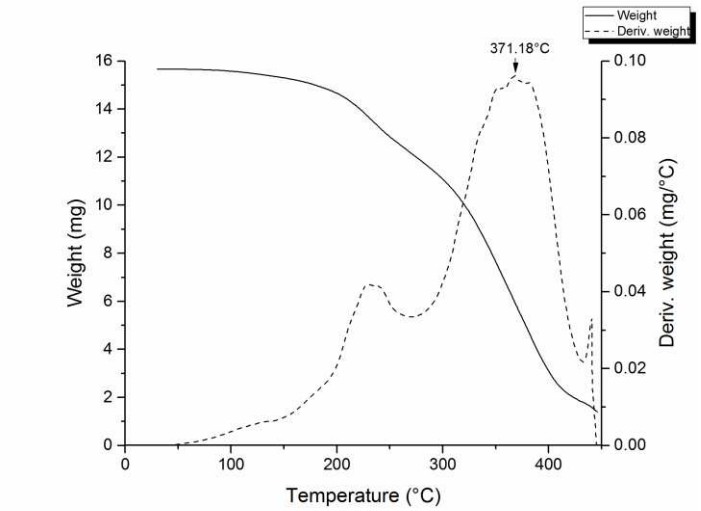

Figure A.12 Thermogravimetric analysis plot of PCMO-ethyl cysteinate. The instrument was set to ramp to 450 °C at a rate of 20 °C min^{-1}, followed by an isothermal step for 2 min.

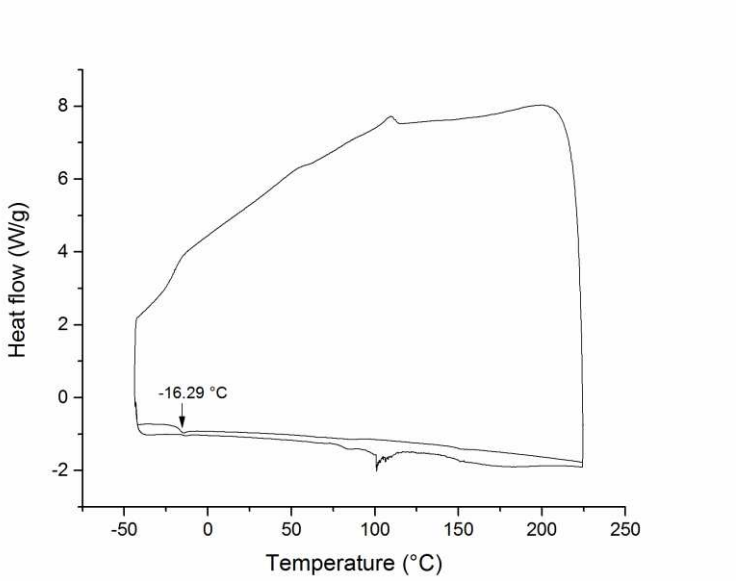

Figure A.13 Differential scanning calorimetry plot of PCMO. The method for data acquisition was the following: The instrument was equilibrated at −40 °C, the temperature was set to ramp to 225 °C at a rate of 2 °C min^{-1}. The process was followed by an isothermal step for 10 min. The cycle was repeated to account for processing methods, thermal history, and hysteresis.

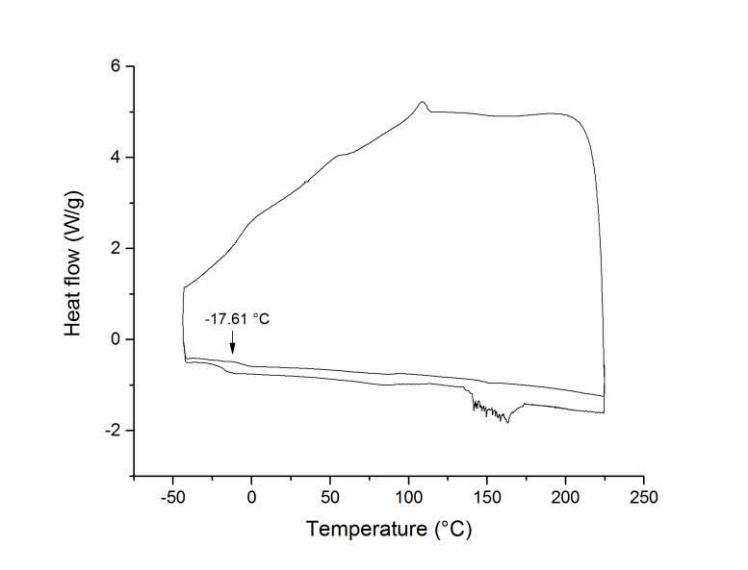

Figure A.14 Differential scanning calorimetry plot of PCMO-cysteamine. The instrument was equilibrated at −40 °C, followed by a temperature increase to 225 °C at a rate of 2 °C min^{-1}, an isothermal step for 10 min followed. The cycle was repeated and the data from the second cycle was used to calculate the thermal transition.

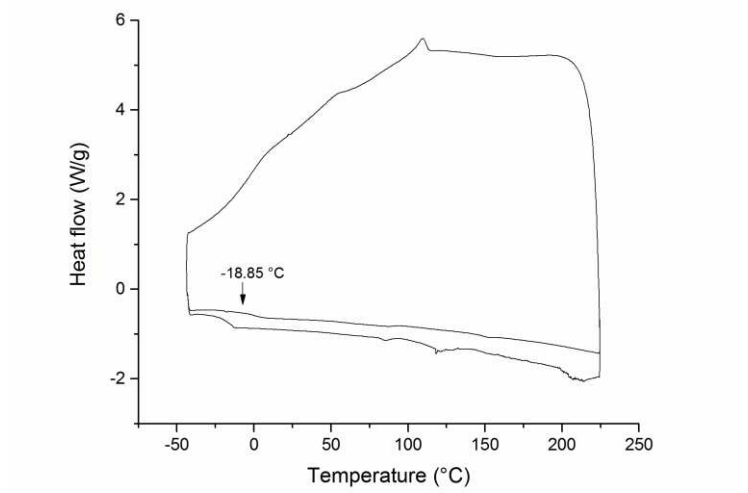

Figure A.15 Differential scanning calorimetry plot of PCMO-ethyl cysteinate. The temperature of the instrument was set to equilibrate at −40 °C, then ramped to 225 °C at a rate of 2 °C min^{-1}. The process was followed by an isothermal step for 10 min. The process was repeated in order to obtain the data that was used to calculate the T_g.

APPENDIX B

EXPERIMENTAL DETAILS AND ADDITIONAL INFORMATION FOR CHAPTER 3

B.1. Additional figures and tables

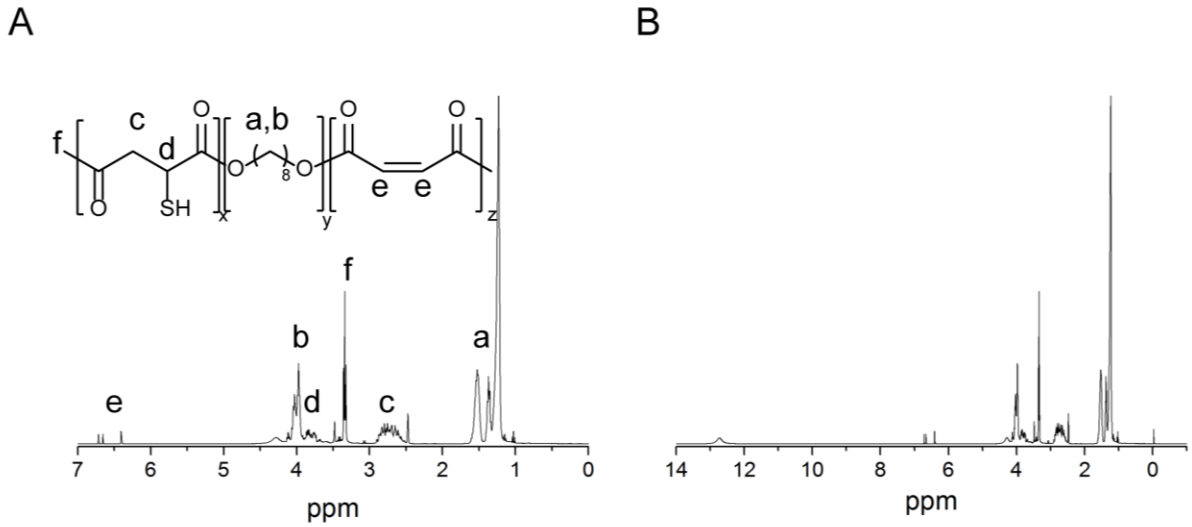

Figure B.1 Selected portion (A) and complete ^{1}H NMR spectrum of PTMO (B). ^{1}H NMR δ_H/ppm (400 MHz, DMSO-d_6): 12.73 (–CO_2*H*), 6.67–6.73 (–*H*C=C*H*–), 3.94–4.07 (–OCH_2–), 3.72–3.89 (–S–C*H*–CO_2–), 3.32–3.35 (–CH_2OH), 2.58–2.91 (–CH_2CO_2–), 2.49 (DMSO), 1.52–1.60 (–CH_2–$(CH_2)_4$–CH_2–),1.34–1.39 (–CH_2–CH_2OH), 1.24 (–$(CH_2)_4$–).

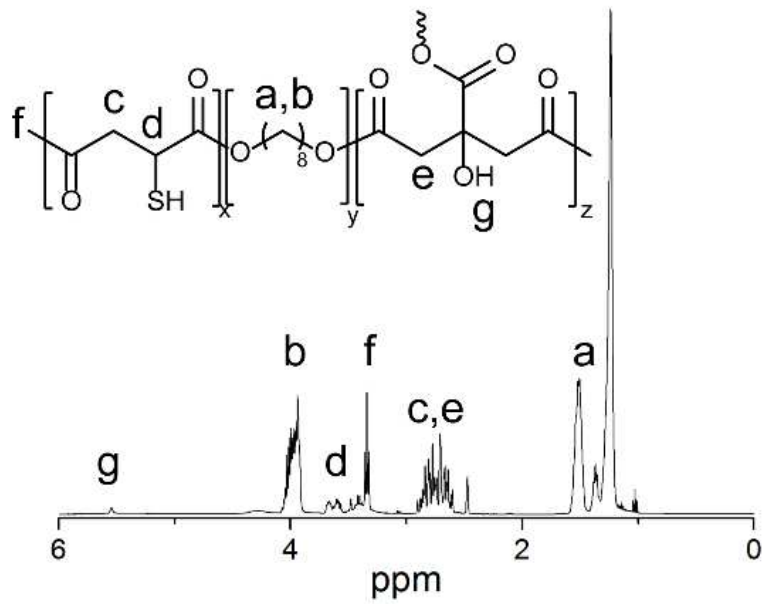

Figure B.2 ^{1}H NMR spectrum of PTCO. ^{1}H NMR δ_H/ppm (400 MHz, DMSO-d+$_6$): 5.56 (–C–O*H*), 3.93–4.07 (–OCH_2–), 3.58–3.69 (–S–C*H*–CO_2), 3.32–3.36 (–CH_2OH), 2.61–2.91 (–CH_2CO_2–), 2.49 (DMSO), 1.51–1.53 (–CH_2–$(CH_2)_4$–CH_2–), 1.36–1.39 (–CH_2–CH_2OH), 1.25 (–$(CH_2)_4$–).

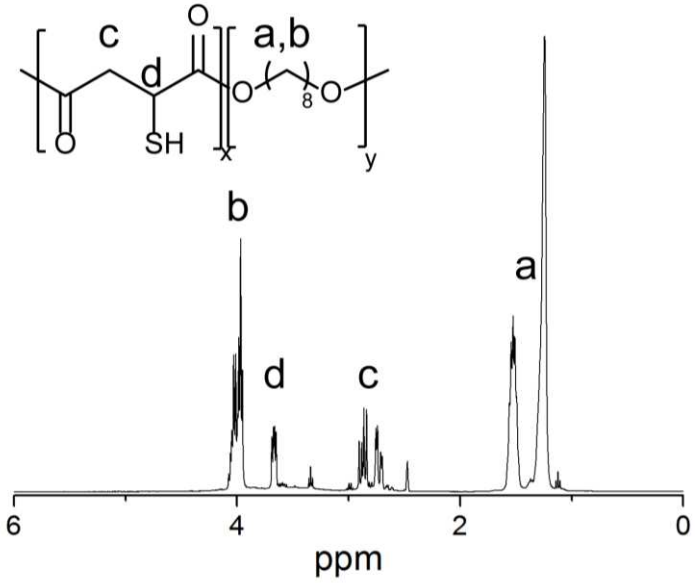

Figure B.3 ^{1}H NMR spectrum of PTO. ^{1}H NMR δ_H/ppm (400 MHz, DMSO-d$_6$): 3.94–4.06 (–OCH_2–), 3.66–3.70 (–S–C*H*–CO_2–), 2.71–2.91 (–CH_2CO_2–), 2.49 (DMSO), 1.57 (–CH_2–$(CH_2)_4$–CH_2–), 1.25–1.30 (–$(CH_2)_4$–).

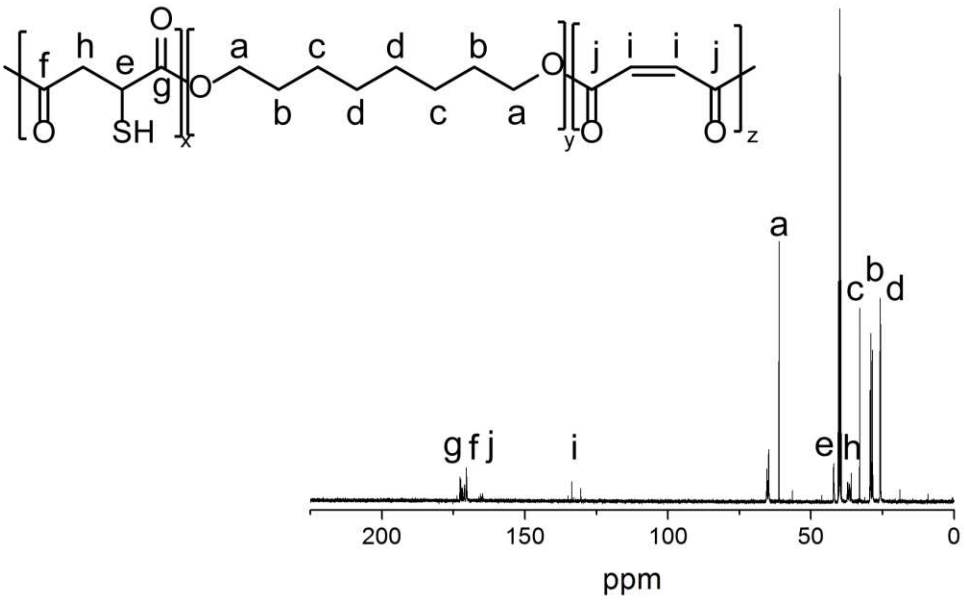

Figure B.4 ^{13}C NMR spectrum of PTMO. ^{13}C NMR δ_C/ppm (100 MHz, DMSO–d_6): 170.3–172.6 (–*C*O_2–), 130.4–133.6 (–H*C*=*C*H–),64.8–65.5 (–*C*H_2OH), 61.2 (–O*C*H_2–), 41.9–42.0 (–S–*C*H–CO_2–), 39.3–40.6 (DMSO), 35.9–37.1 (–*C*H_2CO_2–), 33.0 (–*C*H_2–CH_2OH), 29.0–29.3 (–(*C*$H_2)_2$–), 28.4–28.5 (–*C*H_2–$(CH_2)_4$–*C*H_2–), 25.7–25.9 (–(*C*$H_2)_2$–).

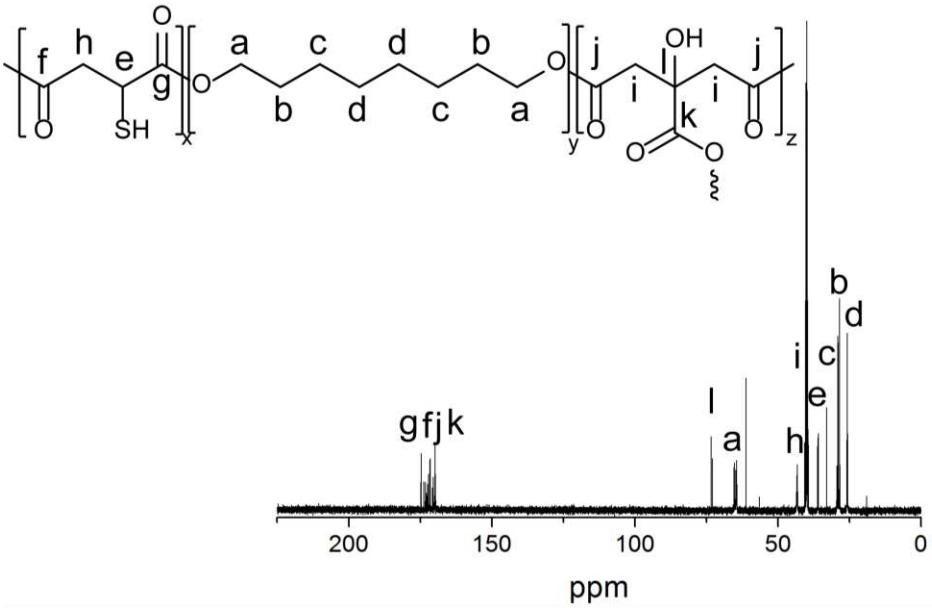

Figure B.5 ^{13}C NMR spectrum of PTCO. ^{13}C NMR δ_C/ppm (100 MHz, DMSO–d_6): 169.6–174.9 (–*C*O_2–), 72.9–73.3 (–*C*–OH), 64.4–65.3 (–O*C*H_2–), 61.2 (–*C*H_2OH), 41.9–42.0 (–*C*H_2CO_2–), 39.3–40.6 (DMSO), 35.8–35.9 (–S–*C*H–CO_2–), 33.0 (–(*C*$H_2)_2$–), 28.4–28.5 (–*C*H_2–$(CH_2)_4$–*C*H_2–), 25.6–25.9 (–(*C*$H_2)_2$–).

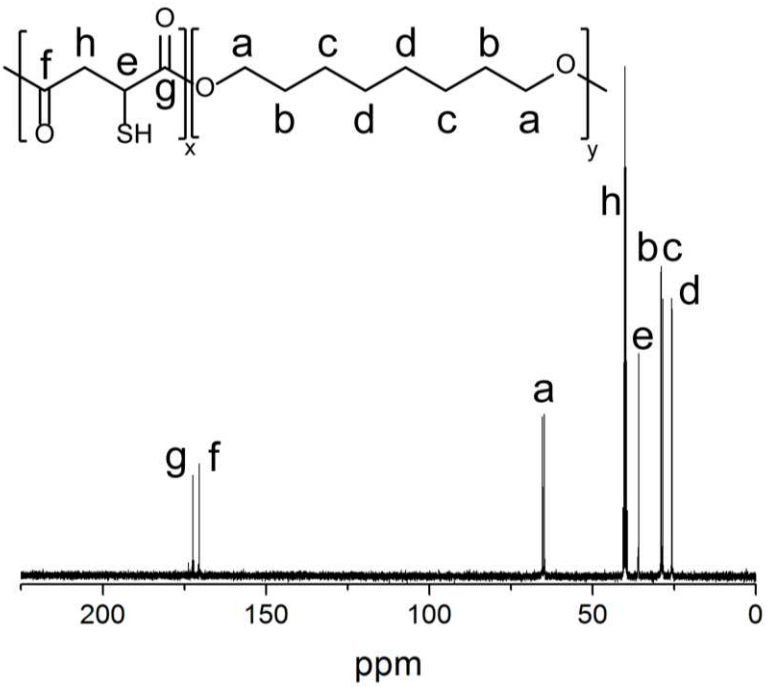

Figure B.6 ^{13}C NMR spectrum of PTO. ^{13}C NMR δ_C/ppm (100 MHz, DMSO–d_6): 170.4–173.7 (–*C*O_2–), 64.7–65.2 (–O*C*H_2–), 39.3–40.6 (DMSO), 39.8 (–*C*H_2CO_2–), 35.9–36.1 (–S–*C*H–CO_2–), 29.0 (–*C*H_2–$(CH_2)_4$–*C*H_2–), 28.4–28.5 (–(*C*$H_2)_2$–), 25.6–25.7 (–(*C*$H_2)_2$–).

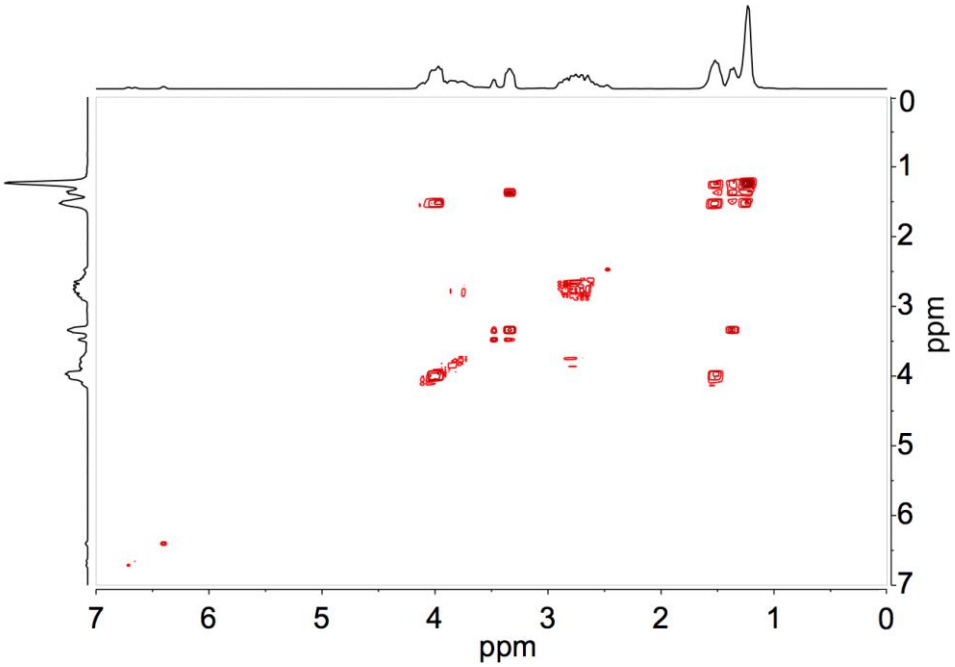

Figure B.7 COSY 2D NMR spectrum of PTMO.

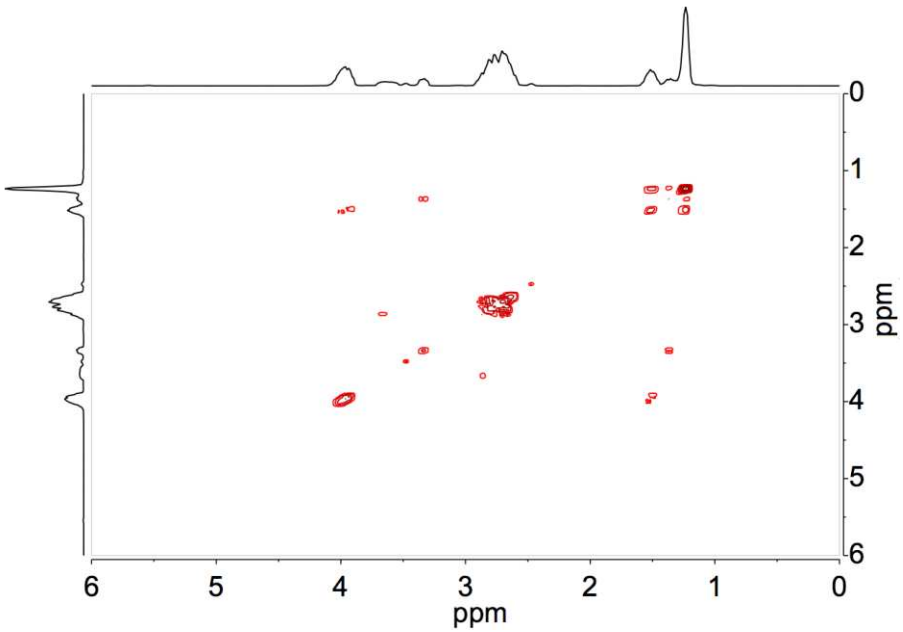

Figure B.8 COSY 2D NMR spectrum of PTCO.

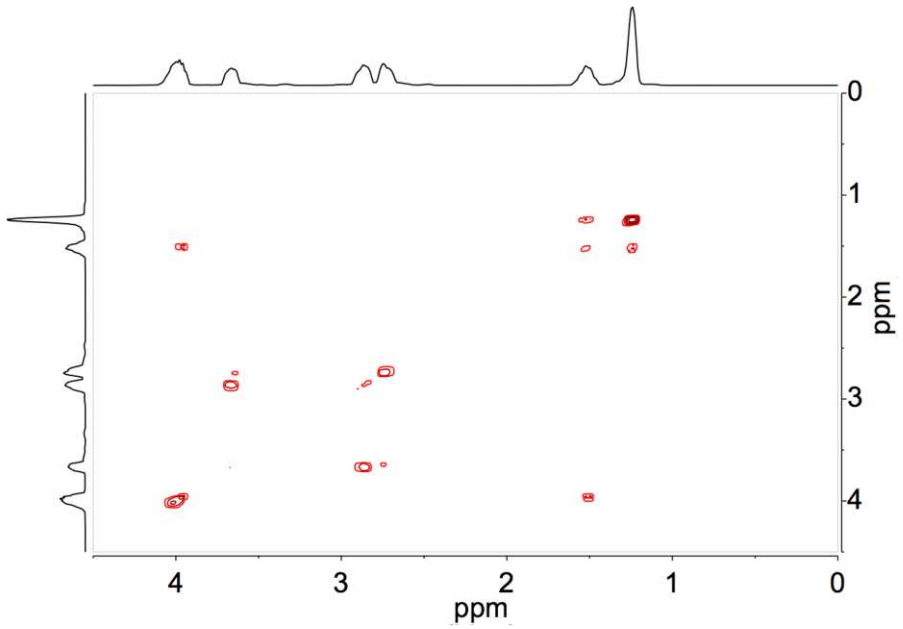

Figure B.9 COSY 2D NMR spectrum of PTO.

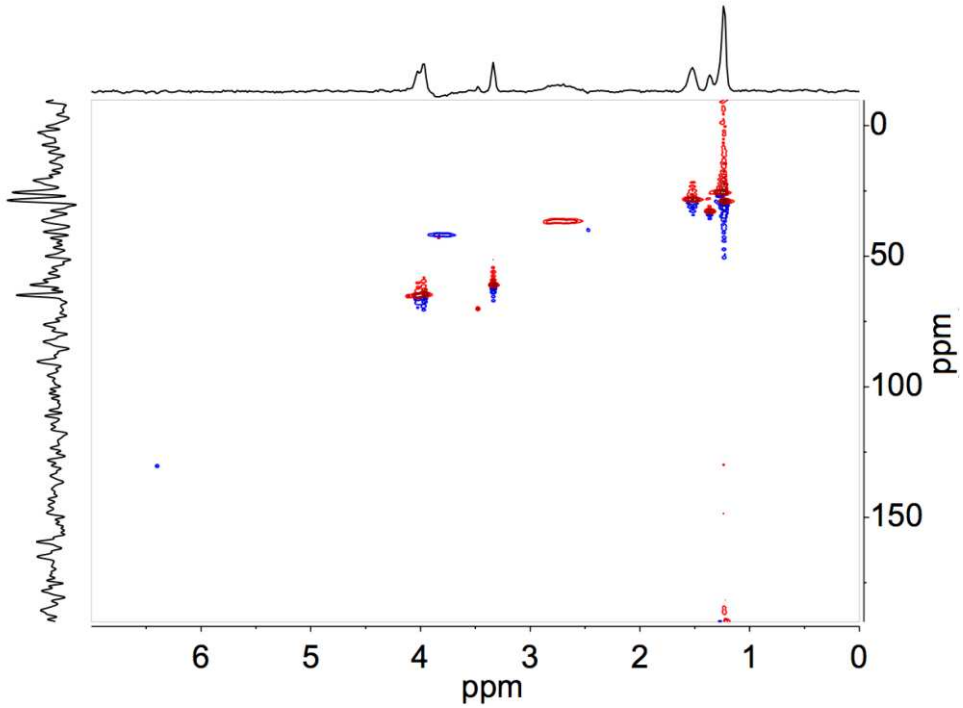

Figure B.10 HSQC 2D NMR spectrum of PTMO.

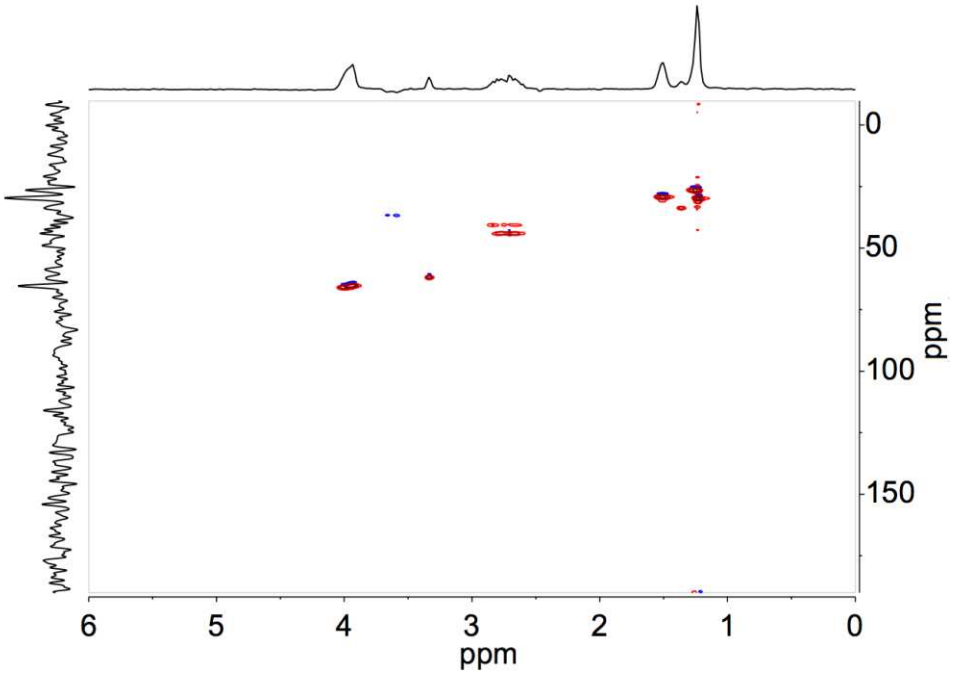

Figure B.11 HSQC 2D NMR spectrum of PTCO.

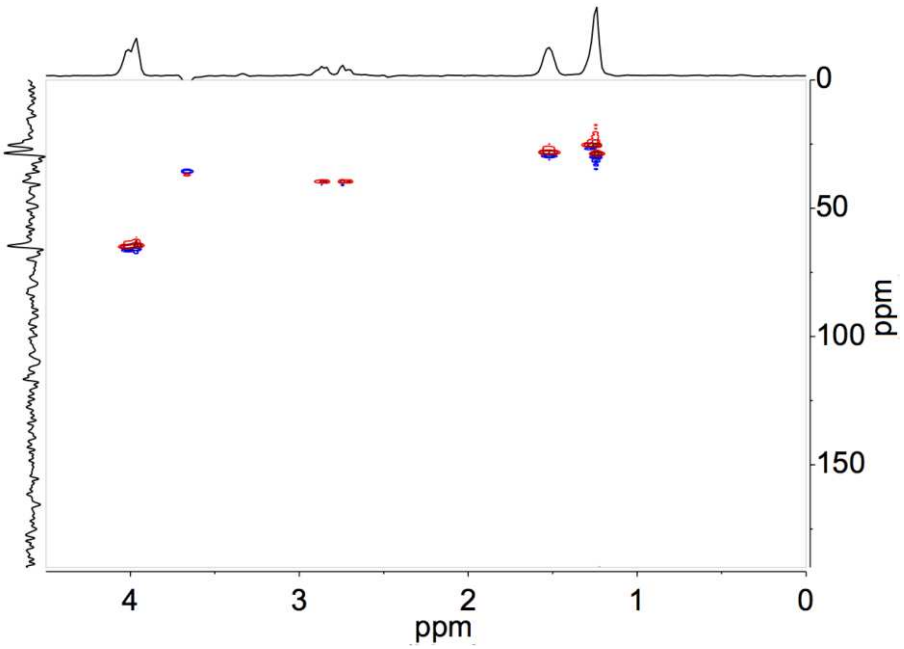

Figure B.12 HSQC 2D NMR spectrum of PTO.

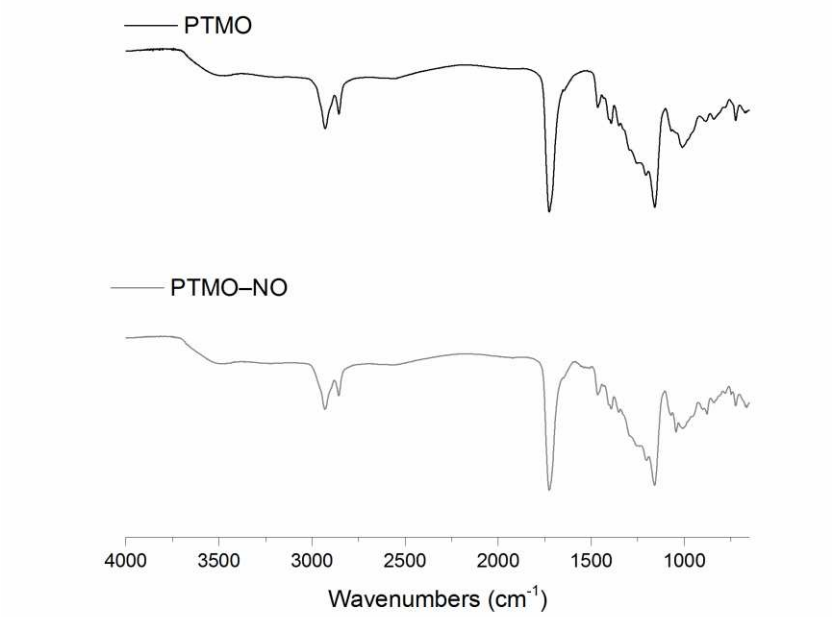

Figure B.13 FTIR-ATR spectra of PTMO and PTMO–NO.PTMO – IR υ_{max}/cm^{-1}: 3468–2400 (O–H), 2929–2856 (C–H), 1725 (C=O) and 1159 (C–O). PTMO–NO – IR υ_{max}/cm^{-1}: 3468–2400 (O–H), 2930–2856 (C–H), 1725 (C=O) and 1159 (C–O).

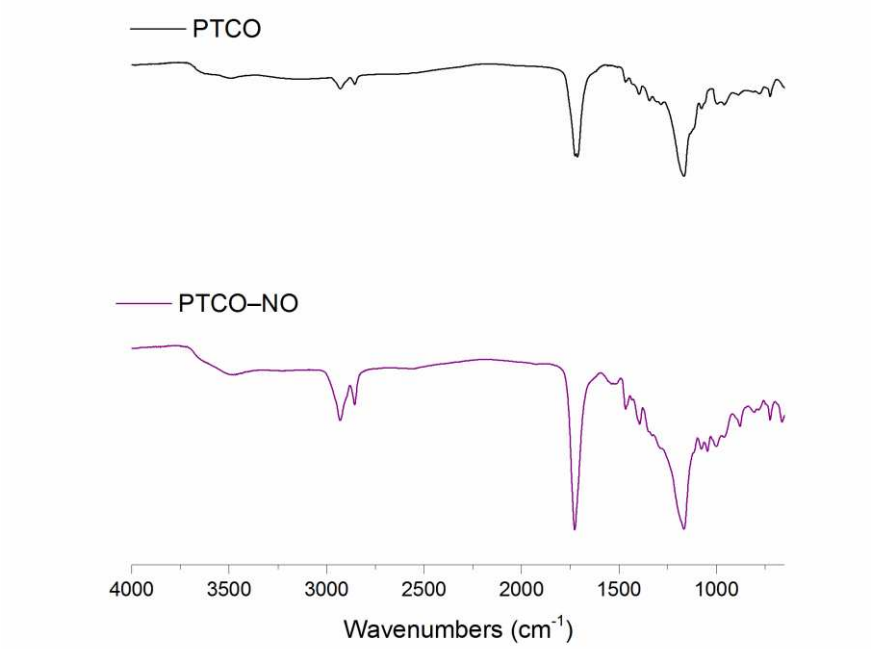

Figure B.14 FTIR-ATR spectra of PTCO and PTCO–NO.PTCO – IR υ_{max}/cm^{-1}: 3494–2400 (O–H), 2928–2855 (C–H), 1725 (C=O), 1167 (C–O). PTCO–NO – IR υ_{max}/cm^{-1}: 3468–2400 (O–H), 2930–2856 (C–H), 1727 (C=O), 1167 (C–O).

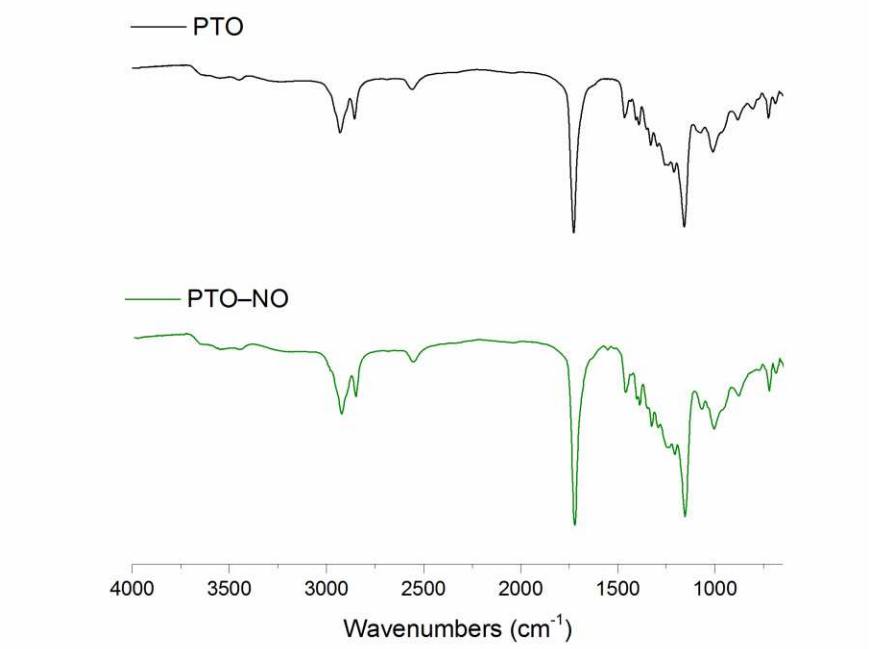

Figure B.15 FTIR-ATR spectra of PTO and PTO–NO .PTO – IR υ_{max}/cm^{-1}: 3544–2400 (O–H), 2930–2856 (C–H), 1727 (C=O), 1158 (C–O). PTO–NO – IR υ_{max}/cm^{-1}: 3544–2400 (O–H), 2927–2900 (C–H), 1728 (C=O), 1159 (C–O).

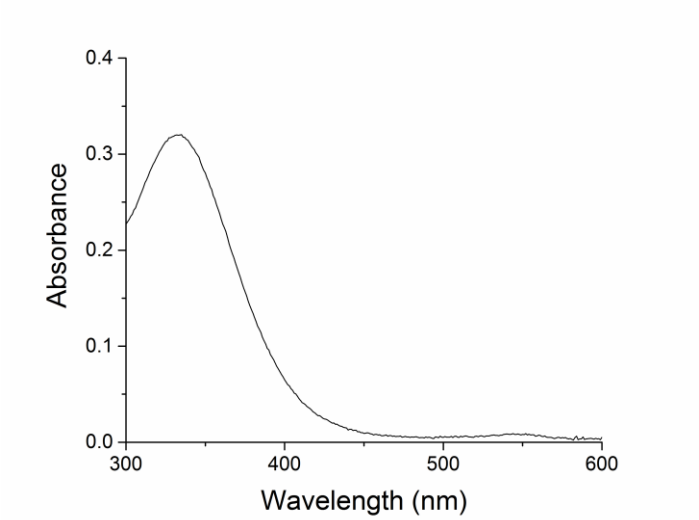

Figure B.16 UV-Vis spectrum of PTMO–NO in DMSO. The spectrum depicts the characteristic transitions of *S*-nitrosothiols at 335 ($\pi \rightarrow \pi^*$) and 544 nm ($n_N \rightarrow \pi^*$).

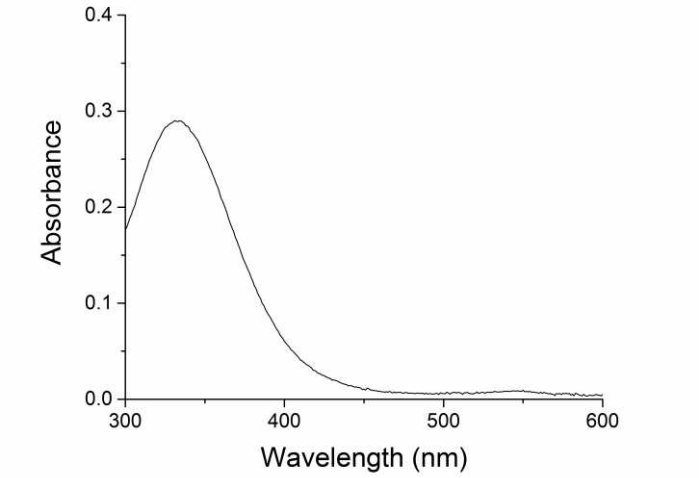

Figure B.17 UV-Vis spectrum of PTCO–NO in DMSO. The spectrum depicts the characteristic transitions of *S*-nitrosothiols at 331 ($\pi \rightarrow \pi^*$) and 544 nm ($n_N \rightarrow \pi^*$).

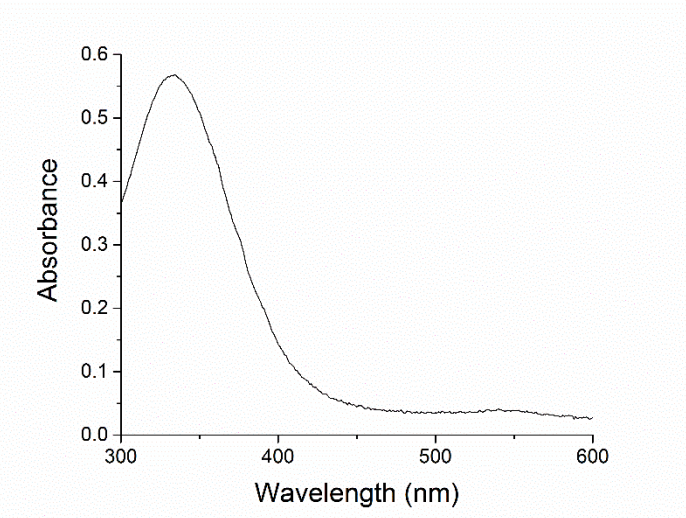

Figure B.18 UV-Vis spectrum of PTO–NO in DMSO. The spectrum depicts the characteristic transitions of *S*-nitrosothiols at 333 ($\pi \rightarrow \pi^*$) and 540 nm ($n_N \rightarrow \pi^*$).

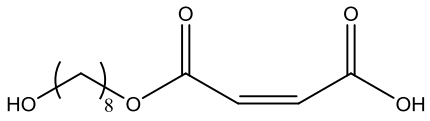

PTMO-P1, PTCO-P1, PTO-P1*‡
4-((8-hydroxyoctyl)oxy-4-oxobut-2-enoic acid.

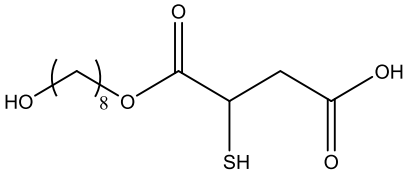

PTMO-P2, PTCO-P2, PTO-P2‡
4-((8-hydroxyoctyl)oxy)-3-mercapto-4-oxobutanoic acid.

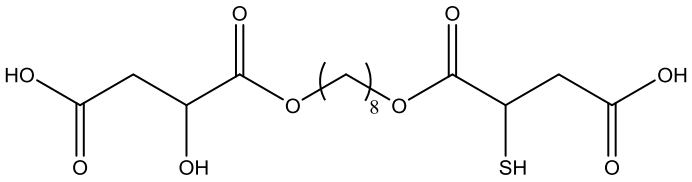

PTMO-P3, PTO-P3*
4-((8-((3-carboxy-3-hydroxypropanoyl)oxy)octyl)oxy)-2-mercapto-4-oxobutanoic acid.

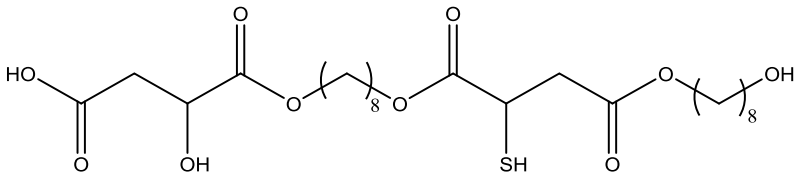

PTMO-P4, PTO-P4*
2-hydroxy-4-((8-((4-((8-hydroxyoctyl)oxy)-3-mercapto-4-oxobutanoyl)oxy)octyl)oxy)-4-oxobutanoic acid.

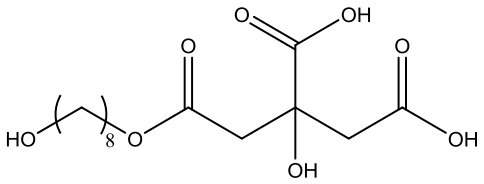

PTCO-P3
2-hydroxy-2-(2-((8-hydroxyoctyl)oxy)-2-oxoethyl)succinic acid.

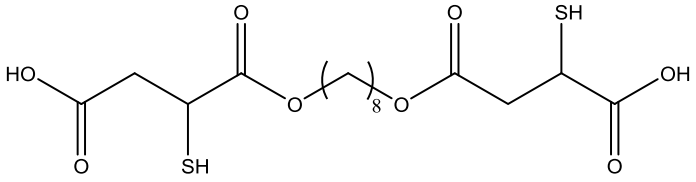

PTCO-P4
4-((8-((3-carboxy-2-mercaptopropanoyl)oxy)octyl)oxy)-2-mercapto-4-oxobutanoic acid.

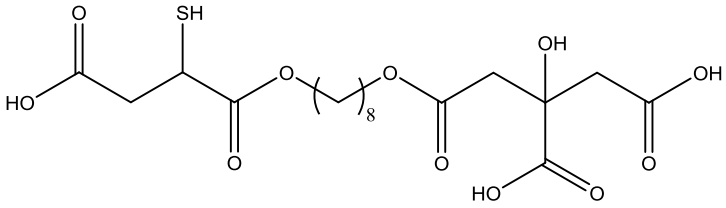

PTCO-P5
2-(2-((8-((3-carboxy-2-mercaptopropanoyl)oxy)octyl)oxy)-2-oxoethyl)-2-hydroxysuccinic acid.

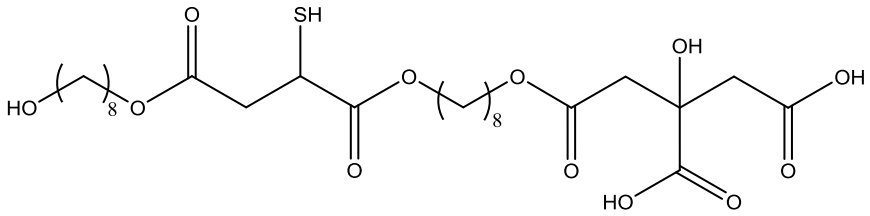

PTCO-P6
2-hydroxy-2-(2-((8-((4-((8-hydroxyoctyl)oxy)-2-mercapto-4-oxobutanoyl)oxy)octyl)oxy)-2-oxoethyl)succinic acid.

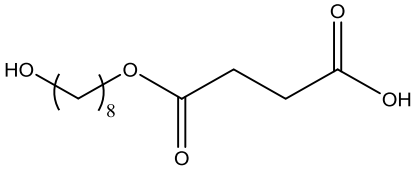

PTCO-P7*†
4-((8-hydroxyoctyl)oxy)-4-oxobutanoic acid

Figure B.19 Structures and names of degradation products identified using mass spectrometry. *Ions also found as byproducts from *S*-nitrosated polymers (PTMO–NO, PTCO–NO and PTO–NO). ‡Ions common to all polymers (PTMO, PTMO–NO, PTCO, PTCO–NO, PTO and PTO–NO) corresponding to dimers composed of the bonded monomers. †Ion only found as byproduct from the *S*-nitrosated polymer PTCO–NO.

Table B.1 Viable bacteria (CFU/mL) obtained after 6 and 24 h exposure to *S*-nitrosated polymers. For all experiments, $n \geq 6$ and results are reported as the mean ± standard deviation.

Viable Bacteria (CFU/mL)

	E. coli		*S. aureus*	
	6 h	24 h	6 h	24 h
PC [a]	$(8.0 \pm 1.2) \times 10^8$	$(5.6 \pm 2.4) \times 10^8$	$(9.1 \pm 5.0) \times 10^7$	$(1.1 \pm 0.4) \times 10^9$
PTMO–NO (**1a**)	1	1	1	1
PTCO–NO (**2a**)	$(5.2 \pm 6.4) \times 10^6$	1	1	1
PTO–NO (**3a**)	$(3.0 \pm 1.4) \times 10^3$	$(3.4 \pm 3.7) \times 10^4$	1	1

[a] Positive control (PC) represents the viable bacteria in the absence of polymer. A value of 1 represents the limit of detection for this technique.

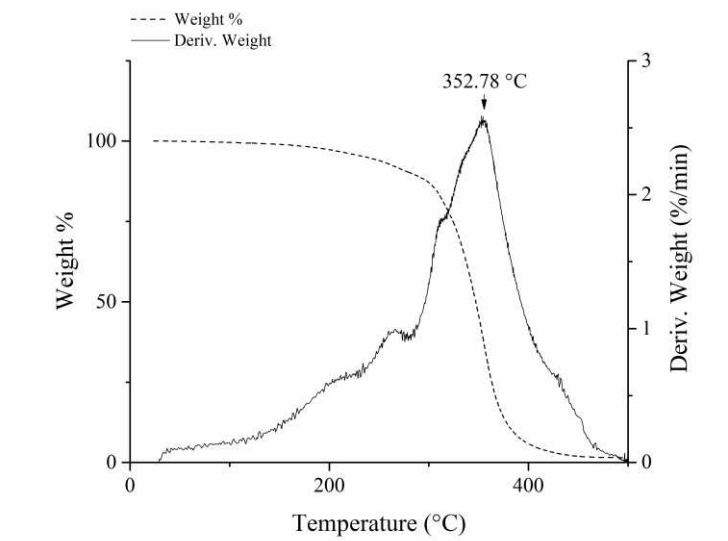

Figure S3.20 Thermogravimetric analysis plot of PTMO. The temperature of the instrument was ramped to 500 °C at a rate of 20 °C min^{-1}, followed by an isothermal step for 5 min.

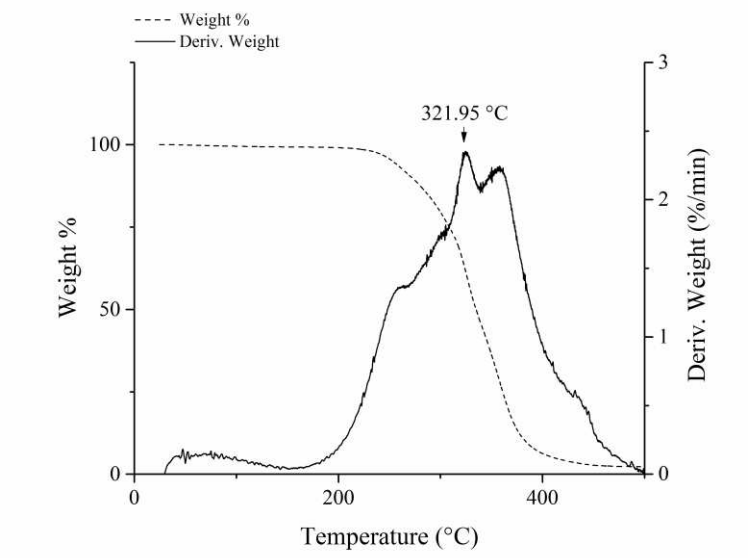

Figure S3.21 Thermogravimetric analysis plot of PTCO. During the experiment, the temperature of the instrument was ramped to 500 °C at a rate of 20 °C min^{-1}. The process was followed by an isothermal step for 5 min.

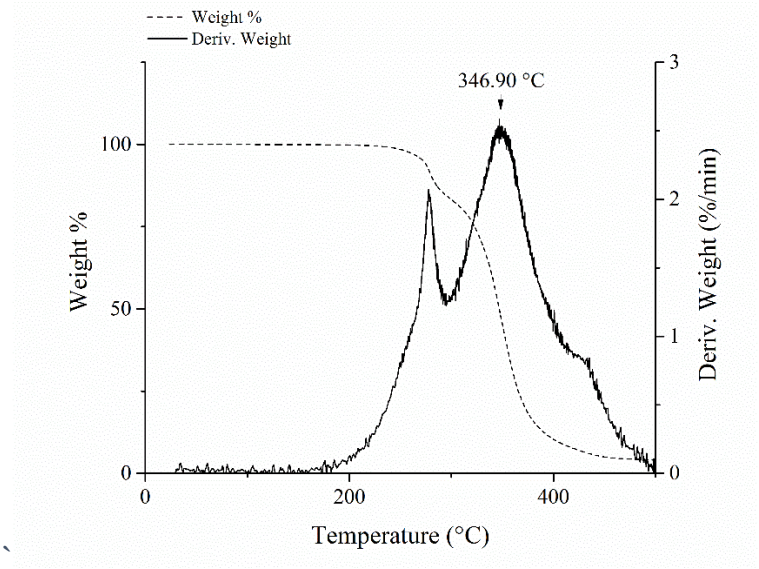

Figure S3.22 Thermogravimetric analysis plot of PTO. The instrument was set to ramp to 500 °C at a rate of 20 °C min^{-1}, followed by an isothermal step for 5 min.

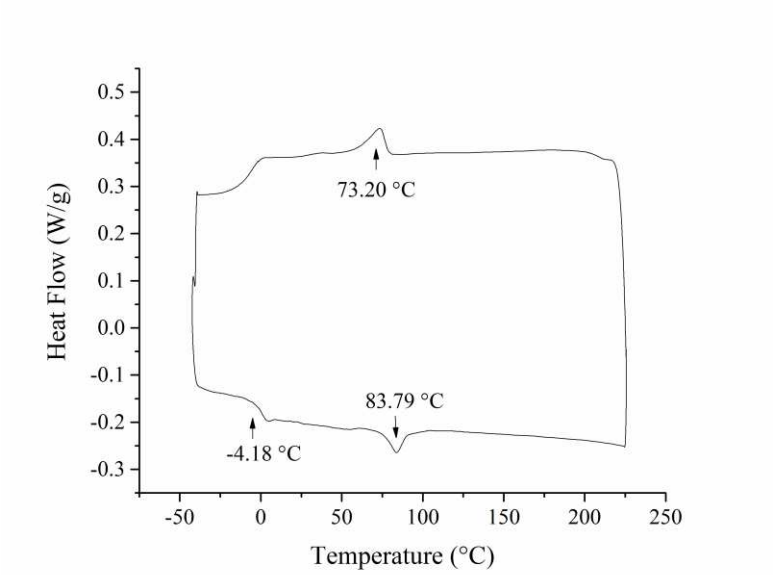

Figure S3.23 Differential scanning calorimetry plot of PTMO**.** The temperature of the instrument was ramped to −40 °C at a rate of 10 °C min^{-1}, then equilibrated at −40 °C. For the following step, the temperature was ramped to 225 °C at a rate of 5 °C min^{-1}. An isothermal step for 5 minutes marked the end of cycle 1, which was repeated once. The temperature was then ramped to 0 °C at a rate of 5 °C min^{-1}.

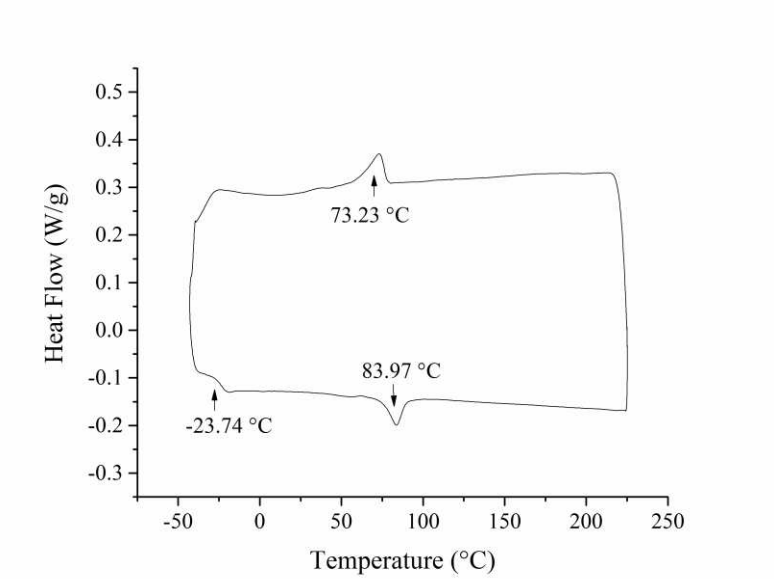

Figure S3.24 Differential scanning calorimetry plot of PTCO**.** The temperature was ramped to −40 °C at a rate of 10 °C min^{-1}, then equilibrated at −40 °C, then ramped to 225 °C at a rate of 5 °C min^{-1}. An isothermal step for 5 minutes marked the end of cycle 1, which was repeated once. The temperature was then ramped to 0 °C at a rate of 5 °C min^{-1}.

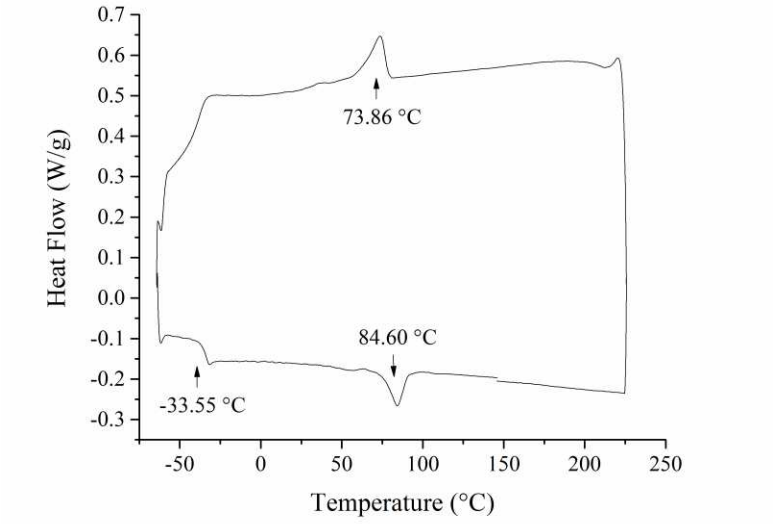

Figure S3.25 Differential scanning calorimetry plot of PTO**.** The temperature of the instrument was ramped to −60 °C at a rate of 10 °C min^{-1}, then equilibrated at −60 °C. For the following step, the temperature was ramped to 225 °C at a rate of 5 °C min^{-1}. An isothermal step for 5 minutes marked the end of cycle 1, which was repeated once. The temperature was then ramped to 0 °C at a rate of 5 °C min^{-1}.

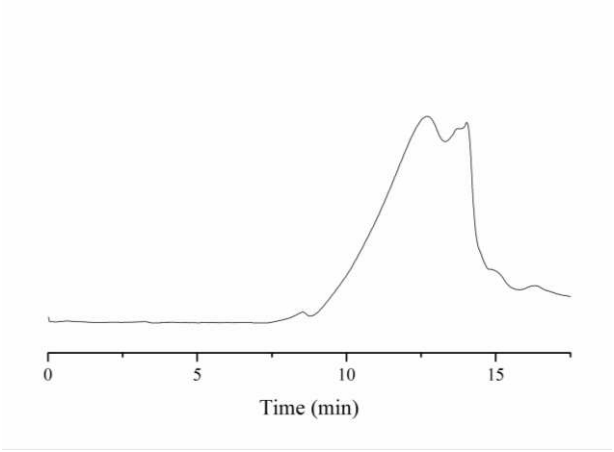

Figure S3.26 Gel permeation chromatography plot of PTMO. The data was acquired from a solution of PTMO in DMF (0.25% w/v). The sample was analyzed using polystyrene standards.

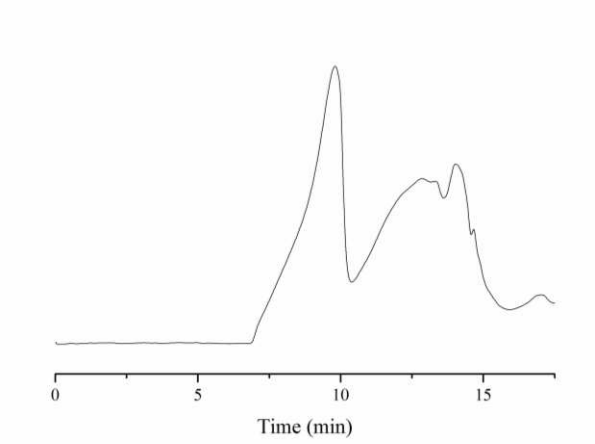

Figure S3.27 Gel permeation chromatography plot of PTCO. The sample was dissolved in DMF (0.25% w/v). Polystyrene standards were used for data analysis.

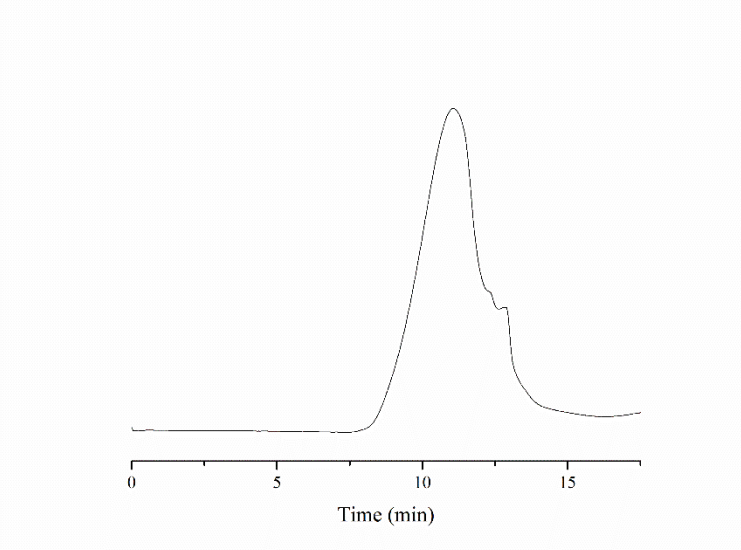

Figure S3.28 Gel permeation chromatography plot obtained from a solution of PTO in DMF (0.25% w/v). The sample was analyzed using polystyrene standards.

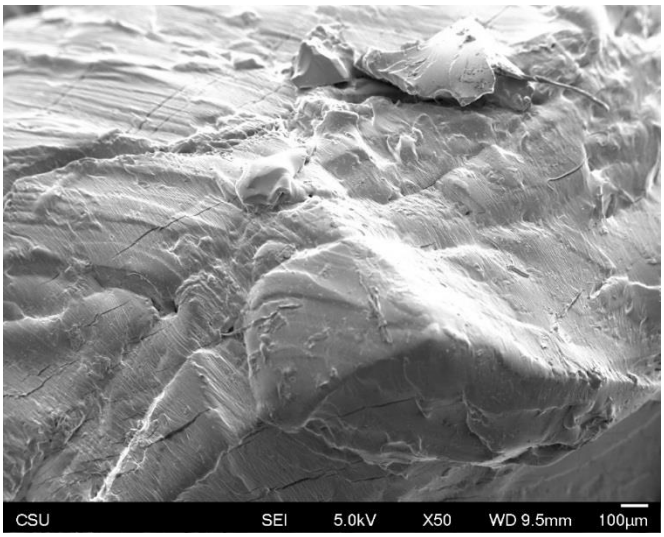

Figure S3.29 Image of PTMO obtained using a scanning electron microscope (SEM)**.**

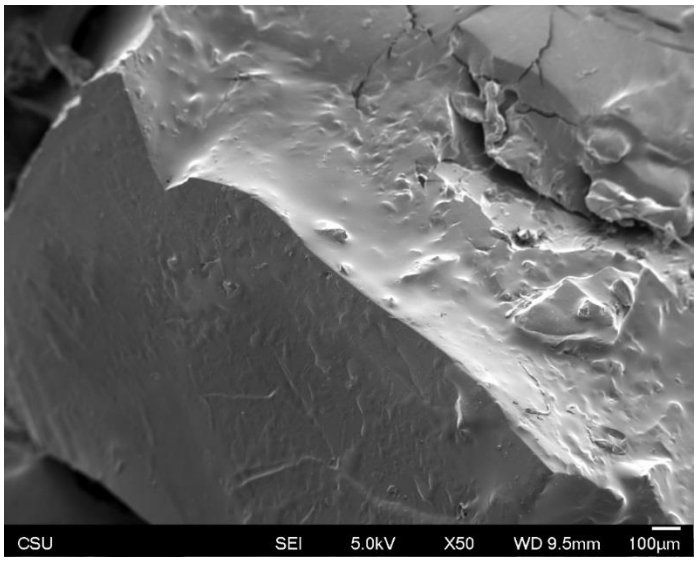

Figure S3.30 SEM image of PTMO–NO**.**

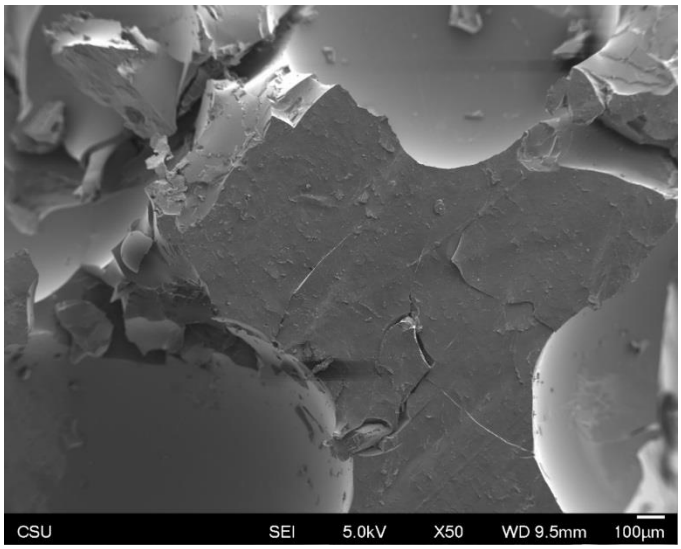

Figure S3.31 SEM image of PTCO**.**

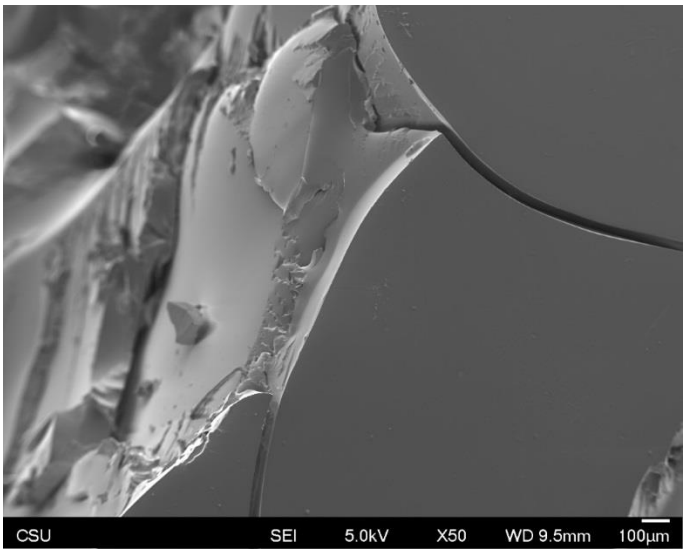

Figure S3.32 SEM image of PTCO–NO**.**

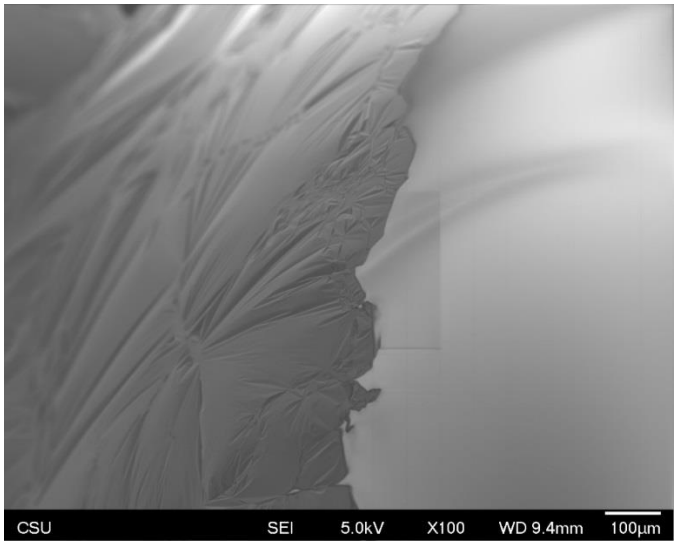

Figure S3.33 SEM image of PTO**.**

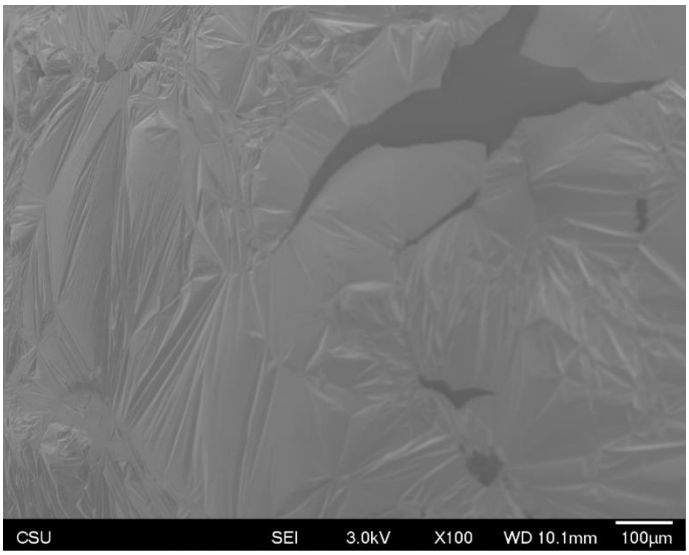

Figure S3.34 SEM image of PTO–NO**.**

APPENDIX C

EXPERIMENTAL DETAILS AND SUPPORTING INFORMATION FOR CHAPTER 5

C.1 Additional figures

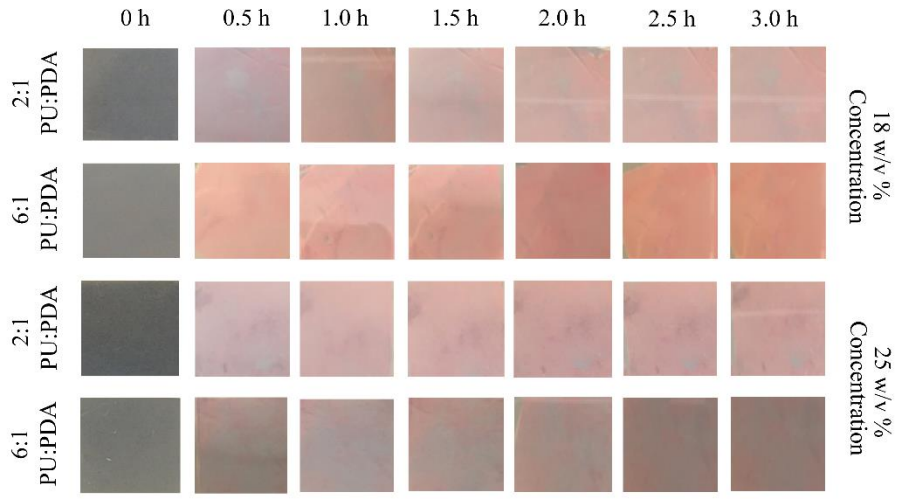

Figure C.1 PU-PDA electrospun fiber mats after exposure to bacterial strain *E. coli* ATCC ™ 25922 at ambient conditions during the course of 3 h. Fibers presented in two upper rows are prepared with 2:1 and 6:1 PU:PDA ratio and 18 % w/v concentration. Fibers presented in the two lower rows are prepared with 2:1 and 6:1 PU:PDA ratio and 25 % w/v concentration. Each column represents the contact time of fiber mats with the bacteria.

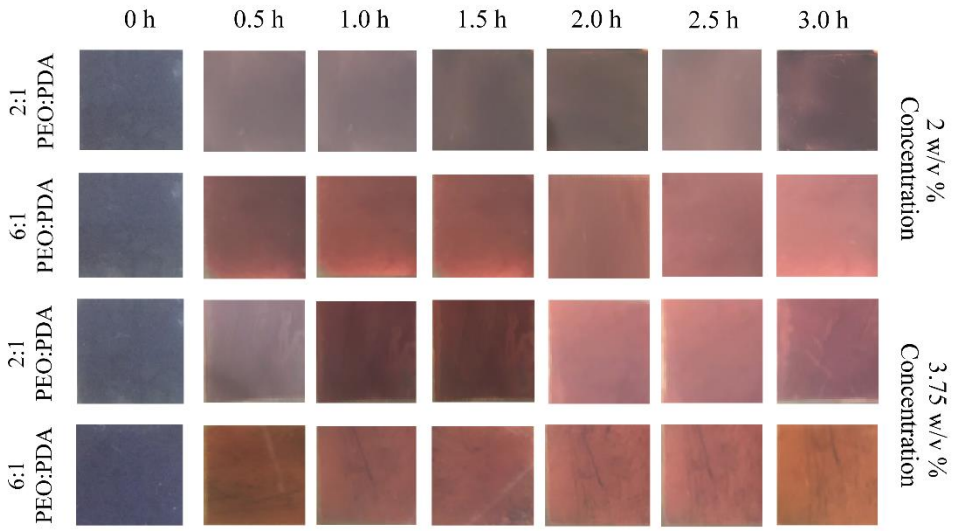

Figure C.2 PEO-PDA electrospun fiber mats after exposure to bacterial strain *E. coli* ATCC ™ 25922 at ambient condition over time. Fibers presented in two upper rows are prepared with 2:1 and 6:1 PEO:PDA ratio and 2% w/v concentration. Fibers presented in the two lower rows are prepared with 2:1 and 6:1 PEO:PDA ratio and 3.75 % w/v concentration. Each column represents the contact time of fiber mats with the bacteria.

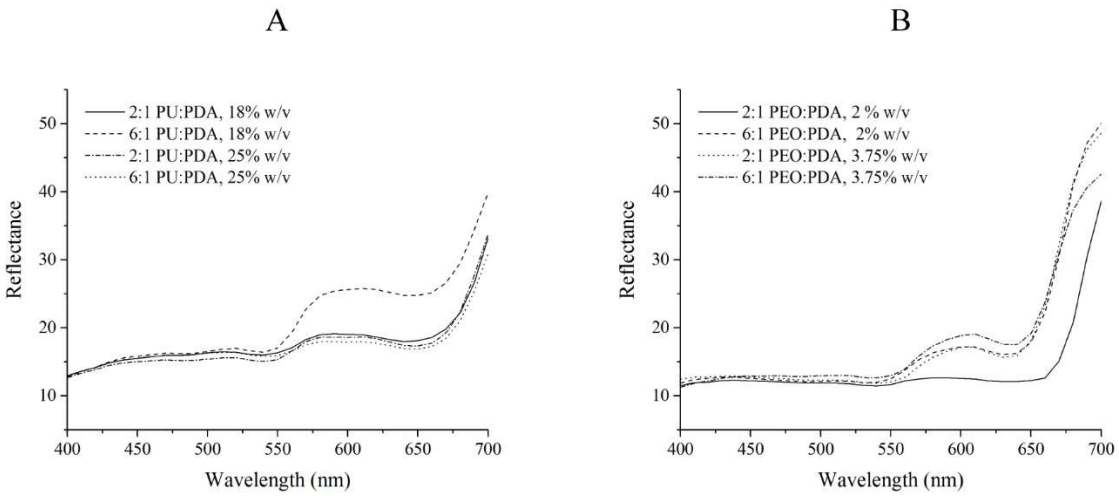

Figure C.3 Plots A and B show the reflectance spectra of the fiber composites that were exposed to *E. coli* for 3 hours for PEO-PDA and PU-PDA fibers, respectively.